



TECHNISCHE UNIVERSITÄT
CHEMNITZ

On the role of dopamine in motivated behavior : a neuro-computational approach

Dr. Julien Vitay

Geboren am 11.12.1979 in Saint-Nazaire (Frankreich)

DISSERTATION ZUR ERLANGUNG DES AKADEMISCHEN GRADES

DR. HABIL

Fakultät für Informatik
Technische Universität Chemnitz

2017

Table of contents

Abstract	1
1 Introduction	3
1.1 Computational neuroscience	5
1.2 Motivated behavior	9
1.3 Reward and the dopaminergic system	11
1.4 Basal ganglia and reinforcement learning	16
1.5 Multiple loops and organization of behavior	21
1.6 Structure of the thesis and contribution	24
List of publications included in the thesis	25
Contribution to each article	25
1.6.1 Chapter 2 : Perirhinal cortex and dopamine	25
1.6.2 Chapter 3 : Basal ganglia and memory retrieval	27
1.6.3 Chapter 4 : WM and multiple basal ganglia loops	29
1.6.4 Chapter 5 : Timing and expectation of reward	31
1.6.5 Chapter 6 : Neural simulator ANNarchy	33
1.7 Conclusion	34
2 Sustained activities and retrieval in a computational model of perirhinal cortex	37
2.1 Introduction	37
2.2 Methods	39
2.2.1 Context	39
2.2.2 Architecture of the model	39
2.2.3 Dopamine modulation	41
2.2.4 Equations for updating the activity	43
2.2.5 Learning rule	45
2.3 Results	46
2.3.1 Learning and propagation of activity within a cluster	46
2.3.2 Sustained activities and intermediate values of dopamine	47
2.3.3 Propagation of activity between clusters	49
2.3.4 Thalamic stimulation	51
2.4 Discussion	52
Appendix: details of the model	54
3 A computational model of basal ganglia and its role in memory retrieval in rewarded visual memory tasks	57
3.1 Introduction	57
3.2 Material and Methods	60
3.2.1 Architecture of the model	60
3.2.2 Perirhinal cortex	61
3.2.3 Dorsolateral prefrontal cortex	62
3.2.4 Ventral-anterior thalamus	63
3.2.5 Caudate nucleus	63
3.2.6 Substantia nigra pars compacta	65

Table of contents

3.2.7	Substantia nigra pars reticulata	66
3.2.8	Experiments	68
3.3	Results	71
3.3.1	Concurrent learning of the different tasks	71
3.3.2	Temporal evolution of the activities after learning	72
3.3.3	Effect of the competition in SNr	75
3.3.4	Influence of the number of cells in SNr	78
3.3.5	Reward-related clustering in CN	79
3.4	Discussion	81
4	Working memory and response selection: A computational account of interactions among cortico-basal ganglio-thalamic loops	89
4.1	Introduction	89
4.2	Material and methods	91
4.2.1	Architecture of the model	91
4.2.2	Experimental setups	99
4.3	Results	102
4.3.1	Task performance	102
4.3.2	Analysis of the model's behavior	103
4.4	Discussion	110
	Appendix A. Full list of equations	114
	Appendix B. Number of simulated cells	119
	Appendix C. Overview of model parameters	120
5	Timing and expectation of reward: a neuro-computational model of the afferents to the ventral tegmental area	123
5.1	Introduction	123
5.2	Material & methods	126
5.2.1	Neurobiological assumptions	126
5.2.2	The proposed model	130
5.3	Results	146
5.3.1	CS-US associations in the amygdala	146
5.3.2	Timecourse of activity in VTA	148
5.3.3	Evolution of VTA activity during conditioning	149
5.3.4	Influence of reward magnitude on conditioning	150
5.3.5	Timing mechanism in NAcc	152
5.3.6	Acquisition rate of temporal prediction	154
5.3.7	Time course of forebrain nuclei	155
5.4	Discussion	157
5.4.1	Relation to other work	159
5.4.2	Biological plausibility	162
5.4.3	Conclusion	166
6	ANNarchy: a code generation approach to neural simulations on parallel hardware	167
6.1	Introduction	167
6.2	Interface of the simulator	170
6.2.1	Structure of a network	170
6.2.2	Equation-oriented description	172
6.2.3	Rate-coded neurons and synapses	173
6.2.4	Spiking neurons and synapses	176
6.2.5	Additional features	181

6.3	Code generation	189
6.3.1	Internal representation of data	189
6.3.2	Simulation steps	190
6.3.3	Mathematical parser	191
6.3.4	Numerical methods	192
6.3.5	OpenMP and CUDA code generation	195
6.4	Benchmarks	197
6.5	Discussion	202
	References	205

Abstract

Neuro-computational models allow to study the brain mechanisms involved in intelligent behavior and extract essential computational principles which can be implemented in cognitive systems. They are a promising solution to achieve a brain-like artificial intelligence that can compete with natural intelligence on realistic behaviors. A crucial property of intelligent behavior is motivation, defined as the incentive to interact with the world in order to achieve specific goals, either extrinsic (obtaining rewards such as food or money, or avoiding pain) or intrinsic (satisfying one's curiosity, fun). In the human brain, motivated or goal-directed behavior depends on a network of different structures, including the prefrontal cortex, the basal ganglia and the limbic system. Dopamine, a neuro-transmitter associated with reward processing, plays a central role in coordinating the activity of this network. Its structures processing in high-level cognitive areas along a limbic-associative-motor gradient and impacts the learning capabilities of the whole system. In this habilitation thesis, I present biologically-constrained neuro-computational models which investigate the role of dopamine in visual object categorization and memory retrieval (Vitay and Hamker, 2008), reinforcement learning and action selection (Vitay and Hamker, 2010), the updating, learning and maintenance of working memory (Schroll et al., 2012) and timing processes (Vitay and Hamker, 2014). These models outline the many mechanisms by which the dopaminergic system regulates cognitive and emotional behavior: bistable processing modes in the cerebral cortex, modulation of synaptic transmission and plasticity, allocation of cognitive resources and signaling of relevant events. Finally, I present a neural simulator able to simulate a variety of neuro-computational models efficiently on parallel architectures (Vitay et al., 2015).

Abstract

Neuronale Modelle nach dem Vorbild des Gehirns bieten die Möglichkeit intelligente, kognitive Prozesse nicht nur besser zu verstehen, sondern sie stellen auch eine vielversprechende Lösung dar, um eine Gehirn-ähnliche künstliche Intelligenz für Wahrnehmung und Verhaltensweisen zu erreichen, die mit natürlicher Intelligenz konkurrieren kann. Eine entscheidende Eigenschaft von intelligentem Verhalten ist Motivation, definiert als der Anreiz mit der Welt zu interagieren, um bestimmte Ziele zu erreichen, sei es extrinsisch (Belohnungen wie Nahrung oder Geld zu erhalten oder die Vermeidung von Schmerzen) oder intrinsisch (die Neugier zu befriedigen, Spaß zu haben). Im menschlichen Gehirn basiert motiviertes oder zielgerichtetes Verhalten auf einem Netzwerk von verschiedenen Strukturen, einschließlich des präfrontalen Cortex, der Basalganglien und des limbischen Systems. Dopamin, ein Neurotransmitter, welcher der Belohnungsverarbeitung zugeordnet wird, spielt eine zentrale Rolle bei der Koordination der Aktivität in diesem Netzwerk. Es strukturiert die Verarbeitung in High-Level-kognitiven Bereichen entlang eines limbischen-assoziativ-motor Gradienten und beeinflusst die Lernfähigkeit des gesamten Systems. In dieser Habilitation, präsentiere ich biologisch motivierte neuronale Modelle, die die Rolle von Dopamin in der visuellen Objektkategorisierung und Gedächtnisabruf (Vitay and Hamker, 2008), Reinforcement Lernen und Aktionsauswahl (Vitay and Hamker, 2010), Aktualisierung, Lernen und Aufrechterhaltung von Arbeitsgedächtnis (Schroll et al., 2012) und Timing Prozessen (Vitay and Hamker, 2014) untersuchen. Diese Modelle beschreiben Mechanismen, durch die das dopaminerge System kognitives und emotionales Verhalten reguliert: bistabile Verarbeitungsmodi in der Hirnrinde, Plastizität und Modulation der synaptischen Übertragung, Zuweisung von kognitiven Ressourcen und Signalisierung von relevanten Ereignissen. Schließlich beschreibe ich einen neuronalen Simulator, der in in der Lage ist, eine Vielzahl von neuronalen Modellen effizient auf parallelen Architekturen zu simulieren (Vitay et al., 2015).

1 Introduction

Minsky (1968) defined the field of Artificial Intelligence (AI) as “the science of making machines do things that would require intelligence if done by humans”. Over its almost 70 years of existence - John MacCarthy invented the term in 1956 -, AI has achieved a lot of progress in specialized areas such as data-mining, machine learning, computer vision, speech recognition or even single cognitive tasks such as chess playing or medical diagnosis. Weak (or applied) AI indeed focuses on methods allowing to solve specific tasks which either necessitate a limited range of human intellectual abilities (e.g. recognizing objects) or even have nothing to do with human intelligence (e.g. search engines). Although these improvements have proven very useful, especially in an industrial context, the real goal of AI - called strong AI by Searle (1980) - is to obtain systems with a general form of intelligence that could be compared with human intelligence on complex behaviors. Despite recent advances in machine learning techniques (e.g. deep learning, LeCun et al., 2015) and prophetic claims that the singularity is approaching (Kurzweil, 2005), one has to admit that strong AI has basically failed until now (Velik, 2012). As Marvin Minsky noticed, all we have is a collection of “dumb” specialists which perform single tasks very well - deep neural networks exceed for example human performance on certain visual recognition tasks - but which, when put together, do not even get close to the cognitive abilities of a rodent. Robotic competitions such as RoboCup are good demonstrators of the limits of strong AI.

Many cognitive architectures for strong AI have been proposed over the years (for a review, see Langley et al., 2009). They usually take the form of conversational agents, virtual reality avatars or robotic platforms, although they may also be used in specific applications. They can be classified generally into two approaches: the symbolic (or cognitivist) approach, which breaks human intelligence into functional components - e.g. attention, long-term memory, sensory processes - and implements each of them with particular symbolic algorithms - production rules, tree searches; and the connectionist (or emergentist) approach which considers distributed systems of functional units (often in the form of neural networks) which interact with each other and learn to perform a task through interacting with an environment. Although the behavior of a symbolic system is easier to analyze, its suitability for real-world problems is problematic: if breaking a task into elementary components makes sense for symbolic problems such as the game of chess, it becomes much harder for recognizing a face, engaging a conversation appropriately or even playing football. The main issue here is symbol-grounding: while manipulating the concept of a cup or a ball is easy for a computer, it is much harder to relate this concept to the visual perception of a cup or ball with any possible shape, under various

1 Introduction

lightning conditions or orientations. This explains why symbolic cognitive architectures have mostly failed to produce interesting behaviors outside restricted lab settings. An additional difficulty is the amount of work required to create the cognitive architecture: each module of the system must communicate symbols adequately to the others, which in turn should be able to cope with potential failures. The resulting architecture becomes quickly tuned to a particular problem, and any significant change in the environmental conditions may require to redevelop the whole system.

The connectionist approach relies heavily on learning to exhibit the desired cognitive functions. Contrary to symbolic architectures, the desired function is not hard-coded in the system but rather emerges from the interaction of multiple units after learning. An example is artificial neural networks, where neurons communicate with each other through connections whose weights evolve with learning: the function performed arises from this interaction, not from the structure of the network itself. The same network can for example learn to perform many different functions, depending on its interaction with the task. The computational properties of neural networks are heavily used in weak AI, especially in machine learning. The drawback of this decoupling between the function and the underlying structure is that it becomes complicated to create complex cognitive architectures: the communication between different modules is not symbolic anymore, but numerical - the activity of a population of neurons. Psychological models of cognition, using generic modules such as planning or long-term memory, do not map easily on a connectionist substrate.

To overcome this problem, a promising direction for AI is to get inspiration from the only truly intelligent system known to date: the brain. The brain has intrinsically a connectionist structure: it is composed of hundreds of billions of neurons, communicating with each other through synapses which undergo plasticity based on experience. The core idea of brain-like AI (or brain-inspired AI) is to study how the brain exhibits natural intelligence and extract the necessary mechanisms to reproduce it in an artificial system. Velik (2012) defined the basic dogma of brain-like AI as such:

It is well appreciated that the human brain is the most sophisticated, powerful, efficient, effective, flexible and intelligent information processing system known. Therefore, the functioning of the human brain, its structural organization, and information processing principles should be used as archetype for designing artificial intelligent systems instead of just emulating its behavior in a black box manner. To achieve this, approaches should not build on work from engineers only but on a close cooperation between engineers and brain scientists.

Brain-like AI covers a variety of approaches, from top-down models simulating the functions of particular brain areas using non-brain-inspired implementations (e.g. Bayesian models for decision making), to bottom-up models simulating with great detail specific brain areas, but without any relationship to their function (e.g. Human Brain Project). The neuro-computational models presented in this thesis aim at finding a middle ground between these approaches: address the

problem of intelligence at the functional level (the models should be useful at the end), while keeping the biological realism high enough to explain and predict biological neural mechanisms. This link between function and structure in the brain is the fundamental question of *computational neuroscience*, which partly overlaps with brain-like AI. Neuro-computational models in this field are by design close to the architecture of the brain; insights from neuroscience on motivated behavior can be rapidly integrated to improve both their plausibility and performance. They furthermore provide an unique way to investigate new computing paradigms.

1.1 Computational neuroscience

Aim

The ambition of computational neuroscience is to bring a computational modeling approach to the interdisciplinary field of neuroscience, aiming concurrently at an explicative role - explaining why the brain behaves in the observed way - and a predictive one - suggesting previously unobserved effects which can be tested. The main challenge is to integrate experimental observations from different levels of description (neuroanatomy, neurochemistry, neurophysiology, neuro-imaging, cognitive science and behavioral studies) into a biologically realistic neural network. Numerical simulations of this model allow to reproduce the underlying observations in a systematic way and to better analyze, interpret and understand the available data. Conversely, predictions can be made based on these simulations, guiding experimentalists in the design of their experiments (theory-driven neuroscience).

Although the term was only first coined by Eric L. Schwartz in 1985, the first examples of computational neuroscience work may be the invention of the integrate-and-fire neuron by Lapique (1907) and the complete mathematical characterization of the initiation and propagation of action potentials in the squid giant axon by Hodgkin and Huxley (1952). Research in computational neuroscience has long focused mostly on characterizing the dynamics of individual neurons or small assemblies. The focus has now shifted toward large-scale models, either at the systems level where functional networks involved in particular processes are investigated (Draniias et al., 2008; Hamker, 2004a), or at the detailed biological level, with the goal of simulating complete brain areas, as in the Blue Brain Project (Markram, 2006), or even the whole brain in its follower Human Brain Project (HBP). Neuro-computational models have virtually addressed over the years all brain structures and functions, including vision in the occipital and temporal lobes (Rolls and Deco, 2001), working memory in the prefrontal cortex and basal ganglia (Frank et al., 2001; Schroll et al., 2012), long-term memory formation in the hippocampal formation (Burgess et al., 2007) or motor learning in the cerebellum (Albus, 1971).

Neuro-computational models

Neuro-computational models typically study the interaction of different brain areas. Each area comprises a certain number of artificial neurons, which are modeled differently depending on the physiological properties of the corresponding biological neuron (pyramidal neuron, medium spiny neuron, basket cell, etc) and the neuro-transmitter they use (e.g. AMPA, NMDA, GABA). Many models however use only two types of neurons: excitatory and inhibitory neurons. When active, excitatory neurons increase the firing rate of neurons receiving synapses from them, while inhibitory neurons decrease it. One of the simplest -although powerful - neuron model is the *rate-coded* neuron, which computes an instantaneous firing rate (corresponding to the frequency of spike emission at a given time t) and exchange it with other neurons. A rate-coded neuron is described by an ordinary differential equation (ODE), which can be of the form:

$$\tau \cdot \frac{dr(t)}{dt} + r(t) = \sum_{i \in \text{Exc}} w_i \cdot r_i(t) - \sum_{j \in \text{Inh}} w_j \cdot r_j(t) + B$$

$r(t)$ is the instantaneous firing rate of a single neuron, τ the time constant defining the speed of its dynamics and B its baseline activity (the firing rate it has without inputs). Inputs are represented by the weighted sums, where each connection to the neuron (a synapse) has a weight w (also called the synaptic efficiency) which multiplies the firing rate of the corresponding pre-synaptic neuron. Two sums are represented here (corresponding to excitatory and inhibitory synapses, as denoted by their respective positive and negative signs), but more complex relationships can be used. For example, modulatory inputs can multiply globally a weighted sum of excitatory inputs. Additionally, a transfer function can be used to restrict the firing rate to positive values, or implement non-linear effects.

If the description of a single neuron is relatively simple, the computational power of a neuro-computational model comes from the interconnection of several populations of neurons, allowing the emergence of complex functions. The projection of a population on another can be dense (all-to-all, i.e. each neuron in the post-synaptic population has a synapse with every neuron in the pre-synaptic one) or sparse (a synapse exists according to a fixed probability or some more complex rule). Moreover, *synaptic plasticity* allows to modify the weights w of a projection based on the activity of the neurons, forming the basis of learning in a neural network. The simplest and most famous rule for synaptic plasticity is the Hebbian learning rule (Hebb, 1949), which states that the weight of a synapse increases when both pre- and post-synaptic neurons are active at the same time (correlation-based learning rule):

$$\Delta w = \eta \cdot r^{\text{pre}} \cdot r^{\text{post}}$$

where w is the weight of the synapse, η a learning rate defining the speed of learning, r^{pre} and r^{post} the instantaneous firing rate of the pre- and post-synaptic neurons, respectively. The disadvantage of this rule being that the weights would increase infinitely, several variants have since

been introduced, among which the Oja learning rule (which adds a regularization term to keep the sum of weights coming to a neuron constant, Oja, 1982) or the Bienenstock-Cooper-Munro rule (BCM, modeling both long-term potentiation - LTP, weight increase - and long-term depression - LTD, weight decrease - Bienenstock et al., 1982), as well as rules modeling the modulatory influence of dopamine on synaptic plasticity. Although there is flexibility in the choice of the rules, a hard constraint to obtain a biologically-realistic model is that all the information needed by the rule should be local to the synapse: the weight change can only depend on variables of the pre- and post-synaptic neurons, but not other neurons. Many classical machine learning algorithms such as backpropagation (Rumelhart et al., 1986) can not be used in this context.

Computer science

The cross-fertilization between computational neuroscience and artificial intelligence is well documented. As explained later, reinforcement learning, a subfield of machine learning (Sutton and Barto, 1998), has been successfully used to interpret the patterns of activity in dopaminergic areas during classical conditioning (Schultz, 1998). As dopamine modulates processing and learning in many brain areas, including the prefrontal cortex and the basal ganglia, this theoretical consideration has radically changed the interpretation of their role in various processes such as motor learning, action selection, working memory or decision-making. This analogy is still widely used by experimentalists and clinicians to interpret their observations, although several computational neuroscientists have since proposed more detailed and realistic neuro-computational models of the dopaminergic system (Brown et al., 1999; O'Reilly and Frank, 2006; Vitay and Hamker, 2014).

On the other hand, deep learning networks (LeCun et al., 2015) are directly derived from computational neuroscience research. The basic structure of a deep learning network for visual recognition is mapped onto the hierarchical organization of the visual cortex, with lower-levels areas extracting simple and local features from the retinal image (edges, gradients), and higher-level areas combining these lower features into complex shapes or even objects (Lecun et al., 1998). The most successful deep learning architectures make also use of sparseness as a regularization method to ensure an efficient coding of visual features, a concept which was first extensively studied by computational neuroscientists (Olshausen and Field, 1997; Spratling, 1999; Wiltschut and Hamker, 2009). Dropout, a regularization technique used to improve generalization in deep networks (Srivastava et al., 2014), is inspired from computational studies of stochastic synaptic transmission (Maass and Zador, 1999).

Challenges

Several issues are faced by computational neuroscience. The first one is the everlasting controversy on the adequate level of description to explain brain processes. Some models can be very detailed, using a model of the 3D morphology of specific neurons and a detailed description of

1 Introduction

chemical processes occurring inside the synapses. This *bottom-up* approach, exemplified by the Human Brain Project, relies heavily on data analysis to find the correct parameters and replicate observations. There is virtually no end to the degree of details that can be incorporated in such models. Despite its ambitious nature on this issue, one of the major criticisms addressed to HBP is that the level of description they chose will not be sufficient to capture all the properties of brain functioning. Contrary to physics or chemistry, neuroscience (including computational neuroscience) is non-paradigmatic in the sense of Thomas Kuhn (Kuhn, 1962): there is no common agreement inside the community on common axiomatic principles or models that could be used as a framework to interpret observations. Based on the enormous amount of unexplained experiments, the different schools of thought can select observations that fit into their paradigm and reject the ones that do not, leading to endless debates. Neuroscience is still in its infancy as a science, but the hope of defining a unified theory of brain functioning has to be maintained.

A more serious criticism to the *bottom-up* approach is that reproducing neural activity does not obligatorily mean to understand it. A complete simulated model of the brain, up to the last molecule involved, may end up as difficult to analyze and understand as an actual brain. What makes a human brain so special is not its number of neurons, nor its variety of cell types and neurotransmitters, but its different levels of organization: the complex and dynamical interaction between biological structures at different scales. The *top-down* approach to computational neuroscience starts from the behavioral function and breaks it iteratively into functional blocks that may eventually map onto the biological substrate. The corresponding models can be high-level mathematical descriptions, such as Bayesian inference (Doya et al., 2006), free-energy minimization (Friston, 2010) or optimization techniques (Sutton and Barto, 1998), while others use simplified neural models (spiking point-neurons, rate-coded neurons) to capture essential computational properties of neural networks. Top-down computational models obviously need to make strong assumptions about the underlying biological substrates and can only explain a limited range of observations. The whole difficulty is to define precisely enough the validity of the model: what can this model explain and predict, and where are its limits. For this kind of models, the key aspect is the ability to make predictions: they usually have enough degrees of freedom to fit virtually any set of experimental data, so their plausibility can only be evaluated by their predictive power.

A second problem faced by computational neuroscience is scalability. As neuro-computational models grow in size, the computational load to run the simulation becomes critical. The human brain comprises around 100 billions of neurons and tenths of trillions synapses. Even when using simple neural and synaptic models, the number of operations per second and the amount of memory needed by a complete brain model exceed the power of current supercomputers. The Human Brain Project has estimated that a complete brain model would require computational power at the exascale (one exaflops - 10^{18} - and 100 petabytes of memory) in order to function in real-time, while the fastest supercomputer at this date only proposes 50 petaflops ($5 \cdot 10^{16}$) of peak performance. The resulting simulation would consume 1.5 GW of energy if today's architectures were simply scaled up (the goal is to reduce it to 20 MW by 2020), while the human

brain merely requires 30W on average. On the short term, there is obviously a need for applying state-of-the-art parallel computing methods to the simulation of neuro-computational models. Several parallel neural simulators exist (NEST, GeNN, Brian, ANNarchy, etc) but they are usually limited to a particular type of neural models and on specific hardware platforms. On the longer term, one may need to rethink computer architectures: neural networks are inherently parallel, with localized processing units - the neurons - interacting through connections - the synapses - in continuous time. Simulating these networks on serial von Neumann architectures, even with many cores, is probably a waste of resources. Dedicated neuromorphic hardware solutions are being developed for the simulation of large-scale neural networks, for example the Spinnaker (Rast et al., 2011) and BrainScaleS (Fieres et al., 2008) projects, or the IBM SyNAPSE (Systems of Neuromorphic Adaptive Plastic Scalable Electronics) chip. They rely on fundamentally different concepts, such as asynchronous and event-driven computations, what leads to fast and energy-efficient simulations. However, these neuromorphic hardware platforms are not commonly available yet and require a strong programming effort.

Despite the different issues inherent to the youth of the field, computational neuroscience is a promising approach to artificial intelligence. It allows to bridge the gap between the quickly expanding knowledge on cognitive and emotional processes involved in behavior and the design of flexible and robust algorithms for intelligent behaving systems.

1.2 Motivated behavior

Animal behavior

Animal behavior can be decomposed into four categories: reflexes (low-level motor responses to stimuli which can not be voluntarily controlled), Pavlovian responses (the acquired association between a stimulus and an outcome, leading to conditioned responses), habits (more or less complex sequences of thoughts or actions which are routinely executed when triggered in a specific context) and goal-directed behavior (or motivated behavior, the ability to perform actions in order to achieve a particular goal) (Balleine and Dickinson, 1998). Pavlovian (or classical) conditioning is a passive learning process: an initially neutral stimulus (conditioned stimulus, CS) is repeatedly paired with a meaningful stimulus (unconditioned stimulus, US, which can be either positive - reward - or negative - punishment). The unconditioned response (UR) usually associated to the US becomes after a variable number of trials associated to the CS, becoming a conditioned response (CR). The classical experiment of Pavlov used a tone (CS) to predict the delivery of food (US) associated with drooling (CR). This form of conditioning does not require any action to be acquired, but can be used to adapt behavior by signaling the relevance of sensory events to higher-level functions. In appetitive conditioning, where the US is a food reward, the appearance of the CS prepares the animal to consumption, mainly through drooling but also possibly by interrupting the current behavior. In fear conditioning, where the US is a painful stimulation, the CS may trigger avoidance behaviors.

1 Introduction

Oppositely, habits and goal-directed behavior are two components of instrumental (or operant) conditioning: the term covers all the processes which lead an animal to *learn* to produce actions in order to obtain rewards (positive reinforcers) or avoid punishments (negative reinforcers) (Skinner, 1938; Thorndike, 1911). While in Pavlovian conditioning the animal merely observes relationships in its environment, in operant conditioning it has control over the occurrence of reinforcers by adapting its behavior both during the learning phase and the exploitation phase. Operant conditioning is the key process in educating animals (for example teaching a dog new tricks by rewarding him after each successful action), but is also fundamental in free behavior: actions are directed toward the achievement of goals. Achieving a goal is a positive reinforcer for behavior, increasing the probability to achieve it again in the future, while failing to do so is a negative reinforcer which forces to adapt the current strategy or find a new one.

Although they are both directed toward goals, the difference between habits and goal-directed behavior is their dependency on the value of the goal. A classical experiment is the devaluation task: when the value of the reward is suddenly decreased (for example by inducing satiety before the experiment), goal-directed processes quickly avoid this outcome, while habitual behavior can persist for a long period of time (Balleine and Dickinson, 1998). Habits are therefore stimulus-response (S-R) mechanisms (a stimulus can trigger the behavior, even when the goal is not interesting anymore) while goal-directed processes are based on action-outcome (A-O) associations (which action do I need to perform to obtain this particular outcome?). The transfer of a goal-directed behavior to the habitual system is possible when the association is repeatedly experienced over an extended period of time. The mechanisms underlying this transfer are not yet fully understood, but they are thought to play an important role in the development of addiction (Everitt et al., 2001).

Explicit vs. implicit motivation

Goals can be extrinsically defined, for example when some food item is available in the environment. If the value of such a goal, possibly previously estimated through classical conditioning processes, exceeds sufficiently the costs associated to obtaining it, the animal engages in a series of actions that may lead to its obtainment, in which case these actions are reinforced. This form of operant conditioning is also called *reinforcement learning*, which is an important issue for both psychology and computer science. However, animals do not only produce actions which are directed toward primary reinforcers such as food, water or sexual partners: they play with their fellows or they explore their environment without any obvious reason for an external observer. The goals of such actions are called intrinsic rewards: satisfying one's curiosity, checking if one's beliefs are true, engaging in social interactions are as important from an evolutionary point of view as ensuring food supplies, reproduction or shelter (Barto et al., 2013; Kaplan and Oudeyer, 2007).

Extrinsic and intrinsic rewards are at the core of motivated behavior, as they determine the choice and intensity of motor plans to achieve them. Importantly, their value depends not only

on the outcome itself, but also on its relevance for the organism: food items have an incentive (motivational) value only when the animal is hungry. This fact highlights the importance of embodiment, i.e. the fundamental link between the body and cognitive, emotional or motivational processes (Price et al., 2012). These processes are not ethereal as suggested by dualist theories of the mind but rather grounded in the body and aimed at ensuring its homeostasis (Cabanac, 1971; Damasio, 1994).

These fundamental properties of animal behavior, especially of human cognitive behavior, are still inaccessible to artificial systems. Current artificial systems mostly respond to specific stimuli by applying predefined or learned rules (stimulus-response associations). They are reactive structures which only seek new and relevant information when instructed to, not when they “want”, “need” or “like” it. There are only a few attempts to implement motivated behavior in such systems, e.g. intrinsic motivation on robotic platforms (Baldassarre et al., 2013; Mirolli et al., 2013), but they are still limited to toy problems. In order to build truly intelligent and autonomous artificial systems, fundamental properties such as intrinsic motivation and transfer of learning must be understood and formalized.

1.3 Reward and the dopaminergic system

Dopaminergic system

Dopamine (DA) is a key neurotransmitter in the brain. It is primarily produced by two small nuclei of the brainstem: the substantia nigra pars compacta (SNc) and the ventral tegmental area (VTA). Dopamine levels are involved in many processes such as the facilitation of approach behavior, incentive learning, motivation, novelty and saliency detection as well as reinforcement learning and action selection (Horvitz, 2000; Ikemoto, 2010; Sesack and Grace, 2010). As shown on Figure 1.1, dopaminergic neurons in SNc and VTA send projections along three different pathways: the nigrostriatal pathway comprises the projections between SNc and the basal ganglia (BG), especially its input structure the striatum. While SNc projects almost entirely to the BG, VTA projects both inside and outside the BG: the mesolimbic pathway reaches subcortical or phylogenetically ancient structures such as the nucleus accumbens (NAcc, also called ventral striatum in primates), the amygdala (a key area for emotional processing), the hippocampus (long-term memory formation and spatial navigation) and the cingulate cortex (error detection, self). VTA also projects diffusely to the cerebral cortex through the mesocortical pathway, reaching primarily the prefrontal cortex (PFC, planning, working memory), but also the motor cortex (movement) and the temporal lobe (visual processing and memory).

Neurons in VTA exhibit a rather low baseline activity (around 5 Hz) and become transiently active in response to various stimuli: novel and salient stimuli (Redgrave and Gurney, 2006), painful stimulations (Matsumoto and Hikosaka, 2009) and reward delivery (Ljungberg et al., 1992). Importantly, Schultz et al. (1997) showed an interesting characteristic of neural firing in VTA during classical appetitive conditioning in the primate. A visual conditioned stimulus

1 Introduction

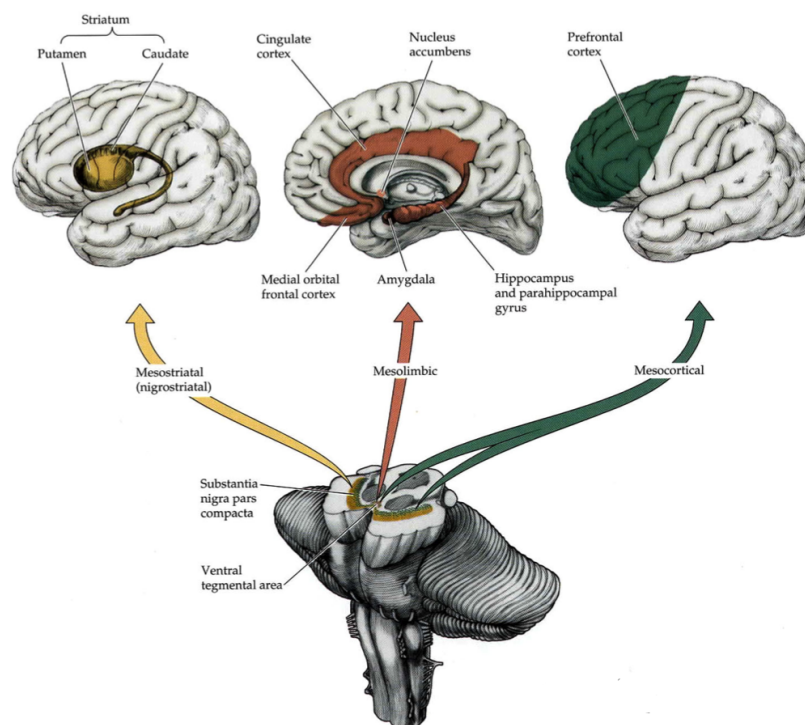


Figure 1.1: Efferent pathways of the dopaminergic system. The nigrostriatal pathway connects SNc to the basal ganglia, especially the striatum. The mesolimbic pathway connects VTA to the nucleus accumbens (or ventral striatum), the amygdala, the hippocampus and the cingulate cortex. The mesocortical pathway connects VTA mainly to the prefrontal cortex, but also the motor cortex and temporal lobe. Adapted from Mancall and Brock (2011).

(CS) is repeatedly paired with a food reward (US). At the beginning of learning, reward delivery generates a burst of activation of the VTA dopaminergic neurons (top of Figure 1.2), but not the appearance of the CS. After a few days of training, the pattern is reversed (middle of Figure 1.2): the appearance of the CS provokes a DA burst, but not reward delivery anymore. Moreover, when the reward delivery is predicted by the CS but omitted (bottom of Figure 1.2), DA cells show a pause in firing (a *dip*) at the time reward is expected.

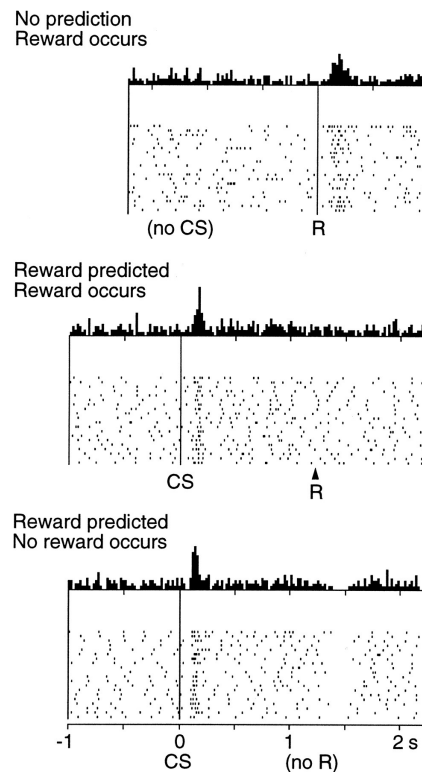


Figure 1.2: Recordings of a single VTA neuron during appetitive conditioning. The raster plots depict the spikes emitted for different trials. The histogram of these spikes is displayed above. Top: reward is delivered unexpectedly. Middle: the CS predicts the delivery of reward. Bottom: the CS predicts a reward, but the reward fails to occur. Adapted from Schultz (1998).

This pattern of activation suggests that VTA cells collectively encode a reward prediction error (RPE), defined as the difference between the reward actually received and the predicted reward. If more reward is received than expected, the RPE is positive, which happens when reward delivery is unexpected (not - yet - predicted) or when a CS appears (the appearance of the CS itself is unpredictable, but it signals that reward will be delivered). If less reward is received than expected, the RPE is negative, corresponding to the dip in VTA activity when reward is omitted. If reward is received as expected, the error is equal to zero. This happens when the CS fully predicts reward delivery.

TD analogy

An analogy between this RPE pattern of VTA cells during conditioning and the *temporal difference* (TD) algorithm of reinforcement learning (Sutton and Barto, 1998) became quickly dominant. In the reinforcement learning framework, each state s of a finite Markovian Decision Process (MDP) is associated with a value function $V^\pi(s)$ which represents the expectation of the sum of rewards that will be obtained after being in the state s and thereafter following a policy π :

$$V^\pi(s) = E_\pi(R_t | s_t = s) = E_\pi\left(\sum_{k=0}^{\infty} \gamma^k r_{t+k+1} | s_t = s\right)$$

γ is a discounting factor allowing to scale the relative importance of immediate rewards (which will be obtained shortly after being in the state s at time t) compared to rewards obtained on the longer term. In the TD algorithm, the value of a state is estimated iteratively after each transition between a state s_t and a state s_{t+1} :

$$V^\pi(s_t) \leftarrow V^\pi(s_t) + \alpha \cdot (r_{t+1} + \gamma \cdot V^\pi(s_{t+1}) - V^\pi(s_t))$$

The TD error signal:

$$\delta_t = R_t - V^\pi(s_t) = (r_{t+1} + \gamma \cdot V^\pi(s_{t+1})) - V^\pi(s_t)$$

is a reward prediction error signal, as it compares the rewards actually received after the state s_t with their prediction $V^\pi(s_t)$. More precisely, the rewards actually received are decomposed into the reward immediately obtained during the transition (r_{t+1}) and an estimation of the rewards that will be obtained after being in s_{t+1} ($V^\pi(s_{t+1})$, discounted by γ). When more reward is obtained than predicted (either because the immediate reward r_{t+1} is high, or because the transition leads to a state with a high value), the RPE signal is positive and increases the value of the state. If less reward is received than expected, the TD error signal is negative and decreases the value of the state.

To account for classical conditioning, states have to represent discrete time events. As by definition no action is required to obtain the rewards, transitions between states occur on a fixed schedule. At the beginning of conditioning, all states are initialized with a value of 0. The first time a reward is delivered, the TD error becomes positive for the preceding state: it was not predicting any reward but one occurred. At the next trial, if the reward arrives at the same time, its value will be slightly higher, so the TD error will be smaller. Meanwhile, the preceding state will see its value increased, because it leads to a state with a positive value. After several conditioning trials, the value of all states preceding reward delivery will be positive. The TD error is zero for the transitions between these states, as they correctly predict reward delivery.

Only the transition to the state corresponding to the appearance of the CS will have a positive TD error signal: the system was in a state where no reward is predicted (the animal is waiting for something to happen) but the transition leads to a state where reward will be delivered after a certain delay. If the reward is not delivered during the usual transition, the TD error becomes negative.

However, over the course of learning multiple trials, the positive TD error signal “travels” back in time, peaking first at reward delivery, then at the preceding state, until it appears at CS onset. In order to fully account for the observations of Schultz et al. (1997), where reward-related activation of VTA cells slowly decreases with learning while the CS-related one increases, but nothing happens in-between, one has to use a modified version of the TD algorithm called TD(λ) (Sutton, 1988). In this variant, when a reward is delivered, not only the value of the preceding state is updated, but also all the preceding states, with a magnitude weighted by the decreasing series λ^{t-k} . Consequently, the state corresponding to CS onset gets also updated the first time reward is delivered. When λ is chosen close enough to 1, the resulting pattern of activation of the TD error signal matches the experimental observations on VTA firing (Schultz, 1998).

Alternative models

This striking analogy was immediately successful and led to many top-down models of the role of DA in both classical and operant conditioning (Daw and Touretzky, 2002; Rao, 2010; Samejima and Doya, 2007; Smith et al., 2006; e.g. Suri and Schultz, 2001). There are however many aspects of DA firing in VTA which are not explained by the TD analogy. When reward is delivered earlier than predicted, VTA cells are activated at reward delivery but stay at baseline at the usual time (Hollerman and Schultz, 1998), contrary to what is predicted by TD. When reward delivery is uncertain, dopaminergic neurons first respond phasically to CS onset and then increase their activity until reward delivery with a slope depending on its probability (Fiorillo et al., 2003). Moreover, DA neurons also respond to novel and salient stimuli which are not predictive of reward (Redgrave and Gurney, 2006).

The main problem is the way time is represented: transitions between states are supposed to occur at a fixed rate, determined by some internal clock. A TD model is only able to learn a single CS-US interval with a constant duration. However, classical conditioning is robust to variability in the CS-US interval (Kirkpatrick and Church, 2000). Many models have been proposed to improve the representation of time in TD models, including serial-compound representations (Suri and Schultz, 2001) and Long Short-Term Memory networks (LSTM, Rivest et al., 2010). More sophisticated neuro-computational models separate the mechanisms responsible for CS-related and US-related activations (Dranias et al., 2008; O’Reilly and Frank, 2006; Vitay and Hamker, 2014). Based on the neuroanatomy of the afferents to the dopaminergic system, they distinguish the sources of excitation and inhibition signaling reward delivery to VTA from the ones signaling predictors of rewards. In Chapter 5, we will discuss these models and explain their importance for motivated behavior.

1 Introduction

Despite these limitations, it is clear that DA firing in VTA represents a RPE that can be used to reinforce actions or plans in other structures such as the BG or the prefrontal cortex. However, if the amount of evidence for the role of positive RPEs is undebatable, it is still unclear what is the effect of negative RPEs, for example when a predicted reward is omitted. VTA cells fire at a rather low baseline activity (5 Hz) and the mechanisms by which a pause in firing can influence plasticity in efferent systems are still a matter of debate (see Shen et al., 2008 for an explanation on its role in the striatum). Moreover, the observed dip in VTA activity when reward is omitted has not been reproduced by other researchers (Joshua et al., 2009). Many efforts remain to be done to fully understand how VTA and SNc signal reward-prediction errors to the BG and prefrontal cortex. VTA is for example known to send also inhibitory projections to the ventral striatum (Brown et al., 2012), what opens new questions on the exact role of VTA in reward processing (Creed et al., 2014).

1.4 Basal ganglia and reinforcement learning

Anatomy

The basal ganglia are a set of nuclei in the basal forebrain (Figure 1.3). They receive inputs from the entirety of the cerebral cortex (although the frontal lobe is dominant) and project to various sub-cortical nuclei such as the brainstem or the thalamus, where the processed information can go back to the cerebral cortex. They are involved in a variety of functions, among which the control of voluntary movements, action selection, sequence learning, habit formation, updating of working memory (WM), motivation and emotion. Their importance for behavior is emphasized by their involvement in many neurological diseases, including Parkinson's disease, Huntington's disease, Tourette syndrome, obsessive-compulsive disorders, addiction and schizophrenia.

The *striatum* (STR) is the main input structure of the BG. In the primate, it is composed of the dorsal striatum (caudate nucleus - CN - and putamen - PUT) and the ventral striatum (nucleus accumbens - NAcc - and olfactory tubercle). It receives massive inputs from the whole cerebral cortex, with the ventral striatum also receiving inputs from sub-cortical structures such as the hippocampus or the amygdala (Humphries and Prescott, 2010). It is principally composed of *medium spiny neurons* (MSNs) which are able to integrate cortical inputs from different areas and project inhibitorily inside the BG on the *globus pallidus* (GP). Two types of MSNs are found in the striatum depending on the dopamine receptors they exhibit: D1-mediated and D2-mediated MSNs. They contribute to different pathways within the BG depending on the part of the GP they project on: its internal part (GPi) for D1 MSNs, the external one (GPe) for D2 MSNs. The second input structure of the BG is the *subthalamic nucleus* (STN). Although much smaller, it also receives massive cortical inputs and projects excitatorily on the GP.

The output structures of the BG are GPi and the *substantia nigra pars reticulata* (SNr). As they are functionally similar, they are often labeled together as GPi/SNr, although they are not

anatomically close. Neurons in GPi/SNr are tonically active, meaning that they have an elevated firing rate baseline (between 60 and 80 Hz). At rest, they exert a strong inhibition on target structures of the BG, including the thalamus. GPi/SNr must be themselves inhibited in order to release this inhibition and allow the target structures to get activated, a phenomenon called *disinhibition* (Chevalier and Deniau, 1990). As a whole, the BG act as a gating regulator of activity in target structures.

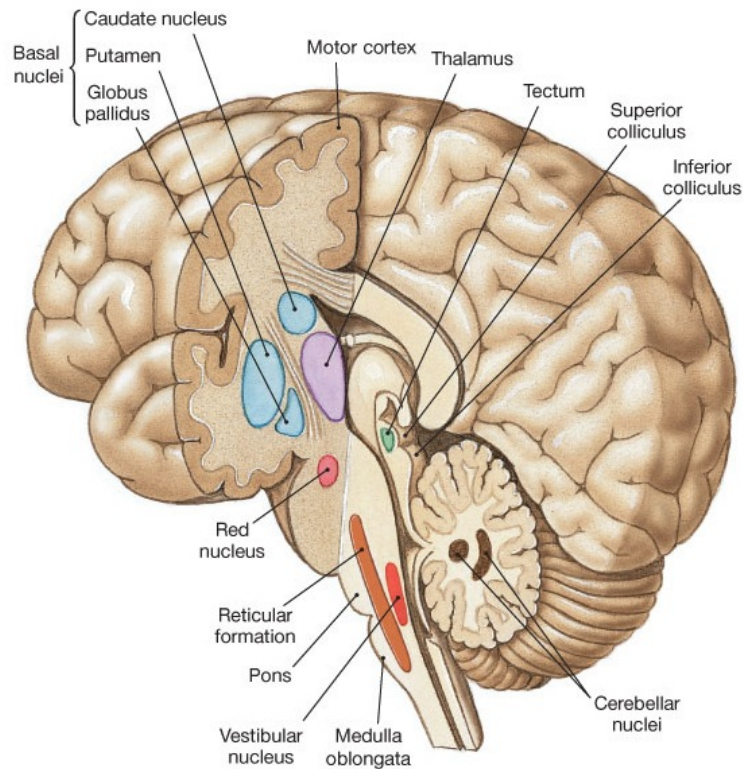


Figure 1.3: Anatomical position of the basal ganglia in the brain. The BG are composed by the striatum (caudate nucleus and putamen), the globus pallidus (internal and external), the substantia nigra (pars reticulata and pars compacta) and the subthalamic nucleus. It receives mainly inputs from the cerebral cortex and projects either directly to the brainstem (red nucleus, superior colliculus) or back to the cortex through the thalamus.

Pathways

The internal connectivity of the BG shows a complex organization (Figure 1.4). Three principal pathways can nevertheless be identified. The *direct* pathway goes directly from D1-mediated MSNs to GPi/SNr. It is the main source of disinhibition for the output of the BG. The *indirect* pathway originates in the D2-mediated MSNs and relays in GPe before targeting GPi/SNr either directly or through STN. The additional inhibitory relay on GPe makes this pathway globally excitatory on GPi/SNr: the activation of D2-mediated MSNs increases firing rates in GPi/SNr, what further prevents target structures to get activated. The opposing effects of the direct and indirect pathways led to the first models of motor processing in the BG (Albin et al., 1989; DeLong, 1990). The balance between their opposing effects (“Go” for the direct pathway, “No Go”

1 Introduction

for the indirect one) allows to control the initiation, vigor and termination of motor movements. Pathological imbalance between the pathways can explain neurological diseases: dopamine loss, characteristic of Parkinson's disease (PD), weakens the direct pathway, as DA has an excitatory effect on D1-mediated MSNs and inhibitory on D2-mediated ones (Gerfen et al., 1990; Surmeier et al., 2007). The resulting increased inhibition on motor centers causes hypokinesia, the inability to initiate movements. On the contrary, excess of dopamine, as in Huntington's disease (Chen et al., 2013) or Tourette syndrome (Albin and Mink, 2006), over-activates the direct pathway and leads to hyperkinetic symptoms, such as involuntary movements and tics.

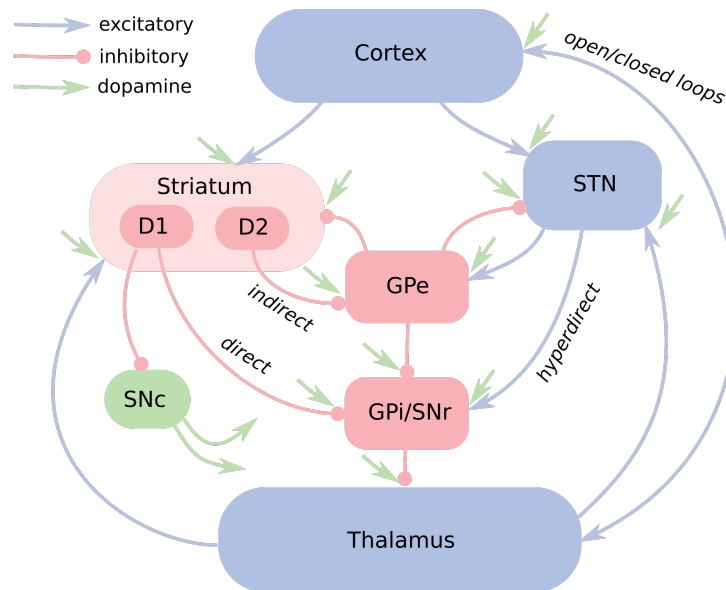


Figure 1.4: Schematic organization of the BG. The BG takes inputs from the cerebral cortex and tonically inhibits the thalamus, modulating closed or open loops between the cortex and the thalamus. The *direct* pathway starts from D1-mediated MSNs of the striatum and ends directly in the output structures GPi/SNr. The *indirect* pathway starts from D2-mediated MSNs, relays in GPe and reaches GPi/SNr either directly or through STN. The *hyperdirect* pathway starts from STN and reaches GPi/SNr either directly or through GPe. Dopaminergic cells in SNc have inputs from the striatum and modulate virtually all projections within the BG.

The *hyperdirect* pathway connects directly STN to GPi/SNr through excitatory synapses, with a much lower latency than the other pathways (Nambu et al., 2002). It allows to send rapidly cortical information to the output nuclei of the BG, bypassing computations in the direct and indirect pathways. Because of its excitatory effect on GPi/SNr and the diffuse projection of SNr on GPi/SNr (a neuron in STN excites many neurons in GPi/SNr), it carries a “Global No Go” signal allowing to suppress involuntary movements or to terminate them prematurely. According to Nambu et al. (2002), the three pathways may cooperate during action selection following a center-surround model: when a voluntary movement is initiated by cortical areas, the hyperdirect pathway first inhibits large areas of the thalamus and cerebral cortex that are related to both the selected movement and its competitors. For example, before moving the arm to the left, any arm movement previously prepared will be wiped out by the increased excitation in GPi/SNr. Some milliseconds later, the direct pathway selects the appropriate motor program

while the indirect pathway selectively inhibits competing movements.

These three pathways form a classical feedforward view of the BG which has been used in many models (Gurney et al., 2001a; O'Reilly and Frank, 2006; Schroll et al., 2012). As depicted in Figure 1.4, there exists many other projections inside the BG which render the understanding of processing within the BG much more complex. The thalamostriatal pathway, formed by projections from the thalamus to the striatum, may for example be involved in attentional processes and help the BG solve the credit-assignment problem (Galvan and Smith, 2011). The reciprocal connections between STN and GPe lead to oscillations under certain circumstances, what could form the basis of an internal pacemaker inside the BG (Plenz and Kital, 1999), but can also become pathological in Parkinson's disease and explain symptoms such as tremor (Levy et al., 2002). Much remains to be done to fully understand the role of the STN-GPe loop (Kumar et al., 2011). The role of the pallidostriatal projection between GPe and the striatum is also still mainly unexplored (Bahuguna et al., 2015; Kita et al., 1999).

Dopamine-mediated plasticity

The striking feature of the BG is their dependency on dopamine, either as a modulator of activity - elevated DA levels increase the excitability of D1-mediated MSNs and decrease the one of D2 cells (Nicola et al., 2000) - or of plasticity - different DA levels can induce selectively *long-term potentiation* (LTP) or *long-term depression* (LTD) at corticostriatal synapses (Calabresi et al., 2007). All nuclei of the dorsal BG receive dopaminergic input from SNc, while the ventral part receives mainly inputs from VTA. Reciprocally, the striatum is a major source of inhibition to the dopaminergic areas, allowing the BG to control their own dopaminergic input (Haber et al., 2000).

Dopamine-mediated plasticity is particularly studied in the striatum. MSNs exhibit particular dynamics: their membrane potential can be either in a hyperpolarized *down-state* or in a depolarized *up-state*. In the down-state, the excitability of the cell is very low and striatal neurons do not emit spikes. In the up-state, the cell is very excitable and responds to its cortical inputs. The transition between these two states can be spontaneous (it occurs at a rate of 0.5 to 2 Hz, Leung and Yim, 1993), induced by a phasic DA burst in VTA/SNc (Gruber et al., 2003) or by a massive cortical input (McGinty and Grace, 2009). For D1-mediated MSNs, LTP is known to occur at corticostriatal synapses in the presence of a strong cortical input and under elevated DA levels when the cell is in the up-state. LTD happens on the contrary when there are weak cortical inputs, low DA levels and the cell is in the down-state (Calabresi et al., 2007; Reynolds and Wickens, 2000). Put together, plasticity at corticostriatal synapses seems to be driven by a three-term DA-modulated Hebbian learning rule, where the change in synaptic efficiency is ruled by the product of the pre-synaptic activity (r^{pre} , presence of cortical inputs), the post-synaptic activity (r^{post} , up- or down-state) and the deviation of the dopamine level from its baseline δ :

$$\Delta w = \delta \cdot r^{\text{pre}} \cdot r^{\text{post}}$$

1 Introduction

The opposite pattern is found for D2-mediated MSNs: high DA levels induce LTD while low levels induce LTP (Shen et al., 2008). With this model of corticostriatal plasticity, DA becomes able to selectively reinforce corticostriatal associations. If a motor plan selected by the direct pathway led to reward, DA will strengthen the corticostriatal synapses to D1-mediated MSNs that were previously activated and reduce the ones to D2-mediated MSNs. This increases the probability that the same motor plan will be selected again in the future by favoring the direct pathway in its competition with the indirect one. Oppositely, if the action leads to less reward than expected, the D1-mediated synapses will be reduced and the D2-mediated ones increased, what strengthens the indirect pathway and prevents further selection of that motor plan.

This mechanism of dopamine-based reinforcement in the BG further emphasized the analogy with reinforcement learning, especially the *actor-critic* architecture (Sutton and Barto, 1998). In this framework, the critic produces the TD error signal which is used both to update the value of a state and to reinforce the state-action association that led to reward. Using this error signal, the actor simply learns to map a state onto the optimal action. In this view, the critic would be composed by the dopaminergic system and the ventral BG, while the actor represents a loop between the cerebral cortex and the dorsal BG. Many neuro-computational models of the BG are based on this architecture (Berns and Sejnowski, 1998; Gurney et al., 2001a; Houk et al., 1995; Joel et al., 2002).

Many criticisms have been formulated to this model. First, DA cells do not only signal RPEs but also respond to aversive, salient and novel stimuli, which does not fit into the reward-prediction error hypothesis (Pennartz, 1995). They also respond to reward-predicting stimuli with a very short latency, raising the issue of how their reward-predicting value can be predicted in such a short time (Redgrave et al., 1999). DA is even not required for acquiring the value of a stimulus (“liking”), only for its motivational effect (“wanting”), so the role of the critic might be misunderstood (Berridge, 2007). Another issue with the actor-critic assumption is the temporal credit-assignment problem: rewards are usually delivered well after the causal action is executed. How can this delayed feedback influence motor representations which have long faded away?

More detailed neuro-computational models have been introduced to overcome these issues. The PBWM (prefrontal cortex, basal ganglia working memory) model of O’Reilly and Frank (2006) makes a strong use of *working memory* (WM) processes to bridge the temporal gap between an action and its consequences. It furthermore provides a mechanism by which the content of WM is gated and updated by functional loops between the PFC and the BG. A similar approach was taken in Vitay and Hamker (2010), which will be presented in Chapter 3. This model was the first to consider the importance of plasticity within the BG (specifically in the projections from the striatum to the globus pallidus) in addition to corticostriatal plasticity.

Generally, the role of the BG in motor learning and action selection is partially understood, but its contribution to other forms of learning has been less extensively studied. An interesting view considers the BG as a fast learning device quickly acquiring rewarded associations and transferring them to the cerebral cortex where they will be generalized and stored in long-term

memory (Ashby et al., 2005). This hypothesis is backed up by the well-accepted role of the BG in habit formation (Seger and Spiering, 2011). Even more generally, one can consider the BG as a trainer for the cerebral cortex. Learning in the cerebral cortex can be characterized as unsupervised, in the sense that cortical neurons self-organize to represent internal and external events in the most efficient way. Cortical areas communicate with and adapt to each other, but there is no obvious objective function guiding the learning process (supervised learning minimizes an error function, which is unavailable at the cortical level), while reinforcement learning has to be ruled out because of the slow temporal dynamics of dopamine in the cortex (the bursts and dips of the DA signal are too smoothed out in the cortex to carry the RPE, Seamans and Yang, 2004). The role of BG would be to transfer specific knowledge acquired by reinforcement learning to the more general unsupervised cortical system. In the view of Stocco et al. (2010), the BG may also act as a conditional information-routing system, enabling transmission between remote cortical areas and allowing the learning of new associations.

1.5 Multiple loops and organization of behavior

It was mentioned that the striatum receives projections from the entirety of the cerebral cortex. However, the organization of these projections follows a specific topology on the surface of the striatum. As depicted in Figure 1.5, different cortical regions project onto different parts of the striatum: the motor and premotor (PMC) cortices project mainly onto the putamen, the dorso-lateral prefrontal cortex (dlPFC) projects mainly on the caudate nucleus, while the orbitofrontal (OFC) and ventromedial prefrontal (vmPFC) cortices project mainly on the nucleus accumbens. As this segregation is preserved throughout the BG, from the projections of the striatum on the GP to the thalamic nuclei relaying the output of the BG back to the cortex, the prefrontal cortex / basal ganglia system is said to be organized in parallel segregated loops (Alexander et al., 1986).

Each loop is therefore specialized in a particular functional domain: the motor loop is involved in motor learning and action selection, the associative loop in cognitive processes such as sequence learning and WM updating, the limbic loop in motivation and goal-directed learning. These subdivisions can be further refined: the motor loop is in fact composed of multiple segregated loops depending on the cortical region of origin (M1, SMA, pre-SMA...). Other loops have been identified, such as the oculomotor loop, devoted to the control of eye movements, or the visual loop, linking the inferotemporal and medial temporal cortices to the tail of the caudate nucleus. The importance of the visual loop will be explained in Chapter 2 and Chapter 3. A similar topological segregation can further be extended to the projections within a functional loop: the topology of the cortical area (e.g. the somatotopic representation of body parts in the motor cortex) is preserved inside the BG (Nambu, 2011). In this view, the PFC/BG system is composed by thousands of small parallel loops (O'Reilly and Frank, 2006).

The segregation is however not total: a certain degree of overlap is observed in the corticostri-

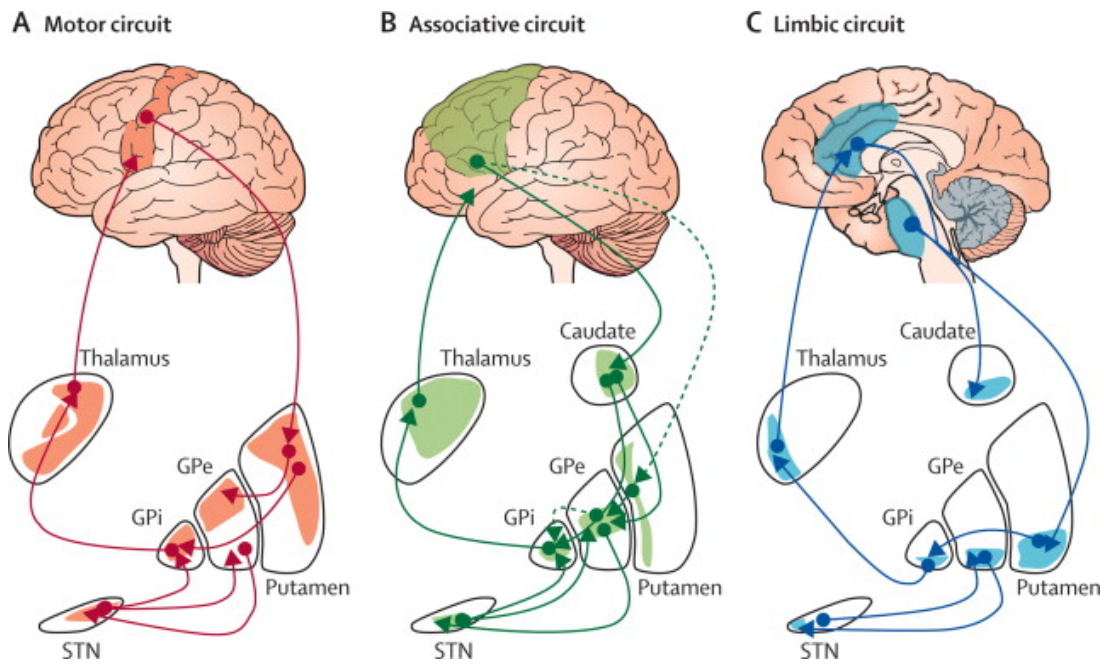


Figure 1.5: Parallel segregated loops between the cerebral cortex and the BG. The motor loop starts from the motor and premotor cortices and involves mainly the putamen. The associative (or cognitive) loop involves the dorsolateral cortex and the caudate nucleus. The limbic loop involves the orbitofrontal and ventromedial cortices to the ventral striatum (nucleus accumbens). Adapted from Rodriguez-Oroz et al. (2009).

atal projections, allowing for example parts of the striatum to integrate both motor and associative information. The funneling structure of the BG - there are 100 times more neurons in the striatum than in GPi/SNr - also increases the probability that the loops communicate with each other inside the BG (Bar-Gad et al., 2003). Finally, the thalamic nuclei relaying the output of the BG back to the cortex do not target only the original cortical area, but reach also adjacent ones. In the PFC / BG system, one distinguishes *closed loops*, where a single cortical area projects to the striatum and receives the processed information back, from *open loops*, where a cortical area sends information to the BG and the result is “forwarded” to another cortical area (Ebner et al., 2015). Category learning in the visual loop between the inferotemporal cortex and the BG is for example transferred to the motor cortex through an open loop (Seger, 2008). The exact organization of the PFC / BG system into closed and open loops is still not precisely known, but this is an important mechanism by which the BG can modulate information transmission in the prefrontal cortex (Stocco et al., 2010).

The question that arises is how these multiple loops could learn useful associations in their respective domains based on a single unitary reward-prediction error signal, as hypothesized by the TD analogy. SNc and VTA actually display a complex topological organization depending on their reciprocal connections with the striatum (striato-nigro-striatal system, Haber et al., 2000). As depicted in Figure 1.6, each region of the striatum engaged in a closed loop with the cerebral cortex forms reciprocal connections with a specific region of the SNc/VTA dopaminergic areas: the striatum sends inhibitory connections to SNc/VTA, which returns a dopaminergic signal. However, each striatal region also projects on the adjacent dopaminergic region along a rostro-

caudal axis, i.e. from limbic to associative to motor domains. This pattern on connectivity forms a spiraling structure which allows different striatal regions to influence others by modulating their dopaminergic inputs.

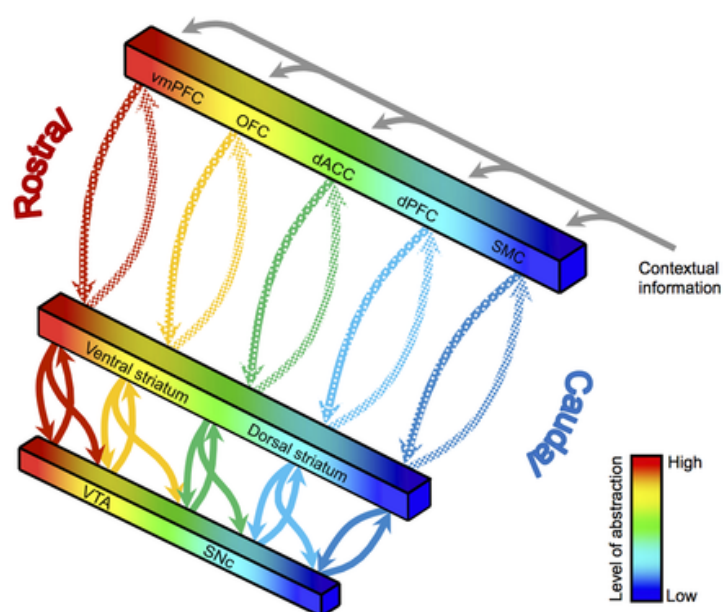


Figure 1.6: Spiraling connectivity pattern in the striato-nigro-striatal system. Different cortical areas (here, vmPFC, OFC, dACC - the dorsal anterior cingulate cortex -, dPFC and SMC - the supplementary motor area) form closed loops with different parts of the striatum (ventral for vmPFC and OFC, dorsal for the others) following a rostro-caudal axis. Each part of the striatum projects on specific regions of the SNc/VTA system, which reciprocate the connections. However, they also project on adjacent dopaminergic regions in the caudal direction, forming a spiraling structure allowing the different closed loops to communicate through dopaminergic activity. Adapted from Keramati and Gutkin (2013).

The resulting organization of PFC-BG loops along a limbic-associative-motor gradient has fundamental consequences on goal-directed behavior. Limbic regions, critical for motivational and affective processes, are in a position to influence how cognitive plans are formed and learned by associative regions, which themselves control how individual movements and actions are executed in motor regions. This highlights the tight integration between cognitive and emotional processes: goals are mainly represented in OFC, which is strongly connected with the limbic system (amygdala, ventral BG) and influences cognitive processes in dPFC. Based on neuro-anatomical evidence, the classical view opposing cognition and emotion as competitors to produce behavior has to be replaced by an emphasis on the cooperation between the two systems.

This gradient also has consequences on learning: striatal regions associated to goal-directed learning influence plasticity in striatal regions associated to habit formation (Khamassi and Humphries, 2012; Yin et al., 2004). This provides a mechanism by which flexible behaviors acquired through goal-directed learning can be transferred into procedural memory to become habits. Similarly, Pavlovian-to-Instrumental transfer (PIT) is the ability to transfer stimulus values acquired through Pavlovian conditioning to instrumental behavior: after a first phase of

1 Introduction

operant conditioning where a rat learns to press levers to obtain different outcomes (say, food and water), a classical conditioning phase is introduced, pairing initially neutral stimuli (tone or light) to the same outcomes. The effect of PIT is that, when back in the operant conditioning room, the conditioned stimuli will now trigger the lever press leading to the same outcome (Corbit and Balleine, 2011). The mechanisms allowing a transfer of learning between classical and instrumental conditioning happen in the cooperation between two loops within the ventral BG, involving two parts of the nucleus accumbens, the core and the shell (Gruber and McDonald, 2012).

Although the concept of multiple parallel PFC/BG loops has been often used in neuro-computational models (N'guyen et al., 2014; e.g. Nakahara et al., 2001; O'Reilly and Frank, 2006), only a few have used the underlying limbic-associative-motor gradient in dopaminergic connectivity to investigate the organization of behavior. Keramati and Gutkin (2013) for example studied this system to explain the mechanisms of addiction. In Schroll et al. (2012) (Chapter 4), we proposed a neuro-computational model of working memory formation and maintenance involving three PFC/BG loops, two associative and one motor, which coordinate their learning through the spiraling striato-nigro-striatal system. The dopaminergic system has a central role in organizing behavior and learning; very simplified models such as TD actually limit our ability to understand the underlying processes.

1.6 Structure of the thesis and contribution

This thesis is composed of five articles published in international peer-reviewed journals. They were selected to be representative of the different aspects of my research on the role of dopamine in motivated behavior. In Vitay and Hamker (2008) (Chapter 2), we studied the influence of dopamine on memory retrieval in the perirhinal cortex, a part of the temporal lobe involved in object recognition and visual memory. In Vitay and Hamker (2010) (Chapter 3), we designed a neuro-computational mode of the BG which is able to solve delayed rewarded visual memory tasks. This fundamental model was the first to introduce plasticity within the BG and was further extended in collaboration with Dr. Henning Schroll to account for working memory formation Chapter 3. In Vitay and Hamker (2014) (Chapter 5), we designed a detailed model of the dopaminergic system during conditioning, with a strong emphasis on its dependency on timing processes. Additionally, in Vitay et al. (2015) (Chapter 6), we present a neural simulator that was developed in parallel and which allows to define these neuro-computational models easily and simulate them efficiently on parallel hardware. A detailed description of the content of these articles is provided in the following sections.

List of publications included in the thesis

1. Vitay, J. and Hamker, F. H. (2008). Sustained activities and retrieval in a computational model of the perirhinal cortex. *Journal of Cognitive Neuroscience*, 20, 11, 1993-2005, doi: [10.1162/jocn.2008.20147](https://doi.org/10.1162/jocn.2008.20147)
2. Vitay, J. and Hamker, F. H. (2010). A computational model of basal ganglia and its role in memory retrieval in rewarded visual memory tasks. *Frontiers in Computational Neuroscience*, 4, doi: [10.3389/fncom.2010.00013](https://doi.org/10.3389/fncom.2010.00013)
3. Schroll, H., Vitay, J., and Hamker, F. H. (2012). Working memory and response selection: a computational account of interactions among cortico-basalganglio-thalamic loops. *Neural Networks*, 26, 59–74, doi: [10.1016/j.neunet.2011.10.008](https://doi.org/10.1016/j.neunet.2011.10.008)
4. Vitay, J. and Hamker, F. H. (2014). Timing and expectation of reward: a neuro-computational model of the afferents to the ventral tegmental area. *Frontiers in Neurorobotics*, 8, 4, doi: [10.3389/fnbot.2014.00004](https://doi.org/10.3389/fnbot.2014.00004)
5. Vitay, J., Dinkelbach, H. Ü., and Hamker, F. H. (2015). ANNarchy: a code generation approach to neural simulations on parallel hardware. *Frontiers in Neuroinformatics*, 9, 19, doi:[10.3389/fninf.2015.00019](https://doi.org/10.3389/fninf.2015.00019)

Contribution to each article

I am the primary author of articles 1, 2 and 4, having conducted the research, implemented the models, performed the experiments, analyzed the results and primarily written the manuscripts. Prof. Hamker supervised the research, guided the whole process and participated in the writing. For article 3, Dr. Henning Schroll is the primary author. He implemented the model, ran the experiments, analyzed the results and primarily wrote the article. I co-supervised the development of the model together with Prof. Hamker and participated in the writing. For article 5, Helge Ülo Dinkelbach was involved in developing the neural simulator and running the experiments, co-supervised by Prof. Hamker and me. I developed equally the neural simulator and wrote primarily the manuscript.

1.6.1 Chapter 2 : Perirhinal cortex and dopamine

Working memory is the ability to temporarily store and manage information in order to use it for cognitive processes (Baddeley, 1986). A typical example is remembering a phone number before typing it: the number is stored in short-term memory as long as it is needed for the action, but the memory fades away when it is not required anymore. The neural correlate of WM processes is *sustained activation*: neurons which are activated by the presence of the information stay active during the whole period between its disappearance and its later use by cognitive processes. Sustained activation has been found in many brain areas, including the

1 Introduction

prefrontal cortex (Funahashi et al., 1989), the parietal cortex (Koch and Fuster, 1989), the inferotemporal cortex (Ranganath et al., 2004) and the medial temporal lobe (Naya et al., 2003). The medial temporal lobe (MTL) has an important role in interfacing high-level visual information represented in the inferotemporal cortex (IT) with long-term mnemonic information encoded in the hippocampal formation. It is composed of the perirhinal (PRh), entorhinal (ERh) and parahippocampal (PHC) cortices.

PRh is in particular involved in visual object categorization (Murray and Richmond, 2001), multimodal integration (Taylor et al., 2006), long-term memory encoding (Buffalo et al., 2000) and retrieval (Brown and Xiang, 1998). In visual object categorization, PRh develops view-independent representation of objects: objects are in general seen from particular angles or are only partially visible. PRh learns to integrate over time these different views and bind them together in a unitary representation. In the model of PRh we developed (Vitay and Hamker, 2008), PRh is represented by two populations of excitatory and inhibitory neurons, respectively, with biologically plausible proportions and connectivity. Different objects are presented to the model through connections from a model of IT to the excitatory neurons. Each object is composed of different parts, which are randomly selected at each presentation: for example the first presentation of a chair would contain its right side and three feet, the second would be its back and only two feet, and so on. Through plasticity in the lateral connections between the excitatory neurons, we observe the formation of connected clusters of neurons which represent the object as whole: individual neurons of the cluster receive visual input from only one part of the object, but they have become connected to neurons representing all the other parts of the object.

Sustained activation has been observed in PRh during delayed matching-to-sample (DMS) tasks, where a visual object (the sample) is shortly presented and removed for a variable duration called the delay period. The same or a different object (the match) is then presented and the subject has to respond if the new object matches the sample. PRh neurons representing the sample object stay active during the delay period (Nakamura and Kubota, 1995). The model reproduces this effect by incorporating the effect of DA on synaptic transmission in the cortex, extrapolated from its known influence in the prefrontal cortex (Durstewitz et al., 2000; Seamans and Yang, 2004). We observed that PRh neurons show sustained activation under intermediate levels of DA, but not low or high doses, a phenomenon known as *inverted-U curve* in the prefrontal cortex (Vijayraghavan et al., 2007). Moreover, intermediate levels of DA favor the propagation of activity within a cluster: while at low DA levels only the neurons receiving visual information get activated, the whole cluster gets activated at intermediate levels because of the enhanced lateral connections within the cluster. Instead of representing a partial view of the object, PRh represents all possible views at the same time, leading to a complete representation of the object. This provides a mechanism by which DA modulates processing in PRh and allows memory retrieval.

The mechanisms used in this model are a very important step for visual processing as they allow view-invariant representations of an object to be formed and retrieved by cognitive pro-

cesses. Under optimal DA levels, object representations can be completed and help categorization. Furthermore, the visual template representing an object in PRh can be activated by cognitive processes (either through direct projections from the PFC or through the thalamus) and used to guide visual search. The visual system is principally organized in two separate pathways: the ventral pathway, originating in the primary visual cortex (V1) and ending in the inferotemporal lobe, is specialized in object recognition; the dorsal pathway, originating in V1 and ending in the parietal cortex, focuses on the localization of visual objects and their manipulation (Ungerleider and Mishkin, 1982). Activating a template in PRh biases IT toward the characteristic features of this object, which itself biases representations in the ventral pathway through feedback projections. Once the corresponding features are enhanced in V1, the dorsal pathway can then locate the object and direct an action toward it (Hamker, 2004a; Hamker, 2005b). Understanding how visual templates are formed and retrieved is a first step toward understanding the cognitive control of vision.

Insights on the role of DA

Tonic levels of DA control the processing properties of PRh by switching from a representational mode - only the perceived information is represented - to a mnemonic one - visual templates are completed or retrieved.

1.6.2 Chapter 3 : Basal ganglia and memory retrieval

Maintaining visual templates in PRh is a critical component of delayed rewarded tasks such as delayed match-to-sample (DMS, reward is delivered if a response is made when the target matches the sample), delayed non-match-to-sample (DNMS, the response is rewarded only if the target does not match the sample) or delayed pair-association (DPA, similar to DMS but there is an arbitrary association between the sample and the rewarded target - e.g. respond for an apple when the sample is a car). The visual loop of the BG, linking high-level visual cortical areas such as IT and PRh with the body and tail of the caudate nucleus, is involved in selectively activating visual templates during the delay period of such tasks in order to prepare the correct response (Levy et al., 1997). The major difficulty of these three tasks is that the visual template to be activated can be different from the presented sample, so the target has to be retrieved from memory.

In Vitay and Hamker (2010), we developed a neuro-computational model of the visual loop of the BG. It is composed of a closed loop between PRh, the caudate nucleus, SNr and the ventro-anterior thalamus, and an open loop with a projection from the dlPFC to the caudate nucleus. Contrary to the generic scheme described on Figure 1.4, we only modeled the direct pathway of this loop. In the experimental setup, a sample is first presented and stored in dlPFC. After a delay of 150 ms, a cue indicated which task to perform (DMS, DNMS or DPA) is presented and stored in dlPFC. Finally, after another delay, two stimuli are presented: the target

1 Introduction

(which matches the sample depending on the task) and a distractor. After a delay, we measure the maximal activity in PRh and deliver reward to SNc if the target has a higher activity. The dopaminergic signal in SNc in response to the reward modulates learning at corticostriatal synapses (both from PRh and dIPFC) according to the three-term DA-modulated Hebbian learning rule presented in this chapter. This is in line with many models of the BG (e.g. Brown et al., 1999; O'Reilly and Frank, 2006). The novelty of this model is that DA also modulates plasticity within the BG, in the connections from the striatum to SNr as well as in the lateral connections of SNr.

This internal plasticity, confirmed by experimental evidence (Rueda-Orozco et al., 2009), releases the constraints on the striatum. In other models, each striatal region converges on a small number of GPi/SNr cells, allowing to disinhibit a single action. The corticostriatal projections must therefore solve two different problems: integrating different cortical representations (here, the sample and the task cue) and map them on the correct action. If plasticity in the projection between the striatum and GPi/SNr is added, corticostriatal projections only need to map cortical associations on the striatum (a form of self-organization), while the striatopallidal ones learn to map these representations onto the correct action. Additionally, plasticity within SNr ensures selectiveness in the output of the BG.

The resulting model is able to learn through reinforcement learning the three tasks using a limited number of objects. It provides a novel mechanism by which cognitive processes in the PFC can learn to influence visual processing by retrieving visual templates. Two limitations of this model should be outlined: first, it only considers the direct pathway of the BG, neglecting the indirect and hyperdirect ones; second, the mechanisms to encode the sample and the task cue in working memory in dIPFC are hard-coded and not learned. The first limitation was since overcome by an extension of this model including the indirect and hyperdirect pathways, with a strong emphasis on the dopamine-modulated plasticity in these pathways. This extended model was successfully used to explain cognitive deficits in various BG-related diseases, such as Parkinson's disease (Schroll et al., 2014) and Huntington's disease (Schroll et al., 2015). Flexible WM mechanisms to learn to maintain relevant information in dIPFC are presented in the next section (Schroll et al., 2012).

Insights on the role of DA

Dopamine regulates plasticity in the projections to the BG, but also between the different nuclei of the BG. Its phasic component carries a reward-prediction error that reinforces successful stimulus-response associations. DA-mediated plasticity occurs only in the acquisition phase, when the success of a response is not predicted yet. When a striatal representation is associated with reward delivery, it cancels dopaminergic activation and suppresses learning.

1.6.3 Chapter 4 : WM and multiple basal ganglia loops

Updating and maintaining information in WM is a complex cognitive process involving mainly the dlPFC and the BG (Frank et al., 2001), although many other cortical areas play a significant role (Ashby et al., 2005; Jonides et al., 1998). Many neuro-computational models consider that the BG is involved only in WM updating, i.e. the conditional entry of stimuli into it (Helie et al., 2013; Uttal, 2015). One of the most prominent models of WM (O'Reilly and Frank, 2006) for example considers the BG as a gating mechanism allowing, based on reinforcement learning, sensory information to enter recurrent loops within the PFC. It has among others been applied to the complex 1-2-AX task, which can be described as followed: a sequence of letters (A, B, X, Y) and digits (1, 2) is displayed on a screen. The subjects have to respond with the left button if they see an A followed by an X, but only if the last digit they saw was a 1. If that last digit was a 2, they have to press left when they see a B followed by a Y. In all other cases, they have to press right.

The 1-2-AX task is very complex, even for humans. It involves maintaining two levels of information in WM: what was the last digit I saw (outer loop) and have I just seen an A or a B (inner loop)? If these two pieces of information are kept in WM, deciding whether to press left or right when an X or Y appears becomes as trivial as a stimulus-response association. The difficulty is to know how a system can learn to maintain the outer and inner loops based solely on reinforcement learning, i.e. without explicit knowledge of the task. O'Reilly and Frank (2006) solve the problem by implementing three parallel PFC/BG loops, one learning to maintain 1 and 2, another A and B and the last one X or Y. The structural credit assignment problem - if the response is incorrect, which of these three loops has failed? - is solved by allowing each loop to modulate its own dopaminergic reward signal, but these loops are mostly independent of each other. Moreover the BG are only used to update WM content, not actually maintain it, contrary to experimental evidence (Landau et al., 2009).

In Schroll et al. (2012), we proposed a neuro-computational model of WM updating and maintenance involving three PFC-BG loops: two associative loops and a motor one. The role of the motor loop is to decide which motor response (left or right) should be executed based on short-term mnemonic information maintained in the associative loops during a 1-2-AX task. The role of the two associative loops is to learn to maintain the outer (1 and 2) and inner (A and B) loops, respectively. Based on an idea by Krueger and Dayan (2009), we posit that shaping plays an important role in organizing the different loops: animals usually don't address complex cognitive tasks directly, but incrementally generate more and more complex behavior by reusing abilities that were previously acquired. In the case of the 1-2-AX task, this would correspond to responding first to a 1 or 2, then to 1 followed by A or 2 followed by B, and finally by the 1-2-AX task itself. Once a subtask is mastered, errors in performance can be interpreted as a change in task complexity, signaling that more cognitive resources should be allocated to solve the problem.

In the first shaping phase (only digits are presented), the motor PFC/BG loop learns to respond

1 Introduction

appropriately using the same mechanisms as in Vitay and Hamker (2010). When the second phase is introduced (A-X or B-Y), the motor loop can not solve the problem because it has no memory of the last digit seen. One of the two associative loops then starts learning to maintain this information through a closed loop. The sustained activation of a digit then biases the motor loop to respond correctly to a 1-A or 2-B association. Finally, when the full 1-2-AX task is introduced, the associative and motor loops fail again, as only the outer loop is maintained. The associative loop sends a “distress” signal, telling the other associative loop to help solve the task. The new loop then learns to maintain A and B, providing enough information to the motor loop to execute the correct motor response.

Associative PFC/BG loops learn from errors as long as they are not confident in their output. When they become confident but the whole behavior fails, they ask for more cognitive resources to be allocated to the task instead of simply unlearning what they were previously correctly doing. Communication between the loops and the subsequent recruitment of cognitive resources is based on the spiraling striato-nigro-striatal connectivity (Haber et al., 2000): each loop has its own dopaminergic signal, which can be activated by loops higher in the hierarchy. When the first associative loop fails to solve the task although it was previously performing well, it signals the second loop through its dopaminergic system that it should get engaged in order to improve the organism’s ability to acquire rewards.

Monitoring of performance is a crucial mechanism by which cognitive resources can be allocated to solve a problem. The brain does not relearn everything every time it is confronted with a new problem, it first tries already acquired solutions and only tries to combine or update them when the performance is not satisfying (Botvinick et al., 2009). Based on neuro-anatomy and the functional importance of dopamine in goal-directed behavior, the spiraling structure of the striato-nigro-striatal system is a good candidate to coordinate the flexible recruitment of PFC-BG loops. However, the anterior cingulate cortex (ACC) is known to be crucial in self-performance assessment and error monitoring. As ACC is involved in a PFC-BG loop located just in between the limbic regions (OFC, vmPFC) and the associative ones (dlPFC) (Haber and Knutson, 2010), its dominating position may be the crucial link to determine the involvement of different associative loops to solve cognitive problems. In all cases, understanding how the dopaminergic system processes reward expectations and errors in these different loops is important for the understanding of the organization of PFC-BG loops.

Insights on the role of DA

The activation of dopaminergic neurons is not uniform but specific to each PFC-BG loop. Different loops can control their learning ability by modulating their influx of dopamine. Moreover, the hierarchical organization of the reciprocal connections between the striatum and the dopaminergic areas allows the flexible recruitment of cognitive resources when needed.

1.6.4 Chapter 5 : Timing and expectation of reward

The TD error signal depends only on two pieces of information: the prediction of the value of a state (or action) and the reward actually received. As shown on Figure 1.7, VTA receives information from many other brain regions: a massive inhibitory projection from NAc (possibly excitatory through a relay on the ventral pallidum - VP), direct cortical excitation from the PFC, excitatory connections from reward-related brainstem regions such as the pedunculopontine tegmental nucleus (PPTN), the lateral habenula (LHb) or the lateral hypothalamus (LH). As discovered recently, it also receives inhibitory connections from the mesopontine rostromedial tegmental nucleus (Bourdy and Barrot, 2012; RMTg, Zhou et al., 2009). Inhibitory neurons in the VTA furthermore control the activity of VTA cells and project on NAc and PFC. The complexity of the afferent system to VTA suggests that it computes more than a simple reward-prediction error signal.

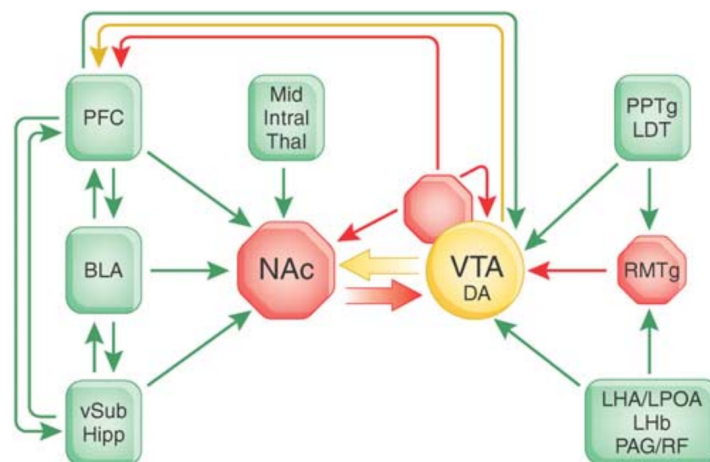


Figure 1.7: Major afferent areas to VTA. The prefrontal cortex (PFC), the basolateral amygdala (BLA), the ventral subiculum of the hippocampus (vSub/Hipp) project on the nucleus accumbens (NAc), which has a strong inhibitory influence on VTA. VTA also receives direct excitatory connections from the PFC. The pedunculopontine tegmental nucleus (PPTg), laterodorsal tegmental nucleus (LDT), lateral hypothalamic and lateral preoptic areas (LHA/LPOA), lateral habenula (LHb), among others, also provide excitatory inputs to the dopaminergic cells of VTA. The mesopontine rostromedial tegmental nucleus (RMTg) provides inhibitory input. VTA also comprises GABAergic cells, which inhibit the dopaminergic ones as well as the PFC and NAc. Adapted from Sesack and Grace (2010).

Several neuro-computational models of the dopaminergic system have been proposed to explain this organization (Brown et al., 1999; O'Reilly et al., 2007; Tan and Bullock, 2008). A common point of these *dual-pathway* models is that they distinguish the excitatory and inhibitory components driving VTA activity for rewards and reward-predicting stimuli, although some debate exists on the exact structures carrying these informations. The DA burst in response to delivery of reward likely originates from the PPTN, while the cancellation of this response when the reward is fully predicted originates from the striatum. Reward-predicting stimuli activate VTA either through the excitatory projection from PFC or from the amygdala. The main differ-

1 Introduction

ence between those models is how the temporal component of the DA signal is computed: in the experiments of Schultz et al. (1997), VTA shows a dip below baseline at the exact time where a reward was expected but did not occur. As no sensory event happens at this time, this indicates that internal timing mechanisms are involved in generating the DA signal.

The hypothesis taken by Brown et al. (1999) and Tan and Bullock (2008) is that the striatum implements a *spectral timing* mechanism (Grossberg and Schmajuk, 1989) where striatal neurons have intracellular calcium levels which peak at different times after stimulus onset: detecting these peaks allows to estimate the time elapsed since onset. Because of the lack of evidence for such a mechanism, we decided in Vitay and Hamker (2014) to investigate alternative mechanisms for interval timing. A successful model of interval timing is the *Striatal-Beat Frequency* model (Matell and Meck, 2004). The basic principle is that cortical neurons behave as oscillators at different frequencies which are synchronized at stimulus onset. The population code composed by these oscillators provides a unique description of the time elapsed since onset: if enough neurons and a large enough range of frequencies are used, the population will never display twice the same pattern, while being reproducible between different trials. Striatal neurons can then detect the elapsed duration by learning to respond to the cortical pattern present when reward is delivered: the DA burst at reward delivery influences plasticity at corticostriatal synapses so they become selective only for that pattern. This model captures many aspects of the link between dopaminergic activity and timing processes, including the accelerated sense of time when DA is elevated - for example in aroused states or during recreational drug use - or the effect of lesions of SNc/VTA or the striatum on interval timing (Coull et al., 2011).

Using this hypothesis, we developed a novel neuro-computational model shedding new light on the afferent system to VTA based on neuro-anatomical evidence. Although the response to primary rewards is classically mediated through PPTN, we propose that conditioned stimuli activate VTA through the existing connection between the amygdala - a structure known for its involvement in classical conditioning - and PPTN. Furthermore, we propose that the cancellation of the DA burst when a reward is predicted and the DA dip when a reward is omitted are processed by two different mechanisms: the direct inhibitory projection from NAcc to VTA can inhibit the response to primary rewards, but bringing VTA activity below baseline requires a complex sub-network linking the ventral BG (NAcc and VP) to VTA through LHb and RMTg.

The model is able to reproduce a wealth of experimental findings: the progressive appearance of phasic bursts at CS onset through classical conditioning, the progressive canceling of the amplitude of the phasic bursts elicited by primary rewards, the strong phasic inhibition at the time when reward is expected but not delivered, the dependency on reward magnitude of the activities in BLA and VTA, the response to reward delivered earlier than expected (Fiorillo et al., 2003; Pan and Hyland, 2005; Schultz et al., 1997). This model is currently limited to VTA activity during classical conditioning but provides a detailed functional basis to address the mechanisms of dopamine release in the PFC-BG system.

Insights on the role of DA

The dopaminergic system integrates information from diverse structures, signaling reward delivery, prediction and omission through different projections. Cognitive, motor and emotional information converge on the dopaminergic system, which then redistributes back the most relevant aspects. It is critically involved in timing processes and therefore the organization of behavior through time.

1.6.5 Chapter 6 : Neural simulator ANNarchy

Neuro-computational models are described by a limited set of information:

1. The number of populations of neurons (or areas), the number of neurons in each population and possibly a topology;
2. A set of ordinary differential equations (ODE) describing the dynamics of each neuron model in the model;
3. Connectivity patterns for the projections between the populations: all-to-all, probabilistic, distance-based, etc;
4. A set of ODEs describing the dynamics of synaptic plasticity for the projections;
5. Methods to provide inputs and read out outputs of the network.

Some of these informations can be inferred from anatomical and physiological data. Neural and synaptic dynamics are well studied, so only small modifications usually need to be applied to standard models. The main difficulty is actually to find sensible values for the free parameters of the model: time constants, learning rates, etc. Although experimental data constrain the range of possible values, this is the most time-consuming part of the design of a neuro-computational model.

Another difficulty is that neural networks can very quickly become expensive to simulate: the number of connections grow quadratically with the number of neurons and the computations can become very slow if no special care is taken about the optimality of the implementation. Parallel computing offers many advantages for the simulation of neural networks as each neuron only processes local information, but writing optimized parallel code on different hardware (shared-memory systems, distributed systems or recently general-purpose graphical cards - GPU) can be quite difficult and time-consuming.

Consequently, researchers in computational neuroscience use neural simulators instead of writing their own simulation code. These are libraries allowing the definition of a model, usually in a high-level scripting language such as Python or Matlab, and hiding from the user all the low-level implementation details necessary to run efficiently simulations in parallel. Another positive side effect is that neural simulators facilitate the exchange of models between researchers for validation and the integration of different models to obtain more functionalities.

1 Introduction

Many different neural simulators are available to the community: NEURON, NEST, GENESIS, Brian, GeNN, Auryn Vitay et al. (2015). They all have different strengths and drawbacks: the exhaustiveness of the set of neural and synaptic models which can be included in a model, the simplicity of the interface, their optimization for a particular parallel hardware, etc. These simulators focus on the simulation of spiking networks, where neurons exchange information through discrete events (spikes), while rate-coded models, where neurons exchange directly a firing rate, are usually impossible or very difficult to define. At the exception of Brian, these simulators provide a fixed set of neural and synaptic models which can only be extended with great difficulty: as long as one only needs standard models, these simulators are very practical, but if one wants to investigate new mechanisms, the programming effort becomes important. Brian proposes a very flexible code generation approach, where neural and synaptic dynamics are described using a text-based equation-oriented mathematical description which is used to generate Python code at run-time (Stimberg et al., 2014). Using code generation allows the user to define virtually any neural or synaptic model.

In parallel to the design of the neuro-computational models presented above, I developed over several years a neural simulator named ANNarchy (Artificial Neural Networks architect), later in collaboration with Helge Ülo Dinkelbach. Two main principles guided the development: first, it should allow the rapid definition of neural networks, for both rate-coded and spiking models. Second, the simulation should be able to run transparently and efficiently on different parallel hardware (using OpenMP for shared-memory systems, MPI for distributed ones and CUDA for GPUs). Code generation is the core principle of the simulator: the definition of the network in a Python script is analyzed and used to generate entirely the simulation code (including a translation from the text-based description of ODEs to executable code statements), using templates adapted to the parallel framework.

In Vitay et al. (2015), we presented the neural simulator to the community and showed that its parallel performance is at least comparable to the alternatives. It is freely available and released under an open-source license. In addition to being used inside the professorship of Artificial Intelligence of the TU Chemnitz, several research groups have shown interest in this simulator and have started using it for their own research. More than just a tool, ANNarchy is also a very promising platform to study the issues raised by neuro-computational models to the parallel computing community: relying on code generation, it allows to explore systematically the different optimizations and algorithms that allow specific networks to be simulated efficiently on different hardware.

1.7 Conclusion

The common theme of this thesis is the role of dopamine in the cognitive, motor and emotional processes involved in goal-directed behavior. Using biologically-realistic neuro-computational models, I investigated its role in visual object categorization and memory retrieval (Vitay and

Hamker, 2008), reinforcement learning and action selection (Vitay and Hamker, 2010), the updating, learning and maintenance of working memory (Schroll et al., 2012) and timing processes (Vitay and Hamker, 2014). The involvement of dopamine in such a wide variety of processes highlights the importance of understanding the mechanisms leading to dopamine release as well as its effect on the activity and plasticity of cortical and subcortical structures.

The different models outline different facets of the effect of DA release in the brain. In the cerebral cortex, the most important effect of DA is the modulation of synaptic transmission in localized networks of excitatory and inhibitory neurons. DA release in the prefrontal cortex influences short-term memory processes by inducing two modes of computation: an “open gate” mode, where multiple sensory information can enter the neural substrate and be represented in parallel; and a “closed gate” mode, where only the strongest and most important representation is maintained, allowing sustained activation (Seamans and Yang, 2004). The transition between these two modes follows an inverted U-curve, where low and high DA levels lead to open gates and intermediate levels to closed gates. The proposed model of PRh (Vitay and Hamker, 2008) exhibits a similar mechanism: PRh can switch between a representational state (driven by inputs) and a mnemonic state (where visual memory is retrieved) depending on the modulatory influence of DA on synaptic transmission. It is likely that DA is able to induce such different modes of computation in all cortical areas receiving dopaminergic input (the whole frontal lobe, the inferotemporal and parietal cortices). The functional consequences of this property still need to be explored, especially with respect to the spatial scale: do all these cortical areas receive the same dopaminergic input from VTA, or is there a functional topology allowing to selectively switch single areas?

In the basal ganglia, the main mode of action considered in the models is the inducement of plasticity by phasic DA bursts or dips. These short-term deviations around the baseline shape synapses coming from the cortex, but also inside the BG. Although more complex models of plasticity have been used, their influence basically follows a three-term DA-modulated Hebbian learning rule. DA bursts reinforce PFC/BG representations which lead to reward, while DA dips “punish” the ones which led to omission of reward or punishment (Schroll et al., 2012; Vitay and Hamker, 2010). This mechanism is fundamentally in line with actor/critic analogies. The short-term duration and the short latency of these phasic responses furthermore allow DA to signal precisely the occurrence of meaningful events, what can be used to learn time intervals and provide an internal sense of elapsed time (Vitay et al., 2015). One aspect of dopamine that will be addressed by future work is the influence of its tonic activity on the BG, which are known to influence the strength and vigor of motor responses as well as the exploration/exploitation trade-off (Beeler et al., 2010; Niv et al., 2007).

An important mechanism proposed in this work is how multiple PFC/BG loops can communicate by influencing each other’s dopaminergic signal. The striato-nigro-striatal connectivity is a remarkable anatomical property whose functional consequences remain largely unexplored. We proposed in Schroll et al. (2012) that it provides a mechanism allowing PFC/BG loops to recruit other loops when the task becomes too complex. The ability of each loop to control its

1 Introduction

dopaminergic input is here fundamental: by knowing how well it performs on a task, it can know if a mistake is its own responsibility, in which case it should continue learning, or if it should rather ask for more cognitive resources to solve the task. This mechanism is fundamental for life-long learning: complex behaviors emerge by composing already acquired simple behaviors, not by learning them from scratch. Future work will broaden this idea to other systems, especially the coordination between the limbic and associative loops which form the basis of goal-directed behavior.

Without a deep comprehension of the neural mechanisms underlying dopamine activity, it would be difficult to design artificial systems showing an intelligent and flexible organization of behavior. Research in computational neuroscience has therefore the opportunity to advance considerably artificial intelligence by transposing biological principles into flexible algorithms. In the proposed work, goal-directed learning focuses on extrinsic rewards. Intrinsic rewards are able to generate more interesting behaviors, such as the discovery of relevant information driven by curiosity or playfulness. Fortunately, dopamine influences similarly the structures responsible for these behaviors and the ones involved with extrinsic rewards, so the principles presented in this thesis will be useful to design such systems. However, intrinsic rewards require an internal state to be acted upon: a core idea of intrinsic motivation is that some actions are directed toward maintaining the system in its "comfort zone" - the homeostasis, for example maintaining the body's temperature, satiety or safeness - while others on the contrary are the consequence of drives that can never be satiated - curiosity can for example never be completely satisfied, so it keeps the organism exploring its environment (see Oudeyer and Kaplan, 2007 for a typology of intrinsic motivation). This internal state obviously requires a body, so that actions acquire a better meaning than simply collecting external rewards. This outlines the importance of embodiment and future work will address the implementation of the proposed models on robotic platforms.

2 Sustained activities and retrieval in a computational model of perirhinal cortex

Abstract

Perirhinal cortex is involved in object recognition and novelty detection, but also in multimodal integration, reward association and visual working memory. We propose a computational model that focuses on the role of perirhinal cortex in working memory, particularly with respect to sustained activities and memory retrieval. This model describes how different partial informations are integrated into assemblies of neurons that represent the identity of an object. Through dopaminergic modulation, the resulting clusters can retrieve the global information with recurrent interactions between neurons. Dopamine leads to sustained activities after stimulus disappearance that form the basis of the involvement of perirhinal cortex in visual working memory processes. The information carried by a cluster can also be retrieved by a partial thalamic or prefrontal stimulation. Thus, we suggest that areas involved in planning and memory coordination encode a pointer to access the detailed information encoded in associative cortex such as perirhinal cortex.

2.1 Introduction

Perirhinal cortex (PRh), composed of cortical areas 35 and 36, is located in the ventromedial part of the temporal lobe. It receives its major inputs from areas TE and TEO of inferotemporal cortex, as well as from entorhinal cortex (ERh), parahippocampal cortex, insular cortex and orbitofrontal cortex (Suzuki and Amaral, 1994). As part of the medial temporal lobe system (with hippocampus and ERh), its primary role is considered to be object-recognition memory, as shown by impairments in delayed matching-to-sample (DMS) or delayed nonmatching-to-sample (DNMS) tasks following PRh cooling or removal (Buffalo et al., 1998; Horel et al., 1987; Meunier et al., 1993; Zola-Morgan et al., 1989). It is thought to be particularly involved in the representation and learning of novel objects (Brown and Xiang, 1998; Pihlajamäki et al., 2003; Wan et al., 1999), with a greater activation for these objects than for familiar ones. suggest that novel objects do not have a strong preexisting representation in inferotemporal cortex, and traces of long-term memory in PRh could be used to manipulate these objects.

2 Sustained activities and retrieval in a computational model of perirhinal cortex

Despite the huge amount of evidence for a mnemonic role of PRh, some recent findings suggest that it is also involved in high-level perception (for a controversy, see and), such as object categorization and multimodal integration, by integrating different sources of information about the identity of an object Taylor et al. (2006). PRh indeed receives connections from insular cortex (somatosensory information) and the dorsal bank of the *superior temporal sulcus* (vision/audition coordination), therefore being at a central place for integrating different modalities of an object. Interestingly, monkeys with lesions of PRh are unable to select a visible object first sampled by touch Goulet and Murray (2001) or by a partial view of that object Murray et al. (1993).

Accordingly, PRh is neither a purely mnemonic nor a perceptual area: it is a multimodal area which is presumably involved in the goal-directed guidance of perception. This link to the goals of the task at hand is reflected by the modulation of PRh activity by reward association (Mogami and Tanaka, 2006), which strongly depends on D2 dopamine receptors (Liu et al., 2004). Also, PRh is involved in visual working memory, which is known to use integrated representations of objects rather than individual features (Lee and Chun, 2001; Luck and Vogel, 1997). showed that PRh cells are more active during a DMS task when their preferred stimulus is the sample (the object to be remembered) than when it is the match (the target) and that this property is actively reset between trials, supporting the evidence of a higher cognitive involvement. Some PRh cells also exhibit sustained activity between sample and match: their proportion has been estimated to 35% compared to 22% in IT or 71% in ERh (Nakamura and Kubota, 1995; Naya et al., 2003). However, contrary to ERh, these sustained activities are not robust to the presentation of distractors between sample and match (Miller et al., 1993b; Suzuki et al., 1997). The exact mechanism and purpose of these sustained activities is still unknown. Are they only provoked by feedback connections from prefrontal cortex where sustained activities are robust to distractors (Miller et al., 1996), or does prefrontal cortex just control the maintenance or suppression of these sustained representations that are created with intrinsic mechanisms in PRh?

This article presents a computational model of PRh focused on the involvement of this cortical area in visual working memory processes, by emphasizing the effect of dopamine modulation on perirhinal cell activation. Our aim is neither to model every aspect of PRh functioning nor to explore the biophysical properties of sustained activation. We rather propose a new interpretation at the functional level of these sustained activities in the framework of multimodal object identification or categorization. The model demonstrates how different aspects of an object or a category are linked into a neural assembly according to their cooccurrence through time and how this assembly can be reactivated for memory retrieval.

2.2 Methods

2.2.1 Context

There are only few computational models of PRh. One of the most famous is the *perceptual-mnemonic feature conjunction* (PMFC) model by Bussey, Saksida and colleagues (Bussey and Saksida, 2002; Cowell et al., 2006). As its name indicates, it is primarily concerned with the interplay of perceptual and mnemonic processes in PRh. PRh is represented by a feature-conjunction layer that integrates individual features and learns to represent effectively objects in concurrent discrimination or configural learning tasks. Learning occurs either through a Rescorla-Wagner rule (Bussey and Saksida, 2002) or through self-association in Kohonen maps (Cowell et al., 2006). Despite its good predictions about the effects of PRh lesions on discrimination and configural learning tasks, it is a purely static model that can not deal with sustained activities. The model by is much more detailed and dynamic (spiking neurons) but only deals with familiarity discrimination: its Hopfield-like structure makes it able to tell rapidly if an object has already been seen but it does not allow to recollect its details. It is a purely mnemonic view of PRh. The model we propose is original with regards to the functions it describes (autoassociative memory, sustained activation, memory retrieval) and its dynamical structure.

2.2.2 Architecture of the model

To keep the model as simple as possible, we do not consider the precise timing of spikes but use mean-rate artificial neurons whose activity is ruled by a dynamical differential equation. This positive scalar activity represents the instantaneous firing rate, which is directly derived through a transfer function from the membrane potential, without using a spike-generation mechanism. As a consequence, the neurons used in this model exchange only this time-varying scalar activity through their connections, similar to dynamical neural fields (Amari, 1977; Taylor, 1999).

The neural network (Figure 2.1 - a) is composed of a population of excitatory pyramidal cells interconnected with a population of inhibitory interneurons. In order to reflect approximately the relative number of GABAergic interneurons in the cerebral cortex, the excitatory population is four times bigger than the inhibitory one Beaulieu (1993). Each inhibitory cell receives excitatory inputs from a subset of excitatory cells, with a gaussian connectivity kernel centered on the corresponding neural location. Reciprocally, each excitatory cell receives connections from a subset of inhibitory cells with a broader gaussian connectivity kernel. Additionally, inhibitory cells are reciprocally connected with each other in an all-to-all manner, with the connection strength decreasing with the distance between cells. Excitatory cells are also reciprocally connected in an all-to-all manner, but the strength of these connections is modifiable with experience.

Each excitatory cell receives a cortical input that could originate in a visual area like TE or in the multimodal parahippocampal cortex. showed that neighbouring cells in PRh tend to represent the same objects after visual experience. This finding could be explained by a self-organization

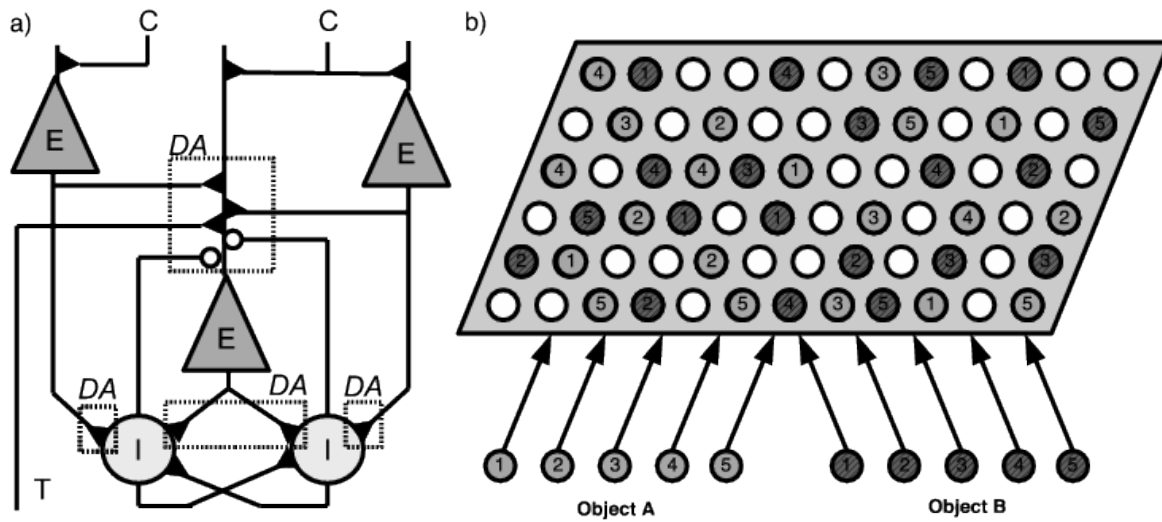


Figure 2.1: a) Architecture of the model. It is composed of $N \times N$ excitatory cells (E) and $\frac{N}{2} \times \frac{N}{2}$ inhibitory cells (I). Excitatory and inhibitory cells are reciprocally connected through gaussian connectivity kernels. Inhibitory cells are also reciprocally connected with each other with a strength decreasing with the distance. Excitatory cells are reciprocally connected with each other, but the strength of the connections is learned. Each excitatory cell receives a cortical input C from other areas. Additionally, some excitatory cells receive a thalamic input T. All connections except the cortical ones are modulated by dopamine (hatched squares). b) Feed-forward connectivity for excitatory cells. Two different objects have to be learned by the model: object A (light grey) and B (dark grey, hatched) are each represented by five parts (numbered from 1 to 5), corresponding to different views or modalities. Each part is represented by a cortical input to four cells, what makes each object being represented by a cluster of 20 cells.

of receptive fields, i.e. the modification of feedforward connections. Our model does not include this feed-forward learning but is rather designed to show how the gathering of these different informations can occur in PRh. The cortical input to a cell will therefore be a time-varying scalar value, reflecting the weighted sum of the activity of its afferent cells, without any information about its origin. The basic idea of the model is that the perirhinal neurons representing a given object or category have receptive fields selective for a particular aspect of that object or category, either in visual space (different views of an object or different exemplars of a category sharing some visual features) or in multimodal space (some neurons are preferentially activated by the sound associated to this object, or its touch). In the following, we will not distinguish between the learning of different views or modalities of an object, or the learning of a category represented by different exemplars: the mechanism remains the same and we will use the term “object” for either a real object or a category. The increase in the strength of the lateral reciprocal connections between excitatory cells will provoke a clustering effect: the representation of an object will be distributed over several cells (forming what is called a *cluster* or an autoassociative pattern) which are individually selective for a particular aspect.

In our simulations, an object is represented by five parts corresponding each to a particular aspect. Each part provides a cortical input to four excitatory cells in PRh (randomly chosen in the population), meaning that the representation of all aspects of an object forms a cluster of twenty neurons (Figure 2.1 - b). During learning, each object will be successively presented during a certain amount of time (250 ms here), but each of its parts will be randomly active with a probability of 0.6. The random activation of parts means that each presentation of an object will be incomplete in most cases. The goal of the learning in the lateral connections will be to correlate the different parts, even if they do not constantly appear together. Unless stated otherwise, all the simulations have been done with two different objects.

2.2.3 Dopamine modulation

Dopamine (DA) modulation is a very important feature of the model, responsible for most of its interesting properties. Unfortunately, little is known about its effects in PRh. We will therefore assume that dopamine modulation in PRh is similar to what occurs in prefrontal cortex, given the fact that PRh has a similar ratio of D1/D2 receptors, even if their density is higher (Hurd et al., 2001). An exhaustive review about dopamine effects on prefrontal cells can be found in . The picture that emerges from experimental observations is very heterogeneous. However, there is some accumulating evidence for the following properties:

- the effect of DA is strictly modulatory: it does not induce excitatory post-synaptic currents by itself (Yang and Seamans, 1996);
- DA modulates both pyramidal and fast-spiking inhibitory interneurons (Gorelova et al., 2002);
- DA modifies the cell’s excitability by modulating intrinsic ionic currents like Na^+ and K^+ (Yang and Seamans, 1996);

2 Sustained activities and retrieval in a computational model of perirhinal cortex

- the effect of DA is dose-dependent: D1 receptor activation can have opposing functional effects depending on the level of stimulation, following an inverted U-shape (Goldman-Rakic et al., 2000);
- the effect of DA is neurotransmitter receptor-dependent: NMDA- (excitatory activity-dependent) and GABA- (inhibitory) mediated currents are enhanced by DA, but AMPA- (excitatory) mediated ones are decreased (Cepeda et al., 1992; Momiyama et al., 1996);
- the effect of DA is dendrite-dependent: DA reduces more strongly the EPSPs generated in apical dendrites (long-distance cortical inputs) than in the basal ones (neighbouring pyramidal cells), through a reduction of dendritic Ca^{2+} currents (Yang and Seamans, 1996; Zahrt et al., 1997);
- the effect of DA is activity-dependent: the more the cell is active, the more DA modulates its inputs (Calabresi et al., 1987);
- DA levels are long-lasting in the target area Huang and Kandel (1995). The phasic DA bursts in the dopaminergic cells are therefore not relevant: we will only consider the tonic component of DA activity, not its phasic component.

Existing models of dopaminergic modulation of sustained activities in prefrontal cortex do not all make the same hypothesis about the exact influence of DA. A detailed model by supposes that DA enhances the persistent Na^+ ionic currents, reduces the slowly inactivating K^+ ionic currents, reduces the efficiency of apical inputs, reduces the amplitude of glutamate-induced EPSPs (including NMDA, even if they admit this is controversial) and increases the spontaneous activity of GABAergic cells as well as the amplitude of IPSPs in pyramidal cells. In their respective models, as well as suppose that DA only enhances NMDA-mediated currents in the basal dendrites in coordination with a simultaneous increase of the amplitude of IPSPs. On the contrary, consider that DA momentarily restricts excitatory inputs on apical dendrites. More recently, considered that DA only modifies the gain of cells by increasing their firing threshold, without being more specific about synaptic currents.

The major link between most of these models is that they distinguish the effects of DA on apical dendrites and on basal dendrites of pyramidal cells: the influence of long-distance cortical inputs is reduced by DA whereas the influence of neighbouring pyramidal cells is increased. This last assumption is coherent with the fact that basal dendrites are primarily NMDA-mediated (Schiller et al., 2000). The reduction of apical currents allows the network to be momentarily insensitive to external inputs, increasing the robustness of sustained activities when they appear. In the case of PRh, as we know that sustained activities are not robust to the appearance of distractors (Miller et al., 1993a), we neglected this effect. Accordingly, the major influences of DA we consider in our model are therefore the increase of the efficiency of lateral connections between excitatory cells (on an activity-dependent manner, as they are mainly mediated by NMDA receptors), the increase of the amplitude of IPSPs (by increasing the efficiency of the connections from inhibitory to excitatory cells) and the increase of the activity of the inhibitory cells through an increase in the efficiency of the connections from excitatory to inhibitory cells. These assumptions are summarized in Figure 2.1 - a. The modification of the excitability of

cells through modulation of ionic currents has not been taken into account since the effects of this mechanism are thought to be similar to the selective modulation of synaptic currents. The differential effects of D1-like and D2-like receptors have not been considered since there exists no sufficient experimental evidence to draw a precise line between them.

2.2.4 Equations for updating the activity

The model consists of a single map of $N \times N$ excitatory units and $\frac{N}{2} \times \frac{N}{2}$ inhibitory units. We use $N = 20$ for the results in this paper, but the properties of the model do not depend on this particular size: it has been tested from $N = 10$ to $N = 40$, showing that distributed computations and flexible learning can induce scalability. We used a mean-field approach, where the activity of each unit follows an ordinary differential equation, discretized with a timestep of 1 ms. In the mean-field approach, a unit represents a population average of a certain number of single cells. Since the true underlying circuitry is not well known, we do not explicitly derive the mean-field solution but describe the dynamics at the macroscopic population level. Nevertheless, for the sake of simplicity, we use the term "cell" for a unit. The mean activity $I_i(t)$ of an inhibitory cell at time t is ruled by Equation 2.1:

$$\tau_I \cdot \frac{dI_i(t)}{dt} + I_i(t) = \sum_{j \neq i} W_{ij}^{II} \cdot I_j(t) + (1 + K^{EI} \cdot DA) \times \sum_k W_{ik}^{EI} \cdot E_k(t) + \eta_i^I(t) \quad (2.1)$$

where $\tau_I = 10$ ms is the net time constant of the unit. W^{II} is the set of connections between inhibitory cells, decreasing with the distance between the cells and W^{EI} is the set of connections from the excitatory cells (activity denoted $E_k(t)$) to the inhibitory cell (formulas given in the appendix). The dopamine level in the network (represented by the scalar value DA between 0 and 1) increases the gain of inputs from excitatory cells. K^{EI} is a fixed scaling parameter. Finally, $\eta^I(t)$ is a noise added to the cell that randomly fluctuates in the range $[-0.1, 0.1]$. The resulting activity is restricted to positive values.

The mean activity $E_i(t)$ of an excitatory cell at time t is ruled by Equation 2.2:

$$\begin{aligned}
 \tau_E \cdot \frac{dE_i(t)}{dt} + E_i(t) = & f((1 + K^{EE} \cdot \sigma^{lat}(DA) \cdot \sigma^{EE}(E_i(t))) \cdot \sum_{j \neq i} W_{ij}^{EE} \cdot E_j(t) \\
 & + (1 + K^{IE} \cdot \sigma^{GABA}(DA) \cdot E_i^2(t)) \cdot \sum_k W_{ik}^{IE} \cdot I_k(t) \\
 & + W_i^C \cdot C_i(t) \\
 & + (1 + K^T \cdot \sigma^T(DA)) \cdot T_i(t) \\
 & + \eta_i^E(t)
 \end{aligned} \tag{2.2}$$

where $\tau_E = 20$ ms is the net time constant of the unit. This value is chosen twice as large as in the inhibitory units to reflect the ratio of membrane time constants between pyramidal cells and inhibitory interneurons in the cortex (McCormick et al., 1985). $f(x)$ is a transfer function, ensuring that the activity of the cell does not reach too high values. It is linear in the range $[0, 1]$ and then saturates slowly to a maximum value of 1.5 (formula given in the appendix). There are five terms inside this transfer function. The first term denotes the influence of the lateral connections between excitatory cells W^{EE} . Its gain depends on dopamine through a sigmoidal term σ^{lat} and a fixed scaling parameter K^{EE} but also on the activity of the cell itself through another sigmoidal function σ^{EE} . For these predominantly NMDA-mediated lateral connections, the influence of DA is therefore activity-dependent. These two sigmoids are independent to ensure that DA only modulates active cells and that effective transmission of activity through NMDA-mediated connections between excitatory cells only occurs in the presence of DA. The second term represents the influence of the connections from the inhibitory cells with a negative strength W^{IE} . Their efficiency also increases with dopamine (sigmoidal function σ^{GABA} and fixed scaling parameter K^{IE}) and the activity of the cell. The feedforward inhibition produced by the increase of the efficiency of IPSPs by high levels of DA on pyramidal cells, as proposed by , is realized through a square of the activity of the cell itself. The third term is the contribution of the cortical input $C_i(t)$ through a random weight W_i^C , without any dopaminergic modulation since they are considered to reach apical dendrites (see the *Dopamine modulation* section). When the cell is stimulated, we set $C_i(t) = 1.0$. The fourth term is the contribution of a possible thalamic input $T_i(t)$, increased by dopamine through σ^T and the scaling parameter K^T . This term is clearly distinct from the cortical inputs: although PRh is dysgranular - with a very thin layer IV (Rempel-Clower and Barbas, 2000) - thalamocortical afferents from the dorsal and medial geniculate nuclei target layers I, III/IV and VI (Furtak et al., 2007; Linke and Schwegler, 2000), therefore on both apical and basal dendrites of pyramidal cells, as well as on various interneurons. We therefore assume that the thalamic input has a driving force through apical dendrites, similar to the cortical input, and a dependence on dopamine through the basal dendrites. The last term $\eta^E(t)$ is a noise randomly fluctuating in $[-0.5, 0.5]$. The resulting activity is restricted to positive values. Details about the sigmoidal functions and other parameters are given in the appendix.

While the general properties of DA modulation are largely supported by the discussed observations, the exact parameters and sigmoid functions have been determined through trial-and-error processes to enable sustained activities. Although the results we present here quantitatively depend on these choices, the global properties we intend to highlight admit some variations in the values of the parameters.

2.2.5 Learning rule

The lateral reciprocal connections between excitatory cells W^{EE} are subject to learning. We considered a covariance rule combining input- and output-dependent LTP (long-term potentiation) and output-dependent only LTD (long-term depression):

$$\tau_W \cdot \frac{dW_{ij}^{EE}(t)}{dt} = (E_i(t) - \hat{E}_i(t))^+ \cdot ((E_j(t) - \hat{E}_j(t))^+ - \alpha_i(t) \cdot W_{ij}^{EE}(t) \cdot (E_i(t) - \hat{E}_i(t))^+) \quad (2.3)$$

where $E_i(t)$ is the pre-synaptic activity of cell i , $E_j(t)$ the post-synaptic activity of cell j . $()^+$ is the positive part function. $\hat{E}_k(t)$ is a temporal sliding-mean of the activity $E_k(t)$ over a window of T ms defined by:

$$\hat{E}_k(t) = \frac{(T - 1) \cdot \hat{E}_k(t - 1) + E_k(t)}{T} \quad (2.4)$$

with $T = 5000$ ms in this model. This term ensures that learning occurs only when pre-synaptic or post-synaptic activities are significantly higher than their baseline value, ruling out learning of noise. However, the final weights determined by this rule alone are strongly dependent on the value of the parameter α_i , which is constant in classical covariance rules. If α_i is set too high, weights will never increase enough to produce post-synaptic activity, but if α_i is too low, the post-synaptic cell will have maximal activity for a too large set of stimuli. As we want our model to deal with different cluster sizes, we had to use a more flexible approach for the learning rule. We therefore focused on homeostatic learning, where the learning rule uses as a constraint that the activity of a cell should not exceed a certain value, in order to save energy (Rossum and Turrigiano, 2001; Turrigiano and Nelson, 2004). Homeostatic learning is possible when the parameter α_i can vary with the experience of the cell, in our case when the cell's activity exceeds a certain threshold. The following rule is used:

$$\tau_\alpha \cdot \frac{d\alpha_i(t)}{dt} + \alpha_i(t) = K_\alpha \cdot H_i(t) \quad (2.5)$$

$$\tau_H \cdot \frac{dH_i(t)}{dt} + H_i(t) = K_H \cdot ((E_i(t) - E_{max})^+)^2 \quad (2.6)$$

with $H_i(t)$ and $\alpha_i(t)$ restricted to positive values and $\alpha_i(0)$ equal to 10.

When $E_i(t)$ exceeds E_{max} (1.0 in our model), $H_i(t)$ becomes rapidly highly positive, leading to a slow increase of $\alpha_i(t)$. The inhibitory part of Equation 2.3 becomes preponderant and all the weights decrease. The reason why $H_i(t)$ is introduced is that $\alpha_i(t)$ must have a slow time constant so that learning is stable. This learning rule is similar to the classical BCM rule (Bienenstock et al., 1982) but is more stable, since the inhibitory term in Equation 2.3 represents a constraint both on a short time scale - by its dependence on $E_i(t)$ and $W_{ij}^{EE}(t)$ - and on a long time scale with $\alpha_i(t)$. The effect of this learning rule is that weights will rapidly increase at the beginning of learning (the Hebbian part of Equation 2.3 is preponderant) but when the cells begin to overshoot, $\alpha_i(t)$ increases and forces the cell to find a compromise between increasing its afferent weights and activity overshooting. When learning is efficient, $\alpha_i(t)$ stabilizes to an optimal value that depends on the mean activity of the cell.

2.3 Results

We will first show the consequence of learning the lateral connections between excitatory cells on the formation of clusters and the propagation of activity within the cluster. We then demonstrate the effect of DA modulation on sustained activities in the network and show that the model follows the classical inverted-U shaped curve. After introducing these basic properties, we then demonstrate the specific properties for memory recall such as the dependence of the propagation of activity between two clusters on the strength of their reciprocal connections, as well as the effect of thalamic stimulation on memory retrieval

2.3.1 Learning and propagation of activity within a cluster

During learning, a sequence of stimuli is shown to the network. The first object is presented for 250 ms, activating a random number of parts of the corresponding cluster. No stimulation is given to the network for the next 250 ms, followed by the second object for 250 ms and further on. This sequence is repeated for 100 times. Please note that this is one particular learning protocol, but that other protocols ensuring that each object is sufficiently often presented also work. The dopamine level is set to a low value of 0.1 during learning, for reasons explained in the *Discussion* section.

After learning, each cell has built connections with the cells representing other parts of an object. Figure 2.2 - a shows the 25 highest connection values for a randomly selected cell in the first cluster. One can observe that this cell has formed positive connections with the 19 other cells of the cluster. The weights within a cluster are not all equal, reflecting the probability of cooccurrence of the different parts during learning. Oppositely, the connections with cells of another cluster have been reduced to neglectable values.

After learning, how do we functionally retrieve the information about the correlation between different parts? Our hypothesis is that the activation of a sufficient number of parts should provoke activity in the remaining parts, at least under certain dopamine levels. Figure 2.2 - b shows the mean activity of the remaining parts dependent on the numbers of parts that receive cortical activation. When dopamine has too low (0.2) or high (0.8) levels, the remaining parts show only little activation, even if four out of five parts are stimulated. When dopamine has an intermediate level (0.4 or 0.6) and three or more parts are activated, the remaining parts show strong activity, as if they actually received cortical input. This shows that under intermediate dopamine levels, the network is able to retrieve all the parts of a cluster if a majority of them is stimulated. We also simulated clusters of bigger size (up to 20 parts of four cells, i.e. 80 cells) and observed that this minimum proportion of stimulated parts is slightly decreasing with the cluster size, but it is always superior to one third.

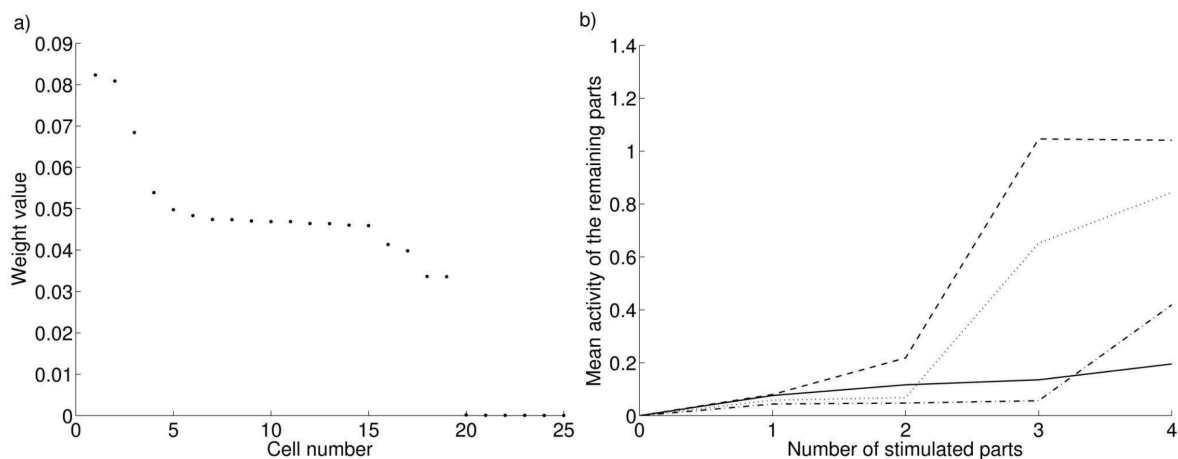


Figure 2.2: a) Weight values for a given cell in the first cluster. Only the 25 highest values are represented in descending order. We observe that this cell has positive connections with the 19 cells that form the cluster and none with other cells. b) Mean activity of unstimulated parts relative to the number of stimulated parts. We observe that for low (0.2) or high (0.8) dopamine levels, the remaining parts are only poorly activated. For intermediate levels (0.4 or 0.6), three stimulated parts are sufficient to provoke a high activity in the remaining two unstimulated parts.

2.3.2 Sustained activities and intermediate values of dopamine

In the following experiments, we stimulate only three parts of a cluster (12 cells out of 20) and record two different neurons, one belonging to these three parts and called the “stimulated” cell, the other to one of the two remaining parts and called the “unstimulated” cell.

To determine the adequate range of dopamine levels, it is interesting to look at the sustained activities observable in the network. Figure 2.3 - a shows the timecourse of the activity of two cells during the successive presentation of the two objects. With a low dopamine level (0.1), only the stimulated cell shows significant activity (around 1.0) during the presentation of the object. With an intermediate dopamine level (0.4), both cells become highly active (around

2 Sustained activities and retrieval in a computational model of perirhinal cortex

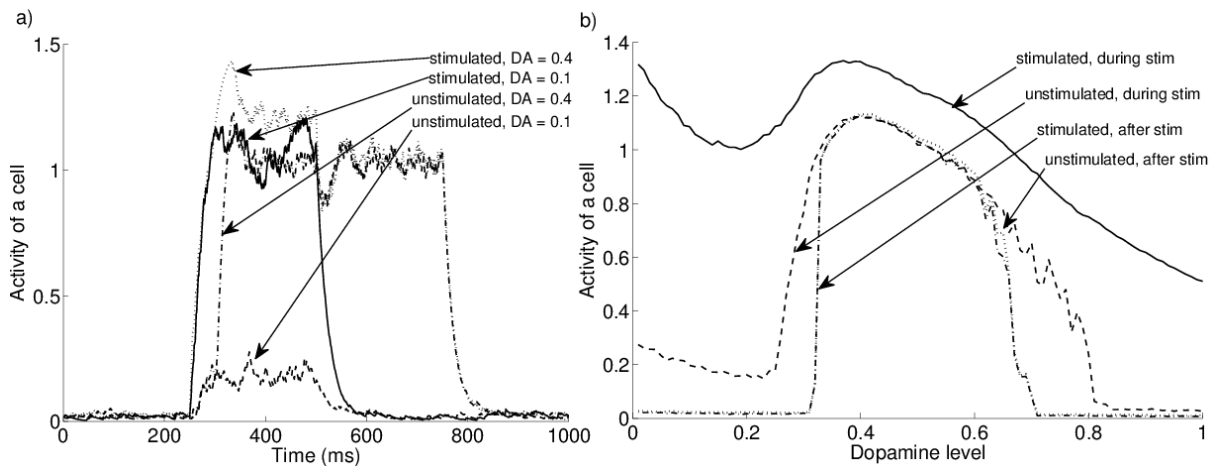


Figure 2.3: a) Time course of the activity of two different cells in the same cluster. The first one (“stimulated cell”) belongs to one of the three parts that receive cortical input, the other one (“unstimulated cell”) receiving no cortical input. When the dopamine level is low ($DA = 0.1$), the stimulated cell responds strongly to the presentation of the object but not the unstimulated one. When the stimulation ends, the activity of these two cells return to baseline. When the dopamine level is intermediate ($DA = 0.4$), the two cells respond equally strong to the presentation of the object. After disappearance, they show sustained activity until a new object is presented. b) Effect of dopamine on two cells in the same cluster. The two upper curves represent the activity of the stimulated and unstimulated cells during stimulation, 200 ms after the corresponding object onset. With intermediate levels of DA, the activity of the unstimulated cell is high and only slightly inferior to the stimulated one (difference of 0.2). With large dopamine levels (> 0.6), the activity of the two cells is drastically reduced because of the enhancement of inhibition by dopamine. The two lower curves (which seem identical) represent the activity of these two cells 100 ms after the end of the stimulation. We observe an inverted-U shape meaning that the level of dopamine necessary to observe sustained activities is between 0.3 and 0.7.

1.2 and 1.0, respectively) during the stimulation, with a little timelag due to the propagation of activity within the cluster. When the stimulation ends, their activity does not fall back to baseline but stays at a high level (1.0). This sustained activity is only due to the reciprocal interactions between excitatory cells and their modulation by dopamine.

When the second object is presented, its representation competes with the sustained activation. If the two representations are equally distributed on the map, which is the case here, some of their excitatory cells will be connected to the same inhibitory cells, leading to enhanced inhibition and disruption of the sustained activities. If the two representations are spatially segregated on the map (corresponding for example to two objects from very different categories, like a face and a tree), the two representations can exist in parallel. Data from about the robustness of sustained activities in PRh does not deal with the distribution of competing stimuli on the surface of the cortex, allowing this property to be a prediction of the model. However, if the distracting stimulus has a low intensity ($C_i(t) < 0.4$) or is not represented by more than two parts, the sustained representation can resist its appearance, thanks to the increased activity of inhibitory cells.

Figure 2.3 - b shows the influence of the dopamine level on the activities of the two considered cells during and after stimulation. When the cluster is partly stimulated, dopamine globally enhances the activity of the stimulated cell when DA is inferior to 0.4 but then begins to depress it. For the unstimulated cell, one can observe a strong enhancing effect when dopamine is around 0.25 due to the propagation of activity within the cluster. When dopamine exceeds 0.8, the activity of this cell falls abruptly to zero, showing that propagation of activity is not possible under high levels of dopamine, because of the enhancement of the reciprocal connections between inhibitory and excitatory cells. The two lower curves of Figure 2.3 - b show the sustained activity of the two cells 100 ms after the end of the stimulation. They have an inverted-U shape which is typical for dopaminergic modulation of working memory in prefrontal cortex (Goldman-Rakic et al., 2000). The graph shows that the values of dopamine in our model that allow to observe sustained activities range between 0.3 and 0.7. The amplitude of the sustained activities is relatively high (up to 80% of the activity during stimulation depending on the dopamine level) but is coherent with cellular recordings (Curtis and D'Esposito, 2003; Naya et al., 2003; Ohbayashi et al., 2003). Due to the balanced background inhibition, we can also change the parameters of the model to obtain lower sustained activities.

2.3.3 Propagation of activity between clusters

The propagation of activity within a cluster is an interesting property in the framework of multimodal object categorisation and identification. However, contrary to the preceding experiments where the two learned objects do not share any parts, learning in the real world does not ensure that parts of two different objects are not activated at the same time in PRh, for example because these objects share these parts. Consequently, the weights between two clusters are

2 Sustained activities and retrieval in a computational model of perirhinal cortex

not necessarily equal to zero. What happens to the propagation of activity if two clusters are reciprocally connected with small weight values?

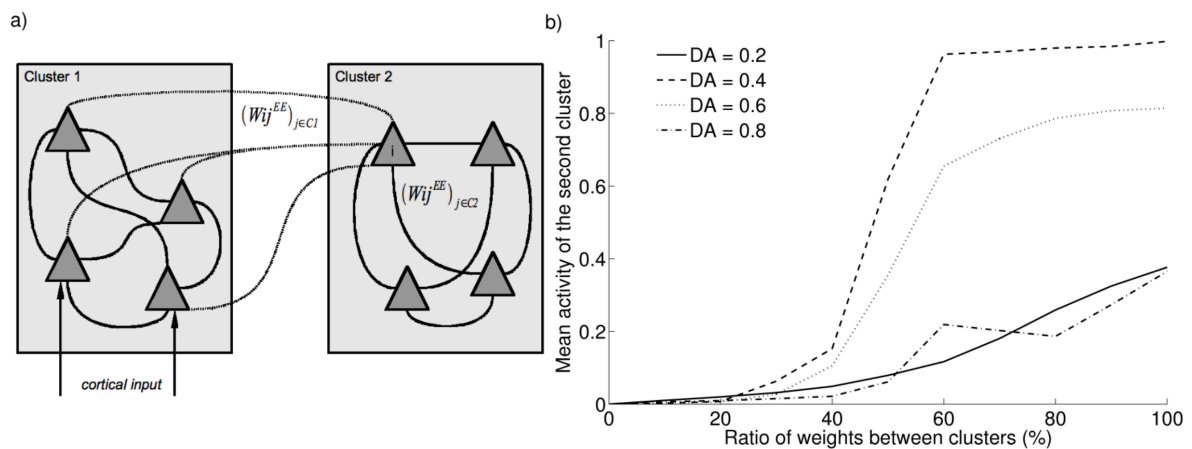


Figure 2.4: a) Influence of the connections between different clusters on the propagation of activity. For simplicity, only four excitatory cells by cluster and just a few connections are shown on the figure. Two clusters C1 and C2 are learned. Each excitatory cell i of the cluster C2 receives connections $(W_{ij}^{EE})_{j \in C1}$ from excitatory cells of the cluster C1, but they are very low after learning. In this experiment, the weights of these inter-cluster connections are artificially set proportional to the mean value of the intra-cluster connections to the corresponding cell in the second cluster $W_i^{mean} = \frac{1}{N} \times \sum_{j \in C2} W_{ij}^{EE}$. b) Results. Three parts of the first cluster are then stimulated and we plot the mean activity of the second cluster after 200 ms. When dopamine is low (0.2) or high (0.8), the second cluster becomes only poorly activated by the first cluster, even when the connections have equal strengths. When dopamine is intermediate, the inter-cluster weights must be below 40% of the intra-cluster weights to avoid the propagation of activity.

Figure 2.4 shows the influence of these inter-cluster connections. After the two clusters have been learned, we artificially increase the strength of connection between the two groups of cells. As each cell does not receive the same amount of cortical input because of the random weights W_i^C , their lateral connections W_{ij}^{EE} are not equal. We therefore computed the mean value of these lateral connections for each cell of the second cluster (called the intra-cluster connection value) and set the connections from the first cluster to the corresponding cell in the second cluster proportional to this value (inter-cluster connection value).

We then stimulate three parts of the first cluster and record the mean activity of the second cluster. Under low or high dopamine levels, inter-cluster connections can be equal to the intra-cluster connections (meaning that they form one bigger cluster) without observing any propagation of activity to the second cluster. Under intermediate dopamine levels, the ratio between these connections must be below 40% to avoid that the activation of one cluster propagates without control to other weakly connected clusters. This result ensures a reasonable trade-off between stability of object representation and propagation of activity.

2.3.4 Thalamic stimulation

The preceding results show that our model is able to learn to correlate different parts of an object through lateral connections and to propagate activity between these parts under intermediate dopamine levels. It also exhibits sustained activity after an object is presented, but which is easily disrupted by similar distractors. What can be the interest of such unrobust sustained activities in the more general framework of visual working memory? Our conviction is that this high-level representation of an object does not need to be actively maintained through time but only regenerated when needed. A cluster describes quite exhaustively the different aspects of an object: what needs to be remembered is more the location of the cluster in PRh than the details of its representation. Propagation of activity within a cluster seems a useful mechanism in the sense that external activation of parts of a cluster can be sufficient under intermediate dopamine levels to retrieve the whole information carried by the cluster. This external activation can take its origins either from prefrontal cortex or from the basal ganglia - through the dorsal nucleus of the thalamus - where sustained activities are robust.

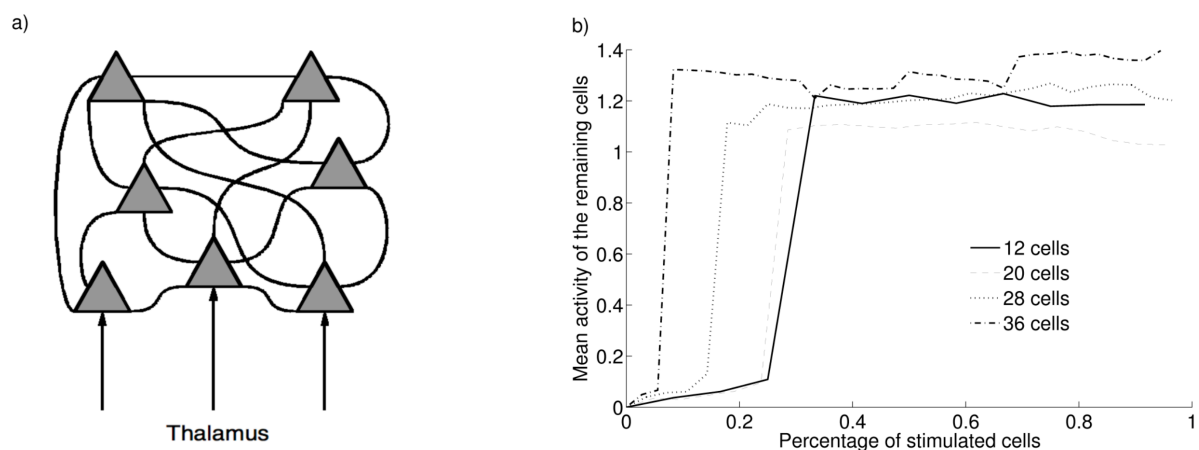


Figure 2.5: a) Thalamic stimulation of clusters of different sizes under intermediate dopamine level ($DA = 0.5$). A certain percentage of the cells of each cluster is fed with a thalamic input. b) Results. With an intermediate dopamine level, propagation of activity within the cluster of 12 cells happens when at least 35% of the cells receive thalamic input. Clusters of bigger size need an even smaller proportion of stimulated cells.

Figure 2.5 shows the influence of partial thalamic stimulation of the cells of a cluster. For this experiment, the network learned simultaneously four clusters of different sizes: 12 cells (3 parts), 20 cells (5 parts), 28 cells (7 parts) and 36 cells (9 parts). A learning cycle (the successive presentation of the four partially stimulated objects) is therefore two times longer (2 seconds) and learning is stopped after 200 cycles. For each cluster, we feed a certain percentage of cells with thalamic input ($T_i = 1.0$) and we record the mean activity of the remaining cells. Using an intermediate dopamine level (0.5), one can observe that, for the cluster of 12 cells, a thalamic stimulation of at least 35% of its cells is sufficient to propagate activity in the cluster. This proportion is even smaller with clusters of bigger sizes. This property allows the *retrieval* of the encoded information in the cluster without knowing all its details. The conse-

quence is that a robust working memory of an object does not require to contact all the cells of a cluster but only a small portion of them, making manipulation easier and more flexible.

2.4 Discussion

The proposed computational model of PRh focuses on multimodal object representation. It learns to integrate different parts of an object, even if they do not all appear together during learning. The resulting clusters of reciprocally interconnected neurons are modulated by dopamine, so that, under an intermediate level, activation of a majority of parts propagates to the rest of the cluster and sustained activities appear after stimulus disappearance. Despite the fact that these sustained activities are not robust to distractors - as experimentally found in -, a cluster can be reactivated through thalamic stimulation of less than 35% of its cells (depending on the size of the cluster) and allows the retrieval of the global information.

The major implication of this model is that the maintenance in working memory of the visual attributes of an object is located in PRh - more precisely in the lateral connections of its cells - but that the manipulation of the content of working memory (robustness to distractors, retrieval) has to come from external regions like the thalamus or prefrontal cortex. A testable prediction is that unrobust sustained activities can be observed in PRh *without* any feedback from prefrontal cortex, as proposed also by or . Similarly to what is observed in prefrontal cortex (Goldman-Rakic et al., 2000), we also suggest that sustained activities in PRh have an inverted-U shape dependence with dopamine levels: no sustained activity for low or high levels of dopamine, sustained activities in the intermediate range. Cellular recordings could also reveal our “propagation of activity” property: cells that are selective for a part of an object that is not presented should respond to the object under intermediate level of DA but not under low levels. Moreover, we predict that these activations will be slightly delayed.

This model principally relies on the modulation by dopamine of various synaptic currents. Although a lot of -sometimes contradictory - data exists regarding the action of DA on prefrontal cells (Seamans and Yang, 2004), little is known about its action on PRh cells. We hypothesized that PRh cells are similarly modulated by DA, but put emphasis on different aspects. In particular, some models of sustained activation in prefrontal cortex (Dreher et al., 2002; Durstewitz et al., 1999) consider that DA primarily restricts the efficiency of cortical inputs on apical dendrites, allowing the network to be isolated from outside distractors. As sustained activities are not robust in PRh, we considered that this apical reduction was not as important as in prefrontal cortex and chose not to use it in the model. On the contrary, we considered that the main influences of DA are to enhance the NMDA-mediated currents provoked by the lateral connections from neighbouring cells and the GABA-mediated currents coming from inhibitory cells like in (Brunel and Wang, 2001; Deco and Rolls, 2003). This assumption is at the core of our model and is susceptible to be experimentally confirmed.

We focused on the tonic component of DA release by considering DA levels in PRh constant over sufficiently long periods. We are not aware of any study that investigated the effect of DA over time in PRh, but our assumption is motivated by observations in hippocampus where the effects of DA can last up to three hours (Huang and Kandel, 1995) and in prefrontal cortex (Grace, 1991) where similar observations have been made. Such long-lasting DA effects can be critical in the learning phase. Here, we set DA to a low value (0.1) since intermediate values partially impair learning: the global efficiency of excitatory lateral connections has to compensate almost exactly the global efficiency of inhibitory connections (which increases faster than the dopaminergic modulation term of excitatory connections). If the DA level is too high during learning, the afferent weights can not increase enough since the homeostatic rule impairs learning when the activity of the cell exceeds a threshold. Thus, the lateral connections will not compensate the disappearance of the cortical input: there will be no sustained activity. However, they remain strong enough to propagate activity within the cluster. Therefore, this model can not handle high constant levels of DA during the whole learning process (what would be however unrealistic), but only some increases to high levels for a finite period of time. These transient increases (which are not however phasic bursts) could momentarily signal the behavioural importance of certain objects and favorize their learning, but on the long-term DA should show habituation to these objects.

The sustained activation in this model relies on the reciprocal interactions between excitatory cells. This concept has already been used in the previously cited computational models of working memory in prefrontal cortex (Brunel and Wang, 2001; Chadderdon and Sporns, 2006; Deco and Rolls, 2003; Dreher et al., 2002; Durstewitz et al., 1999). The major differences with most of these models is that in our model these lateral connections are primarily relevant for memory recall and that they adapt to the experience of the system so that the attractors of the network can evolve through time. Another remarkable property is that the cells of a cluster do not need to receive input at the same time: a partial activation is enough to propagate activity and to create sustained activities in the whole cluster. It could be possible that the sustained activities in PRh have no direct purpose but they occur as a side effect of the propagation of activity for memory retrieval.

What do the clusters of cells in PRh exactly represent? We used the term “object” in a very broad sense, as a collection of parts that frequently appear together during learning. This could relate to spatial arrangements of parts of an object (the back, the seat and the feet of a chair, for example) that do not all appear at the same time depending on the point of view to the object, but partly view-invariant cells are already present in IT (Booth and Rolls, 1998). However, When PRh is functional, learning to discriminate a set of visual objects under a certain viewpoint can be easily transferred to the same objects under another viewpoint, whereas this capacity is severely impaired without PRh (Buckley and Gaffan, 1998). Another level of abstraction for PRh is multimodal integration, i.e. linking the visual representation of an object with its tactile information, its sound or the associated action (grasping, pushing, sitting, etc).

A cluster could also represent a subordinate-level category in the sense of: different objects

sharing a sufficient number of sensory features (parts) would be represented by the same cluster. For example, a cluster could be generic for different espresso cups but not mugs, lacking the genericity of the “cup” basic-level category but providing a minimal sensory abstraction. This is coherent with the study by that indicates that PRh is only involved in fine-grained categorization. Such narrow categories could be used as “templates” to guide attention to the corresponding target through feedback connections to the ventral pathway (Hamker, 2005b), as broader categories have been shown to be useless in visual search (Smith et al., 2005).

Our primary aim has been to extend the concept of visual working memory to association areas where the detailed visual properties of an object are stored. Most computational models of working memory make no such distinction and primarily deal with sustained activities in prefrontal cortex. We propose that memory retrieval is achieved through a loop between PRh, basal ganglia and thalamus. PRh receives thalamocortical connections from dorsal and medial geniculate nuclei of the thalamus and in turn projects heavily to the caudate putamen, a part of the main input structure of the basal ganglia, the striatum (Furtak et al., 2007). When a given object has to be retrieved, the basal ganglia can selectively disinhibit the thalamus and therefore favorize the thalamic stimulation of the cluster to be retrieved.

This pathway through the basal ganglia significantly compresses the information encoded in the cerebral cortex and can not represent its rich and detailed representations: as pinpoints, the number of neurons projecting to the striatum is two orders of magnitude greater than the number of striatal neurons (Kincaid et al., 1998). We propose that the basal ganglia acts as a pointer that allows to retrieve the detailed representation when necessary through the disinhibition of thalamus. Similarly, prefrontal cortex is probably not encoding the content of memory, but rather a rule to retrieve this content. In a realistic DMS task, basal ganglia and prefrontal cortex have to learn which object has to be retrieved and which should be forgotten. This work is facilitated by the fact that the exact content of a cluster in PRh does not need to be known by this external loop: stimulating 35% of its cells (or even less for bigger clusters) is sufficient to retrieve its details.

Acknowledgements

This work has been supported by the HA2630/4-1 grant of the German research foundation (Deutsche Forschungsgemeinschaft, DFG).

Appendix: details of the model

All equations described in the *Materials and methods* section are numerized according to the finite difference method, with a timestep of 1 ms. Their evaluation occurs asynchronously: cells

are randomly evaluated and their new activity is immediately used in the rest of the computations, in order to emphasize the competition between neuronal representations (Rougier and Vitay, 2006).

The model is composed of 20×20 excitatory cells and 10×10 inhibitory cells. Excitatory and inhibitory cells are reciprocally connected through gaussian connectivity kernels. We thus defined a distance between cells: let the excitatory cell E_i have coordinates $(x_i, y_i) \in [0..20]^2$ on the map and the inhibitory cell I_j have coordinates $(x_j, y_j) \in [0..10]^2$. The distance $d_{EI}(i, j)$ between the two cells is therefore given by:

$$d_{EI}(i, j) = \sqrt{(x_i - 2 \times x_j)^2 + (y_i - 2 \times y_j)^2}$$

Similarly, the distance $d_{II}(i, j)$ between two inhibitory cells I_i with coordinates $(x_i, y_i) \in [0..10]^2$ and I_j with coordinates $(x_j, y_j) \in [0..10]^2$ is given by:

$$d_{II}(i, j) = \sqrt{(x_i - x_j)^2 + (y_i - y_j)^2}$$

We then define the gaussian connectivity kernels by:

$$W^{IE}(i, j) = -0.12 \times \exp\left(-\left(\frac{d_{EI}(i, j)}{2.5}\right)^2\right)$$

$$W^{EI}(i, j) = 0.3 \times \exp\left(-\left(\frac{d_{EI}(i, j)}{2}\right)^2\right)$$

The connections between two inhibitory cells are given by:

$$W^{II}(i, j) = \begin{cases} 0.02 \times \exp\left(-\left(\frac{d_{II}(i, j)}{5}\right)^2\right) & \text{if } i \neq j \\ 0 & \text{else.} \end{cases}$$

The parameters of Equation 2.1 are the same for each inhibitory cell: $\tau_I = 10$ ms, $K^{EI} = 1.2$ and $\eta_i^I(t)$ is a random value uniformly distributed between -0.1 and 0.1. The parameters of Equation 2.2 are: $\tau_E = 20$ ms, $K^{EE} = 3.0$, $K^{IE} = 3.0$, $K^T = 1.0$ and $\eta_i^E(t)$ a random value uniformly distributed between -0.5 and 0.5. Cortical weights W^C are randomly chosen in the range [0.8, 1.2]. The sigmoidal functions $\sigma^{lat}(x)$, $\sigma^{EE}(x)$, $\sigma^{GABA}(x)$, $\sigma^T(x)$ all have the same shape:

$$\sigma(x) = \frac{1}{1 + \exp(-l \cdot (x - c))} - \frac{1}{1 + \exp(l \cdot c)}$$

2 Sustained activities and retrieval in a computational model of perirhinal cortex

with l and c being: for $\sigma^{lat}(x)$ $c = 0.3, l = 20$; for $\sigma^{EE}(x)$ $c = 0.3, l = 20$; for $\sigma^{GABA}(x)$ $c = 0.5, l = 10$; for $\sigma^T(x)$ $c = 0.5, l = 10$. The transfer function $f(x)$ is defined as follows:

$$f(x) = \begin{cases} 0 & \text{if } x < 0 \\ x & \text{if } 0 \leq x \leq 1 \\ \frac{0.5}{1 + \exp(-10.0 \cdot (x-1))} + 0.75 & \text{if } x > 1 \end{cases}$$

The parameters of Equation 2.3, Equation 2.5 and Equation 2.6 are: $\tau_W = 50000$ ms, $\tau_\alpha = 50000$ ms, $K_\alpha = 100$, $\tau_H = 100$ ms, $K_H = 200$, $E_{max} = 1.0$.

3 A computational model of basal ganglia and its role in memory retrieval in rewarded visual memory tasks

Abstract

Visual working memory tasks involve a network of cortical areas such as inferotemporal, medial temporal and prefrontal cortices. We suggest here to investigate the role of the basal ganglia in the learning of delayed rewarded tasks through the selective gating of thalamocortical loops. We designed a computational model of the visual loop linking the perirhinal cortex, the basal ganglia and the thalamus, biased by sustained representations in prefrontal cortex. This model learns concurrently different delayed rewarded tasks that require to maintain a visual cue and to associate it to itself or to another visual object to obtain reward. The retrieval of visual information is achieved through thalamic stimulation of the perirhinal cortex. The input structure of the basal ganglia, the striatum, learns to represent visual information based on its association to reward, while the output structure, the substantia nigra pars reticulata, learns to link striatal representations to the disinhibition of the correct thalamocortical loop. In parallel, a dopaminergic cell learns to associate striatal representations to reward and modulates learning of connections within the basal ganglia. The model provides testable predictions about the behavior of several areas during such tasks, while providing a new functional organization of learning within the basal ganglia, putting emphasis on the learning of the striatonigral connections as well as the lateral connections within the substantia nigra pars reticulata. It suggests that the learning of visual working memory tasks is achieved rapidly in the basal ganglia and used as a teacher for feedback connections from prefrontal cortex to posterior cortices.

3.1 Introduction

During object-based visual search, target templates stored in visual working memory (WM) can bias attentional processing in visual areas to favorize the relevant objects (Desimone and Duncan, 1995; Woodman and Luck, 2007). Visual WM can be investigated through a number of different tasks in rats, primates or humans, among which change detection, recall procedures, delayed matching to sample (DMS), delayed nonmatching to sample (DNMS) or delayed pair-association (DPA) tasks are frequently used. These experiments have allowed to shed light

3 *A computational model of basal ganglia and memory retrieval*

on the psychophysical mechanisms involved in visual WM (Luck and Vogel, 1997) as well as to delineate the neural substrates subserving these functions (Ranganath, 2006). Visual WM has several computational aspects: encoding of the relevant items (potentially in an abstract manner), maintenance of the items through time in face of distractors, retrieval of the sensory content of the item, abstraction of the underlying rule. It faces both a structural credit assignment problem (which item to store and retrieve) and a temporal assignment problem (how to link encoding in WM with the delayed delivery of reward).

Specific attention has been directed towards the prefrontal cortex which is well-known to be involved in WM maintenance and manipulation in various modalities (Funahashi et al., 1989; Fuster and Alexander, 1971). Prefrontal lesions do not totally eliminate visual WM but impairs the ability to maintain it during long delays or in front of distractors (D'Esposito et al., 2006; Petrides, 2000). Neurons in PFC exhibit robust object-specific sustained activities during the delay periods of visual WM tasks like DMS or DNMS (Miller et al., 1996). However the informational content of WM-related activities in PFC is still unclear (Romanski, 2007). Inferotemporal (IT) neurons have been shown to encode object-specific information (Nakamura et al., 1994) as they are located at the end of the ventral visual pathway (Ungerleider and Mishkin, 1982). They have been shown to be critical for visual WM (Fuster et al., 1981; Petrides, 2000) and also exhibit sustained activation during the delay period, even if their responses can be attenuated or cancelled by intervening distractors (Miller et al., 1993a), what can be partly explained by feedback cortico-cortical connections originating from PFC (Fuster et al., 1985; Webster et al., 1994).

The medial temporal lobe (MTL, composed of perirhinal - PRh -, entorhinal - ERh - and parahippocampal - PH - cortices) also plays an important also not essential role in visual WM. Compared to IT, a greater proportion of neurons in PRh and ERh exhibit sustained activation during the delay-period (Nakamura and Kubota, 1995) and are robust to distractors (Suzuki et al., 1997). They are especially crucial when visual objects are novel and complex (Ranganath and D'Esposito, 2005). Particularly, PRh cells are more strongly involved in visual recognition when it requires visual WM processes (Lehky and Tanaka, 2007). They are reciprocally connected with IT neurons and can provide them with information about novelty or category membership since they can rapidly encode relationship between visual features (Murray and Bussey, 1999; Rolls, 2000), as well as the association of objects to reward (Mogami and Tanaka, 2006). Ranganath (2006) provided a complete account of the functional relationship between IT, PFC and MTL in visual WM. He considers that the visual aspects of the remembered object are maintained in the ventral pathway at various levels of complexity (low-level features in V1 or V4, object-related representations in IT) through sustained activation of cells. Top-down activation of these neurons by MTL would provide them with information about novelty and help to reconstruct a coherent mental image of the objects composing the visual scene, thanks to the link between MTL and hippocampus. Top-down activation by PFC helps the ventral stream to maintain representations in face of distraction and also allows stimulus-stimulus associations (like in the delayed pair-association task) in IT (Gutnikov et al., 1997).

A structure that is absent in this scheme but that is nevertheless very important in visual WM is the basal ganglia (BG), a set of nuclei in the basal forebrain. Human patients with BG disorders (such as Parkinson's disease) show strong deficits in delayed response tasks (Partiot et al., 1996). Several experiments have recorded visual WM-related activities in various structures composing the BG, especially the striatum (STR) (Chang et al., 2007; Hikosaka et al., 1989; Lewis et al., 2004; Mushiake and Strick, 1995). Almost all cortical areas send projections to the input nuclei of BG (STR and the subthalamic nucleus STN), while the output nuclei of BG (the internal segment of globus pallidus GPi and the substantia nigra pars reticulata SNr) tonically inhibit various thalamic nuclei, allowing selective modulation of corticothalamic loops (Parent and Hazrati, 1995b). The BG are organized through a series of closed loops, which receive inputs from segregated cortical regions and project back to them quite independently (see Haber (2003) for a review). The number and functional domain of these loops is still an open issue (Alexander et al., 1986; Lawrence et al., 1998; Nambu et al., 2002), but two of them are of particular relevance for our model. The executive loop involves the dorsolateral part of PFC (dlPFC), the head of the caudate nucleus (a region of the dorsal striatum), GPi-SNr and the mediodorsal nuclei of thalamus (MD). The structures involved in this loop have all been shown to be involved in WM processes in various modalities and provide a basis for the maintenance and manipulation of items in cognitive tasks (see Frank et al. (2001) for a review about the functional requirements of WM). The visual loop involves the inferotemporal and extrastriate occipital cortices, the body and tail of the caudate nucleus, SNr and the ventral-anterior nucleus of the thalamus (VA) (Middleton and Strick, 1996; Seger, 2008). This loop is particularly involved in visual categorization and visual discrimination, but also sends output to premotor areas to link category learning with appropriate behavior. In addition to IT neurons, the body of the caudate nucleus is involved in visual WM tasks, what suggests a role of the entire visual loop in visual WM (Levy et al., 1997).

What remains unknown is how these two loops can interact together in order to subserve visual WM functions in the context of efficient behavior. Previous models have particularly addressed the updating of working memory content as part of the executive BG loop (e.g. Brown et al. (1999) or O'Reilly and Frank (2006)). We here focus on how such memory content can be used to bias the visual loop allowing for a goal-directed memory recall in the context of rewarded tasks such as DMS, DNMS or DPA. Among the different mechanisms by which two BG loops can interact, we focus on the overlapping projection fields of cortical areas: a cortical area sends principally projections to a limited region of the striatum, but its axons send collaterals along the surface of the striatum. In particular, the body of the caudate, which is part of the visual loop and principally innervated by inferotemporal projection neurons, also receives connections from the dorsolateral prefrontal cortex (Selemon and Goldman-Rakic, 1985). This model is thus composed of the visual loop linking PRh with BG and the thalamus, while the executive loop is reduced to sustained activation in dlPFC which projects on the region of the striatum belonging to the visual loop. The model is alternatively presented with specific combinations of visual cues and tasks symbols that allow the system to perform actions leading to the delivery of reward (as proposed by Gisiger and Kerszberg (2006)). Our emphasis is on

the reward-modulated self-organization of connectivity between distributed populations. The model provides hypotheses about how sustained representations in dlPFC can bias learning in the visual loop so that object-related activities in the ventral visual pathway can be retrieved through thalamic stimulation in the context of a particular cognitive task to provide anticipatory top-down signals for the visual system, as observed physiologically (Naya et al., 2003; Takeda et al., 2005). In particular, self-organization in the model relies on the competitive selection of relevant cortical representations in the output structures of the BG.

3.2 Material and Methods

3.2.1 Architecture of the model

Each structure used in this model is composed of a set of dynamical neurons, whose membrane potential is governed by a time-dependent differential equation and transformed into a mean firing rate through a non-linear transfer function. These neurons therefore exchange a real instantaneous value instead of spikes, as it saves considerably computational costs and allows to use efficient learning rules that are not yet available for spiking neurons. Although we do not capture some biophysical details, this paradigm is sufficiently complex to show the emergence of dynamic behaviors through the interaction of distributed computational units (Rougier, 2009). The differential equation that rules the evolution of the activity of each neuron is discretized according to the Euler method with a time-step of 1 ms and is evaluated asynchronously to allow stochastic interactions between functional units (Rougier and Vitay, 2006).

Biological details gave us some insights on the choice of certain parameters, such as the time constants for the different neurons, as we know for example that striatal cells are faster than cortical cells (Plenz and Aertsen, 1996). Other parameters have been set to bring the model into a functionally meaningful range. Control simulations showed that minor variations on their values do not change qualitatively the results presented here.

The architecture of the model is depicted in Figure 3.1 A. Visual inputs are temporally represented in the perirhinal cortex (PRh), each cell firing for a particular visual object. These perirhinal representations project to the prefrontal cortex (dlPFC) where they are actively maintained for the duration of the task. These sustained activations in dlPFC are artificially controlled by a set of gating signals, leaving unaddressed the temporal credit assignment problem. PRh and dlPFC both project extensively to the caudate nucleus (CN), which learns to represent them in an efficient manner according to the task requirements. Depending on reward delivery in the timecourse of learning, each active striatal cell learns to integrate perirhinal and prefrontal information in a competitive manner due to inhibitory lateral connections. This mechanism leads to the formation through learning of clusters of striatal cells that represent particular combinations of cortical information depending on their association to reward. These CN cells send

inhibitory projections to the SNr, whose cells are tonically active and learn to become selective for specific striatal patterns. This learning between CN and SNr is also dependent on reward delivery. Learning of the lateral connections between SNr cells additionally allows to limit the number of simultaneously inhibited SNr cells. These cells in SNr tonically inhibit thalamic cells (VA) which have reciprocal connections with PRh. The connections from SNr to VA and between VA and PRh are not learned but focused (one-to-one connection pattern), meaning that the inhibition of one SNr cell leads to the thalamic stimulation of a unique cell in PRh. A dopaminergic cell (SNc) receives information about the delivered reward (R) and learns to associate it with striatal activities. Its signal modulates learning at the connections between cortical areas (PRh and dIPFC) and CN, between CN and SNr, as well as within SNr. We now present in detail each structure and the differential equations followed by their neurons.

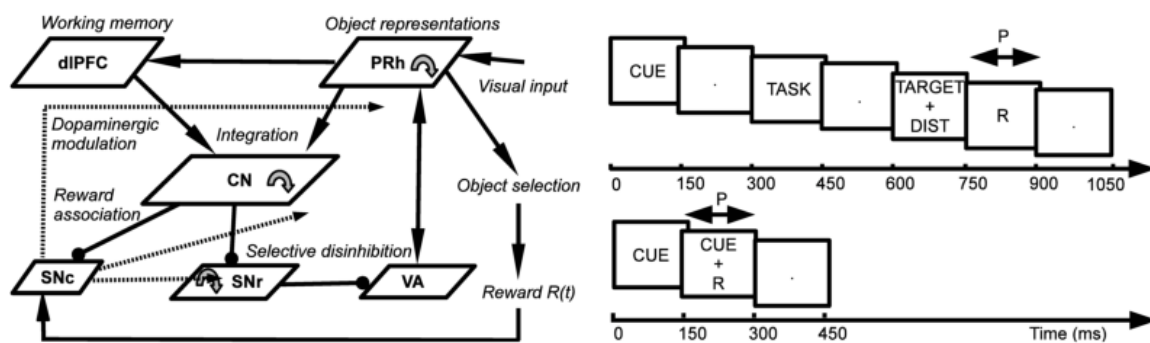


Figure 3.1: (A) Architecture of the model. Pointed arrows denote excitatory connections and rounded arrows denote inhibitory ones. Circular arrows within an area represent lateral connections between the cells of this area. (B) Timecourse of the visual inputs presented to the network. Top: rewarded trials like DMS, DNMS or DPA. Bottom: delay conditioning.

3.2.2 Perirhinal cortex

The input of our model is a high-level visual area with mnemonic functions which is able to bias processing in the ventral visual stream. In general, the area TE of the inferotemporal cortex is a potential candidate, but we particularly focused on PRh, as it has been shown to be preferentially involved in recognition tasks that require visual WM (Lehky and Tanaka, 2007). We previously designed a detailed computational model of PRh that is able to learn object-related representations in clusters of cells based on partial information (Vitay and Hamker, 2008). These clusters linked through lateral connections are able to exhibit sustained activation when the dopamine (DA) level in the network is within an optimal range. The visual information that they contain can also be easily retrieved through a partial stimulation coming from the thalamus. We hypothesize that this memory retrieval through thalamic stimulation under an accurate level of DA can be a basis for the guidance of visual search.

Here, we reduced the size of PRh to δ cells, each of them representing a particular object that

3 A computational model of basal ganglia and memory retrieval

is presented to the network (see Section 3.2.8 for the description of these objects). In our previous model, PRh contained hundreds of cells and each object was represented by a cluster of different cells. Each cell i has a membrane potential $m_i(t)$ and an instantaneous firing rate $u_i^{\text{PRh}}(t)$ which are governed by the following equations:

$$\tau \cdot \frac{dm_i(t)}{dt} + m_i(t) = V_i(t) + W_i^{\text{VA}} \cdot u_i^{\text{VA}}(t) + \sum_{j \in \text{PRh}} W_{i,j}^{\text{PRh}} \cdot u_j^{\text{PRh}}(t) + \epsilon(t) \quad (3.1)$$

$$u_i^{\text{PRh}}(t) = (m_i(t))^+$$

where $\tau = 20$ ms is the time constant of the cell, $V_i(t)$ its visual input (see Section 3.2.8) and $W_i^{\text{VA}} = 0.5$ the weight of a connection coming from the corresponding thalamic cell whose firing rate is $u_i^{\text{VA}}(t)$. $\epsilon(t)$ is an additional noise whose value varies uniformly at each time-step between -0.3 and 0.3 . The transfer function used for perirhinal cells is simply the positive part of the membrane potential $()^+$. Each perirhinal cell additionally receives inhibitory lateral connections from the seven neighboring perirhinal cells with a fixed weight of $W_{i,j}^{\text{PRh}} = -0.3$ to induce competition between the perirhinal cells.

3.2.3 Dorsolateral prefrontal cortex

We do not model explicitly the executive loop and rather use a very simple WM representation in dlPFC, including mechanisms of updating and resetting. Future work will address these questions in the context of WM gating in the executive loop (Frank et al., 2001; Gruber et al., 2006). The dlPFC is here composed of 8 cells which keep track of activity in PRh through temporal integration:

$$\tau \cdot \frac{dm_i(t)}{dt} = G(t) \cdot W_i^{\text{PRh}} \cdot (u_i^{\text{PRh}}(t) - 0.5)^+$$

$$u_i^{\text{dlPFC}}(t) = \begin{cases} 0 & \text{if } m_i(t) < 0 \\ m_i(t) & \text{if } 0 \leq m_i(t) \leq 1 \\ 1 & \text{if } m_i(t) > 1 \end{cases} \quad (3.2)$$

where $\tau = 10$ ms is the time constant of the cell and $G(t)$ a gating signal allowing the entry of an item in working memory. Each dlPFC cell receives only one connection from a PRh cell with the weight $W_i^{\text{PRh}} = 1.0$. As soon as the activity of a PRh cell exceeds 0.5, it is integrated in the corresponding prefrontal cell, whose activity saturates to a maximum value of 1.0 thanks to the transfer function and stays at this value even if the perirhinal stimulation ends. The gating signal $G(t)$ is manually set to a value of 1.0 when objects have to be maintained in WM and

to a value of 0.0 otherwise. The activity of the prefrontal cells is manually reset to zero at the end of a trial.

3.2.4 Ventral-anterior thalamus

The portion of the ventral-anterior nucleus of the thalamus we consider here is represented by eight cells that are reciprocally connected with PRh. Its 8 cells send and receive a connection with only one perirhinal cell, forming segregated thalamocortical loops. In a more biologically detailed model, we would have to take into account the difference in the number of cells between VA and PRh, as well the more diffuse pattern of connections from thalamus to cortex. However, this simplification is justified by our previous detailed model of PRh, where we have shown that a thalamic cell can activate a functional cluster of cells representing a single object (Vitay and Hamker, 2008). The membrane potential and firing rate of these thalamic cells are ruled by the following equations:

$$\begin{aligned} \tau \cdot \frac{dm_i(t)}{dt} + m_i(t) &= W_i^{\text{PRh}} \cdot u_i^{\text{PRh}}(t) + W_i^{\text{SNr}} \cdot u_i^{\text{SNr}}(t) + M + \epsilon(t) \\ u_i^{\text{VA}}(t) &= (m_i(t))^+ \end{aligned} \quad (3.3)$$

where $\tau = 15$ ms and $M = 0.8$. In addition to the connection coming from one PRh cell with a weight of $W_i^{\text{PRh}} = 0.5$, a thalamic cell also receives an inhibitory connection from one cell of SNr with a weight of $W_i^{\text{SNr}} = -0.7$.

3.2.5 Caudate nucleus

The caudate nucleus of the striatum learns to represent the cortical information in PRh and dIPFC in an efficient manner based on dopaminergic signaling of reward-related information in SNc. Although some evidences suggest that the DA level can even influence the firing rate of striatal cells (Nicola et al., 2000), we here exclusively focus on the effect of DA on the synaptic learning of corticostriatal connections (Di Filippo et al., 2009). The striatum is mostly composed of medium spiny neurons that integrate cortical information and directly inhibit several structures such as the substantia nigra or the globus pallidus. These cells have also lateral inhibitory connections, either directly or through fast-spiking interneurons (Tepper et al., 2008). CN contains here 64 cells ruled by the following equations:

$$\begin{aligned} \tau \cdot \frac{dm_i(t)}{dt} + m_i(t) &= \sum_{j \in \text{Cx}} W_{i,j}^{\text{Cx}}(t) \cdot u_j^{\text{Cx}}(t) + \sum_{j \in \text{CN}} W_{i,j}^{\text{CN}} \cdot u_j^{\text{CN}}(t) + M + \epsilon(t) \\ u_i^{\text{CN}}(t) &= (m_i(t))^+ \end{aligned} \quad (3.4)$$

3 A computational model of basal ganglia and memory retrieval

where $\tau = 10$ ms and $M = 0.3$. Each striatal cell receives inhibitory lateral connections from the 63 other striatal cells with a weight of $W_{i,j}^{\text{CN}} = -0.2$. The corticostriatal connections $W_{i,j}^{\text{Cx}}(t)$ coming either from PRh or dIPF_c are learned according to a homeostatic covariance learning rule:

$$\eta \cdot \frac{dW_{i,j}^{\text{Cx}}(t)}{dt} = (\text{DA}(t) - \overline{\text{DA}}) \cdot (u_i^{\text{CN}}(t) - \overline{\text{CN}})^+ \cdot (u_j^{\text{Cx}}(t) - \overline{\text{Cx}}) - \alpha_i(t) \cdot ((u_i^{\text{CN}}(t) - \overline{\text{CN}})^+)^2 \cdot W_{i,j}^{\text{Cx}}(t)$$

where $\eta = 100$ is the rate of learning, $\text{DA}(t)$ represents the synaptic level of DA (considered equal to the activity of the SNc cell), $\overline{\text{DA}}$ the baseline activity of the SNc cell, $u_i^{\text{CN}}(t)$ the firing rate of the striatal cell, $\overline{\text{CN}}$ the mean firing rate of the CN cells, $u_j^{\text{Cx}}(t)$ the firing rate of the cortical cell, $\overline{\text{Cx}}$ the mean firing rate of the considered cortical area and $\alpha_i(t)$ a cell-dependent regularization factor. The weights are randomly initialized with a value between -0.1 and 0.1 .

The first part of the right term of Equation 3.5 is a classical Hebbian learning rule (correlation between the activities of the presynaptic and postsynaptic cells) modulated by the DA level. The positive function applied to the striatal activity ensures that only the cells which are significantly activated compared to the rest of the population will update their selectivity for cortical patterns. The exact influence of DA on corticostriatal learning is still a matter of debate and depends on the type of dopaminergic receptor (D1 or D2) involved, the state of the membrane potential of the striatal cell ("up" and "down" states) and on the cortical patterns (Calabresi et al., 2007). We do not model in detail these mechanisms and consider that a phasic burst of DA (transient activity of the SNc cell above its baseline) globally favors long-term potentiation (LTP) of corticostriatal synapses, while DA depletion (activity below baseline) globally induces long-term depression (LTD) of the same synapses (Reynolds and Wickens, 2000).

The second part of the right term of Equation 3.5 performs a homeostatic regularization of the corticostriatal synapses. Its shape is similar to the classical Oja learning rule (Oja, 1982) to avoid an infinite increase of the weight values, but the difference is that the regularization factor $\alpha_i(t)$ is not fixed but varies with the activity of the cell (Vitay and Hamker, 2008). Homeostatic plasticity allows cells to adapt their learning behavior to ensure stability (Turrigiano and Nelson, 2004). In our case, we want to avoid that the striatal cells fire too much in order to save energy, by scaling down proportionally the weights of all the connections. $\alpha_i(t)$ therefore becomes positive when the firing rate of the cell exceeds a defined threshold u^{MAX} :

$$\tau \cdot \frac{d\alpha_i(t)}{dt} + \alpha_i(t) = (u_i^{\text{CN}}(t) - u^{\text{MAX}})^+$$

{eq-ficn:alphanacc}

with $\tau = 20$ ms and $u^{\text{MAX}} = 1.0$. In addition to dynamically and locally normalizing the afferent connections to the cells, this homeostatic regularization term also allows to sharpen

the selectivity of the cell. Homeostatic plasticity has been observed in the nucleus accumbens, a part of the striatum (Ishikawa et al., 2009).

3.2.6 Substantia nigra pars compacta

The dopaminergic cells contained in SNc have the property to respond to the delivery of unexpected rewards by a phasic burst of activity above baseline (Mirenowicz and Schultz, 1994). However, in conditioning tasks, the amplitude of this response to primary rewards gradually decreases through learning and is transferred to the appearance of the conditioned stimulus (Pan et al., 2005). In addition, when reward is omitted, these dopaminergic cells show a phasic depletion of activity (below baseline) at the time reward was expected (Schultz et al., 1997). Several theories have tried to explain this behavior related to reward expectation, including an analogy with the error signal of the temporal difference (TD) algorithm of reinforcement learning (Suri and Schultz, 1999) or more biologically detailed models (Brown et al., 1999; O'Reilly et al., 2007). The TD analogy considers that DA phasic activation or depletion at the time of reward delivery or conditioned stimulus appearance are due to a unique mechanism. The more biologically detailed approaches contrarily highlight the role of afferent structures in the different components of this behavior: the phasic activation to primary rewards may be due to excitatory connections coming from the pedunculopontine tegmental nucleus, and its amplitude is gradually decreased by the learning of the reward expectation through inhibitory connections coming from the striatum. In these models, the DA phasic activation for the appearance of a conditioned stimuli is provoked by different mechanisms than for the delivery of primary rewards. The depletion in DA activity when reward is omitted is controlled by an external timing mechanism, presumably computed by an intracellular calcium-dependent mechanism in striatal cells (Brown et al., 1999) or by an external signal computed in the cerebellum (O'Reilly et al., 2007). We followed the assumptions of these models, but did not model explicitly this timing signal.

We used only one cell in SNc, which receives information about the received reward $R(t)$ and learns to predict its association with striatal representations through learnable inhibitory connections. The activity of this cell is ruled by the following equations:

$$\tau \cdot \frac{dm(t)}{dt} + m(t) = R(t) + P(t) \cdot \sum_{j \in \text{CN}} W_j^{\text{CN}}(t) \cdot u_j^{\text{CN}}(t) + \overline{\text{DA}} \quad (3.5)$$

$$\text{DA}(t) = (m(t))^+$$

where $\tau = 10$ ms, $\overline{\text{DA}} = 0.5$. The reward $R(t)$ (set to 0.5 when received, 0.0 otherwise) and the timing of its occurrence $P(t)$ (set to 1.0 when expected, 0.0 otherwise) are external to the neuronal model. When reward is delivered, $R(t)$ will drive the activity of the cell above its baseline but this effect will be reduced by the learning of the inhibitory connections between the striatum and SNc. When reward is expected but not delivered, the striatal inhibition will

force the cell to exhibit an activity below baseline. The connections between CN and SNc are learned according to the following rule:

$$\eta \cdot \frac{dW_j^{\text{CN}}(t)}{dt} = -f(\text{DA}(t) - \overline{\text{DA}}) \cdot (u_j^{\text{CN}}(t) - \overline{\text{CN}})^+ \quad (3.6)$$

$$f(x) = \begin{cases} x & \text{if } x > 0 \\ 5 \cdot x & \text{else.} \end{cases} \quad (3.7)$$

where $\eta = 10000$. The weights are initialized with a value of 0.0, so that striatal representations have initially no association to reward. When $\text{DA}(t)$ is above baseline (reward has been delivered), the inhibitory connections are further decreased, which means that the striatal representation increases its associative value. When $\text{DA}(t)$ is below baseline (reward has been omitted), the same striatal representation decreases its association to reward. This dopaminergic signal is used to modulate learning in CN and SNr.

3.2.7 Substantia nigra pars reticulata

The output nuclei of the BG (GPi and SNr) have the particularity to be tonically active (with an elevated firing rate of 25 Hz at rest and pause in firing when inhibited by striatal activity). They send inhibitory projections to ventral thalamic nuclei as well as various subcortical structures such as the superior colliculi. The SNr cells are selective for particular motor programs and can disinhibit various thalamocortical loops (Chevalier and Deniau, 1990). Their selectivity is principally due to the inhibitory connections originating from the striatum and GPe, but they also receive excitatory inputs from the subthalamic nucleus. However, the SNr cells also tonically inhibit each other, with a particular connectivity pattern suggesting they may subserve an important functional role (Mailly et al., 2003). When a SNr cell is inhibited by striatal activation, it stops inhibiting the other SNr cells, who consequently increase their firing rate and inhibit more strongly their efferent thalamic cells. Inhibitory connections within SNr may therefore help focusing on the disinhibition of the desired thalamocortical loop by suppressing the competing other loops (Gulley et al., 2002). Instead of considering the inhibitory effect of high nigral activity, we modeled this competition between SNr cells by an excitatory effect of low nigral activity, what is functionally equivalent. The 8 cells in SNr evolve according to the following equations:

$$\tau \cdot \frac{dm_i(t)}{dt} + m_i(t) = \sum_{j \in \text{CN}} W_{i,j}^{\text{CN}}(t) \cdot u_j^{\text{CN}}(t) + \sum_{j \in \text{SNr}} W_{i,j}^{\text{SNr}}(t) \cdot (M - u_j^{\text{SNr}}(t))^+ + M + \epsilon(t)$$

$$u_i^{\text{SNr}}(t) = \begin{cases} 0 & \text{if } m_i(t) < 0 \\ m_i(t) & \text{if } 0 \leq m_i(t) \leq M \\ \frac{1}{1 + e^{-\frac{m_i(t)-M}{20}}} + 0.5 & \text{if } m_i(t) > M \end{cases}$$

where $\tau = 10$ ms, $M = 1.0$ and $\epsilon(t)$ is an additional noise randomly picked between -0.3 and 0.3 . The excitatory connections from neighboring SNr cells are active when their corresponding activity is below baseline. The transfer function ensures that activities exceeding M saturate to a value of 1.5 with a sigmoidal shape. The inhibitory connections originating in CN are learned according to an equation similar to Equation 3.5. Even if little is known about synaptic learning in SNr, the strong dopaminergic innervation of nigral cells (Ibañez-Sandoval et al., 2006) makes it reasonable to hypothesize that DA modulates the learning of striatonigral connections in a way similar to the corticostriatal ones.

$$\eta^{\text{inh}} \cdot \frac{dW_{i,j}^{\text{CN}}(t)}{dt} = f(\text{DA}(t) - \overline{\text{DA}}) \cdot g(\overline{\text{SNr}} - u_i^{\text{SNr}}(t)) \cdot (u_j^{\text{CN}}(t) - \overline{\text{CN}})^+ - \alpha_i^{\text{inh}}(t) \cdot ((\overline{\text{SNr}} - u_i^{\text{SNr}}(t))^+)^2 \cdot W_{i,j}^{\text{SNr}}(t) \quad (3.8)$$

$$f(x) = \begin{cases} x & \text{if } x > 0 \\ 10 \cdot x & \text{else.} \end{cases} \quad (3.9)$$

$$g(x) = \frac{1}{1 + e^{-\frac{x}{20}}} - 0.5 \quad (3.10)$$

$$\tau_\alpha^{\text{inh}} \cdot \frac{d\alpha_i^{\text{inh}}(t)}{dt} + \alpha_i^{\text{inh}}(t) = K_\alpha^{\text{inh}} \cdot (m_i(t))^-$$

where $\eta^{\text{inh}} = 500$, $\overline{\text{SNr}}$ is the mean activity of all the cells in SNr, $\tau_\alpha^{\text{inh}} = 10$ ms, $K_\alpha^{\text{inh}} = 2.0$ and $()^-$ is the negative part of the membrane potential. The weights are randomly initialized between -0.15 and -0.05 and later restricted to negative values. DA depletion (below baseline) has been given a greater influence in the learning rule through the $f()$ function, because at the beginning of learning DA depletion has a much smaller amplitude than the DA bursts. Contrary to the classical Hebbian learning rule, the postsynaptic activity influences here the learning rule through a sigmoidal function $g()$, what makes it closer to the BCM learning rule (Bienenstock et al., 1982). Similarly to BCM, there is a threshold (here the mean activity of the

nuclei) on the postsynaptic activity that switches the learning rule from LTD to LTP. This learning rule is meant to increase the selectivity of each SNr cell regarding to its neighbors as well as the signal-to-noise ratio in the population. Another way for the nigral cells to increase their selectivity is competition through their lateral connections. There are two different learning rules used depending on whether the DA level is above or below baseline. When DA is above its baseline, the lateral connections are updated according to the following equation:

$$\eta^{\text{lat}} \cdot \frac{dW_{i,j}^{\text{SNr}}(t)}{dt} = (\text{DA}(t) - \overline{\text{DA}}) \cdot (\overline{\text{SNr}} - u_i^{\text{SNr}}(t))^+ \cdot (\overline{\text{SNr}} - u_j^{\text{SNr}}(t))^+ - \alpha_i^{\text{lat}}(t) \cdot ((\overline{\text{SNr}} - u_i^{\text{SNr}}(t))^+)^2 \cdot W_{i,j}^{\text{SNr}}(t) \quad (3.11)$$

where $\eta^{\text{lat}} = 500$. The weights are initially set to 0.0. This rule is similar to a classical anti-Hebbian learning, as it favors the competition between two cells when they frequently have simultaneously low firing rates. In the case of a DA depletion, an important feature of the model is that the symmetry of the lateral connections between two inhibited cells has to be broken. DA depletion has then a punishing effect on the most inhibited cells, which will later receive much more excitation from previously moderately inhibited cells:

$$\eta^{\text{lat}} \cdot \frac{dW_{i,j}^{\text{SNr}}(t)}{dt} = (\overline{\text{DA}} - \text{DA}(t)) \cdot \sqrt{(\overline{\text{SNr}} - u_i^{\text{SNr}}(t))^+} \cdot (\overline{\text{SNr}} - u_j^{\text{SNr}}(t))^+ - \alpha_i^{\text{lat}}(t) \cdot ((\overline{\text{SNr}} - u_i^{\text{SNr}}(t))^+)^2 \cdot W_{i,j}^{\text{SNr}}(t) \quad (3.12)$$

In both cases, two simultaneously inhibited cells will increase their reciprocal lateral connections. However, in the case of DA depletion, the square root function applied to the postsynaptic activity breaks the symmetry of the learning rule and the most inhibited cell will see its afferent lateral connections relatively more increased than the other cells. Thus, the inhibited cells which won the competition through lateral connections but provoked a DA depletion will be more likely to loose competition at the next trial. The effect of these asymmetric learning rules will be presented in section Section 3.3.3, where we will show that they are able to eliminate distractors. Both learning rules use the same equation for the updating of the regularization factor:

$$\tau_{\alpha}^{\text{lat}} \cdot \frac{d\alpha_i^{\text{lat}}(t)}{dt} + \alpha_i^{\text{lat}}(t) = K_{\alpha}^{\text{lat}} \cdot (m_i(t) - M)^+ \quad (3.13)$$

where $\tau_{\alpha}^{\text{lat}} = 10$ ms and $K_{\alpha}^{\text{lat}} = 1.0$.

3.2.8 Experiments

In order to test the ability of our model to perform visual WM tasks, we focused on three classical experimental paradigms: the delayed matching-to-sample (DMS), the delayed nonmatching-

to-sample (DNMS) and the delayed pair-association (DPA) tasks. These three tasks classically consist in presenting to the subject a visual object (called the cue), followed after a certain delay by an array of objects, including a target towards which a response should be made (either a saccade or a pointing movement or a button press). In DMS, the target is the same object as the cue; in DNMS, the target is the object that is different from the cue; in DPA, the target is an object artificially but constantly associated to the cue. These three tasks are known to involve differentially IT, MTL, PFC and BG (Chang et al., 2002; Elliott and Dolan, 1999; Sakai and Miyashita, 1991).

Similarly to the mixed-delayed response (MDR) task of Gisiger and Kerszberg (2006), we want our model to acquire knowledge about contextual information, allowing it to learn concurrently these three tasks with the same cued visual objects. We therefore need to provide the network with a symbol specifying which task has to be performed. The meaning of this symbol is however initially not known by the model and must be acquired through the interaction within the tasks. The top part of Figure 3.1 b shows the time course of the visual inputs presented to the network during a trial. Each trial is decomposed into periods of 150 ms. During the first period, a cue is presented to the network, followed by a delay period without visual stimulation. A visual object representing which task to perform (DMS, DNMS or DPA) is then presented, followed by the same delay period. During this presentation phase, the signal $G(t)$ in Equation 3.2 is set to 1.0 to allow the sustained activation in dIPFC of these two objects.

In the choice period, two objects are simultaneously presented to the network: the target (whose identity is defined by the cue and the task symbol) and a distractor chosen randomly among the remaining cues. At the end of this period, the response of the network is considered to be performed, and reward is given accordingly through a probabilistic rule during the following reward period. For the entire duration of this reward period, the signal $R(t)$ in Equation 3.5 is set to 0.5 if reward is given and to 0.0 otherwise. $P(t)$ is set to 1.0, denoting that reward is expected to occur. This reward period is followed by another delay period, the activities in dIPFC being manually reset to their baseline, allowing the network to go back to its resting state before performing a new trial.

In these experiments, we use four different cues (labelled A, B, C and D) and three task symbols (DMS, DNMS and DPA) that stimulate each a different cell in PRh. The corresponding cells will therefore be successively activated according to the timecourse of the trial described on the top part of Figure 3.1 B. In the Results section, we will only consider subsets of combinations of cues and tasks. For example, we define DMS-DNMS_AB as a combination of four different trials: A followed by DMS (A+DMS), A followed by DNMS (A+DNMS), B followed by DMS (B+DMS) and B followed by DNMS (B+DNMS). These four different trials are randomly interleaved during the learning period. In the DMS trials, the target of the task is the same as the cue, the distractor being chosen in the remaining possible cues. In the DNMS trials, the target is the object that is different from the cue. In the DPA task, the target is an object artificially associated to the cue. In DMS-DPA_AB, the target of the trial A+DPA is C and the one of B+DPA is D.

Each PRh cell is stimulated by its corresponding visual object by setting the signal $V_i(t)$ in

3 A computational model of basal ganglia and memory retrieval

Equation 3.1 to a value of 1.0 during the whole period. In the choice period, $V_i(t)$ is limited to 0.5 for both cells (to mimic competition in the lower areas). To determine the response made by the system, we simply compare the activities of the two stimulated PRh cells at the end of the choice period. If the activity of the cell representing the target is greater than for the distractor, we hypothesize that this greater activation will feed back in the ventral stream and generate an attentional effect that will guide a saccade toward the corresponding object (Hamker, 2004a; Hamker, 2005b). We assume that this selection is noisy, what is modeled by introducing a probabilistic rule for the delivery of reward that depends on the difference of PRh activity for the two presented stimuli.

If we note u^{target} the activity of the PRh cell representing the target at the end of the choice period and u^{dist} the activity of the cell representing the distractor, the signal $R(t)$ in Equation 3.5 has the following probability to be delivered during the reward period:

$$\mathcal{P}(R) = 0.5 + u^{\text{target}} - u^{\text{dist}} \quad (3.14)$$

This probability is of course limited to values between 0.0 and 1.0. When the activities of the two cells are equal, reward is delivered randomly, as we consider that a saccade has been performed randomly towards one of the two objects, as the feedback from PRh to the ventral pathway is not sufficiently distinct to favorize one of the two targets. When the activity of the target cell becomes relatively higher, the probability of executing the correct saccade and receiving reward is linearly increased. When reward is delivered, the signal $R(t)$ has a value of 0.5 during the whole reward period, whereas it is set to 0.0 otherwise. We do not consider here the influence of rewards with different amplitudes.

In delay conditioning, reward is delivered randomly with a fixed probability during the presentation of a visual object (called X). The timecourse of this task is depicted on the bottom part of Figure 3.1 B. This task is described in Section 3.3.5 to study the effect of the probability of reward delivery on striatal representations and reward prediction in SNc.

In Section 3.3.4, we will study the influence of the number of cells in SNr on the performance of the network. While this number is equal to 8 in the previous experiments, we vary it here from 6 to 16. When the number of cells in SNr exceeds 8, we simply added cells in SNr which receive striatal inhibition and compete with the others, but which do not inhibit any thalamic cell. When there is only 6 cells, we suppressed in SNr and VA the cells corresponding to the objects DPA and X, which are not used in this experiment.

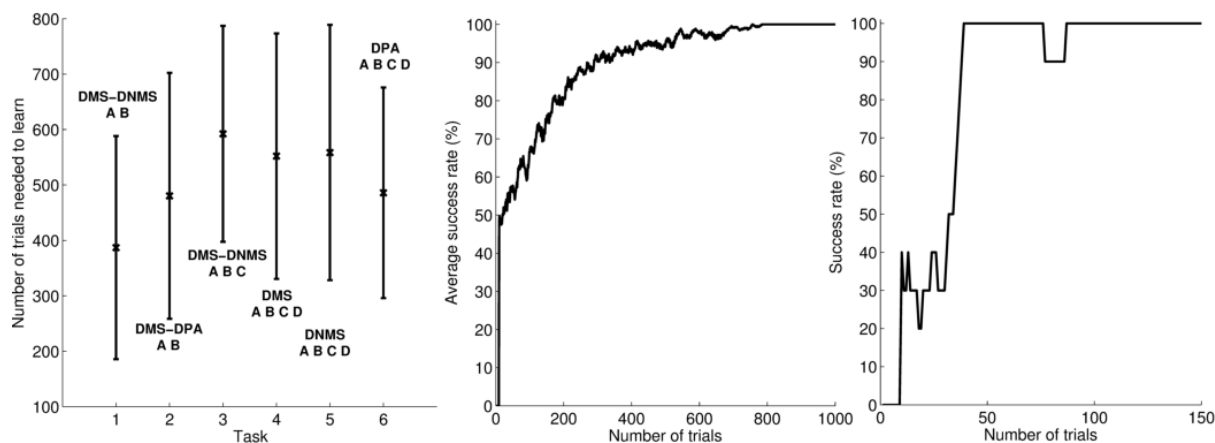


Figure 3.2: Different success rates. (A) Mean value and standard deviation of the last incorrect trial during learning of 50 randomly initialized networks for different combinations of cues and tasks: 1) DMS-DNMS_AB; 2) DMS-DPA_AB; 3) DMS-DNMS_ABC; 4) DMS_ABCD; 5) DNMS_ABCD; 6) DPA_ABCD. (B) Average success rate of 50 networks presented with DMS-DNMS_AB. (C) Success rate of a particular network which learned DMS-DNMS_AB, but computed only on the trials composed of A as a cue followed by DNMS as a task symbol.

3.3 Results

3.3.1 Concurrent learning of the different tasks

Figure 3.2 A shows the learning behavior of the model when different combinations of tasks are presented. Each network was fed 1000 times with randomly alternated trials. The Y-axis represents the rank of the last trial during the learning sequence where the network produced a incorrect answer, which is a rather conservative measurement of behavior. After this last mistake, the performance of all networks are stable, even when more than 1000 trials are presented as further tests have shown. We represent here the performance of different combinations of tasks: DMS-DNMS_AB, DMS-DPA_AB, DMS-DNMS_ABC, DMS_ABCD, DNMS_ABCD and DPA_ABCD. For each combination of tasks, we used fifty different networks that were initialized randomly. One can notice that the different networks learn at very variable speeds, as shown by the standard deviation. For example, for the DMS-DNMS_AB task, some networks converged after 200 different trials whereas a few others needed 800 trials, what denotes the influence of initialization as well as the one of noise. The only significant difference between the combinations of tasks is that DMS-DNMS_AB is learned faster than DMS-DNMS_ABC, DMS_ABCD, DNMS_ABCD and DPA_ABCD (two-sample K-S test, $P < 0.05$). However, this can be simply explained by the fact that DMS-DNMS_ABC uses six different trials instead of four for DMS-DNMS_AB (C+DMS and C+DNMS have to be learned at the same time), and that DMS_ABCD, DNMS_ABCD and DPA_ABCD use a bigger set of possible distractors during the choice period. We will investigate in Section 3.3.3 the influence of distractors on performance. The distributions of the numbers of trials needed to learn for each combination have no significant shape, though a Gaussian fit can not be rejected (χ^2 -test, $0.2 \leq P \leq 0.6$).

Figure 3.2 B shows the average success rate of 50 networks presented with the DMS-DNMS_AB task. The success rate of a network is computed after each trial during learning as the percentage of rewarded trials for the last ten trials: if the last ten trials were rewarded, the success rate is 100%, if only one trial was not rewarded, the success rate is 90% and so on. All networks have reached the maximum success rate before the 800th trial, but some only need 200 trials. At the beginning of learning, the success rate is 50%, as the network does not really select a response and reward is given randomly according to the probabilistic rule of reward we use. This success rate quickly increases to a high value in around 300 trials, followed by a more flat phase where the competition in SNr temporarily deteriorates the performance of the networks.

This flattening of the average success rate can be explained by observing Figure 3.2 C. We represent the success rate of a particular network which learned DMS-DNMS_AB, but this success rate is plotted for analysis purpose only from trials composed of A as a cue followed by DNMS as a task symbol. We see that the network performs this task accurately after only 40 trials and stays at this maximum until it makes a mistake shortly before the 80th trial. We will later show that this temporary decrease in performance is due to the late involvement of selection in SNr. To quantify this behavior, we examined the success rates of the 50 networks used in Figure 3.2 B and decomposed them regarding to the four types of trials involved in the learning phase (A followed by DMS and so on). We found that 32.5% of trial-specific networks showed this type of behavior, by reaching success in at least ten successive trials before performing again a mistake. In average, these trial-specific networks reach stable success after only 14 trials and stay successful for 17 trials before performing a mistake. They then need on average 47 other trials before reaching definitely 100% success (last mistake after the 78th trial). In comparison, the other trial-specific networks (67.5%) perform their last mistake at the 64th trial on average, which is significantly shorter (χ^2 -test, $P \leq 0.05$).

3.3.2 Temporal evolution of the activities after learning

Figure 3.3 shows the temporal evolution of some cells of a particular network that successfully learned DMS-DNMS_AB. The learning phase consisted of 1000 randomly interleaved trials. At the end of learning, the network was able to generate systematically correct responses which all provoked the delivery of reward. The selectivity of CN cells developed to represent the different combinations of cues and task symbols through clusters of cells (see Section 3.3.5). SNr cells also became selective for some of these clusters and the learned competition between them ensured that only one SNr cell can be active at the same time in this context. The temporal evolution of the activity of the cells on Figure 3.3 was recorded during the course of a trial using A as a cue and DNMS as a task symbol. However, this pattern is qualitatively observed in every network that successfully learned the task and similar activation patterns occur for different tasks. The cells which are not shown on this figure do not exhibit significant activity after learning.

When the object A is presented as a cue in PRh (and simultaneously enters the working memory

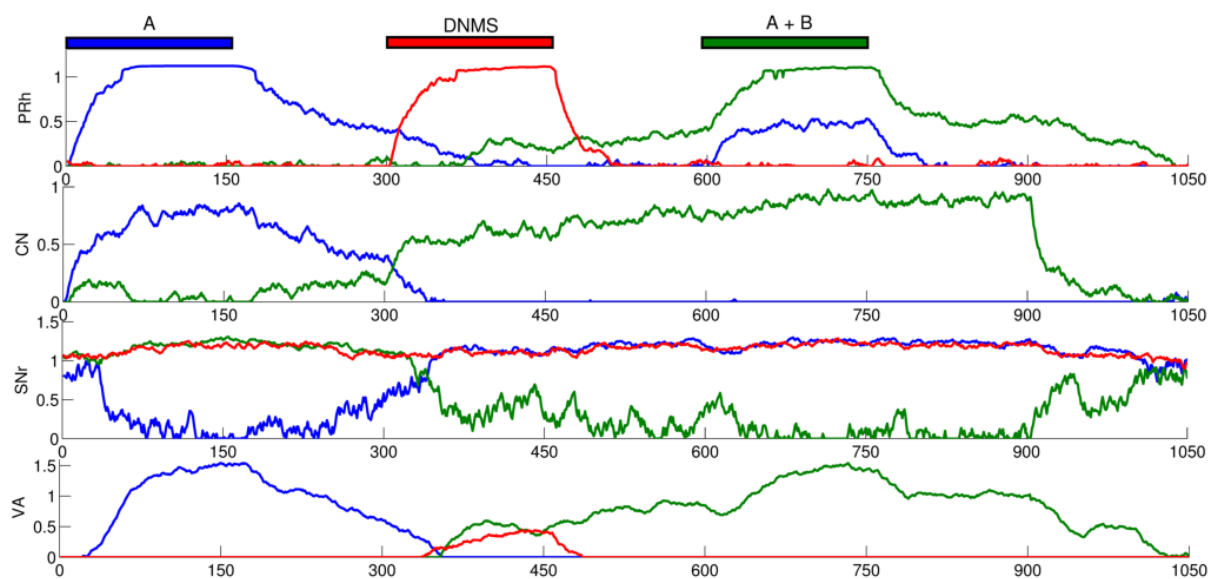


Figure 3.3: Temporal evolution of the activity of several cells in a network which successfully learned DMS-DNMS_AB. The activities are plotted with regard to time (in ms) during a trial consisting of A as a cue, DNMS as a task symbol and B as a target. The first row represents the activities of three cells in PRh which are respectively selective for A (blue line), DNMS (red line) and B (green line). The second row shows the activities of two cells in CN, one being selective for the pair A+DMS (blue line), the other for the pair A+DNMS (green line). The third row represents the activities of three cells in SNr which are respectively selective for A (blue line), DNMS (red line) and B (green line). The fourth row represents the activities of three cells in VA which are respectively selective for A (blue line), DNMS (red line) and B (green line).

in dIPFC), it excites a cluster of cells in CN which, in this example, represents the couple A+DMS (blue line). This cluster inhibits the cell representing A in SNr which in turn stops inhibiting the corresponding cell in VA. The thalamocortical loop is then disinhibited and the two cells representing A in PRh and VA excite each other. After 150 ms, the stimulation corresponding to the cue ends and the activity of the cells representing A slowly decreases to their baseline. At 300 ms, the object specifying the task (DNMS) stimulates a cell in PRh and enters WM in dIPFC. This information biases processing in CN so that a new cluster representing A+DNMS gets activated (green line) and disinhibits through SNr the cell in VA representing the object B, which is the target of the task. At 600 ms, when both objects A (distractor) and B (target) stimulates PRh, the perirhinal cell A only receives visual information, while the cell B receives both visual and thalamic stimulation. Consequently, its activity is higher than the cell A and will be considered as guiding a saccade toward the object B. The cell representing DNMS in SNr never gets inhibited because it has never been the target of a task during learning. The corresponding thalamic cell only shows a small increase during the presentation of the object in PRh because of the corticothalamic connection. In the Discussion, we will come back on the fact that, in this particular example, the system has learned to select B instead of avoiding A as it should do in a DNMS task.

Three features are particularly interesting in this temporal evolution and have been observed for every network used in Section 3.3.1. The first one is that the perirhinal and thalamic cells corresponding to the object B are activated in advance to the presentation of the target and the distractor. The network developed a predictive code by learning the input, context and target association. For example, the behavior of the perirhinal cell correlates with the finding of pair-recall activities in IT and PRh during DPA tasks: some cells visually selective for the associated object have been shown to exhibit activation in advance to its presentation (Naya et al., 2003). Similarly, the behavior of the thalamic cell can be compared to the delay period activity of MD thalamic cells (part of the executive loop) during oculomotor WM tasks (Watanabe and Funahashi, 2004). The second interesting observation is the sustained activation of the perirhinal cell B after the disappearance of the target (between 750 and 900 ms on the figure) which is solely provoked by thalamic stimulation (as the WM in dIPFC still excites CN), whereas classical models of visual WM suggest that it is due a direct feedback from dIPFC (Ranganath, 2006).

The third interesting feature is the fact that the network, when only the cue was presented in PRh and dIPFC, already started to disinhibit the corresponding thalamic cell, somehow anticipating to perform the DMS task. We tested the 50 networks used in Section 3.3.1 after learning the DMS-DNMS_AB task and presented them with either A or B for 200 ms. By subsequently recording the activity of the corresponding cells in SNr, we noticed that they all tended to perform DMS on the cue, i.e. disinhibiting the corresponding thalamic cell. This can be explained by the fact that the representation of the cue in PRh is also the correct answer to the task when DMS is required, and the projection from PRh to CN therefore favors the selection of the striatal cluster representing A+DMS compared to A+DNMS. This can be interpreted such that the “normal” role of the visual loop is to maintain the visually presented objects, but that this behavior can be modified by additional prefrontal biasing (here the entry of DNMS into WM and

its influence on striatal activation), as suggested by Miller and Cohen (2001).

3.3.3 Effect of the competition in SNr

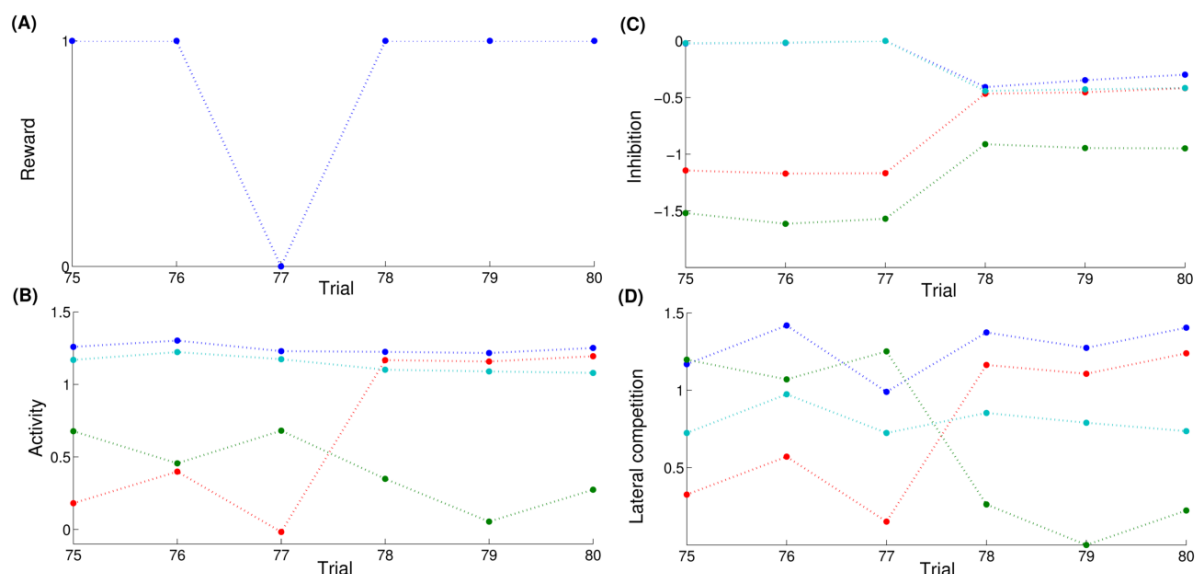


Figure 3.4: Evolution of internal variables in SNr for trials surrounding the mistake performed by the network on Figure 3.2 C. (A) Reward received at each trial. (B) Activity of four SNr cells at the time reward is received or expected during the trial. These cells are selective respectively for A (blue line), B (green line), C (red line) and D (turquoise line). (C) Striatal inhibition received by these four cells. (D) Competition term received by the same four cells.

We focus now on what happens around the late incorrect trial in Figure 3.2 C to show that the first phase of learning corresponds to the selective learning of connections from cortex to CN and from CN to SNr, whereas the second one corresponds to the learning of lateral connections within SNr to decorrelate the activities in the structure. Figure 3.4 shows the evolution of some internal variables of SNr cells between the trials surrounding the mistake produced at the trial number 77 of Figure 3.2 C. These trials are all composed of A as a cue, DNMS as a task symbol and therefore B as a target. Figure 3.4 A shows that the preceding and following trials were rewarded, but not the trial 77. Figure 3.4 B shows the activity of four SNr cells at the exact time when reward is delivered or expected to be delivered (750 ms after the beginning of the trial on Figure 3.3). These cells are selective respectively for A (blue line), B (green line), C (red line) and D (turquoise line). The four remaining cells in SNr are not plotted for the sake of readability, but they are not active anymore at this stage of learning. Figure 3.4 C represents the inhibition received by these cells at the same time, which means the weighted sum of inhibitory connections coming from CN. Figure 3.4 D represents the competition term received by these cells, which means the weighted sum of lateral connections in SNr (see Equation 3.8).

Through learning in the 76 first trials consisting in A followed by DNMS, the cells B and C became strongly inhibited during the choice period. In the rest of the article, we will call “active” a cell

which is strongly inhibited and has an activity close to 0.0. Both cells receive a strong inhibition from the same CN cluster but they still do not compete enough with each other so that only one remains active. As B is a target, this provokes the disinhibition of the thalamocortical loop corresponding to B, so that the cell B in PRh is much more active than the cell A, leading to a correct response and subsequent reward. The cell C is not involved in this particular task, so it is just a distractor: its activation does not interfere with the current task. However, this cell may be useful in other tasks, but the strong striatal inhibition it receives will make it harder to recruit it for other tasks. At the trial 77, the cell C in SNr competes sufficiently with the cell B so that the activity of the cell B becomes close to its baseline (around 0.7 on Figure 3.4 B). The difference between the activities of cells A and B in PRh becomes small, leading to an omission of reward on Figure 3.4 A according to the probabilistic rule we used. This omission has two effects through the depletion of DA: first, it reduces the striatal inhibition received by the two active cells, as seen on Figure 3.4 C; second, it increases the competition between the two active cells, but in an asymmetrical manner (Figure 3.4 B). According to Equation 3.12, the excitatory connection from the cell B to C will be much more increased than the one from the cell C to the cell B, as the cell C is much more inhibited than the cell B. Consequently, at trial 78, the cell C receives much more excitation from the cell B and its activity becomes above baseline. The cell B is then strongly inhibited by the same cluster in CN and generates a correct rewarded response. In the following trials, the cell B will further increase its selectivity for this cluster, whereas the other cells in SNr (including the cell C) will totally lose theirs and can become selective for other clusters.

What happened around this trial shows the selection of a unique cell in SNr, even when the network already had a good performance. This selection relies on four different mechanisms. First, the network should have selected a number of cells in SNr which produce a correct answer. These cells include the target, but also distracting cells that are also selective for the same cluster in CN but which disinhibit irrelevant thalamocortical loops. Second, as the network produces correct answers, the cluster in CN becomes associated to a high reward-prediction value in SNC. The amplitude of phasic DA bursts is accordingly reduced. However, omission of reward will generate a greater depletion of the DA signal, compared to the beginning of learning when CN clusters had no association to reward and provoked no DA depletion. Third, omission of reward reduces the striatal inhibition received by active cells in SNr. However, if this was the only “punishing” mechanism, all the active cells will lose their selectivity. In this particular example, the cell B would gradually stop receiving inhibition from CN and all the preceding learning would be lost. Fourth, the learning of lateral connections in SNr is asymmetric with respect to DA firing: when a distractor progressively wins the competition until the response associated to the target is attenuated, this distractor becomes disadvantaged in the competition with the target. This is an indirect memory effect: as the cell corresponding to the target was previously activated and provoked reward delivery, the cease of its activation (provoking reward omission) is transmitted to the other cells in SNr through DA depletion, which “understand” that their activation is irrelevant and “get out” of the competition.

It is important to note that this competition between cells in SNr stays completely local to

the cells: there is no winner-take-all algorithm or supervising mechanism deciding which cell should be punished. This competition emerges only through the interaction of the cells and the learning of their reciprocal connections. As stated in Section 3.3.1, the scheme described before occurs during learning in 32.5% of the networks we studied: the target cell in SNr temporarily loses the competition before being reselected. However, in other cases the target directly wins the competition and the distractors fade: there is no degradation in performance, what can explain the great variability in the number of trials needed to learn correctly all the tasks on Figure 3.2 A.

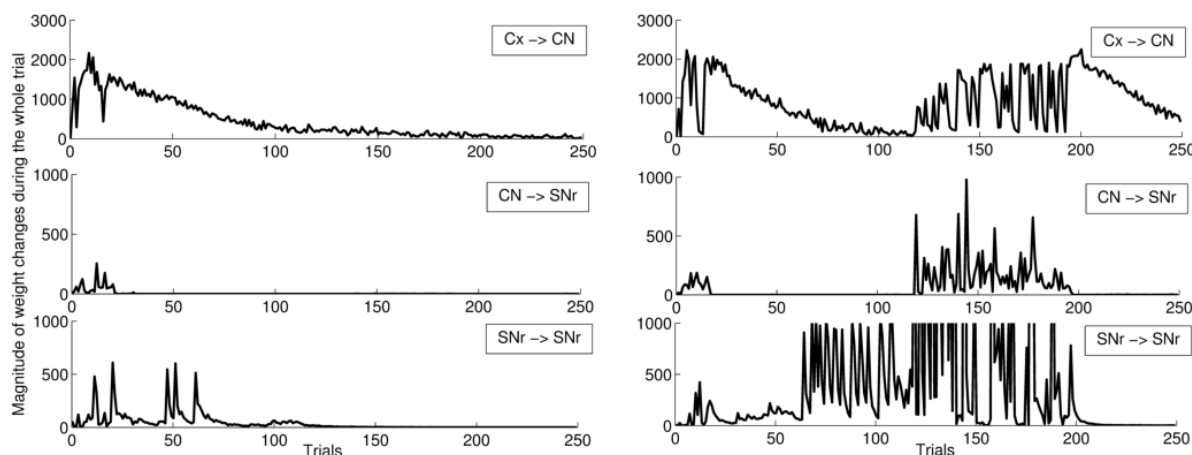


Figure 3.5: Magnitude of weight changes during learning of DMS-DNMS_AB for two different networks, plotted here only for A+DMS trials. The top line corresponds to global weight changes in CN (projections from PRH and dIPFC), the middle one to the connections from CN to SNr, the bottom one to lateral connections within SNr. (A) Network showing a late competition mechanism in SNr selecting directly the correct target without provoking a mistake. (B) Network showing a late competition mechanism in SNr that led to the performance of mistakes and to a long period of instability. The amplitude of lateral weight changes has been thresholded during this unstable phase (it reaches up to 5000) in order to allow a better comparison with the first network.

In order to better describe these two schemes of learning, we show on Figure 3.5 the magnitude of weight changes in CN and SNr during learning for two different networks. This magnitude is computed for each trial in the learning session by summing the absolute values of the discretized variations of weight values ($|dW_{i,j}(t)|$ in Equation 3.5, Equation 3.8, Equation 3.11 and Equation 3.12 for all neurons in the considered area and for all computational timesteps in the entire trial (1050 in our design). These two networks have both learned the DMS-DNMS_AB task, but we represent here only the magnitude of weight changes occurring during A+DMS trials. The top row represents the magnitude of weight changes for striatal cells (Equation 3.5), the middle row for the inhibitory connections from CN to SNr (Equation 3.8) and the bottom one for lateral connections within SNr (both Equation 3.11 and Equation 3.12). The absolute amplitude of these weight changes is meaningless, as it depends on the number of cells in each areas and the number of afferent connections. On Figure 3.5 A, the network shows an early learning phase in the first thirty trials where both striatal and pallidal cells show great

variations in weight values, denoting that the network tries to find a correct answer to the task. After this first period, the connections from CN to SNr cease to fluctuate, while the connections from PRh and dIPFC to CN gradually stabilize (rather slowly, as the computed magnitude also takes into account the regularization term in Eq. Equation 3.5, as the striatal cells always tend to overshoot, and this magnitude only decays with the association to reward). However, after the 50th trial, the lateral connections within SNr show another peak of variation. This corresponds to the simultaneous activation of two SNr cells, including the target. In this case, the correct target wins the competition and eliminates the distractor without provoking a mistake. The task has been correctly learned and the network slowly stabilizes its learning. Oppositely, the network shown on Figure 3.5 B has the same early phase of learning, but the late increase in magnitude of lateral weight changes is much higher and lasts for about 50 trials. This inefficient selection process might be due to interference with learning in other trials, but provokes no mistake for the task. However, around the 120th trial, this competition leads the network to perform a mistake (as what happens in Figure 3.4), and the connections within the network vary for a certain number of trials before finding the correct solution and stabilizing. The first scheme of learning is the most frequently observed, while the second one corresponds roughly to the 32.5% of networks found in Section 3.3.1. We observed a third infrequent scheme of learning similar to the second one, but where only the connections from CN to SNr are modified in the second phase of learning, not the lateral ones. This can be explained by the fact that the target and the distractor have already learned to compete with each other during the learning of another type of trial.

3.3.4 Influence of the number of cells in SNr

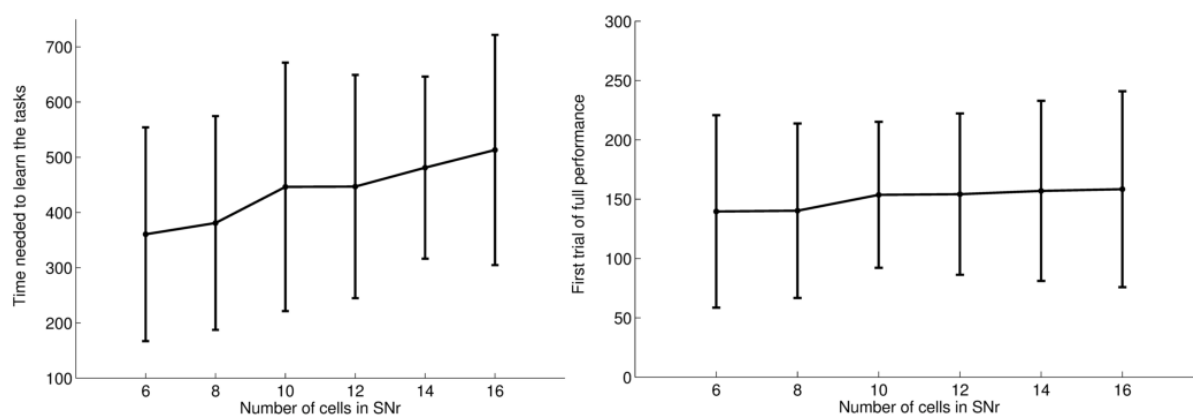


Figure 3.6: Influence of the number of cells in SNr. (A) Mean value and standard deviation of the last incorrect trial during learning of 50 randomly initialized networks learning DMS-DNMS_AB, depending on the number of cells in SNr. (B) Rank of the first trial during learning which got a success rate of 100% (computed on the ten preceding trials), depending on the number of cells in SNr.

As the number of possible distractors in SNr may influence the number of trials needed to learn the tasks, we investigated the influence of the number of cells in SNr (method described in

Section 3.2.8). Figure 3.6 A shows the average number of trials needed to learn DMS-DNMS_AB by fifty randomly initialized networks. One can observe that the mean number of trials needed to learn increases monotonically with the number of cells in SNr, but in a quite flat manner: from 360 trials with 6 cells to 510 trials with 16 cells (regression analysis $y = 15.16 * x + 271.9$, with x the number of cells in SNr and y the time needed to learn, $r^2 = 0.25$). This rather slow increase can be explained by the fact that the selection process in SNr through lateral connections do not concern cells two-by-two as shown on Figure 3.4, but can eliminate several distractors at the same time. In addition, the variability of these numbers of trials is rather high, and some networks with 16 cells in SNr converge faster than some networks with only 6 cells depending on initialization and noise.

As a matter of comparison, Figure 3.6 B shows for the same networks the rank of the first trial in the learning sequence where the success rate was 100% (ten preceding trials were rewarded). One can observe that this first successful trial occurs on average at the same time in the learning sequence (around 150 trials), independently of the number of cells in SNr. We estimated the proportion of trial-specific networks that reached an early phase of success during at least ten consecutive trials before performing a mistake again. This proportion stays rather constant with the number of cells in SNr, the minimum being 32.5% for 8 cells and the maximum 40% for 14 cells. Taken together, the result presented here confirm that there are globally two stages of learning regarding SNr: a first stage of parallel search independent of the number of cells in SNr, where the system selects through striatal inhibition an ensemble of cells in SNr able to obtain rewards (including the target and several distractors) and a second stage of partially sequential search that depends on the number of cells in SNr, where the system tries to eliminate the distractors through lateral competition, what needs more time when the number of possible distractors increases.

3.3.5 Reward-related clustering in CN

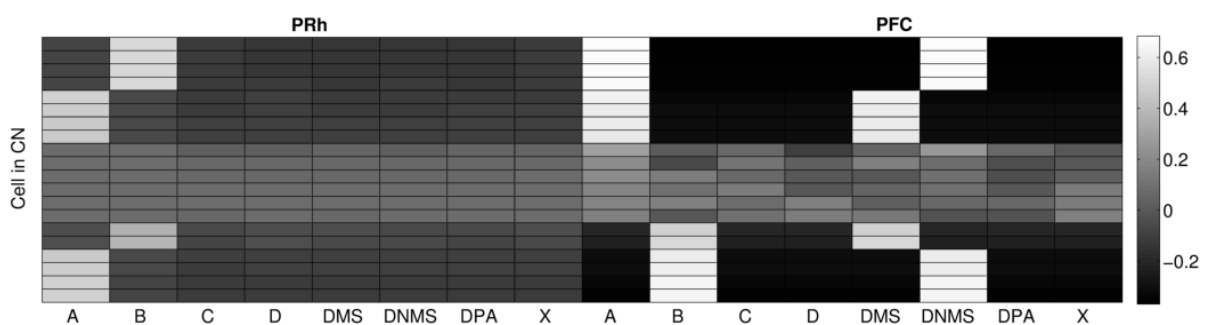


Figure 3.7: Receptive fields of some CN cells after learning DMS-DNMS_AB. The X-axis represent the cells in PRh and dIPFC and the Y-axis the different cells in CN. A white color represents a positive weight for the connection, grey represents a weight close to zero and black a negative weight.

The CN cells learn to represent cortical information from PRh and PFC during the first stage of learning, together with the parallel selection in SNr. As the competition between CN cells is not

3 A computational model of basal ganglia and memory retrieval

very strong, a cluster of a few CN cells gradually become selective for a particular pattern of cortical activity which is rewarded. Each rewarded combination of cue and task symbols in the cortical areas gets represented by 2 to 5 cells in CN, whose identity may change through learning depending on reward delivery. Figure 3.7 shows the receptive fields (connection pattern with the cortical neurons) of several cells in CN after learning DMS-DNMS_AB. One can observe that some cells developed a very sharp selectivity to the cue and task symbols in dIPFC, as well as for the target in PRh. They have very strong positive connection weights to these cells, and relatively strong negative connection weights to the others. For example, the four cells on the top of the figure are selective for A and DNMS in dIPFC and B in PRh. After learning, this cluster will selectively inhibit the cell B in SNr and generate a correct response towards B.

According to these receptive fields, when a cue (e.g. A) is presented at the beginning of a trial, it will be represented in both PRh and dIPFC and therefore activate preferentially the cluster in CN selective for A+DMS. This explains the activation pattern of CN cells on Figure 3.3: the presentation of the cue favors the DMS-related clusters. However, when DNMS or DPA appear, they tend to inhibit these clusters so that the correct cluster can emerge from the competition. This tendency of the network to perform the DMS task even when the task is not known may have some advantages: a cue which is reliably associated to reward will see its representation in PRh enhanced through disinhibition of its thalamocortical loop, compared with visual objects which were never associated with rewards. This is coherent with the findings of Mogami and Tanaka (2006) who showed that the representation of visual objects in PRh is modulated by their association to reward.

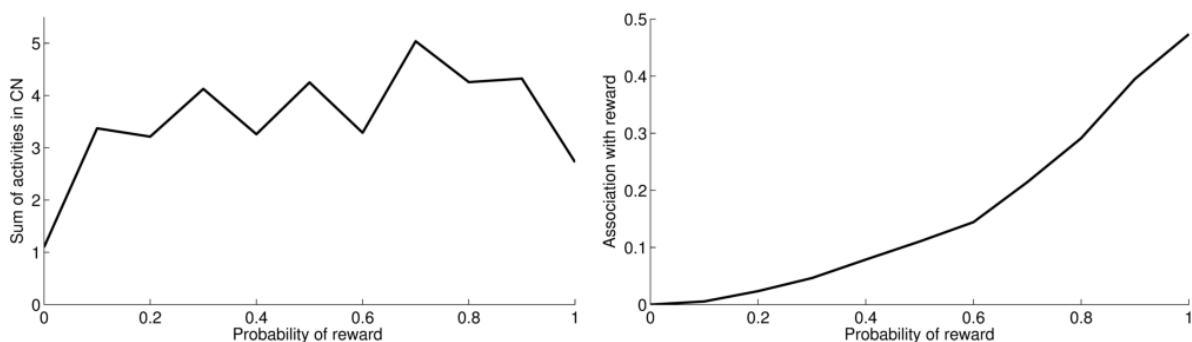


Figure 3.8: (A) Sum of activities in CN depending the probability of reward associated to the object X. (B) Association with reward of the cluster representing X in CN, depending on the probability of reward delivery.

At the end of the learning phase, the clusters in CN are fully associated with reward, which means that they totally cancel the phasic DA bursts and could generate a maximal depletion of DA if reward was omitted. The question that arises is whether all rewarded objects get represented equally in CN. In order to investigate this issue, we now use the trace conditioning that we presented in Section 3.2.8. This task consists in presenting to the network a visual object X which is randomly associated to reward with a fixed probability, whatever the response of the system. This trace conditioning task is randomly intermixed with the learning of DMS-DNMS_AB, for a total number of 1000 trials. Figure 3.8 A shows the sum of the activities of

all CN cells at the time reward is given or expected, averaged over the last 50 conditioning trials of the learning sequence. Even with a low probability of reward like 0.1, the object X gets represented in CN by a sum of activity comprised between 3.0 and 5.0. This value must be compared to the sum of activities in CN when reward is never given (1.1) and which solely consists in weight initialization and noise. This sum of activities can represent a cluster of 3 to 6 cells depending on their activity.

Figure 3.8 B shows the association with reward associated of the object X at the time reward is given or expected, averaged over the last 50 conditioning trials of the learning sequence. This prediction of reward is computed as the absolute value of the weighted sum of connections from CN to SNc. Contrary to the striatal representations, this association to reward strongly depends on the probability of reward. It explains that even rarely rewarded objects can get represented in CN: the received reward generates a DA burst of activity that increases the corresponding corticostriatal connections, but it never becomes sufficiently associated to reward to generate a DA depletion that would decrease the same connections.

3.4 Discussion

We designed a computational model inspired by the functional anatomy of the visual loop connecting a high-level visual cortical area (PRh), some structures of BG (CN, SNc and SNr) and the corresponding thalamic nuclei (VA). The functioning of this closed loop is biased by the sustained activation of some prefrontal cells (dIPFC) which here artificially keep track of activity in PRh. This model is able to learn a mixture of visual WM tasks like DMS, DNMS and DPA in the context of reinforcement learning, where only a reward signal is delivered when the system answers correctly. This reward signal drives the activity of a dopaminergic cell which modulates Hebbian learning in the connections between the neurons of the model. With the combinations of tasks we tested, the network was able to learn perfectly the tasks after an average of 500 trials. Even if this number of trials may seem huge in comparison to experimental data on human adults, one has to consider that the system has absolutely no prior knowledge about the task: the symbols representing the tasks to perform within a trial are initially meaningless and the system only sees a couple of visual objects before being forced to make a choice in an array of objects.

Even if the architecture of the visual BG loop has been simplified compared to the known literature (only the direct pathway is implemented) and some known mechanisms have not been taken into account (like the modulation of the activity of striatal cells by DA firing), this model is able to exhibit some interesting emergent behaviors which can be considered as predictions. First, we have observed sustained activation of PRh cells which is only due to thalamic stimulation. As we hypothesized in (Vitay and Hamker, 2008), the observed sustained activation in PRh (and IT) may not only be the consequence of direct feedback from prefrontal areas to temporal areas, but may also pass through the thalamus via the BG in order to gain more control on

the relevance of this behavior during the reinforced learning phase. After this learning phase, the fronto-temporal connections may replace the BG-thalamus system and directly provoke the sustained activation. Second, the tendency of the model after learning to start performing DMS right after the presentation of the cue (as the cue is represented both in PRh and dlPFC) enhances the perirhinal representation of items that are reliably associated to reward, what is in agreement with the findings of Mogami and Tanaka (2006). It suggests that the default role of the visual loop of the BG is to favorize the representation of rewarded visual objects that are present in the visual scene, and that the role of the connections from dlPFC to the visual loop is to bias this behavior towards cognitively defined targets, as suggested by Miller and Cohen (2001). Third, cells in PRh and VA corresponding to the target in the task are activated in advance of the presentation of the search array. Especially in DNMS and DPA where the target differs from the cue, this behavior reminds the pair-recall activities found in IT and PRh (Naya et al., 2003), as well as the presaccadic activities in the medio-dorsal nucleus (MD) of the thalamus (Watanabe and Funahashi, 2004). We have not found similar results concerning the VA nucleus of the thalamus, but we predict that VA cells responsive for paired target of a DPA task will exhibit pair-recall activity.

There are three different stages of learning in the model. The first stage consists in the representation of cortical information by the striatal cells based on the delivered reward. This striatal representation combines the content of the WM (a representation of the cue and the task in dlPFC) with the perirhinal representation of the target through the activation of a cluster of cells. These clusters are composed of a limited number of cells due to competition among striatal cells. The second stage of learning consists in the selective inhibition of a group of SNr cells by these clusters of striatal cells. This selective inhibition is strongly modulated by reward delivery, so that the inhibited SNr cells are able to disinhibit the perirhinal representation of the target but not the distractor. This phase is performed in a parallel manner which does not depend on the number of cells in SNr. The third stage of learning is the enhanced competition between SNr cells to decorrelate their activities. This phase is sometimes characterized by a temporary degradation of the performance of the network until the target cell gets selected by the competitive mechanism, what makes this phase sequential with regard to the number of cells in SNr. This phase strongly relies on the learned reward-association value of striatal clusters in SNc, so that omission of reward can generate a depletion of DA. However, this distinction into three different stages is made *a posteriori*, as all cells learn all the time through the experiments without any change of parameters in the learning rules.

The role of the learned competition in SNr is to ensure that only the useful thalamocortical loop is disinhibited according to task requirements. Without this competition, several SNr cells would be inhibited by the same striatal cluster because the initialization of the connections between CN and SNr is randomly distributed. This could provoke parasitic disinhibition of thalamocortical loops, leading to involuntary movements or visual hallucinations. Without an additional self-organization of thalamocortical connections the search for the target cell requires in the progressive elimination of those distractors that strongly compete with the target, eventually leading to DA depletion to resolve the ambiguity. For large real-world networks one potential

way to keep the sequential search in a reasonable bound would be to consider the topographical projections from cortex to striatum as well as from striatum to SNr. In our model, these projections are all-to-all and only become selective for particular patterns through learning. Zheng and Wilson (2002) showed that adjacent cells in striatum have very little common input, leading to a sparse representation of cortical information. Similarly, projections from striatum to GPi and SNr also have a sparse connectivity (Bar-Gad et al., 2003), although some GPi cells have been shown to receive input from functionally different striatal regions (Flaherty and Graybiel, 1994). Wickens and Oorshcot (2000) observed that striatal cells are organized into small assemblies of neurons that have mutually inhibitory connections. The number of such compartments is remarkably similar to the number of GPi neurons, what could suggest a topographical pattern of convergence from cortex to SNr through striatum that could allow to limit this competition in SNr to limited sets of functionally related cells instead of the whole population. This would be in agreement with the found pattern of lateral connections between SNr cells belonging to the same or adjacent functional subdivision (Mailly et al., 2003).

To our knowledge, this model is the first to address the issue of learning at the level of SNr, either from striatum to SNr or within SNr. The late selection of the useful-only SNr cells may allow the prediction that the mean activity of the SNr population will be lower during learning than after, in the sense that more SNr cells will be inhibited in the first stages of learning than when the competition takes place. In addition, one may observe that the performance of the subject could temporarily be degraded after a certain number of successful trials, due to the late involvement of competition in SNr. From a computational point of view, our model assigns a new functional role to SNr (and GPi) in the general framework of BG functioning and may guide to the development of a new class of BG models.

The model currently solves the DNMS task by learning to select the target, not by learning to avoid the cue. If a novel target were presented together with the cue after the learning phase, the system would not respond systematically towards it. In this respect, what is learned by the model when DNMS is required is more a version of DPA that associates cues together than truly DNMS. In order to learn DNMS, we would have to close the thalamocortical loop corresponding to the cue even more strongly than when SNr cells are at their baseline level. That could be achieved by exciting strongly the SNr cell corresponding to the cue, therefore inhibiting the neighboring cells in SNr which can then let other thalamocortical loops become active. The indirect pathway of BG is a possible candidate to truly learn DNMS: the additional inhibitory relay through GPe allows striatal activation to indirectly excite the output nuclei GPi/SNr (Albin et al., 1989; DeLong, 1990). This indirect pathway is also particularly involved in the processing of DA depletion, as the striatal cells participating in this pathway have mainly D2-type DA receptors and are globally inhibited by DA release. Dopamine depletion could then favorize this pathway and signal precisely to the output nuclei the omission of the expected reward. Incorporating this indirect pathway could allow us to truly learn DNMS and might also allow to simplify the learning rules in SNr which treat differentially over- and below- baseline DA activities. The balance between the direct and indirect pathway may signal more elegantly these two different situations, without modifying the principal results presented here.

3 *A computational model of basal ganglia and memory retrieval*

On top of this possible influence of the indirect pathway on learning DNMS, Elliott and Dolan (1999) showed that DMS and DNMS involve differentially cortical or subcortical structures, the MD nuclei of the thalamus (part of the executive loop) being for example more implicated in DNMS than DMS. This raises the issue of the involvement of the executive loop in solving these rewarded visual WM tasks. In the current model, only the connections originating from dIPFC (which simply stores perirhinal information) bias representations in CN to perform the tasks. The purpose of this model is only to show that it is possible to retrieve object-related information in high-level visual areas like IT or PRh through behaviorally-relevant BG gating. The role of the executive loop in rewarded visual WM tasks is obviously much more complex than just maintaining perirhinal representations: gating the entry of items in WM (if a distractor is systematically presented during the task but has no behavioral relevance, it should not enter WM), manipulating them (abstracting sensory information and applying rules) and eventually actively suppressing items from WM (at the end of a trial or when a new item makes it obsolete). Gating and suppression of items are manually performed in our current dIPFC model but can be learned through the loop linking dIPFC with the corresponding BG structures modulated by DA firing (O'Reilly and Frank, 2006). Manipulating and abstracting representations is a harder issue that involves specifically the prefrontal cortex, but some computational models have already started to address this problem (Rougier et al., 2005). It would be also interesting not only to learn to represent specific combinations of cues and task symbols, but also to abstract the rule behind the task: if a new cue is presented, the system has to learn again this specific combination. This generalization to novel cues may be the role of the executive loop which may bias the visual loop in a more abstract manner than just storing cues and task symbols. This view is supported by the findings of Parker et al. (1997) which showed that MD (thalamic nuclei part of the executive loop) is crucial for learning DMS when the set of cues is big, but not when the set is small (what could be learned solely in the visual loop).

An extension of our model that would be able to fully learn the DMS, DNMS and DPA (with generalization to novel cues for all tasks and avoidance of the cue instead of selection of the target for DNMS) would therefore be composed of the visual and executive loops of the BG, both incorporating at least the indirect pathway. The role of the visual loop would be to retrieve the visual information associated to rewarded objects in the temporal lobe, acting by default on visually presented objects. The role of the executive loop would be to bias this processing, either by forbidding the visual loop to perform its automatic behavior (as in DNMS) or by guiding this behavior towards objects retrieved from memory (as in DPA). The executive loop would also be responsible for managing the task in time (gating and updating the entry of items into WM) in order to solve the temporal credit assignment problem, which is hard-coded in the current model. It would also manage the generalization of the learned task to bigger sets of cues and ultimately abstract the underlying rule. The interaction between the executive and visual loops will still rely on overlapping projection fields from PRh and dIPFC on the caudate nucleus, but their synchronized learning will necessitate to explore the spiraling pattern of connections between dopaminergic cells in SNc and the striatum discovered by Haber (2003), suggesting a hierarchical organization of BG loops in guiding behavior. However, we expect the principal results of

the current model to remain true in this extended version: the sustained activation of the target is only due to the classical disinhibition mechanism of the BG; the anticipatory activities in the thalamus are due to the maintenance of cues and task symbols in the executive loop; and the split of learning in two phases at the level of SNr should not be affected by the incorporation of the indirect pathway, whose role would be rather a simplification of the treatment of dopamine depletion than a modification of the competition mechanism.

The way we modeled the dopaminergic firing in SNc is rather simple from a computational point of view. It receives information about the delivery of reward and learns to associate it with striatal representations. This reward association progressively cancels through learning the amplitude of the phasic DA bursts and provokes DA depletion at the time reward is expected (through an external timing signal) but not delivered. This behavior is consistent with the observations of Schultz et al. (1997) about DA firing at the time of reward in conditioning tasks. It does not reproduce the observed phasic burst that appears after learning at the presentation of the conditioned stimuli (or cue in our case). However, contrary to the classical approach comparing DA firing with the error signal of the temporal difference (TD) algorithm (Suri and Schultz, 1999), we consider that this pattern of activation is computed by a separate mechanism, presumably by the selective entry in WM of the cue in the executive loop, as suggested by Brown et al. (1999) and O'Reilly and Frank (2006). This entry of the cue in the executive loop will provide a timing signal which, combined with the reward association of the corresponding CN representation, is able to gradually provoke a DA phasic burst at the appearance of a cue which is reliably associated to reward. From a conceptual point of view, our current implementation of the DA firing considers that DA firing only enables the learning of the link between a context (here the content of WM), an action (the response made by the system) and the consequences of this action (here the delivery of reward), as suggested by Redgrave and Gurney (2006).

The DA phasic burst generated by the executive loop could allow to signal the behavioral relevance of a stimulus instead of its association to reward. In the trace conditioning that we performed, even rarely rewarded stimuli get represented in CN, although they do not acquire a strong association to reward. By signaling that these stimuli may be rewarded but do not have a great importance for behavior, this cue-related DA firing may allow to reduce or even suppress their representation in CN so that the corresponding cells can focus on more important events. This DA-mediated behavioral relevance may act on the learning of corticostriatal connections (as we implemented it) or through the modulation of the membrane potential of striatal cells through the activation of D1 or D2 receptors (Calabresi et al., 2007). Linking striatal representations to behavioral relevance instead of just reward-association may allow a more efficient and selective encoding of external events that can occur in natural scenes.

A few computational models have addressed the issue of memory retrieval in the context of delayed visual WM tasks (Gisiger and Kerszberg, 2006; Mongillo et al., 2003; Morita and Suemitsu, 2002). These models are mainly attractor networks which focus on the interplay between inferotemporal and prefrontal cortices, but do not consider the influence of BG on learning through reinforcement. The model by Gisiger and Kerszberg (2006) learns concurrently DMS and DPA

3 *A computational model of basal ganglia and memory retrieval*

with a paradigm similar to the one we used. It is composed of three interconnected cortical structures performing respectively visual representation, working memory and planning, and is able to reproduce electrophysiological data on IT and PFC functioning. However, it only learns to associate visual representations together, without learning to schedule the tasks. For example, the execution in time of DPA compared to DMS is controlled by manually computed gating signals, whereas, in our model, the only external gating signals concern the entry of visual representations into WM, independently of the particular task. Even if our model does not either solve the temporal credit assignment problem, we consider that the BG loops are an important site where the temporal execution of a task is learned, and that this functioning in time has important consequences on the content of cortical processing itself, such as anticipatory activities.

A comparison with other BG models is more difficult as we apply our model to a different paradigm. Some models deal with the influence of BG on reinforcement learning, particularly in classical or operant conditioning. The model of Suri and Schultz (1999) principally focuses on the computational aspects of DA firing which is considered similar to the error signal of the TD algorithm and which biases a direct mapping between stimuli and actions, within an actor-critic architecture. The model of Brown et al. (1999) is more biologically detailed and proposes a distinction between the different sources of information reaching SNc. The rest of the architecture of the BG is nonetheless kept simple and learning occurs only at the corticostriatal level. Other models focus more on the executive loop, especially with regard to WM gating and maintenance. Similarly to our approach, the model of O'Reilly and Frank (2006) uses the BG as a gating device for specific thalamocortical loops. It is successfully applied to complex WM tasks such as 1-2-AX, where it learns to generate a binary motor response depending on the content of WM. It is also applied to the store ignore recall (SIR) task, where it is presented with successions of visual objects, together with task symbols like "store" (where it should copy the object into WM) or ignore (where it should not copy). When the "recall" signal is presented alone, the system should respond towards the object that is currently stored in WM, whereas ordinarily it should just respond towards what is visually available. This task is similar to how we simulated DMS (PRh represents the visual input except when thalamic stimulation tells the opposite), but their model has the great additional ability to ignore intervening distractors by selectively updating the content of WM depending on task requirements. The main differences with our model is that the output of their model is segregated from the input and that cues and task symbols have to be presented simultaneously. Adding an efficient executive loop to our model may allow us to better compare with this model. The model of Ashby et al. (2005) also focuses on working memory maintenance (although in the spatial modality) through selective disinhibition of thalamocortical loops by the direct pathway only and considers elegantly the role of the feedback connections between PFC and posterior cortices. A very functionally different model was proposed by Gurney et al. (2001b), who place the subthalamic nucleus (STN) at a very central place in the functioning of the BG. They claim that STN mediates the interplay between the selection pathway (similar to the direct pathway in other models) and the control pathway which biases processing in the selection pathway instead of acting in the opposite

direction as suggested in the classical direct/indirect (or Go/NoGo) dichotomy. Although DA has there only a tonic effect, the concepts introduced in this model allow to reconsider the functional connectivity between BG structures.

Our proposed model is coherent with most cortical functional models of visual WM, such as Ranganath (2006). It considers that relevant visual objects are actively maintained in dIPFC and fed back in high-level visual areas. These visual areas themselves modulate visual processing in the ventral pathway through feedback connections, in order to create object-based attention that helps selecting the correct target in space (Hamker, 2005a). However, we propose that in the first phase of learning, BG learns to associate prefrontal representations with visual representations through reinforced trial-and-error learning in order to acquire the correct behavior. In parallel, but more slowly, the top-down connections from PFC to IT or PRh learns the same task in a supervised manner, BG acting as the teacher. After this second stage of learning, this prefrontal feedback on high-level visual areas can become the unique source of memory retrieval, as suggested by the results of Tomita et al. (1999).

Acknowledgments

This work has been supported by the German Research Foundation (Deutsche Forschungsgemeinschaft) grant “A neurocomputational systems approach to modeling the cognitive guidance of attention and object/category recognition” (DFG HA2630/4-1) and by the European Union grant “Eyeshots: Heterogeneous 3-D Perception across Visual Fragments”.

4 Working memory and response selection: A computational account of interactions among cortico-basal ganglio-thalamic loops

Abstract

Cortico-basal ganglio-thalamic loops are involved in both cognitive processes and motor control. We present a biologically meaningful computational model of how these loops contribute to the organization of working memory and the development of response behavior. Via reinforcement learning in basal ganglia, the model develops flexible control of working memory within prefrontal loops and achieves selection of appropriate responses based on working memory content and visual stimulation within a motor loop. We show that both working memory control and response selection can evolve within parallel and interacting cortico-basal ganglio-thalamic loops by Hebbian and three-factor learning rules. Furthermore, the model gives a coherent explanation for how complex strategies of working memory control and response selection can derive from basic cognitive operations that can be learned via trial and error.

4.1 Introduction

Working memory (WM) is a key prerequisite for planning and executing responses. In a prominent notion (Repovs and Baddeley, 2006), WM consists of the capability to maintain information over limited periods of time and the ability to manipulate that information. By maintaining information in WM, an organism can detach its responses from its immediate sensory environment and exert deliberate control over its actions. Healthy human adults demonstrate an enormous flexibility in WM control in that WM is eligible for a tremendous multitude of stimuli, each of which can be maintained over adjustable periods of time and manipulated in various ways. However, that flexibility has to be acquired meticulously over many years of childhood and adolescence. In the early years of childhood, even WM tasks as simple as a Delayed-Match-to-Sample task pose a serious challenge (Luciana and Nelson, 1998).

While several brain structures have been shown to contribute to WM and response selection (cf. Bird and Burgess, 2008; Bunge et al., 2002; Jonides et al., 1998; McNab and Klingberg, 2008;

4 Working memory and response selection

Rowe et al., 2000), we here focus on the role of basal ganglia (BG) as part of a looped cortico-BG-thalamic architecture: closed cortico-BG-thalamic loops, connecting a particular area of cortex to itself, can be anatomically distinguished from open loops, linking in an ascending manner areas involved in motivation, cognition and motor execution (Haber, 2003; Voorn et al., 2004). This architecture of parallel and hierarchically interconnected loops provides a potential anatomic substrate for both WM processes and response selection: closed loops allow maintaining information for extended periods of time and flexibly updating it (i.e. two major WM processes); open loops allow information that is maintained in hierarchically superior WM loops to bias response selection within hierarchically inferior motor loops (cf. Haber, 2003).

With regard to plasticity, BG are assumed to take part in visual and motor category learning (Seger, 2008) and in establishing associations between stimuli and responses (Packard and Knowlton, 2002). Probably most eminently, they are believed to have an important role in reinforcement learning: BG receive dopaminergic afferents from substantia nigra pars compacta (SNc), a nucleus of the midbrain, that provides them with an error signal of reward prediction (Hollerman and Schultz, 1998; Schultz et al., 1997): Relative to a tonic baseline dopamine emission of nigral neurons, dopamine bursts result from unexpected rewards and from reward-predicting stimuli while dopamine depletions follow omissions of expected rewards. Dopamine levels have been shown to modulate long-term synaptic plasticity within BG, especially in its major input structure, the striatum (Reynolds et al., 2001; Shen et al., 2008).

In recent years, several computational models of BG functions have been developed, pinpointing their role in WM and motor control (Ashby et al., 2007; Brown et al., 2004; Gurney et al., 2001a; O'Reilly and Frank, 2006; Vitay and Hamker, 2010). It has been shown that reinforcement learning mechanisms within biologically inspired cortico-BG-thalamic loops can solve conditional Delayed-Match-to-Sample and Delayed-Paired-Association tasks (Vitay and Hamker, 2010) and the 1-2-AX task of WM (O'Reilly and Frank, 2006). Moreover, it has been proven that shaping (i.e. a procedure of teaching a task via successively more complex approximations, Skinner, 1938) can provide computational models with benefits to learn demanding WM tasks (Krueger and Dayan, 2009): notably, shaping can speed up the learning process and provide sub-strategies to an agent that can later be used to cope with similar problems. In animal training and human education, shaping is a standard procedure to guarantee learning of complex behaviors: conditional WM tasks like the 1-2-AX task would not be trainable to animals or infant humans without such a procedure.

Given the huge variety of functions that BG contribute to and the multitude of brain areas that they interact with, a fundamental question in BG research is how different BG loops coherently interact. Here we follow a model-driven approach to gain insight into how dopamine-modulated learning in BG controls a combined WM-response selection system acting within different cortico-BG-thalamic loops. We propose a single set of Hebbian and three-factor learning rules for two different levels of the cortico-BG-thalamic hierarchy: prefrontal loops learn to flexibly switch between WM update and WM maintenance and a hierarchically inferior motor loop learns selection of rewarded responses based on WM content and visual stimulation.

Our model's functional abilities are demonstrated on delayed response (DR) tasks, a delayed alternation (DA) task and on the 1-2-AX task of WM (O'Reilly and Frank, 2006), the latter being trained in a three-step shaping procedure. We provide interpretations of the roles of BG pathways in WM control and response selection and propose a mechanism of how task monitoring for unexpected errors instigates learning processes. The purpose of our approach is to show how reinforcement learning processes within separate but interconnected cortico-BG-thalamic loops can in parallel establish WM control and response selection.

4.2 Material and methods

4.2.1 Architecture of the model

BG loops can be classified according to their contributions to different functional domains (Alexander et al., 1986): loops traversing the caudate nucleus and lateral prefrontal cortex contribute to the executive domain. They are involved in goal-directed learning, action-outcome associations and WM (Redgrave et al., 2010); loops traversing the putamen as well as premotor and sensorimotor cortices contribute to the motor domain and are involved in action selection, stimulus-response associations and habitual control (Horvitz, 2009). Different types of loops interact through various kinds of fibers (Haber, 2003). Among these fibers, cortico-striatal connections allow for a convergence of inputs from distinct frontal cortical areas onto key striatal regions (Calzavara et al., 2007; Takada et al., 1998). Thereby, these fibers create a hierarchy of information flow from the executive/prefrontal domain to the sensorimotor domain and provide a potential substrate for how cognitive processes guide motor processes (Calzavara et al., 2007). Figure 4.1 shows the general layout of our model which is consistent with cortico-BG-thalamic circuitry (Braak and Del Tredici, 2008; DeLong and Wichmann, 2007; Haber, 2003). The model consists of parallel and hierarchically interconnected cortico-BG-thalamic loops that all have the same general architecture and obey the same learning rules. Prefrontal cortico-BG-thalamic loops (as shown on the left of Figure 4.1) control WM by flexibly switching between maintenance and updating of information. They bias a motor loop (shown on the right of Fig. Figure 4.1) to decide between a set of possible responses. As previously motivated by others (e.g. Krueger and Dayan, 2009; O'Reilly and Frank, 2006), our model contains multiple independent prefrontal loops. While there is no upper limit to the number of loops that can be incorporated, we kept it as small as possible to minimize computational costs: two prefrontal loops are sufficient to have the model learn the tasks analyzed in this paper. Differential recruitment of these loops is controlled by the pedunculopontine nucleus (PPN) as detailed in the corresponding subsection below.

The general functional framework of our model is straightforward. During stimulus presentation, visual input is externally fed into inferior temporal cortex (ITC). Stimulus-related activity can then spread through the model and bias processing within prefrontal and motor loops. Motor responses are read out of primary motor cortex (MI) activity and rewarded if correct. When

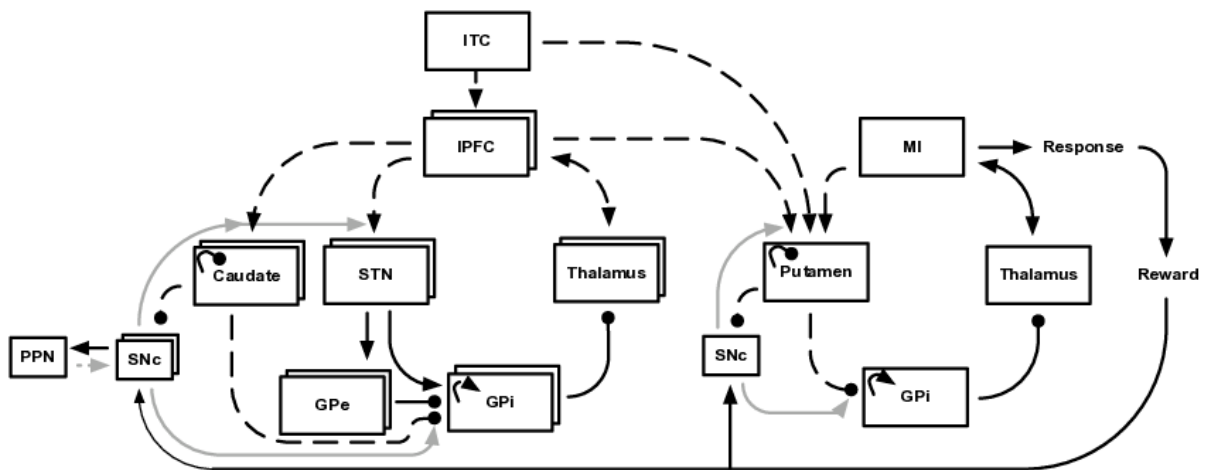


Figure 4.1: Architecture of the proposed model: prefrontal cortico-BG-thalamic loops flexibly control WM and guide a motor loop to choose between a set of possible responses. While the general layout of prefrontal and motor loops is the same, the motor loop is simplified as explained in the main text. Boxes represent the different layers of the model, arrows the connections between them. ‘Double’ boxes represent dual prefrontal circuits. Solid arrows denote hard-coded connections between or within layers, dashed arrows learnable ones. Pointed arrows symbolize excitatory connections, rounded arrows inhibitory ones. The solid gray arrows deriving from SNc represent a modulatory ‘dopaminergic’ influence on learning within BG synapses. The dotted gray arrow from PPN to SNc denotes a ‘cholinergic’ recruitment of SNc neurons through PPN. Explanations are given in the main text. GPe: globus pallidus external segment; GPi: globus pallidus internal segment; IPFC: lateral prefrontal cortex; MI: primary motor cortex; ITC: inferior temporal cortex; PPN: pedunclopontine nucleus; SNc: substantia nigra pars compacta; STN: subthalamic nucleus.

a reward is given, reward information is fed into SNc where an error signal of reward prediction is computed. From this error signal, BG learn to self-organize in such a way that the model's responses maximize rewards.

The cortico-BG-thalamic loops' functional architecture works as follows. Activation of cortex excites striatal and subthalamic neurons. Striatum then inhibits tonically active neurons of the internal segment of globus pallidus (GPi) via striato-pallidal connections that are usually referred to as the direct BG pathway. Decreases of GPi firing in turn disinhibit thalamic neurons that excitatorily connect back to cortex. In global terms, the direct pathway serves to establish WM maintenance within prefrontal loops by mapping cortical representations onto themselves. Within the motor loop, it links WM content to appropriate responses by mapping prefrontal-loop representations onto specific motor-loop representations. In contrast, activation of the subthalamic nucleus (STN) causes a strong and global excitation of GPi via subthalamo-pallidal fibers that are usually referred to as the hyperdirect pathway. As activity is spreading from STN to the external segment of globus pallidus (GPe), inhibitory GPe-GPi connections cancel the excitatory effects of STN on GPi. The hyperdirect pathway (which is modeled only in prefrontal loops) thus gives a brief and global reset pulse to GPi, allowing the respective loop to update. The interplay of the various layers will in detail be analyzed in Section 4.3.2.

In constructing the model, we included only those nuclei and pathways that were necessary to have the model perform response selection, WM maintenance and updating of WM. These functions are required by a set of prominent WM tasks (described in Section 4.2.2). As detailed later in this section as well as in Section 4.3.2, we assume response selection to be subserved by the direct pathway of the motor loop, WM maintenance by the direct pathway of prefrontal loops and WM updating by the hyperdirect pathway of prefrontal loops. We did not model the hyperdirect pathway of the motor loop and the 'indirect' striato-GPe-GPi pathway (within neither loop). As detailed in Section 4.4, empirical evidence implicates these pathways in functions other than the ones targeted in this paper. To keep the motor loop simple, pallido-pallidal, cortico-thalamic and thalamo-cortical connections were rendered hard-coded instead of learnable. Importantly: wherever a nucleus is present in both types of loops, activities are computed via the same equations. And: wherever a connection is learnable in both types of loops, the learning rules are the same.

The mathematical implementation of our model is inspired by a previous model from our group (Vitay and Hamker, 2010) that consists of a single-loop BG architecture without the ability to learn WM control: each of the modeled layers consists of dynamic, firing rate-coded neurons (exact numbers are reported in Table ?? of the Appendix B). For each neuron, a membrane potential is determined via a differential equation, discretized according to the Euler method (first-order) with a time step of 1 ms; a cell-specific transfer function turns membrane potentials into firing rates. The differential equations are evaluated asynchronously to allow for stochastic interactions between functional units. As a general template, membrane potentials $m_i^{\text{post}}(t)$ are computed by the following differential equation:

4 Working memory and response selection

$$\tau \cdot \frac{dm_i^{\text{post}}(t)}{dt} + m_i^{\text{post}}(t) = \sum_{j \in \text{pre}} w_{i,j}^{\text{pre-post}}(t) \cdot u_{\text{pre},j}(t) + M + \epsilon_i(t) \quad (4.1)$$

where τ is the time constant of postsynaptic cell i , $u_{\text{pre},j}(t)$ the firing rate of presynaptic cell j , $w_{i,j}^{\text{pre-post}}(t)$ the weight between these cells, M a baseline parameter and $\epsilon_i(t)$ a random noise term. The noise term supports exploration of WM control and action selection by introducing independent random fluctuations to the membrane potentials of different cells. Firing rates $u_i^{\text{post}}(t)$ are computed from membrane potentials via cell-specific transfer functions $f_u(x)$:

$$u_i^{\text{post}}(t) = f_u(m_i^{\text{post}}(t)) \quad (4.2)$$

As defined in Appendix A, $f_u(x)$ defines negative values to be set to zero and for some layers additionally specifies sigmoid functions.

Loops are not predetermined to represent particular stimuli: each prefrontal loop receives the same visual input and only by accumulating knowledge about its environment will it learn to encode certain stimuli and ignore others. Figure 4.1 depicts all learnable connections of the model by dashed arrows. As explained in detail in the next paragraphs, thalamo-cortical and cortico-thalamic learning is Hebbian-like whereas learning in BG relies on three-factor rules, involving a reward-related dopaminergic term (Reynolds and Wickens, 2002). Dopamine levels are controlled by SNc firing rates and encode an error signal of reward prediction.

Dopaminergic learning poses an obvious challenge on modeling: as stimuli are typically presented (and responses performed) some time before reward delivery, there will be a delay between concurrent activity of pre- and postsynaptic cells and the dopamine levels resulting from that activity. The brain's probable solution to this problem are synapse-specific calcium eligibility traces: concurrent pre- and postsynaptic activities lead to a sudden rise in input-specific postsynaptic calcium concentrations ($Ca_{i,j}^{\text{post}}(t)$) that decrease only slowly when concurrent activity ends.

$$\eta^{\text{Ca}} \cdot \frac{dCa_{i,j}^{\text{post}}(t)}{dt} + Ca_{i,j}^{\text{post}}(t) = f_{\text{post}}(u_i^{\text{post}}(t) - \overline{\text{post}}(t) - \gamma_{\text{post}}) \cdot f_{\text{pre}}(u_j^{\text{pre}}(t) - \overline{\text{pre}}(t) - \gamma_{\text{pre}}) \quad (4.3)$$

$$\eta^{\text{Ca}} = \begin{cases} \eta^{\text{inc}} & \text{if } dCa_{i,j}^{\text{post}}(t) > 0 \\ \eta^{\text{dec}} & \text{else.} \end{cases} \quad (4.4)$$

η^{Ca} is the time constant of the calcium trace, $\overline{\text{pre}}(t)$ the mean firing rate of afferent layer pre at time t , $\overline{\text{post}}(t)$ the mean firing rate of postsynaptic layer post at time t , η^{inc} a parameter controlling the speed of calcium level increase and η^{dec} a parameter controlling the speed of

calcium level decline. γ_{pre} and γ_{post} allow to adjust thresholds for pre- and post-synaptic activities that separate between increases and decreases of calcium traces. Functions $f_{\text{pre}}(x)$ and $f_{\text{post}}(x)$ can restrict pre- and post-synaptic terms to positive values or introduce sigmoid functions as detailed in Appendix A. $dC a_{i,j}^{\text{post}}(t)$ gives a positive value when at the same point in time, both presynaptic cell j and postsynaptic cell i fire more than the adjusted mean activities of their respective layers. As η^{Ca} is set to the relatively small value of η^{inc} in that case, the corresponding calcium level increases rapidly. In contrast, $dC a_{i,j}^{\text{post}}(t)$ becomes negative when concurrent activity ceases. As η^{Ca} is set to a relatively large value (η^{dec}) in that case, the calcium level does not directly drop to zero but declines rather smoothly. Calcium eligibility traces are inspired by findings that calcium levels stay heightened for some interval longer than actual pre- and postsynaptic activities (Kötter, 1994) and that postsynaptic calcium is required for striatal dopamine-mediated learning (Cepeda et al., 1998; Suzuki et al., 2001).

To determine changes in BG-related weights ($w_{i,j}^{\text{pre-post}}(t)$), a three-factor learning rule is used, comprising the calcium trace described above (which contains the two factors pre- and post-synaptic activity) and a dopaminergic term ($\text{DA}(t)$) linked to reward delivery:

$$\eta \cdot \frac{dw_{i,j}^{\text{pre-post}}(t)}{dt} = f_{\text{DA}}(\text{DA}(t) - \text{DA}_{\text{base}}) \cdot C a_{i,j}^{\text{post}}(t) - \alpha_i(t) \cdot (u_i^{\text{post}}(t) - \overline{\text{post}}(t))^2 \cdot w_{i,j}^{\text{pre-post}}(t) \quad (4.5)$$

$$\tau \cdot \frac{d\alpha_i(t)}{dt} + \alpha_i(t) = K_{\alpha} \cdot (u_i^{\text{post}}(t) - u^{\text{MAX}})^+ \quad (4.6)$$

$$f_{\text{DA}}(x) = \begin{cases} x & \text{if } x > 0 \\ \varphi \cdot x & \text{else.} \end{cases} \quad (4.7)$$

$\text{DA}(t)$ is the dopamine level of the respective loop at time t , DA_{base} the baseline dopamine level of 0.5, $\alpha_i(t)$ a regularization factor, u^{MAX} the maximal desired firing rate of cell i , φ a constant regulating the strength of long-term depression (LTD) relative to the strength of long-term potentiation (LTP) and K_{α} a constant that determines the speed of increases of $\alpha_i(t)$. In case of a dopamine burst (i.e. when dopamine levels rise above baseline), all weights are increased in proportion to the strengths of their calcium traces; dopamine depletions (i.e. dopamine levels below baseline) decrease recently active synapses accordingly. The subtractive term of the equation ensures that weights do not increase infinitely: when connections are strong enough to push firing of a postsynaptic cell above a threshold defined by u^{MAX} , α_i increases and all weights to that postsynaptic cell are decreased. This ensures homeostatic synaptic plasticity, i.e. it provides negative feedback to level excessive neuronal excitation (cf. Pozo and Goda, 2010 for a biological review on the phenomenon). Technically, the homeostatic term is derived from Oja's rule (Oja, 1982), but α_i is made dependent upon postsynaptic activity to avoid arbitrary parameter values. Biologically, homeostatic synaptic plasticity has been shown to arise

4 Working memory and response selection

from alterations in the composition and abundance of postsynaptic AMPA receptors (Pozo and Goda, 2010). Increases of α_i can be fast or slow depending on the value of K_α .

By applying a single set of learning principles to all loops, we show their flexibility to subserve two highly different functions, namely to establish flexible control of WM and to link distinct cortical representations in a stimulus-response manner, thereby linking WM to motor control. While the general learning rules for prefrontal and motor loops are the same, the parameter values regulating LTD in the case of dopamine depletion differ. In particular, LTD in prefrontal loops is assumed to be slower than in the motor loop. Functionally, this ensures that after a sudden change in reward contingencies (resulting in dopamine depletions), re-learning in the motor loop is faster than re-learning in prefrontal loops: attempts to map priorly relevant stimuli onto different responses will thus be undertaken faster than gating previously irrelevant stimuli into WM.

The following paragraphs will focus on the different functional parts of the model and more thoroughly explain the supposed architecture.

Cortex

The model contains the cortical structures of lateral prefrontal cortex (IPFC) and MI. IPFC is assumed to take part in WM control (Owen et al., 1999); MI integrates cortical and subcortical inputs to send an emerging motor command to the motoneurons of the spinal cord. As a simplification, we assume each visual stimulus and motor command to be represented by a single computational unit within cortex. All cortical cells receive excitatory thalamic input; IPFC additionally receives cortico-cortical afferents from ITC which is involved in visual object recognition. In the mammal brain, prefrontal cortex is innervated by dopaminergic fibers. Prefrontal dopamine has been shown to modulate WM processes (Seamans and Yang, 2004; Vijayraghavan et al., 2007). However, these dopamine signals appear to last for several minutes (Feenstra et al., 2000; Feenstra and Botterblom, 1996; van der Meulen et al., 2007; Yoshioka et al., 1996) and are therefore not well suited to reinforce particular stimulus-response associations in a timely precise manner. Within the model, learning of thalamo-cortical weights is therefore assumed to be Hebbian-like (i.e. to not be modulated by dopamine). As our model is essentially an account of how learning in BG guides the organization of cortico-BG-thalamic loops, we do not model prefrontal dopamine signals.

Thalamus

Thalamus is assumed to relay information to cortical areas (Guillery and Sherman, 2002) and to control cortical activation and deactivation (Hirata and Castro-Alamancos, 2010). Consistent with this, maintenance of a representation in WM and selection of a response require thalamic disinhibition through GPi in the model. Thalamic cells receive inhibitory pallidal and excitatory cortical input (cf. Figure 4.1). As with prefrontal cortex, there is evidence for dopaminergic

innervation of the thalamus (Melchitzky and Lewis, 2001; Sánchez-González et al., 2005). The nature of the dopamine signals provided, however, has not yet been clearly elucidated. Conservatively, we thus assume cortico-thalamic learning to be Hebbian-like (i.e. not to be modulated by dopamine).

Striatum

There are two input structures to the BG: striatum and STN. Both receive glutamatergic cortical afferents and both are organized topographically (Ebrahimi et al., 1992; Miyachi et al., 2006). Striatum can be subdivided into putamen, receiving mostly motor-cortical afferents, and caudate nucleus, innervated by IPFC (Alexander et al., 1986). Next to excitatory cortical afferents, striatal cells receive inhibitory input from a network of GABAergic interneurons (Suzuki et al., 2001). In the model, these are hard-coded for means of simplicity and serve to downsize the number of striatal cells that become associated to each cortical representation. Activity of caudate nucleus has been shown to be negatively correlated with progress in reward-related learning (Delgado et al., 2005). Lesioning dorsolateral parts of the striatum leads to disabilities in stimulus-response learning (Featherstone and McDonald, 2004). Within the model, striatum learns to efficiently represent single or converging cortical afferents in clusters of simultaneously activated cells as previously shown by Vitay and Hamker (2010). Striatum gives rise to the direct BG pathway, that connects striatal cell clusters to single GPi cells. Thereby, it is vital both for WM maintenance and stimulus-response mapping.

Subthalamic nucleus

STN is considered part of the hyperdirect BG pathway that links cortex with GPi via two excitatory connections (Nambu et al., 2002). Also, STN excitatorily innervates GPe (Parent and Hazrati, 1995a). Recently, STN has become a key target for deep brain stimulation (DBS) in Parkinsonian patients in order to alleviate dyskinesia (Kleiner-Fisman et al., 2006) and to improve mental flexibility (Alegret et al., 2001; Witt et al., 2004). STN DBS has been reported to cause WM deficits in spatial delayed response tasks (Hershey et al., 2008) and nn-back tasks (Alberts et al., 2008), thereby further underlining its contribution to cognitive processing. Electrical stimulation of STN in monkeys yields a short-latency, short-duration excitation of GPi, followed by a strong inhibition, the latter being mediated by GPe (Kita et al., 2005). Based on these findings, we assume STN within prefrontal loops to give a global (learned) excitatory reset signal to GPi that is canceled by STN-GPe-GPi fibers shortly after.

Globus pallidus external segment

The role of GPe in BG functioning is still rather elusive. Historically, GPe has been considered a relay station on a striato-GPe-subthalamo-GPi pathway, often referred to as the indirect BG

4 Working memory and response selection

pathway (DeLong, 1990). More recently, such a simple notion has been challenged and GPe has been hypothesized to have a more prominent processing function in BG (Obeso et al., 2006). Our model contains a reduced set of GPe connections, accounting for afferents from STN and efferents to GPi only. Thereby, GPe is modeled only in its potential contribution to the hyperdirect (and not the indirect) pathway.

Globus pallidus internal segment

The internal segment of globus pallidus is a major BG output structure receiving and integrating subthalamic, external pallidal and striatal input (DeLong and Wichmann, 2007). GPi has a high baseline firing rate by which it tonically inhibits thalamic neurons (Chevalier and Deniau, 1990). Striatal and GPe inputs inhibit GPi cells below this baseline, thus disinhibiting thalamic neurons and opening a gate for mutually excitatory cortico-thalamic loops (DeLong and Wichmann, 2007). Subthalamic input in contrast excites GPi, thus further inhibiting thalamic neurons and preventing cortico-thalamic loops from firing (Nambu et al., 2002). The interplay of afferents to GPi which is critical for the model's functioning, will be studied in detail in Section 4.3.2 of this paper.

Lateral competition in GPi ensures that each striatal cell cluster connects to a single pallidal cell only. While this is of course a simplification, it reasonably reflects the much smaller number of pallidal cells relative to striatal ones (Lange et al., 1976). As shown in Eq. (A.23) of the Appendix A, lateral weights evolve according to an Anti-Hebbian learning rule.

Substantia nigra pars compacta

Inspired by the findings of Schultz and co-workers (Hollerman and Schultz, 1998; Schultz et al., 1997) and in line with other computational accounts of reinforcement learning O'Reilly and Frank (2006), we assume SNc neurons to compute an error signal of reward prediction. This signal is then relayed to BG to modulate learning of afferent connections. A detailed account of the underlying rationale can be found in Vitay and Hamker (2010). Briefly, SNc neurons compute a difference signal between actual and expected rewards and add the resulting value to a medium baseline firing rate of 0.5. Thereby, unexpected rewards lead to activities above this baseline while omissions of expected rewards result in decreases in SNc firing. Information about actual rewards is set as an external input while stimulus-specific reward expectations are encoded in learnable striato-nigral afferents.

Each prefrontal and motor loop is connected to a separate SNc neuron. This is based upon reports showing SNc to have a topographical organization and reciprocal connections with striatum (Haber, 2003; Joel and Weiner, 2000). Inspired by evidence showing SNc neurons to broadly innervate striatal subregions (Matsuda et al., 2009), we assume a single dopamine neuron to innervate all BG cells of a corresponding loop.

Pedunclopontine nucleus

As outlined above, the model contains multiple prefrontal loops. Following an idea by Krueger and Dayan (2009), recruitment of these loops is dependent upon error detection after prior successful task performance. The framework of our model allows us to develop a biologically plausible mechanism of error detection: highly unexpected errors (i.e. errors after prior successful task performance) lead to relatively large dips in SNc firing. These dips can be used as a signal to recruit additional SNc neurons, thereby enabling learning within additional prefrontal loops.

A potential anatomic substrate for subserving such a recruitment is a part of the brainstem named pedunclopontine nucleus (PPN). PPN has been associated to the phenomena of attention, arousal, reward-based learning and locomotion (Winn, 2006); activation of cholinergic fibers from PPN to SNc has been shown to recruit quiescent dopamine neurons (Di Giovanni and Shi, 2009). As PPN is innervated by many BG structures (Mena-Segovia et al., 2004), it presumably also receives information about reward prediction. In our model, PPN constantly receives input from the SNc. Whenever the most recently recruited prefrontal-loop SNc neuron fires below a fixed threshold of 0.05 because of a highly unexpected error, PPN sends an activation signal back to the SNc to recruit an additional SNc neuron. Through this simple operation, PPN subserves a basic form of task monitoring, reacting whenever unexpected omissions of reward occur. In employing this mechanism, we do not artificially decrease learning rates within those prefrontal loops that previously recruited SNc neurons belong to. This contrasts with the model of Krueger and Dayan (2009).

Of course, the mechanism we propose may be largely simplified: other brain areas than the PPN have been linked to error detection as well, in particular the anterior cingulate (Holroyd and Coles, 2002). Further, PPN output is not restricted to SNc but also reaches other BG nuclei, most notably STN (Winn, 2006). Thus, PPN will neither be the only brain structure involved in error detection nor will recruitment of dopamine neurons be the only way it assists in modulating learning in cortico-BG-thalamic loops.

4.2.2 Experimental setups

We demonstrate the model's learning capabilities on DR tasks as well as on the 1-2-AX conditional WM task.

Delayed response and delayed alternation tasks

We trained the model on an unconditional DR task, a conditional DR task and a DA task. In all three tasks, the model is exposed to a continuous array of trials. Within each trial, it has to choose between two responses and is rewarded if it picks the correct one. When a network has

4 Working memory and response selection

performed correctly for 100 trials in a row, we assume it to have learned the task successfully. A failure is admitted if a network does not reach this criterion within 10,000 trials.

In the unconditional DR task (cf. Figure 4.2 (A)), one of two stimuli (i.e. either stimulus A or stimulus B) is presented for 400 ms at the beginning of each trial. After a delay period of 200 ms, the model's response is evaluated. For stimulus A, the left button has to be selected while stimulus B requires a right-button press. The model has no prior knowledge about associations between stimuli and buttons. The conditional DR task (cf. Figure 4.2 (B)) differs from the unconditional DR task in that two stimuli are displayed and that both of them have to be considered to achieve a correct response: if stimuli A and X (or B and Y) have been shown, a left-button press is required while presentation of stimuli A and Y (or B and X) requires a right-button press. In the DA task (cf. Figure 4.2 (C)), the model is supposed to alternate between left- and right-button presses every 1200 ms. Reward is given whenever it chooses the button that it did not choose in the previous trial. For the DA task, we make the additional assumption that the model visually perceives the response that it decides for. Each response is thus fed into the model as a stimulus.

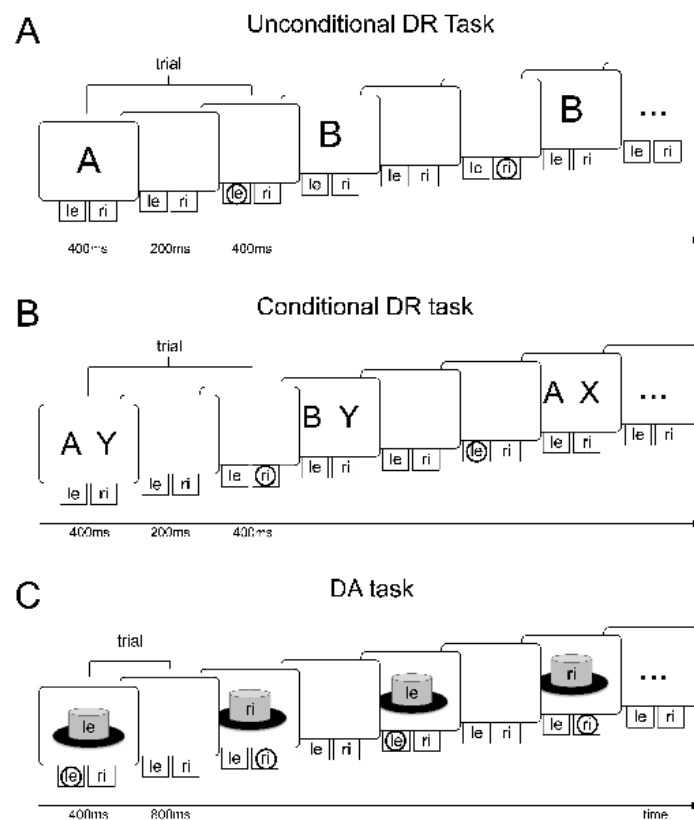


Figure 4.2: Delayed response tasks and delayed alternation task: In each task, the model is confronted with a successive array of trials. Within each trial, it has to choose between a left- and a right-button press. Circles indicate correct responses. Depending on the task, stimuli may or may not be presented. Detailed explanations are given in the main text. (A) Unconditional DR task. (B) Conditional DR task. (C) DA task. DR: delayed response; DA: delayed alternation; le: left button; ri: right button.

1-2-AX task

Within each trial of this task, one of a set of eight possible stimuli (1, 2, A, B, C, X, Y and Z) is shown and the model is required to decide for one of two buttons (cf. Figure 4.3). Only and exactly one of these buttons will lead to reward when pressed. The task has a complex inner-outer loop structure that is not known to the model: numbers (1 and 2) represent context cues and constitute the outer loop. To correctly perform the task, the last outer-loop stimulus has to be kept in WM at any time. Whenever the last outer-loop stimulus has been a 1, presentation of an X requires a right-button press when it has been directly preceded by an A; if the last outer-loop stimulus has been a 2, a Y that directly follows a B requires a right-button response. In all other cases, a left-button press has to be performed. The model has to decide for a response within each trial. There are several versions of this task regarding the sequence of stimuli. We will here use the version employed by O'Reilly and Frank (2006): First, an outer-loop stimulus (i.e. 1 or 2) is randomly chosen. Then, with equal probabilities, one to four inner loops are generated. With a probability of 0.5, an inner loop consists of a potential target sequence (i.e. A-X or B-Y); otherwise, any of the inner-loop stimuli (i.e. A,B or C) is followed by any of X,Y or Z, all probabilities being equal.

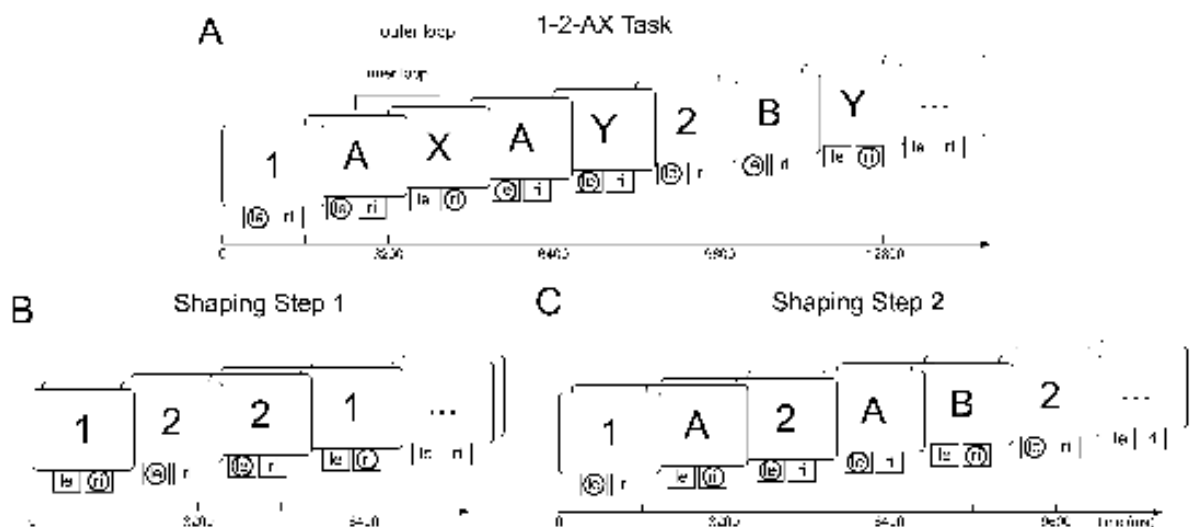


Figure 4.3: The 1-2-AX conditional WM task and the shaping procedure proposed to train the model. In each trial, a stimulus is presented and the model has to choose between a left- and a right-button press. Circles indicate correct responses. Please refer to the main text for detailed explanations. (A) Full 1-2-AX task. (B) Step 1 of the shaping procedure involving only the outer-loop stimuli 1 and 2. (C) Step 2 of the shaping procedure involving outer-loop stimuli (1 and 2) plus inner-loop stimuli (A,B and C). le: left button; ri: right button.

Teaching this task to the model requires a three-step shaping procedure as depicted in Figure 4.3. In a first step, only the outer-loop stimuli 1 and 2 are presented, probabilities being equal. Each 1 requires a right-button press, each 2 a left-button press. When the model has reliably acquired this task (which is conservatively assumed to be the case after 100 correct responses in a row), the inner-loop stimuli A,B and C are added to the sequence. An outer-loop

stimulus can be followed by one or two inner-loop stimuli, all probabilities again being equal. A right-button press is required when an A comes up and the last number has been a 1 and when a B comes up and the last number has been a 2. In all other cases, a left-button press is required. Finally, when the second step is securely coped with, the full task is presented. After 150 correct responses in a row, the model is classified as having solved the task; if this criterion is not reached within 10,000 trials, we admit that the model has failed. In the first two steps of shaping, stimulus presentation (lasting for 400 ms) is separated from response requirement by a 400 ms delay period. This is to ensure that the model learns to make use of WM, preventing it from solving the task by simply associating visual ITC representations to responses. By employing the latter strategy, the model would not develop the ability to maintain the stimuli in WM as is required to successfully master the subsequent steps of shaping. For the full task, responses are required while visual stimulation is still on as proposed by O'Reilly and Frank (2006). Each stimulus is presented for 800 ms. 400 ms after each stimulus onset, the model's response is evaluated.

4.3 Results

4.3.1 Task performance

Delayed response and delayed alternation tasks

Fig. Figure 4.4 (A) shows the model's performance in learning the DR/DA tasks. For each of the three versions of the task, 50 randomly initialized networks were run. For each task, box plots show the number of trials needed until the last error occurs.

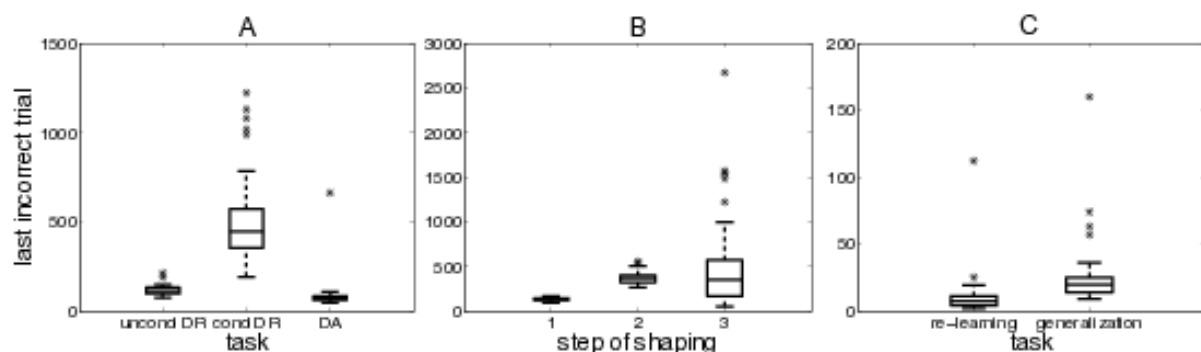


Figure 4.4: The model's performance in learning several WM tasks. (A) Performance on the DR/DA tasks. (B) Performance on the 1-2-AX task, separately for each step of shaping. (C) Performance on the generalization test described in Section 4.3.2. For each of the tasks, 50 randomly initialized networks were run. Box plots show the number of trials needed until the last error occurs. The boxes' upper and lower borders represent upper and lower quartiles, respectively; the median value is shown as a line crossing each box. Whiskers extend to a maximal length of 1.5 times interquartile range, outliers are represented by asterisks.

One network failed to learn to criterion. Two-sided Mood's median tests provide difference statistics for the number of trials needed until the last error occurs. Thanks to the stability of these non-parametric tests in the presence of outliers, we kept the failing network for statistical analyses, charging the maximum number of 10,000 trials: the unconditional DR task (Mdn=111, IQR=33) requires significantly less trials than the conditional DR task (Mdn=443.5, IQR=221), $\chi^2(1) = 92.16$, $p < 0.001$. Clearly, this is because of its simpler rules. The DA task (Mdn=70.5, IQR=22) takes significantly less trials than both the unconditional DR task, $\chi^2(1) = 51.84$, $p < 0.001$, and the conditional DR task, $\chi^2(1) = 84.64$, $p < 0.001$.

1-2-AX task

Figure 4.4 (B) shows the performance of 50 randomly initialized networks learning the 1-2-AX task. For each step of the shaping procedure, box plots show the number of trials needed until the last error occurs.

All networks learned the task to criterion. Two-sided Wilcoxon signed-rank tests provide difference statistics for the number of trials needed to cope with the different steps: the second step of shaping (Mdn=365, IQR=78) takes significantly longer than the first step (Mdn=130, IQR=23), $z=6.15$, $p<0.001$, as can be explained by the more complex set of rules to learn and the higher number of additional WM representations to develop. The third step (Mdn=352.5, IQR=402) requires significantly more trials than the first step, $z=5.49$, $p<0.001$, but does not differ significantly from the second step, $z=0.50$, $p=0.62$. In the third step, a highly complex set of rules has to be learned while no additional WM representations have to be developed.

4.3.2 Analysis of the model's behavior

Re-learning and generalization

To demonstrate the model's abilities to profit from previous experiences, we evaluated its performance both in re-learning a task that has previously been learned and in generalizing from previous experiences to a new but structurally similar task. To this end, we trained 100 randomly initialized networks on the first two steps of the shaping procedure designed for the 1-2-AX task. Once the second step was learned to criterion, we again changed the rules: for 50 networks, we went back to the first step of shaping to evaluate re-learning. Note that learning the second step could have overwritten the knowledge acquired in the first step. For the 50 remaining networks, we changed the meanings of the two outer-loop stimuli to evaluate generalization. Previously, a right-button press had been required for an AA if the most recent number had been a 1 and for a BB if it had been a 2. Now it was required for an AA when the last number had been a 2 and for a BB when it had been a 1. Note that in this test for generalization the stimuli stay the same while responses have to be adapted.

4 Working memory and response selection

Figure 4.4 (C) shows the model's performance on these tests of re-learning and generalization. All networks learned to criterion. Difference statistics are based on two-sided Wilcoxon signed-rank tests. Re-learning the first step of shaping (Mdn=7.5, IQR=7) is significantly faster than the initial process of learning it (Mdn=129, IQR=25), $z=6.15$, $p<0.001$. Learning the generalization task (Mdn=19.5, IQR=11) takes significantly less trials than learning the first plus the second step of shaping (Mdn=493.5, IQR=112), $z=6.15$, $p<0.001$. Thus, the generalization task is learned a lot faster than the equally complex task that is learned during the first two steps of shaping. In fact, the generalization task is even learned significantly faster than both the first step of shaping by itself (Mdn=127.5, IQR=35), $z=6.14$, $p<0.001$, and than the second step of shaping by itself (Mdn=360.5, IQR=88), $z=6.15$, $p<0.001$. Thereby, it is clearly shown that the model profits from previous experiences: the more it has already learned about its environment, the better become its abilities to solve further problems.

Spread of activity within cortico-BG-thalamic loops

When a stimulus is presented to the model, it can either become maintained in WM or it fades away as visual stimulation ends. Figure 4.5 illustrates how a target stimulus—once associated to reward—is actively maintained in WM: when the target comes up in ITC, target-related activity (black line) is relayed to IPFC. IPFC then activates associated striatal and subthalamic cells. Subthalamic activity rises fast leading to a global increase in GPi firing via all-to-all excitatory connections. This breaks the circle of reverberating activity in the respective prefrontal loop, erasing any previously maintained stimulus (see gray lines) from WM. In the meantime, GPe activity rises through subthalamic excitation. By all-to-all inhibitory connections to GPi, GPe counterbalances the excitatory effect of STN on GPi and thereby—with a brief delay—brings WM reset to an end. As the previously maintained stimulus is erased from WM, target-related IPFC activity can activate striatal target-coding cells. Via inhibitory connections, these striatal cells then decrease firing of a GPi neuron that is associated to the target. This neuron in turn disinhibits a corresponding thalamic cell. Thalamus then excites cortex so that target-associated activity can reverberate in the prefrontal loop.

Figure 4.6 depicts the effects of target presentation on the motor loop: the target-coding cells within IPFC and ITC excite striatal cells of the motor loop. These cells then inhibit an associated GPi cell that in turn disinhibits a corresponding thalamic cell. Thalamus then excites the particular MI cell that codes the response that the target stimulus has been mapped on.

4.3.2.1 Development of WM control

Figure 4.7 shows the development of WM control. Firing rates are taken from a randomly initialized network learning the unconditional DR task. Intra-temporal, lateral prefrontal, striatal, subthalamic and pallidal activities of the prefrontal loop are shown for four periods along the

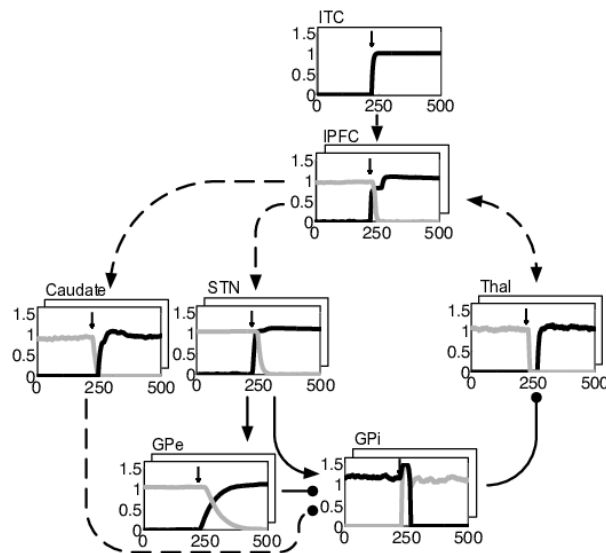


Figure 4.5: Prefrontal-loop effects of presenting a task-relevant stimulus (target) to the model when another stimulus is currently kept in working memory. For various layers of a prefrontal loop, subplots present firing rates of selected cells within a 500 ms time period covering target presentation onset (denoted by arrows). Firing rates of cells coding the target are shown as black lines while gray lines correspond to the previously maintained stimulus. All firing rates are taken from a randomly initialized network successfully coping with an unconditional DR task. Explanations are given in the main text. GPe: globus pallidus external segment; GPi: globus pallidus internal segment; ITC: inferior temporal cortex; IPFC: lateral prefrontal cortex; STN: subthalamic nucleus; Str: Striatum; Thal: thalamus.

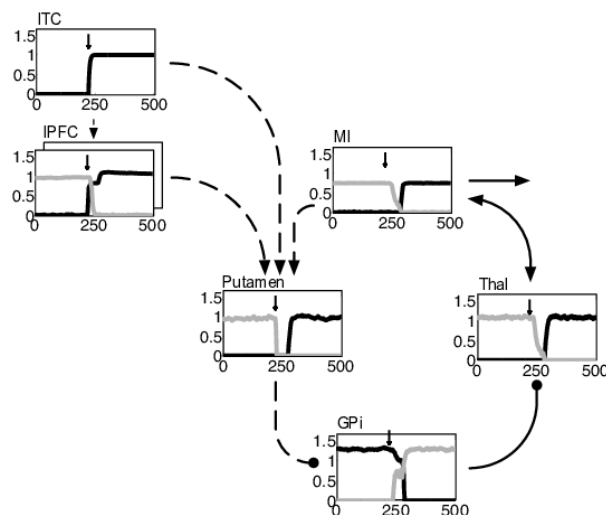


Figure 4.6: Motor-loop effects of presenting a task-relevant stimulus (target) to the model when another stimulus is currently kept in working memory. For various layers of the motor loop, subplots present firing rates of selected cells within a 500 ms time period covering target presentation onset (denoted by arrows). Firing rates of cells associated to the target and its associated response are shown as black lines, gray lines correspond to the previously maintained stimulus and its associated response. All firing rates are taken from a randomly initialized network successfully coping with an unconditional delayed response task. Explanations are given in the main text. GPi: globus pallidus internal segment; ITC: inferior temporal cortex; IPFC: lateral prefrontal cortex; MI: primary motor cortex; Str: Striatum; Thal: thalamus.

4 Working memory and response selection

process of learning (trials 1-5, 52-56, 91-95 and 129-133). The unconditional DR task we employed contains two stimuli, AA and BB. Black lines show firing rates of cells that can a posteriori be identified as having learned to code stimulus AA, gray lines correspond to stimulus BB.

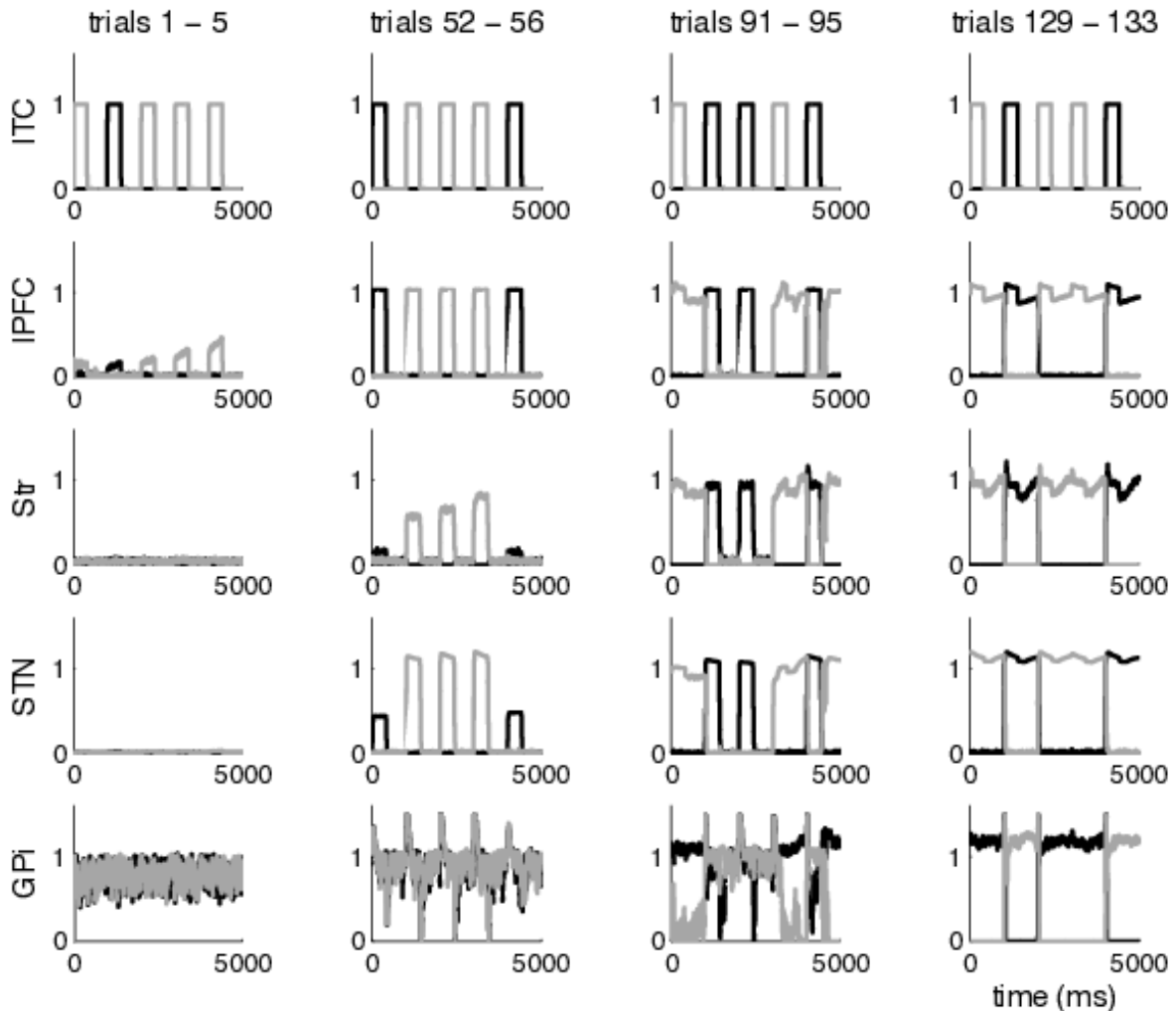


Figure 4.7: Development of WM control in the prefrontal loop that is directly subject to learning during an unconditional delayed response task. Subplots show firing rates of various prefrontal-loop layers for 5000 ms periods at different stages of the learning process (trials 1-5, 52-56, 91-95 and 129-133). Black lines depict firing rates of cells coding stimulus AA while gray lines correspond to stimulus (BB). Explanations are given in the main text. GPI: globus pallidus internal segment; ITC: inferior temporal cortex; IPFC: lateral prefrontal cortex; STN: subthalamic nucleus; Str: striatum.

The leftmost column (trials 1-5) shows prefrontal-loop activities soon after the model is exposed to the task: IPFC task-related activities begin to emerge through the development of Hebbian connections from ITC. The corresponding IPFC cells have, however, not yet learned to activate striatal or subthalamic cells so that all representations fade away from WM when visual stimulation ends. Some decades of trials later (trials 52-56), cortico-subthalamic connections have largely developed as evidenced by the existence of task-related subthalamic activity upon stimulus presentation. Further, cortico-striatal connections have begun to emerge, result-

ing in some striatal activity upon stimulus presentation. Pallidal representations have not yet clearly developed as evidenced by the more or less uniform firing of GPi across trials. Thus, stimulus-associated activity cannot reverberate within cortico-BG-thalamic loops and IPFC representations still fade away when visual stimulation ends. Another four decades of trials later (trials 91-95), pallidal representations have started to evolve: stimulus BB (gray lines) shows clear task-related GPi activity (i.e. decreases of firing rates contingent upon stimulus presentation). This stimulus is now maintained in the loop independent of visual stimulation (which can be seen by ongoing activity after visual input ends). It can be concluded that a closed loop of connections that subserve the observed maintenance has been developed for this stimulus. Stimulus AA (black lines) however is still not clearly represented in the layers and mostly fades away when visual input ceases. The rightmost column shows the network when it has fully learned the DR task (trials 129-133): all brain areas show clear task-related activities. Both stimuli are maintained throughout the delay periods. Notice that when a stimulus is presented twice in a row, WM is not reset in between.

Recruitment of prefrontal loops

As outlined in Section 4.2.1, in cases of unexpected changes of reward contingencies, PPN triggers the activation of quiescent SNc neurons through dips in dopamine levels. This behavior can be well observed in networks learning the 1-2-AX task (Figure 4.8).

In the first step of shaping, two SNc neurons are active: the one neuron associated to the motor loop and one of the two neurons associated to prefrontal loops; the third SNc neuron is fixed to the baseline firing rate of 0.5 and awaits its activation by PPN. As the model learns the first step of shaping and becomes successful in predicting reward, firing rates of all active SNc neurons asymptotically approach baseline level (which can be seen around trial 200). As soon as the model has performed correctly for 100 trials in a row, the second step of shaping begins. Thereby, the rules of the task switch and the model cannot predict rewards accurately anymore. As it, however, still expects to be able to, SNc firing rates dip much below baseline. This activates the SNc neuron of the second prefrontal loop (as can be seen around trial 260). Around trial 700, the model has learned to cope with the second step of shaping and dopamine levels approach baseline again. After 100 correct responses in a row, the rules of the task switch again and SNc firing dips. This would now activate an SNc neuron of a third prefrontal loop (which, however, we did not include to save computational time as the tasks presented can be learned without it).

How shaping helps

To support the model in learning the 1-2-AX task, we train it using a three-step shaping protocol as described in Section 4.2.2. This protocol breaks down the inner-outer-loop structure of the task to assist the model in learning it. Figure 4.9 shows mean cortical activities for a network

4 Working memory and response selection

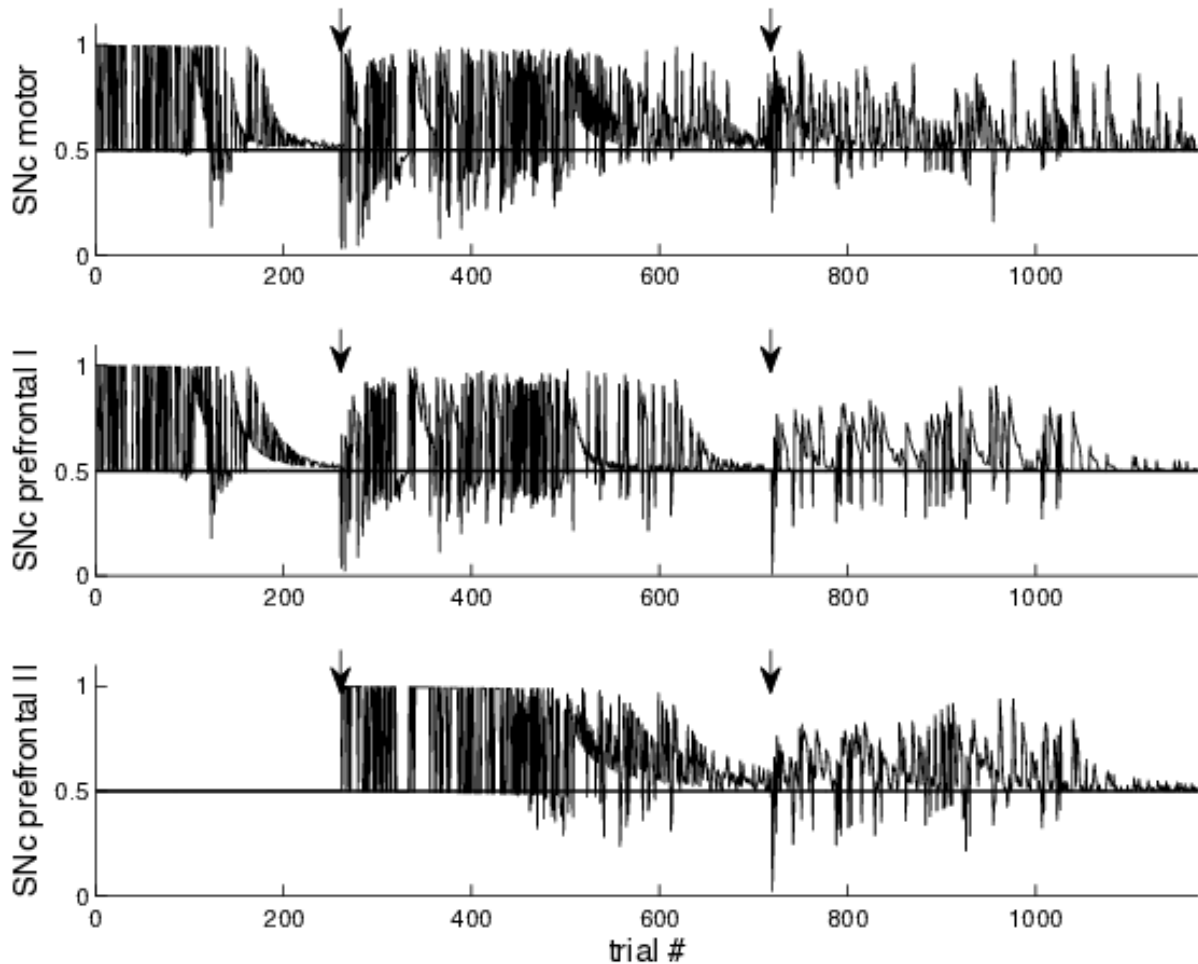


Figure 4.8: Activity of SNc neurons over the course of trials, taken from a randomly initialized network learning the 1-2-AX task. Subplots show firing rates for each of the three SNc neurons involved in the task. Arrows indicate where a switch of rules takes place. Explanations are given in the main text. SNc motor: substantia nigra pars compacta (SNc) cell of the motor loop; SNc prefrontal I: SNc cell of the prefrontal loop that is directly subject to dopaminergic modulation; SNc prefrontal II: SNc cell of the prefrontal loop that becomes modulated by dopamine when activated by the pedunculopontine nucleus.

that successfully copes with the full 1-2-AX task. Firing rates of cells that belong to ITC and both parts of IPFC are each averaged over 100 consecutive trials.

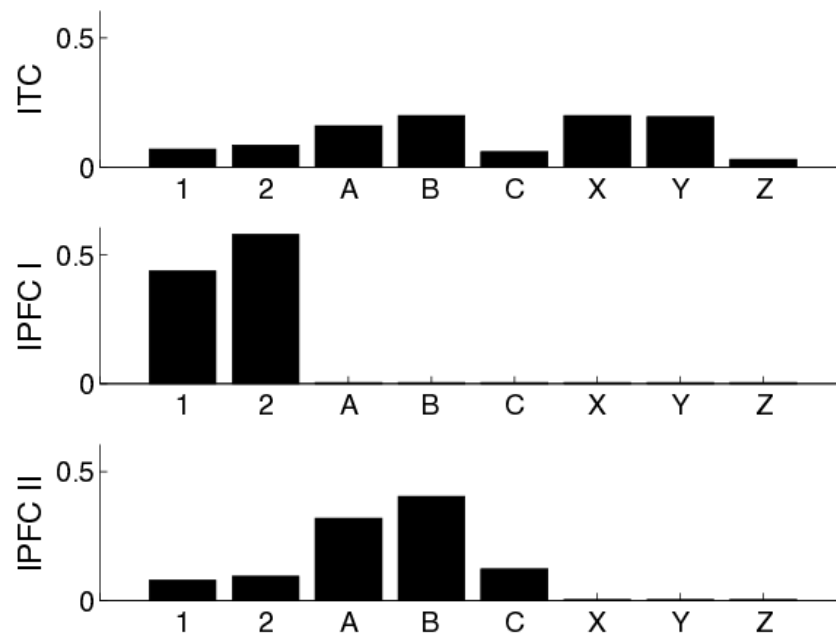


Figure 4.9: WM control strategies of prefrontal cortex. For a network that successfully copes with the 1-2-AX task, subplots show mean activities within inferior temporal cortex and both parts of lateral prefrontal cortex: For each cortical cell, mean firing rates are depicted as averaged over 100 trials. ITC: inferior temporal cortex; IPFC I: part of lateral prefrontal cortex that belongs to the prefrontal loop that is directly subject to dopaminergic modulation; IPFC II: part of lateral prefrontal cortex that belongs to the loop that becomes modulated by dopamine when activated by the pedunculo-pontine nucleus.

As described in Section 4.2.1, visual input is directly fed into ITC. Obviously therefore, ITC shows above-zero activities for all of the task's stimuli. The different mean firing rates reflect the stimuli's different probabilities of appearance as defined by the task. In particular, stimuli A,B,XA,B,X and YY are presented most often. IPFC activities are shown separately for the two prefrontal loops. Within the prefrontal loop which is subject to dopaminergic modulation directly, IPFC shows non-zero activities for stimuli 1 and 2. This indicates that this loop alternates between maintenance of the two outer-loop stimuli, ignoring all other stimuli. It thereby follows precisely the strategy of WM control that it has learned during the first step of shaping. The part of IPFC that belongs to the prefrontal loop which is recruited by PPN later shows strong activities for stimuli 1, 2, A,BA,B and CC. Clearly, these are the stimuli presented during the second step of shaping. This loop thereby maintains the last inner-loop stimulus that has been presented. From a global viewpoint, the model therefore maintains both the last outer-loop stimulus and the last inner-loop stimulus in WM at all times. In addition, ITC represents the stimulus presently shown. Via connections from ITC and IPFC to putamen, the motor loop is thus equipped with all the necessary information to choose its responses correctly: it receives information about the last outer-loop stimulus, the last inner-loop stimulus and the currently presented stimulus.

4.4 Discussion

We have shown how interactions among hierarchically interconnected cortico-BG-thalamic loops allow for flexible control of WM and for adaptive stimulus-response mappings. We thereby find that the anatomically well-defined cortico-BG-thalamic architecture is flexible enough to subserve both WM control and response selection. This implies that the same BG nuclei and pathways can subserve different functions on different levels of the system's hierarchy. The striatum and its associated direct pathway allows for WM maintenance in prefrontal loops and for stimulus-response associations in motor loops. Within the cortico-BG-thalamic architecture, we show how complex strategies of WM control and response selection can be learned by methods of successive approximations and that these methods allow to generalize previously learned behaviors to new situations.

The need for shaping in complex WM tasks

As outlined above, the model relies on a three-step shaping procedure to solve the 1-2-AX task. To understand why shaping is vital to solve a complex task like that, it is necessary to understand its structure: in the 1-2-AX task, different stimuli have to be maintained in WM for differing periods of time. Moreover, they have to be updated independently depending on WM content and visual input. Specifically, outer-loop stimuli have to be deleted from WM only when the next outer-loop stimulus appears, while inner-loop stimuli have to be maintained for one trial only; all other stimuli should not be maintained at all. To make the task even more difficult, the model further has to learn how to correctly respond based on WM content. Decisions about rewards are based upon the final response only, not upon WM control. This poses the need of inferring both correct WM control and response behavior from a binary and thus relatively unspecific reward signal. One way to enable an agent to find out complex strategies of WM control and response behavior is to have it randomly permute the space of potential solutions (i.e. to try out each possible configuration of WM content and responses). O'Reilly and Frank (2006) employ such an approach. In their model, the maintenance of representations in WM is not subject to learning, only the gating of stimuli into WM. In order to learn correct WM control and stimulus-response associations, these stimuli must first be gated into WM, otherwise their information is lost before anything can be learned. To get the learning going, their model randomly gates stimuli into WM in an early phase of learning. Sooner or later, this will lead to finding the correct solution. However, such an approach is quite a computational effort and soon becomes practically infeasible as the number of potential stimuli and reactions increases. This is reflected in the much higher number of trials the PBWM model requires to learn the 1-2-AX task (being in the order of 30,000 compared to approximately 1000-1500 for our model, taking our definition of a trial). In contrast, our model allows each stimulus to enter IPFC and then learns WM maintenance and stimulus-response associations via calcium trace learning. As a consequence of this approach, our model does not learn the 1-2-AX task without a shaping procedure. While this might appear as a disadvantage at first sight, we consider it to be advantageous in

terms of biological plausibility and flexibility: a human subject who is supposed to learn the 1-2-AX task without being told about its rules (and who has to find them find out through trial and error) will have a pretty hard time. Infant humans who cannot access a similarly broad range of previous experiences surely will not learn it without a shaping procedure. At the beginning of learning, our model does not have any knowledge, either (making infant learning a fair comparison). However, as outlined by Krueger and Dayan (2009), shaping allows an agent to develop sub-strategies for solving complex tasks. These can be kept in memory and be reactivated when an agent faces new but similar problems. Our model develops one sub-strategy within each step of shaping. When facing new tasks, it will use prior strategies in parallel with developing new ones and thus constantly enlarges its knowledge about its environment (cf. Section 4.3.2). By quickly re-learning previous WM-motor strategies and by generalizing from previous strategies (cf. Section 4.3.2), our model's dependency on shaping for solving complex tasks gradually decreases. It thereby gives an explanation of how high-level cognitions can develop from basic cognitive operations.

Limitations of the model

The model employs a considerable number of simplifications: it does not contain the indirect BG pathway. This pathway and its predominantly D2-type dopamine receptors appear to be prominently engaged in learning to reverse dominant behaviors (Izquierdo et al., 2006; Lee et al., 2007; Tanimura et al., 2011). Also, the hyperdirect pathway of the motor loop has been omitted. Empirically, it appears to provide (relatively global) stop signals to prevent execution of responses (Aron and Poldrack, 2006; Eagle et al., 2008). This paper is restricted to the functions of response selection, WM maintenance and WM updating as required by most basic WM tasks. Therefore, we do not model these additional pathways. As a further simplification, we do not consider exact timing of responses: as stated in Section 4.2.2, the motor responses of the model are read out at predefined time-steps. Each decision about reward delivery thus depends upon the dominant response at only one particular time-step—and therefore neither upon the latency nor the duration of the response. Moreover, as the focus of this paper is on the contribution of BG reinforcement learning processes to the establishment of WM control and response selection, we do not provide an interpretation on the contribution of prefrontal dopamine signals to WM processes.

Comparison to other computational models of reinforcement learning in BG

A prominent account of the role of BG in WM is the PBWM model proposed by O'Reilly and Frank (2006). They provide a model of prefrontal cortico-BG-thalamic loop functioning, not including any explicit motor loop. This model requires BG for gating stimuli into prefrontal cortex while maintenance of information is subserved by locally self-excitatory prefrontal cortical loops; the direct and indirect BG pathways provide Go and NoGo signals for WM update, respectively. These assumptions contrast with our suppositions, implicating the whole cortico-BG-thalamic

4 Working memory and response selection

loop, via the direct BG pathway, in learning to maintain information (however, we agree that in well-learned tasks cortico-cortical connections might progressively take over control and supersede BG participation). Existing empirical evidence does not clearly favor one or the other assumption as several types of task-related activity seem to exist in striatal neurons. Cromwell and Schultz (2003) for instance found five such types in a spatial DR task. Consistent with our approach, one of these types showed sustained activity for the whole delay period. The relatively small number of cells in GPi (Lange et al., 1976) might at first sight argue against our hypothesis that WM maintenance is learned via cortico-BG-thalamic loops. But note that other types of connections (e.g. cortico-cortical ones) might develop as WM maintenance of a particular stimulus has been reliably learned, and release GPi to learn something new.

Ashby et al. (2007) propose a single-loop model of perceptual category learning (SPEED) that does not account for WM. They use a three-factor learning rule, much like ours, to map cortical representations onto striatal cells. However, BG learning is restricted to cortico-striatal connections, thus rendering their model less powerful in stimulus-response mapping. In particular, it will have severe problems mapping stimuli onto responses when relevant information lies within stimulus compounds instead of single stimuli. By allowing cortico-cortical connections to shortcut BG in case of well-learned, automatic behavior, however, their model provides an interesting concept beyond the scope of our model.

Brown et al. (2004) present an account of how learning within a single cortico-BG-thalamic loop assists in deciding between reactive and planned behaviors. Their TELOS model manages to learn several saccadic tasks and offers much anatomical detail. The authors assume cortico-cortical learning to be subject to the same phasic dopamine modulation as learning between cortex and BG. As explained above, this assumption is somewhat challenged by the long-lasting nature of prefrontal dopamine signals. WM is modeled as a hard-coded entity that is anatomically restricted to PFC: visual representations are predetermined to be gated in when PFC activity surmounts a certain threshold and to be deleted from it when the next sufficiently strong input appears.

Vitay and Hamker (2010) propose a computational account on how learning in BG guides visual attention in Delayed-Match-to-Sample and Delayed-Paired-Association tasks. The model contains only one cortico-BG-thalamic loop which is connected to infero-temporal cortex. It does not have the abilities to learn WM control. BG connectivity is restricted to the direct pathway. We here adapt and extend their account to model WM and motor control. To that end, we kept the general procedure of computing membrane potentials and firing rates. We also kept the concept of three-factor learning rules within BG—but sophisticated them to contain calcium eligibility traces. We newly devised an architecture of parallel cortico-BG-thalamic loops and allowed for interactions among these loops. We included additional BG nuclei and pathways and made the lateral inhibition in GPi independent of dopaminergic modulation to improve the model's performance and to be in better accord with empirical data.

Predictions

Our model provides falsifiable predictions with regard to both behavioral and electrophysiological data. It predicts that re-organization of overt responses (i.e. within motor loops) is faster than a re-organization of WM control (i.e. within prefrontal loops). In particular, tasks that can be learned by utilizing a previously valid strategy of WM control (i.e. tasks in which only responses have to be adapted) will be learned significantly faster than tasks for which no previous strategy of WM control is available (cf. Section 4.3.2). Experimentally, this can be investigated by training animals or infant humans on the unconditional DR task described in Section 4.2.2 and by then changing the rules without announcement. In one condition, the same stimuli as in the original DR task will be used, but responses will have to be reversed to obtain reward. In the other condition, two new stimuli will be introduced, each of which has to be associated to one of the two responses. Our model predicts that the first condition will be learned significantly faster than the second one. The experimenter should use stimuli that the animal or infant has never seen before.

As we designed our shaping procedure to optimally suit the learning algorithms of our model, experimental evidence about the procedure's adequacy tells about the biological plausibility of our algorithms. For the 1-2-AX task, we propose that in a first step of shaping, only the outer-loop stimuli 1 and 2 should be presented while in a second step, the outer-loop stimuli plus the inner-loop stimuli A,BA,B and CC should be shown. The efficiency of this procedure can for instance be compared to the protocol that Krueger and Dayan (2009) propose to train an LSTM network (Hochreiter and Schmidhuber, 1997). Showing our procedure to establish the desired behavior faster and more reliably will be a piece of evidence for the biological plausibility of our approach.

Neurophysiologically, our model makes clear predictions about the functions of BG nuclei: STN (via the hyperdirect pathway) is assumed to provide reset signals for WM update in prefrontal loops. STN lesions that are confined to prefrontal loops should thus result in severe difficulties to flexibly update WM. We predict that those lesions will cause failures to delete previously maintained stimuli from WM in delayed match to sample tasks. This will show up as perseverative errors, i.e. subjects will continue to base their answers on stimuli that were relevant in previous trials. The caudate nucleus (via the direct pathway) is supposed to support WM maintenance. Lesions should result in impairments to learn maintenance of stimuli in WM. In a delayed match to sample task, this will show up as an increase in 'random' (i.e. unsystematic) errors. Putamen is supposed to establish associations between WM content and appropriate responses. Lesions will cause severe impairments in learning stimulus-response associations. The impact on well-learned behavior, however, is less clear due to a potential buildup of cortico-cortical connectivity. Another physiological prediction is the increase in the number of active SNc neurons when a highly expected reward does not occur (i.e. after reward contingencies change in an unpredictable way). PPN lesions should attenuate SNc recruitment. Heightened SNc activity is supposed to correspond with an increase in alertness and concentration.

Conclusion

We propose an anatomically detailed computational model of how reinforcement learning contributes to the organization of WM and overt response behavior. To our knowledge, our model is the first to prove the functional flexibility of cortico-BG-thalamic loops: we show that both WM control and response selection can develop in parallel within separate but interacting loops. Within this framework, we show how complex cognitive operations can develop from basic strategies of WM control and response selection.

Acknowledgments

This work has been supported by the German Research Foundation (Deutsche Forschungsgemeinschaft) grant “The cognitive control of visual perception and action selection” (DFG HA2630/4-2) and by the EC Project FP7-ICT “Eyeshots: Heterogeneous 3-D Perception across Visual Fragments”.

Appendix A. Full list of equations

We here give a full overview on the model's equations that will allow to reproduce the model. To facilitate reading and allow for an easy comparison, all parameters are shown in Table ?? and Table ?. Equation 4.4, Equation 4.6 and Equation 4.7 of the main text identically apply to all learning rules unless a deviation is specified.

Cortex

Membrane potentials ($m_i^{\text{Cx}}(t)$) and firing rates ($u_i^{\text{Cx}}(t)$) of prefrontal and motor cortical cells are given by

$$\tau \cdot \frac{dm_i^{\text{Cx}}(t)}{dt} + m_i^{\text{Cx}}(t) = w_{i,i}^{\text{Cx-Cx}} \cdot u_i^{\text{ITC}}(t) + \sum_{j \in \text{Thal}} w_{i,j}^{\text{Thal-Cx}}(t) \cdot u_j^{\text{Thal}}(t) + M + \epsilon_i(t)$$

$$u_i^{\text{Cx}}(t) = \begin{cases} 0 & \text{if } m_i^{\text{Cx}}(t) < 0 \\ m_i^{\text{Cx}}(t) & \text{if } 0 \leq m_i^{\text{Cx}}(t) \leq 0.7 \\ 0.2 + \frac{1}{1 + \exp \frac{0.7 - m_i^{\text{Cx}}(t)}{2}} & \text{if } m_i^{\text{Cx}}(t) > 0.7 \end{cases} \quad (4.8)$$

ITC simply reproduces sensory input. As motivated by Vitay and Hamker (2010), the transfer function of Equation 4.8 ensures that a broad range of membrane potentials above the value of 0.75 results in a relatively constant firing rate. This guarantees more stability in maintaining

eligible WM representations in prefrontal loops when visual stimulation ends. Thalamo-cortical weights ($w_{i,j}^{\text{Thal-Cx}}(t)$) are updated according to

$$\eta \cdot \frac{dw_{i,j}^{\text{Thal-Cx}}(t)}{dt} = (u_j^{\text{Thal}}(t) - \overline{\text{Thal}}(t)) \cdot (u_i^{\text{Cx}}(t) - \overline{\text{Cx}}(t) - \gamma) - \alpha_i(t) \cdot (u_i^{\text{Cx}}(t) - \overline{\text{Cx}}(t))^2 \cdot w_{i,j}^{\text{Thal-Cx}}(t)$$

The threshold parameter γ ensures that only those prefrontal cells become associated to thalamic neurons that are activated by visual stimulation (i.e. not just by random noise). Weights are impeded to decrease below zero. Cortico-cortical weights from ITC to IPFC ($w_{i,j}^{\text{Cx-Cx}}(t)$) are updated according to:

$$\eta \cdot \frac{dw_{i,j}^{\text{Cx-Cx}}(t)}{dt} = (u_j^{\text{Cx}_{\text{ITC}}}(t) - \overline{\text{Cx}_{\text{ITC}}}(t))^+ \cdot (u_i^{\text{Cx}_{\text{PFC}}}(t) - \overline{\text{Cx}_{\text{PFC}}}(t)) - \alpha_i(t) \cdot (u_j^{\text{Cx}_{\text{ITC}}}(t) - \overline{\text{Cx}_{\text{ITC}}}(t)) \cdot ((u_i^{\text{Cx}_{\text{PFC}}}(t) - \overline{\text{Cx}_{\text{PFC}}}(t)) \cdot w_{i,j}^{\text{Cx-Cx}}(t))$$

Weights are not allowed to decrease below zero.

Thalamus

Membrane potentials ($m_i^{\text{Thal}}(t)$) and firing rates ($u_i^{\text{Thal}}(t)$) of thalamic neurons are governed by

$$\tau \cdot \frac{dm_i^{\text{Thal}}(t)}{dt} + m_i^{\text{Thal}}(t) = w_{i,i}^{\text{GPi-Thal}} \cdot u_i^{\text{GPi}}(t) + \sum_{j \in \text{Cx}} w_{i,j}^{\text{Cx-Thal}}(t) \cdot u_j^{\text{Cx}}(t) + M + \epsilon_i(t)$$

$$u_i^{\text{Thal}}(t) = (m_i^{\text{Thal}}(t))^+$$

Cortico-thalamic weights ($w_{i,j}^{\text{Cx-Thal}}(t)$) are updated according to

$$\eta \cdot \frac{dw_{i,j}^{\text{Cx-Thal}}(t)}{dt} = (u_j^{\text{Cx}}(t) - \overline{\text{Cx}}(t))^+ \cdot (u_i^{\text{Thal}}(t) - \overline{\text{Thal}}(t) - \gamma) - \alpha_i(t) \cdot (u_i^{\text{Thal}}(t) - \overline{\text{Thal}}(t))^2 \cdot w_{i,j}^{\text{Cx-Thal}}(t)$$

Weights are impeded to decrease below zero.

4 Working memory and response selection

Striatum

Membrane potentials ($m_i^{\text{Str}}(t)$) and firing rates ($u_i^{\text{Str}}(t)$) of striatal cells are governed by

$$\tau \cdot \frac{du_i^{\text{Str}}(t)}{dt} + u_i^{\text{Str}}(t) = \sum_{j \in \text{Cx}} w_{i,j}^{\text{Cx-Str}}(t) \cdot u_j^{\text{Cx}}(t) + \sum_{j \in \text{Str}, j \neq i} w_{i,j}^{\text{Str-Str}} \cdot u_j^{\text{Str}}(t) + M + \epsilon_i(t)$$

$$u_i^{\text{Str}}(t) = (m_i^{\text{Str}}(t))^+$$

Cortico-striatal weights ($w_{i,j}^{\text{Cx-Str}}(t)$) are updated by the following calcium trace dependent three-factor learning rule:

$$\eta^{\text{Ca}} \cdot \frac{d\text{Ca}_{i,j}^{\text{Str}}(t)}{dt} + \text{Ca}_{i,j}^{\text{Str}}(t) = (u_j^{\text{Cx}}(t) - \overline{\text{Cx}}(t) - \gamma)(u_i^{\text{Str}}(t) - \overline{\text{Str}}(t))^+$$

$$\eta \cdot \frac{dw_{i,j}^{\text{Cx-Str}}(t)}{dt} = f_{\text{DA}}(\text{DA}(t) - \text{DA}_{\text{base}}) \cdot \text{Ca}_{i,j}^{\text{Str}}(t) - \alpha_i(t) \cdot (u_i^{\text{Str}}(t) - \overline{\text{Str}}(t))^2 \cdot w_{i,j}^{\text{Cx-Str}}(t)$$

γ encourages weights to become negative, thereby instigating different inputs to connect to non-overlapping clusters of striatal representations.

Subthalamic nucleus

Membrane potentials ($m_i^{\text{STN}}(t)$) and firing rates ($u_i^{\text{STN}}(t)$) of STN cells are governed by

$$\tau \cdot \frac{du_i^{\text{STN}}(t)}{dt} + u_i^{\text{STN}}(t) = w_{i,i}^{\text{Cx-STN}}(t) \cdot u_i^{\text{Cx}}(t) + M + \epsilon_i(t)$$

$$u_i^{\text{STN}}(t) = \begin{cases} 0 & \text{if } m_i^{\text{STN}}(t) < 0 \\ m_i^{\text{STN}}(t) & \text{if } 0 \leq m_i^{\text{STN}}(t) \leq 1 \\ 0.5 + \frac{1}{1 + \exp\left(\frac{1 - m_i^{\text{STN}}(t)}{2}\right)} & \text{if } m_i^{\text{STN}}(t) > 1 \end{cases}$$

Cortico-subthalamic weights ($w_{i,j}^{\text{Cx-STN}}(t)$) are updated according to

$$\eta^{\text{Ca}} \cdot \frac{d\text{Ca}_{i,i}^{\text{STN}}(t)}{dt} + \text{Ca}_{i,i}^{\text{STN}}(t) = (u_i^{\text{Cx}}(t) - \overline{\text{Cx}}(t))^+ \cdot (u_i^{\text{STN}}(t) - \overline{\text{STN}}(t) - \gamma)^+$$

$$\eta \cdot \frac{dw_{i,i}^{\text{Cx-STN}}(t)}{dt} = f_{\text{DA}}(\text{DA}(t) - \text{DA}_{\text{base}}) \cdot \text{Ca}_{i,i}^{\text{STN}}(t) - \alpha_i(t)(u_i^{\text{STN}}(t) - \overline{\text{STN}}(t))^2 \cdot w_{i,i}^{\text{Cx-STN}}(t)$$

γ again ensures that only those prefrontal cells become associated to subthalamic neurons that receive visual stimulation. Weights are restricted to not decrease below zero.

Globus pallidus external segment

Membrane potentials ($m_i^{\text{GPe}}(t)$) and firing rates ($u_i^{\text{GPe}}(t)$) of GPe cells are given by

$$\begin{aligned} \tau \cdot \frac{du_i^{\text{GPe}}(t)}{dt} + u_i^{\text{GPe}}(t) &= w_{i,i}^{\text{STN-GPe}} \cdot u_i^{\text{STN}}(t) + M + \epsilon_i(t) \\ u_i^{\text{GPe}}(t) &= (m_i^{\text{GPe}}(t))^+ \end{aligned}$$

Globus pallidus internal segment

GPi membrane potentials ($m_i^{\text{GPi}}(t)$) and firing rates ($u_i^{\text{GPi}}(t)$) are ruled by

$$\begin{aligned} \tau \cdot \frac{dm_i^{\text{GPi}}(t)}{dt} + m_i^{\text{GPi}}(t) &= \sum_{j \in \text{Str}} w_{i,j}^{\text{Str-GPi}}(t) \cdot u_j^{\text{Str}}(t) + \sum_{j \in \text{GPi}, j \neq i} w_{i,j}^{\text{GPi-GPi}} \cdot (M - u_j^{\text{GPi}}(t))^+ \\ &+ \sum_{j \in \text{STN}} w_{i,j}^{\text{STN-GPi}} \cdot u_j^{\text{STN}}(t) + \sum_{j \in \text{GPe}} w_{i,j}^{\text{GPe-GPi}} \cdot u_j^{\text{GPe}}(t) + M + \epsilon_i(t) \end{aligned}$$

GPi has a high baseline firing rate; low GPe firing rates denote high activity in a functional sense. Lateral afferents therefore have the presynaptic term $(M - u_j^{\text{GPi}}(t))^+$: the lower the firing rate of a GPi cell, the higher its impact on other cells. The transfer function of Equation 4.9 ensures a slow increase of firing rates when membrane potentials rise above the value of 1.0. Striatal afferents are learnable while subthalamic and external pallidal inputs are assumed to be hard-coded for simplicity. Striato-pallidal inhibitory weights ($w_{i,j}^{\text{Str-GPi}}(t)$) evolve according to

$$\eta^{\text{Ca}} \cdot \frac{d\text{Ca}_{i,j}^{\text{GPi}}(t)}{dt} + \text{Ca}_{i,j}^{\text{GPi}}(t) = (u_j^{\text{Str}}(t) - \overline{\text{Str}}(t))^+ \cdot g(\overline{\text{GPi}}(t) - u_i^{\text{GPi}}(t))$$

$$g(x) = \frac{1}{1 + \exp -2x} - 0.6 \quad (4.9)$$

4 Working memory and response selection

$$\eta \cdot \frac{dw_{i,j}^{\text{Str-GPi}}(t)}{dt} = -f_{\text{DA}}(\text{DA}(t) - \text{DA}_{\text{base}}) \cdot \text{Ca}_{i,j}^{\text{GPI}}(t) - \beta \cdot \alpha_i(t) \cdot (\overline{\text{GPi}}(t) - u_i^{\text{GPI}}(t))^2 \cdot w_{i,j}^{\text{Str-GPi}}(t)$$

$$\tau_{\alpha} \cdot \frac{d\alpha_i(t)}{dt} + \alpha_i(t) = (-m_i^{\text{GPI}}(t) - 1.0)^+$$

The constant β attenuates the strength of the regularization term. The sigmoidal function $g(x)$ guarantees selectivity of striato-pallidal mappings by ensuring a clear separation between GPi firing rates that favor an increase of striato-pallidal weights and those that favor a decrease of weights. $\alpha_i(t)$ increases when $(-m_i^{\text{GPI}}(t) - 1.0)$ becomes positive. Weights are restricted to not become larger than zero. Lateral weights ($w_{i,j}^{\text{GPI-GPi}}(t)$) evolve according to

$$\eta \cdot \frac{dw_{i,j}^{\text{GPI-GPi}}(t)}{dt} = (\overline{\text{GPi}}(t) - u_j^{\text{GPI}}(t))^+ \cdot (\overline{\text{GPi}}(t) - u_i^{\text{GPI}}(t))^+ - \beta \cdot \alpha_i(t) \cdot (\overline{\text{GPi}}(t) - u_i^{\text{GPI}}(t))^2 \cdot w_{i,j}^{\text{GPI-GPi}}(t)$$

Weights are restricted to not become smaller than zero.

Substantia nigra pars compacta

Membrane potentials ($m_i^{\text{DA}}(t)$) and firing rates ($u_i^{\text{DA}}(t)$) of SNc cells are given by

$$\tau \cdot \frac{dm_i^{\text{DA}}(t)}{dt} + m_i^{\text{DA}}(t) = R(t) + P(t) \cdot \sum_{j \in \text{Str}} w_{i,j}^{\text{Str-SNc}}(t) \cdot u_j^{\text{Str}}(t) + \text{DA}_{\text{base}}$$

$$\text{DA}_i(t) = (m_i^{\text{DA}}(t))^+$$

Reward $R(t)$ is set to 0.5 when received and to 0.0 otherwise; when above zero, $R(t)$ decreases by one-thousandth of its value at each time step. The timing factor of reward prediction $P(t)$ is set to 1.0 when reward is expected and to 0.0 else. For the time constant τ we chose a relatively small value of 10 ms to set only a small temporal delay between reward-related events (i.e. rewards and their omissions) and changes in SNc firing (that then cause phasic changes in dopamine levels). Thereby, we ensure that the time period where reward-related events (i.e. via dopamine) are associated to neuronal eligibility traces ($d\text{Ca}_{i,j}^{\text{post}}(t)$) is temporally close to when these events take place. Larger values of τ would result in eligibility traces decaying further before dopamine levels rise. This would result in smaller weight changes per trial and would thereby slow down learning of WM control and response selection. Furthermore, much larger values of τ could be problematic in case of short inter-trial-intervals since reward-related events could then be associated to future (instead of previous) eligibility traces.

Learnable, negatively weighted striato-nigral afferents encode reward prediction. Depending on the balance between actual reward and reward prediction, firing rates above or below the

baseline level (DA_{base}) of 0.5 can result. Striato-nigral weights ($w_{i,j}^{\text{Str-SNc}}(t)$) encoding reward prediction are learned via

$$\eta \cdot \frac{dw_{i,j}^{\text{Str-SNc}}(t)}{dt} = -(u_j^{\text{Str}}(t) - \overline{\text{Str}}(t)) + f_{\text{DA}}(DA_i(t) - DA_{\text{base}})$$

The postsynaptic and the dopaminergic term are identical in this equation, resulting in a two-factor ‘‘Hebbian’’ learning rule.

Relationship between motor activity and overt responses

To account for imprecision in the motor command system, response selection is assumed to be based upon brain activity in a probabilistic way: The higher the activity of a particular MI cell, the greater the probability of the associated response. In case of equal activity among motor cells, the probability of each response is the inverse of the number of possible alternatives. The probability of response R_i is therefore given by

$$P(R_i) = 0.5 + u_i - u_j$$

where u_i is the firing rate of the cell associated to the response R_i and u_j the firing rate of the respective other MI cell. Probability values are reasonably restricted to the interval $[0, 1]$.

Appendix B. Number of simulated cells

Table 4.1 presents the numbers of cells in each of the model’s layers. The two prefrontal loops each contain eight cells within IPFC, STN, GPe and GPi so that each of the 1-2-AX task’s stimuli can in principle become represented within at least one cell. MI contains two cells: one for each response. The number of striatal cells has to be considerably larger since clusters of striatal cells become receptive to various combinations of cortical afferents. The motor part of striatum exceeds the prefrontal part in size as cells from all cortical areas have to converge there.

Table 4.1: Numbers of cells within the model’s layers. GPe: globus pallidus external segment; GPi: globus pallidus internal segment; SNc: substantia nigra pars compacta; STN: subthalamic nucleus.

Cell type	Prefrontal loop	Motor loop	Visual
Cortex	8	2	8
Striatum	25	49	0
STN	8	0	0
GPe	8	0	0

Cell type	Prefrontal loop	Motor loop	Visual
GPI	8	2	0
Thalamus	8	2	0
SNC	1	1	0

Appendix C. Overview of model parameters

To allow for an easy overview and comparison of the model's parameters, these are systematically listed in Table 4.2 and Table 4.3. Table 4.2 contains the parameters for computing membrane potentials and firing rates, Table 4.3 the parameters for computing weights.

Table 4.2: Parameters for computations of membrane potentials and firing rates. The table shows time constants (τ), feedforward weights (w^{ff}), lateral weights (w^{lat}), baseline membrane parameters (M) and random noise terms (ϵ) for each of the model's layers. All learnable weights (denoted by l) are randomly initialized with values between 0.05 and 0.10, except for connections from inferior temporal to lateral prefrontal cortex ($w_{i,i}^{\text{Cx-Cx}}$) which are uniformly initialized with 0.1. Cx: cortex; GPe: globus pallidus external segment; GPI: globus pallidus internal segment; SNC: substantia nigra pars compacta; STN: subthalamic nucleus; Str: striatum; Thal: thalamus. ^a: Weights are of this value for the motor loop only while they are learnable in prefrontal loops.

Cell type	τ (ms)	w^{ff}	w^{ff}	w^{ff}	w^{lat}	M	ϵ
Cx	5	$w^{\text{Thal-Cx}}: 1.0^a$	$w^{\text{Cx-Cx}}: 0.0^a$	-	-	0.0	[-0.05; 0.05]
Str	10	$w^{\text{Cx-Str}}: l$	-	-	$w^{\text{Str-Str}}: -0.3$	0.3	[-0.1; 0.1]
STN	10	$w^{\text{Cx-STN}}: l$	-	-	-	0.0	[-0.01; 0.01]
GPe	50	$w^{\text{STN-GPe}}: 1.0$	-	-	-	0.0	[-0.1; 0.1]
GPI	10	$w^{\text{Str-GPI}}: l$	$w^{\text{STN-GPI}}: 8.0$	$w^{\text{GPe-GPI}}: -8.0$	$w^{\text{GPI-GPI}}: 1.0^a$	0.8	[-0.75; 0.75]
Thal	5	$w^{\text{Cx-Thal}}: 0.5^a$	$w^{\text{GPI-Thal}}: -1.0$	-	-	0.7	[-0.1; 0.1]
SNC	10	$w^{\text{Str-SNC}}: l$	-	-	-	0.5	0.0

Table 4.3: Parameters for computations of weights. The table shows time constants (η and τ_α), threshold parameters (γ), parameters controlling the relative strength of long-term depression (φ), parameters controlling the speed of calcium increase (η^{inc}) and decline (η^{dec}), parameters controlling the maximal desired firing rates for cells with learnable inputs (u^{MAX}), homeostatic regularization factors (β) and parameters controlling the speed of increases of α_i (K_α) for each of the model's connection types; when two values are given, the first corresponds to the motor loop and the second to prefrontal loops. Cx: cortex; GPi: globus pallidus internal segment; SNc: substantia nigra pars compacta; STN: subthalamic nucleus; Str: striatum; Thal: thalamus.

Connection type	η (ms)	τ_α (ms)	γ	φ	η^{inc} (ms)	η^{dec} (ms)	u^{MAX}	β	K_α
$w^{\text{Cx-Cx}}$	800	20	0.0	-	-	-	1.0	-	10
$w^{\text{Thal-Cx}}$	450	20	0.25	-	-	-	1.0	-	10
$w^{\text{Cx-Str}}$	250	20	0.55; 0.4	0.5; 0.1	1	500	1.0	-	10
$w^{\text{Cx-STN}}$	250	20	-	0.2	1	500	1.0	-	1
$w^{\text{Str-GPi}}$	500	2	-	10.0; 0.2	1	250	-	0.03; 1.0	-
$w^{\text{GPi-GPi}}$	100	2	-	-	1	250	1.0	0.06	1
$w^{\text{Cx-Thal}}$	700	20	0.1	-	-	-	0.8	-	10
$w^{\text{Str-SNc}}$	10000	-	-	5.0	-	-	-	-	-

5 Timing and expectation of reward: a neuro-computational model of the afferents to the ventral tegmental area

Abstract

Neural activity in dopaminergic areas such as the ventral tegmental area is influenced by timing processes, in particular by the temporal expectation of rewards during Pavlovian conditioning. Receipt of a reward at the expected time allows to compute reward-prediction errors which can drive learning in motor or cognitive structures. Reciprocally, dopamine plays an important role in the timing of external events. Several models of the dopaminergic system exist, but the substrate of temporal learning is rather unclear. In this article, we propose a neuro-computational model of the afferent network to the ventral tegmental area, including the lateral hypothalamus, the pedunculo-pontine nucleus, the amygdala, the ventromedial prefrontal cortex, the ventral basal ganglia (including the nucleus accumbens and the ventral pallidum), as well as the lateral habenula and the rostromedial tegmental nucleus. Based on a plausible connectivity and realistic learning rules, this neuro-computational model reproduces several experimental observations, such as the progressive cancellation of dopaminergic bursts at reward delivery, the appearance of bursts at the onset of reward-predicting cues or the influence of reward magnitude on activity in the amygdala and ventral tegmental area. While associative learning occurs primarily in the amygdala, learning of the temporal relationship between the cue and the associated reward is implemented as a dopamine-modulated coincidence detection mechanism in the nucleus accumbens.

5.1 Introduction

Dopamine (DA) is a key neuromodulator influencing processing and learning in many brain areas, such as the basal ganglia (Bolam et al., 2000; Haber et al., 2000), the prefrontal cortex (Goldman-Rakic et al., 1992; Seamans and Yang, 2004) or the amygdala (Bissière et al., 2003; Pape and Pare, 2010). Dopaminergic neurons in the ventral tegmental area (VTA) and substantia nigra pars compacta (SNc) are phasically activated by unexpected rewards, aversive, salient or novel stimuli (Horvitz, 2000; Mirenowicz and Schultz, 1994; Redgrave et al., 2008; Schultz et al., 1993). During classical conditioning with appetitive rewards (unconditioned stimulus US),

5 Timing and expectation of reward

cells in VTA gradually show the same phasic activation at the onset of a reward-predicting cue (conditioned stimulus CS), but stop responding to the US when it is fully predicted (Ljungberg et al., 1992; Pan and Hyland, 2005; Schultz et al., 1997). If the reward is expected but omitted, VTA cells show a complete and long-lasting pause (or dip) in firing shortly after the time when the US was expected; if the reward is delivered earlier than expected, VTA cells respond phasically as if it were not predicted, but do not show a dip at the expected time (Hollerman and Schultz, 1998).

This phasic behavior linked to temporal expectation of reward (cancellation of US-related bursts after sufficient training, pause in firing after reward omission, normal bursts if the reward is delivered earlier) indicates that timing mechanisms play an important role in dopaminergic activation. Conversely, DA is well known to influence other timing processes, such as interval timing and duration estimation (Coull et al., 2011; Kirkpatrick, 2013). Reward magnitudes can alter the estimation of time in peak-interval procedures (where the consumatory response rate in anticipation of an expected reward usually peaks at the learned time), either leftward (the temporal estimation is earlier than what it really is) or rightward (later), the same effect being observed with elevated or reduced DA activity in SNc/VTA (Galtress and Kirkpatrick, 2009). Understanding the interaction between the reward/motivational systems and timing processes is therefore of critical importance (Galtress et al., 2012; Kirkpatrick, 2013). The objective of this article is to propose a neuro-computational model incorporating the afferent structures to the dopaminergic system which are involved in appetitive conditioning and to better describe the neural mechanisms leading to the observed temporal behaviour of dopaminergic neurons.

The *temporal difference* (TD) algorithm originally proposed by (Sutton and Barto, 1981) has become an influential model linking DA activity to timing mechanisms (Montague et al., 1996; Schultz et al., 1997). TD is a unitary mechanism describing DA activity as a reward-prediction error: the difference between the reward expectation in a given state and the actually received reward. Early implementations of TD have used serial-compound representations to represent the presence of a stimulus over time, allowing to reproduce some aspects of DA firing during classical conditioning by chaining backwards in time the association between the CS and the US (Suri and Schultz, 1999, 2001). This would predict a progressive backward shift of the US-related burst during learning, what is experimentally not the case, as the CS- and US-related bursts gradually increase and decrease with learning, respectively. Different temporal representations of the stimuli can overcome this issue. Using long eligibility traces (TD(λ), (Sutton and Barto, 1998)), the algorithm can be turned into a more advanced associative learning rule to better fit the experimental data (Pan and Hyland, 2005). Using a series of internal microstimuli growing weaker and more diffuse over time also allows to overcome this problem as well as to better capture DA activity when a reward is delivered earlier as predicted (Ludvig et al., 2008). An adequate temporal representation of stimuli can even be learned in an unsupervised manner through the use of long short-term memory (LSTM) networks (Rivest et al., 2010; Rivest et al., 2013). Overall, TD-based algorithms are an important model of DA activity, both because of their mathematical elegance and predictive power, and are widely used for explaining experimental data in decision-making (for example Daw et al. (2005; Rao, 2010; Samejima and Doya,

2007)) and in neurorobotical systems (for example (Krichmar, 2013; Sporns and Alexander; 2002)).

Other models have been proposed to better explain the experimental data while improving the biological plausibility. One important class of models are the *dual-pathway* models, which hypothesize that the different components of DA activation are computed in segregated brain areas projecting onto the SNc/VTA (Brown et al., 1999; Hazy et al., 2010; O'Reilly et al., 2007; Tan and Bullock, 2008). These models share some common assumptions about the mechanisms, although the putative brain areas may differ: reward delivery provokes DA bursts through glutamatergic projections from the pedunculo-pontine nucleus (PPTN); the conditioning strength of the CS is first acquired in the amygdala or the ventral striatum and then transferred to the DA cells either directly or through PPTN; the cancellation of predicted US bursts and the dips at reward omission originate from the striosomes of the dorsal or ventral striatum which project inhibitorily to VTA/SNC. The origin of the latter signals, which have a strong temporal component, differ however between these models. The models by Brown et al. (1999) and Tan and Bullock (2008) consider that cells in the striosomes of the dorsal and ventral striatum implement an *intracellular spectral timing* mechanism (Grossberg and Schmajuk, 1989), where each cell in these populations has an internal calcium variable peaking at a given time after the CS onset and emits delayed spikes. The cell being active at reward delivery (signaled by the DA burst) becomes representative of the elapsed duration. The models by O'Reilly et al. (2007) and Hazy et al. (2010) more abstractly consider a ramping function peaking at the estimated reward delivery time, and originating from the cerebellum. How this timing signal from the cerebellum is adapted to different CS-US intervals is not explicitly modeled.

Spectral timing mechanisms have been observed in the cerebellum (Fiala et al., 1996) but not in the striatum. The cerebellum is critically involved in aversive conditioning such as the rabbit eye-blink conditioning (Christian and Thompson, 2003; Thompson and Steinmetz, 2009), but its involvement in appetitive conditioning is still unknown (see Martin-Soelch et al. (2007)). Moreover, the intracellular mechanisms necessary for spectral timing may not efficiently apply to the supra-second range used in most appetitive conditioning experiments (Coull et al., 2011; Matell and Meck, 2004). The neural substrate of temporal learning in dual-pathway models of the dopaminergic system needs further investigation.

The goal of the the present article is to investigate how far dual-pathway models of reward prediction can be adapted to take into account the recent wealth of experiments investigating timing processes in the brain (Coull et al., 2011; Kirkpatrick, 2013). Although most of them focus on operant conditioning, they point at a critical role of the striatum in learning supra-second durations. One of the most biologically plausible model of interval timing to date is the *Striatal-Beat Frequency* model (Lustig et al., 2005; Matell and Meck, 2000; Matell and Meck, 2004), which proposes that striatal neurons act as coincidence detectors, reacting maximally when a series of cortical oscillators, synchronized at CS onset, is in a particular configuration. We propose that a similar mechanism is used to control the temporal behavior of dopaminergic cells during appetitive conditioning.

We present a neuro-computational model incorporating many areas involved in appetitive conditioning and reward processing, including the amygdala, the ventral basal ganglia and various forebrain nuclei projecting to VTA/SNc. It focuses on the phasic components of dopaminergic activation and reproduces the behavior of VTA cells during conditioning, especially with respect to different reward magnitudes, reward omission or earlier delivery. However, it is not designed to address the tonic component of DA activation, nor the observed dependency of VTA firing on reward probability (Fiorillo et al., 2003). From the computational point of view, it provides a robust and autonomous mechanism to learn CS-US associations with variable durations.

5.2 Material & methods

5.2.1 Neurobiological assumptions

Appetitive delay conditioning

The proposed model of dopaminergic activation during conditioning is restricted in its current form to appetitive conditioning, where the US is a physical reward such as food. Aversive conditioning, where the US is a painful stimulation or a frightening stimulus, engages similar structures - in particular, the amygdala, the ventral striatum and the dopaminergic system (Delgado et al., 2008; LeDoux, 2000; Matsumoto and Hikosaka, 2009) - but the model does not aim at reproducing these effects. The cerebellum plays a much more important role in aversive than in appetitive conditioning (Thompson and Steinmetz, 2009). There is still a debate on whether the same DA cells are activated by appetitive and aversive rewards or if two segregated populations exist (Lammel et al., 2012).

The model is also limited to delay conditioning, where the CS is still physically present (visually or auditorily) when the US arrives. Trace conditioning introduces a temporal gap between the CS and the US. In this case, even small intervals can impair the learned association strength (Raybuck and Lattal, 2013). The medial prefrontal cortex and hippocampus are necessary for trace conditioning to take place, but not delay conditioning (Ito et al., 2006; Walker and Steinmetz, 2008; Wu et al., 2013). This indicates that working memory processes (either through sustained activation or synaptic traces) are involved in trace conditioning, what is not covered by this model. Some TD-based implementations are able to learn both delay and trace conditioning tasks: the model of Ludvig et al. (2008) uses a series of temporal basis functions to represent the trace of the stimuli, what allows the TD algorithm to associate reward delivery to the correct timing. The model of Rivest et al. (2010; Rivest et al., 2013) learns an adequate temporal representation for both CS and US using a long short-term memory (LSTM) network (Hochreiter and Schmidhuber, 1997) which is able to fill an eventual gap between the CS and the US.

Dual-pathway models focus mainly on delay conditioning: Brown et al. (1999) propose that a bistable representation of CS information, mimicking the sustained activation in the prefrontal

cortex during working memory processes (Funahashi et al., 1993), could bridge the temporal gap between the CS and the US, while O'Reilly et al. (2007) couple their model of DA activity with a neuro-computational model of working memory involving the prefrontal cortex and the basal ganglia in order to address trace conditioning (O'Reilly and Frank, 2006).

In the experiments shown in this article, the CS is an individual visual stimulus that activates specific clusters of cells in the inferotemporal cortex (IT). Object-level representations in IT allow to provide the prefrontal cortex, the amygdala and the basal ganglia with rich detailed representations of visual objects (Tanaka, 2000). However, inputs to the model could be easily adapted to auditory inputs. The US is a food reward, activating the lateral hypothalamus (LH). Neurons in LH are activated by the specific taste components of a single reward, proportionally to their magnitude (Nakamura and Ono, 1986). Rewards are therefore represented by a combination of tastes (for example fat, sugar, salt, umami, as in the MOTIVATOR model of Dranias et al. (2008)) allowing to distinguish different rewards from each other by their nature instead of only their relative magnitude.

Role of VTA and forebrain structures

The midbrain dopaminergic system is predominantly composed of the SNc and VTA. VTA plays a specific role in the facilitation of approach behaviors and incentive learning (Fields et al., 2007), while SNc is more involved in motor and cognitive processes, although this functional distinction is more based on anatomical considerations than direct observations (Haber, 2003). The proposed model focuses on VTA activation during conditioning because of its central role in the reward circuitry (Sesack and Grace, 2010), but it is not excluded that a similar behaviour is observed in SNc because of the spiraling structure of striato-nigro-striatal pathways (Haber et al., 2000).

Dopaminergic neurons in VTA exhibit a relatively low tonic activity (around 5Hz), but react phasically with a short-latency (< 100ms), short-duration (< 200ms) burst of high activity in response to unpredicted rewards, aversive, salient or novel stimuli (Horvitz, 2000; Mirenowicz and Schultz, 1994; Redgrave et al., 2008; Schultz et al., 1993). After appetitive conditioning, the same cells also react phasically to reward-predicting stimuli (Schultz et al., 1997). These phasic bursts of activity for both unpredicted rewards and reward-predicting cues are dependent on glutamatergic activation by PPTN (Dormont et al., 1998; Lokwan et al., 1999; Pan et al., 2005), which is itself driven by inputs from LH and the central nucleus of the amygdala (CE) (Semba and Fibiger, 1992). Excitatory inputs from the prefrontal cortex (PFC) to VTA, PPTN and LH exert a regulatory role on this bursting behavior (Fields et al., 2007; Geisler and Wise, 2008) and regulate plasticity in VTA (Wolf et al., 2004).

The mechanisms underlying inhibitory control of VTA are less clear. VTA receives predominantly GABAergic synapses from the ventral basal ganglia (BG), especially from the ventromedial shell of the nucleus accumbens (NAcc) and the ventral pallidum (VP) (Usuda et al., 1998; Zahm and Heimer, 1990). These inhibitory projections are known to control the number of DA

5 *Timing and expectation of reward*

neurons in VTA able to switch from an hyperpolarized state to an irregular spontaneous firing rate around 5Hz. There is also a large number of GABAergic neurons in VTA (around 30%) but they predominantly project outside VTA (Carr and Sesack, 2000). A recently labeled area posterior to the VTA, the rostromedial tegmental nucleus (RMTg), has been shown to provide a strong GABAergic inhibition on dopaminergic VTA cells, able to produce the dip observed at reward omission (Bourdy and Barrot, 2012; Jhou et al., 2009; Lavezzi and Zahm, 2011). Neurons in RMTg are excited by aversive events and reward omission, and this activation is provoked by excitatory projections from the lateral habenula (LHb) which is activated in the same conditions (Balcita-Pedicino et al., 2011; Bromberg-Martin and Hikosaka, 2011; Hikosaka et al., 2008; Hong et al., 2011).

Role of the amygdala

The amygdala is long known for its involvement in acquiring and expressing auditory fear conditioning (LeDoux, 2000). Neurons in the basolateral amygdala (BLA), the major input structure of the amygdala, learn to associate CS and US representation, based either on thalamic or cortical information (Doyère et al., 2003), with long-term potentiation being modulated by dopaminergic innervation from VTA (Bissière et al., 2003). The output structure of the amygdala, the central nucleus of the amygdala (CE) is critical for expressing fear conditioning (conditioned responses), through its projections on various brainstem nuclei (Koo et al., 2004).

However, the amygdala is now recognized to be also involved in appetitive conditioning and reward processing (Baxter and Murray, 2002; Murray, 2007). The amygdala and LH both react to the palability of rewards, suggesting either common afferences in the brainstem, a direct projection from LH to BLA (Sah et al., 2003) or an indirect one through the gustatory thalamus, as lesions of the gustatory brainstem nuclei abolish food-elicited responses in both LH and the amygdala (Nishijo et al., 2000). In this model, we assume a direct projection from LH to BLA, but how the amygdala gets access to the value of a food reward is still not clear.

BLA neurons have been shown to respond proportionally to reward magnitude (Bermudez and Schultz, 2010). They also respond to both reward-predicting cues and the associated rewards, with a sustained activation during the delay (Nishijo et al., 2008; Ono et al., 1995). This places the BLA at a central position for learning CS-US associations, or more precisely associating the value of the US to the sensory representation of the CS. This information is transferred to CE, which is able to activate VTA, either through direct projections (Fudge and Haber, 2000) - although they are quite weak and have only been observed in primates -, or more likely indirectly through excitation of PPTN (Lee et al., 2011; Semba and Fibiger, 1992).

Role of the ventral basal ganglia

The ventral BG plays a critical role in learning goal-oriented behaviors and is considered as an interface between the limbic and motor systems, as it receives converging inputs from the

amygdala, hippocampus and prefrontal cortex (Humphries and Prescott, 2010; Nicola, 2007). Its major input structure, the ventral striatum, is mostly composed of the nucleus accumbens (NAcc), itself decomposed into core and shell territories, but also extends without a clear demarcation into the caudate nucleus and the putamen, accounting for around 20% of the whole striatum (Haber and Knutson, 2010). It is primarily composed of GABAergic medium-spiny projection neurons (MSN, 90%), as well as tonically-active cholinergic neurons (TAN) and GABAergic interneurons. MSN neurons project on the ventral pallidum (VP), VTA, SNc, LH and PPTN. They receive inputs from VP, VTA, LH, BLA and the subiculum (part of the hippocampal formation) (Humphries and Prescott, 2010; Sesack and Grace, 2010).

NAcc is involved in learning the incentive motivational value of rewards (Galtress and Kirkpatrick, 2010; Nicola, 2007; Robbins and Everitt, 1996). Excitatory inputs from the BLA have been shown necessary to promote reward-seeking behaviors and enable the cue-evoked excitation of NAcc during operant conditioning. NAcc is also involved in Pavlovian reward learning, with single neurons being phasically activated by both CS and US after sufficient training (Day and Carelli, 2007). Learning in NAcc has been shown to depend strongly on dopaminergic innervation from VTA (Eyny and Horvitz, 2003).

VP, the output structure of the ventral BG, is also strongly involved in reward processing and reward expectation (Smith et al., 2009; Tachibana and Hikosaka, 2012). It receives GABAergic projections from NAcc, excitatory projections from PPTN, and projects to SNc/VTA, LHb, RMTg and the mediodorsal nucleus of the thalamus (MD) (Haber and Knutson, 2010; Hallanger and Wainer, 1988; Jhou et al., 2009). During classical conditioning, VP cells are excited by reward-predicting cues and the associated reward when the reward is large, but inhibited by small rewards (Tindell et al., 2004). The NAcc → VP pathway is therefore considered a major route for disinhibiting efferent structures at CS onset and reward delivery and guide reward-orienting behaviors (Sesack and Grace, 2010).

Regarding the involvement of the ventral BG in timing, the current evidence is rather controversial. Two lesion studies showed no involvement of NAcc in the timing of instrumental responding (Galtress and Kirkpatrick, 2010; Meck, 2006), but Singh et al. (2011) showed that lesions of NAcc induce a deficit in learning the timing of Pavlovian responses. The NAcc and the medial caudate nucleus robustly activate during reward anticipation (Deadwyler et al., 2004), while the rostroventral putamen most reliably deactivates in response to nonreward delivery (McClure et al., 2003; O'Doherty et al., 2003). Lesions of NAcc have recently been shown to disrupt reinforcement-omission effects (Judice-Daher and Bueno, 2013). However, no cellular recordings have yet shown that NAcc cells react specifically to reward omission.

In this model, we form the hypothesis that a subset of NAcc cells learns the precise time when a reward is expected and gets activated when it is omitted. Recent advances in the neurobiology of interval timing show that a similar mechanism is likely to occur in the dorsal striatum during peak-interval tasks (Coull et al., 2011; Matell and Meck, 2004). The *Striatal-Beat Frequency* model (Lustig et al., 2005; Matell and Meck, 2000) has proposed that striatal cells act as coincidence detectors, learning to react to a particular configuration of cortical inputs when

5 Timing and expectation of reward

a DA burst occurs and to signal the temporal expectation of reward. In this framework, cortical inputs oscillate at various frequencies in the alpha range (8-13Hz) and are synchronized at cue-onset. This provides an unique population code for the time elapsed since cue onset, so striatal cells can learn to react to a specific duration through dopamine-modulated long-term potentiation (LTP) or depression (LTD) (Calabresi et al., 2007; Shen et al., 2008). We consider a similar mechanism here for learning CS-US interval durations in NAcc.

Synaptic plasticity at corticostriatal synapses depends on the polarization of the membrane potential: in the hyperpolarized state (-90mV, called the down-state), striatal cells exhibit mostly LTD at active synapses; in the depolarized state (-60mV, the up-state), these cells exhibit LTP or LTD depending on the extracellular dopamine level (Calabresi et al., 2007; Shen et al., 2008). Neurons in NAcc exhibit these up- and down-states (O'Donnell and Grace, 1995), and the transition from the down-state to the up-state depends either on phasic DA release from VTA (Goto and Grace, 2005; Gruber et al., 2003), afferent input from the ventral subiculum of the hippocampus (O'Donnell and Grace, 1995) or a conjunction of medial prefrontal cortex and amygdala inputs (McGinty and Grace, 2009). This mechanism is thought to help restricting striatal firing to the exact time when reward is expected: NAcc cells are brought in the up-state by DA bursts at reward delivery, allowing the to learn the precise cortical pattern. After learning the same cell could be brought in the up-state only by this cortical pattern (in conjunction with BLA inputs), even if VTA is not bursting (Matell and Meck, 2004).

5.2.2 The proposed model

Overview

In this section, we will explain the major flows of information and learning in the model before describing more precisely the details of the model, depicted on Figure 5.1. Most experiments in this article will concern the concurrent learning of three different CS-US associations, each using different visual and gustatory representations, and with different CS-US intervals (see Section 5.2.2.1). The first phase of learning represents sensitization to the rewards, by presenting each reward individually ten times. The US representation activates a set of cells in LH, depending of the basic tastes composing it, what in turn activates the US-selective population of PPTN, provoking a phasic DA burst in VTA which gates learning in BLA. After sufficient exposure to each reward, BLA has self-organized to represent them individually by the activation of a single cell. Meanwhile, BLA progressively learns to activate CE, which in turn activates the CS-selective population of PPTN (Figure 5.1). However, when reward is delivered, the preceding activation of the US-selective population inhibits activation in the CS-selective one. During the sensitization phase, a similar self-organizational mechanism occurs in NAcc: individual rewards become represented by different single neurons.

The second phase of learning concerns conditioning *per se* with distinct trials for each CS-US association: an initially neutral visual stimulus (CS) activates a distributed representation

5 Timing and expectation of reward

in IT, which lasts for a fixed duration before the US is delivered. This visual representation projects onto BLA, and, through DA-modulated learning in BLA at reward-delivery, becomes able through repetitive pairing to activate the same BLA cell that would be activated by the US alone. Homeostatic regulation in BLA ensures that the BLA activity at CS onset has the same amplitude as the reward-related activity. CS-related activation in BLA becomes able to activate CE, which becomes able to provoke VTA bursts through excitation of PPTN. This mechanism is sufficient to explain the progressive phasic DA bursts in VTA at CS onset during learning.

In parallel, CS onset activates a bank of oscillators in the ventromedial prefrontal cortex (vmPFC) at different frequencies. During conditioning, the phasic DA burst at US delivery brings the corresponding NAcc cell into the up-state, allowing it to become selective to the precise configuration of cortical oscillators corresponding to the elapsed duration since CS onset. This progressive activation at US delivery diminishes the amplitude of the US-related VTA burst through the direct NAcc \rightarrow VTA inhibitory projection. Meanwhile, NAcc learns to inhibit VP at reward delivery, what could potentially lead to the disinhibition of LHb, provoking a dip of activity in VTA through RMTg. However, reward delivery activates the US-selective population of PPTN, which excites VP: the inhibitory influence of NAcc is counterbalanced by PPTN, what leaves VP above its baseline level and avoid unwanted inhibition of VTA.

After a sufficient number of conditioning trials, we investigate reward omission, where the CS is presented for the usual duration, but not the US. In this case, one NAcc cell goes into the up-state when the reward is expected because of its strong vmPFC input at this time and inhibits VP. This inhibition is then not counterbalanced anymore by US-related PPTN activation, so this disinhibits LHb, activates RMTg and finally provokes a strong inhibition of VTA, bringing it below baseline for a certain duration (the dip).

Computational principles

Each area in the proposed model is composed of a given number of computational units, where each unit computes the mean activity of a population of neurons. The dynamics of each unit is described by the evolution of its time-dependent firing rate (Dayan and Abbott, 2001). The firing rate $r(t)$ of an unit is a positive scalar describing the instantaneous number of spikes per second emitted by neurons in the corresponding population. In this model, it is taken to be the positive part of the so-called *membrane potential* $m(t)$ of the unit, which follows a first order differential equation depending on the firing rate of other units. In this model, the absolute value of the firing rate is usually restricted to the range $[0, 1]$ through homeostatic regulation of learning (see for example Equation 5.12), where 1 represents the maximal instantaneous firing rate that the considered type of cell can have. Typical units in the model are governed by Equation 5.1 and Equation 5.2:

$$\tau \cdot \frac{dm(t)}{dt} + m(t) = g_{\text{exc}}(t) - g_{\text{inh}}(t) + B + \eta(t) \quad (5.1)$$

$$r(t) = (m(t))^+ \quad (5.2)$$

where τ is the time constant of the cell (expressed in milliseconds), B is its baseline activity, $\eta(t)$ an additive noise term chosen randomly at each time step from a uniform distribution between -0.1 and 0.1, $g_{\text{exc}}(t)$ and $g_{\text{inh}}(t)$ being the weighted sum of excitatory and inhibitory afferent firing rates, respectively. $()^+$ is the positive function, which only keeps the positive part of the operand and outputs 0 when it is negative. In the rest of this article, we will only describe how the membrane potential $m(t)$ of each unit evolves, the corresponding firing rate being always the positive part.

Units in this model can differentially integrate their inputs depending on their assigned type (here exc, inh, mod and dopa). This type corresponds either to the neurotransmitter type (exc and mod represent glutamergic synapses, inh GABAergic ones and dopa represents dopaminergic receptors) or the region of origin (exc and mod connections have both an excitatory effect but arise from different areas and are integrated differently).

For a given type of synapses, the weighted sum of of inputs is defined by Equation 5.3:

$$g_{\text{type}}(t) = \sum_i^{\text{type}} w_i(t) \cdot r_i(t) \quad (5.3)$$

where i is the index of a synapse of this type, $r_i(t)$ the firing rate of the presynaptic neuron at time t and $w_i(t)$ the weight of the connection (or synaptic efficiency).

Some computational principles in this model rely on the conversion of the onset of a tonic input $x(t)$ (reward delivery, CS presentation) into a short-term phasic component. For convenience, we define here a function $\Phi_{\tau,K}(x)$ allowing this transformation according to Equation 5.4 and Equation 5.5:

$$\tau \cdot \frac{d\bar{x}(t)}{dt} + \bar{x}(t) = x(t) \quad (5.4)$$

$$\Phi_{\tau,k}(x(t)) = (x(t) - k \cdot \bar{x}(t))^+ \quad (5.5)$$

$\bar{x}(t)$ integrates the input $x(t)$ with a time constant τ , while $\Phi_{\tau}(x(t))$ represents the positive part of the difference between $x(t)$ and $\bar{x}(t)$. k is a parameter controlling which proportion of the input will be kept on the long-term (if $k = 0$ the tonic component is preserved, if $k = 1$ $\Phi_{\tau,k}(x(t))$ will converge towards zero). If $x(t)$ is for example an Heaviside function (switching from 0 to 1 at $t = 0$), $\Phi_{\tau,0}(x(t))$ will display a localized bump of activation with a maximum at $t = \tau$, as depicted on Figure 5.2.

5 Timing and expectation of reward

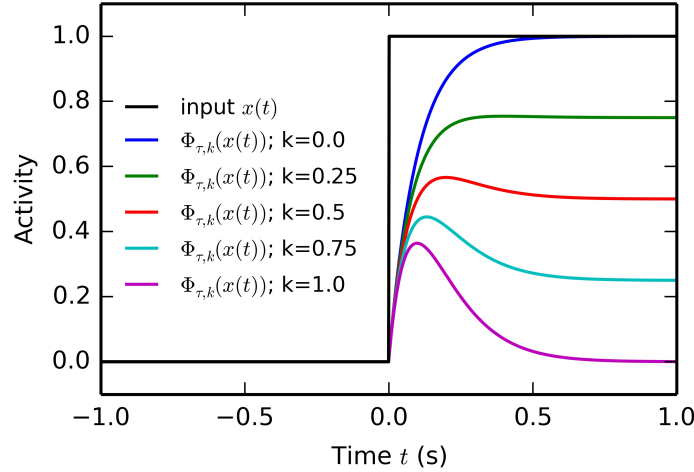


Figure 5.2: Temporal profile of the phasic function $\Phi_{\tau,k}(x)$ defined by Equation 5.5}. At $t = 0$, the Heaviside input $x(t)$ goes from 0 to 1. The temporal profile of five phasic functions $\Phi_{\tau,k}(x)$ with $\tau = 50$ ms and k ranging from 0 to 1 is displayed. If $k = 0$, the phasic function is a simple leaky integrator with time constant τ . If $k = 1$, the output of the filter is a localized bump peaking at $t = \tau$ and converging towards 0.

Another useful function is the threshold function, which outputs 1 when the input exceeds a threshold Γ , 0 otherwise (Equation 5.6):

$$\Delta_{\Gamma}(x) = \begin{cases} 0 & \text{if } x < \Gamma \\ 1 & \text{otherwise.} \end{cases} \quad (5.6)$$

The learning rules used in the model derive from the Hebbian learning rule. The simplest variant of this learning rule in the model is a thresholded version described in Equation 5.7. The evolution over time of the weight $w_{i,j}(t)$ of a synapse between the neuron i in population pre (presynaptic neuron) and the neuron j of population post (postsynaptic neuron) is governed by:

$$\epsilon \cdot \frac{dw_{i,j}(t)}{dt} = (r_{\text{pre}}^i(t) - \theta_{\text{pre}})^+ \cdot (r_{\text{post}}^j(t) - \theta_{\text{post}})^+ \quad (5.7)$$

where $r_{\text{pre}}^i(t)$ and $r_{\text{post}}^j(t)$ are the pre- and post-synaptic firing rates, θ_{pre} and θ_{post} are fixed thresholds, and ϵ is the learning rate. The thresholds can be adjusted to take baseline firing rates into account and restrict learning to significant deviations from this baseline. Weight values are restricted to the range $[w_{\text{min}}, w_{\text{max}}]$, where w_{min} is usually 0.

Another learning rule used in the model derives from the covariance learning rule (Dayan and Abbott, 2001; Schroll et al., 2012; Vitay and Hamker, 2010). In this framework, only those cells whose firing rate is significantly above the mean firing rate in their respective population can participate to learning. The evolution over time of the weights is described by Equation 5.8:

$$\epsilon \cdot \frac{dw_{i,j}(t)}{dt} = (r_{\text{pre}}^i(t) - \bar{r}_{\text{pre}}(t))^+ \cdot (r_{\text{post}}^j(t) - \bar{r}_{\text{post}}(t))^+ \quad (5.8)$$

where $\bar{r}_{\text{pre}}(t)$ and $\bar{r}_{\text{post}}(t)$ are the average firing rate in the pre- and post-synaptic populations, respectively. This mean activity allows to adapt more dynamically the learning behavior between two populations. Dopamine-modulated learning rules will be described in the rest of the text, together with the corresponding populations (BLA and NAcc). The parameters of all learning rules are described in Table 5.2.

All equations in the model are solved using the forward Euler method, with a time step of 1 ms. The model is implemented in the neurosimulator ANNarchy (Artificial Neural Network architect), which combines a Python interface to a high-performance parallel simulation kernel in C++.

5.2.2.1 Representation of inputs

The network is presented with two kinds of inputs: the visual representation of the CS and the gustatory representation of the US. In this article, we will concurrently learn three CS-US associations (CS1+US1, CS2+US2, CS3+US3), with different parameters (magnitude and time interval) in order to show the robustness of the model. Other combinations of magnitude and duration provoke similar results of the model.

The CS are represented by a three-dimensional binary vector, where each element represents the presence (resp. absence) of the corresponding CS with a value of 1 (resp. 0). The US are represented by a four-dimensional vector, where each element represents a single taste component (for example salt, sugar, fat and umami as in (Draniyas et al., 2008)). As shown in Table 5.1, there is an overlap between the different tastes of the US, rendering harder the task to distinguish them. Moreover, each US representation is multiplied by a magnitude, representing the quantity of food delivered. In this article, this magnitude is the same for all tastes composing the US.

Table 5.1: Definition of the inputs to the model. Each CS-US association is defined by unique CS and US vectors. During conditioning, rewards are presented with a certain magnitude, and after a certain delay after CS onset.

Number	CS	US	Magnitude	Interval (s)
1	[1, 0, 0]	[1, 1, 0, 0]	0.8	2
2	[0, 1, 0]	[1, 0, 1, 0]	0.5	3
3	[0, 0, 1]	[1, 0, 1, 1]	1.0	4

A conditioning trial is composed of a first reset interval of 1 second where no input is given to the network (all elements of the CS and US representations are set to 0). At time $t = 1s$, the CS representation is set to the corresponding vector. This input is maintained for a given duration,

5 Timing and expectation of reward

whose value depend on the CS-US association (2 seconds for CS1-US1, 3 seconds for CS2-US2, 4 for CS3-US3). These different interval durations are chosen to show that the network can indeed learn different CS-US intervals without any modification, but different combinations would lead to similar results.

Once the delay is elapsed, the US representation is set for 1 second, with the CS representation maintained. In extinction trials, the US representation is not set. After this duration of one second, all elements of the CS and US representations are reset to 0, and the network can settle for one more second, so the duration of one trial is equal to the interval plus 3 seconds.

The visual input to the model is represented by the population IT, composed of 9 units. The CS representations activate different neurons in IT with a specific one-to-many pattern: one element of the CS vector activates exactly 3 units in IT (called a cluster), without overlap. This activation is excitatory, with a fixed weight value of 1.0 (see Table 5.2 for the weight value of all projections.). Each neuron in IT has a membrane potential governed by Equation 5.9, with the firing rate being its positive part (Equation 5.2):

$$\tau \cdot \frac{dm(t)}{dt} + m(t) = g_{\text{exc}}(t) + \eta(t) \quad (5.9)$$

with $\tau = 10$ ms, $\eta(t)$ randomly chosen at each time step in $[-0.1, 0.1]$ and $g_{\text{exc}}(t)$ the input from the CS representation. The gustatory inputs are similarly represented by LH, with a one-to-one projection (one neuron in LH represents one element of the US representation). Thus, neurons in LH are also governed by Equation 5.9, with $\tau = 10$ ms.

Table 5.2: Parameters of the projections in the model. Pre and Post describe the pre- and post-synaptic populations, respectively. Type denotes the type of the synapses in the projection, as they are differentially integrated by the postsynaptic neurons (exc, inh, mod, dopa). Pattern denotes the projection pattern between the pre- and post-synaptic populations: all-to-all means that all post-synaptic neurons receive connections from all presynaptic neurons; one-to-one means that each postsynaptic neuron receives exactly one connection from the pre-synaptic population, without overlap. one-to-many and many-to-many refer to specific projection patterns for the clusters in IT, please refer to Section 5.2.2.1 for a description. Eq represents the number of the equation governing plasticity in the projection. Weight describe the initial value for the weight of each synapse (non-learnable connections keep this value through the simulation). w_{min} is the minimal value that a learnable weight can take during learning, while w_{max} is the maximal value (if any). The other parameters correspond to the respective equations of the learning rules, please refer to them for details.

Pre	Post	Type	Pattern	Eq.	Weight	w_{extmin}	w_{max}	θ_{pre}	θ_{post}	K	τ_{dopa}	k	τ_{α}
VIS	IT	exc	one-to-many	-	1.0	-	-	-	-	-	-	-	-

Pre	Post	Type	Pattern	Eq.	Weight	w_{extmin}	w_{max}	θ_{pre}	θ_{post}	K	τ_{dopa}	k	τ_{α}
GUSLH	exc	one-	-	-	1.0	-	-	-	-	-	-	-	-
		to-											
		one											
LH	BLA	exc	all-	Equation	50.3 ± 0.2	$[0, -]$	100	-	-	10	100	1	1
		to-	all										
		all											
IT	BLA	mod	all-	Equation	50	-	300	-	-	-	-	-	-
		to-	all										
		all											
BLA	BLA	inh	all-	Equation	50	$[0, 3]$	100	-	-	-	-	-	-
		to-	all										
		all											
BLACE	exc	all-	-	-	1.0	-	-	-	-	-	-	-	-
		to-											
		all											
CE	PPT	exc	all-	-	1.5	-	-	-	-	-	-	-	-
		to-	one										
		one											
LH	PPT	exc	all-	-	0.75	-	-	-	-	-	-	-	-
		to-	one										
		one											
PPT	PPT	inh	all-	-	2	-	-	-	-	-	-	-	-
		to-	all										
		all											
PPT	NTA	exc	all-	-	1.5	-	-	-	-	-	-	-	-
		to-	all										
		all											
PPT	MP	exc	all-	-	0.5	-	-	-	-	-	-	-	-
		to-	all										
		all											
VP	RMT	inh	all-	-	1	-	-	-	-	-	-	-	-
		to-	all										
		all											
VP	LHb	inh	all-	-	3	-	-	-	-	-	-	-	-
		to-	all										
		all											
LHb	RMT	exc	all-	-	1.5	-	-	-	-	-	-	-	-
		to-	all										
		all											

5 Timing and expectation of reward

Pre	Post	Type	Pattern	Eq.	Weight	w_{extmin}	w_{max}	θ_{pre}	θ_{post}	K	τ_{dopa}	k	τ_{α}
RMTg	VTA	inh	all-to-all	-	1.0	-	-	-	-	-	-	-	-
IT	vmPFC	exc	many-to-many	-	0.3	-	-	-	-	-	-	-	-
vmPFC	NAcc	mod	all-to-all	Equation 501	1	$[-0.2, -]$	50	-	-	5	10	1	10
BLA	NAcc	exc	one-to-one	-	0.3	-	-	-	-	-	-	-	-
VTA	NAcc	dopa	all-to-all	-	0.5	-	-	-	-	-	-	-	-
NAcc	NAcc	inh	all-to-all	Equation 503	5	$[0, 1]$	1000	-	-	-	-	-	-
NAcc	VP	inh	all-to-all	Equation 507	7	$[0, 2]$	100	0	0.5	-	-	-	-
NAcc	VTA	inh	all-to-all	Equation 507	7	$[0, 2]$	500	0	0	-	-	-	-

Amygdala

The amygdala is decomposed into its input structure, BLA, and its output structure, CE. BLA receives visual information from IT, gustatory information from LH and dopaminergic innervation from VTA. Its role is to learn to associate the CS and US representations: a BLA cell which was previously activated by the food reward alone, proportionally to its magnitude (Bermudez and Schultz, 2010), should become activated with the same firing rate at CS onset, indicating a transfer of the value of the US to the CS.

As depicted on Figure 5.3, the BLA is composed of 36 units, reciprocally connected with each other through inhibitory connections (inh). Excitatory connections from LH (exc) interact with the excitatory ones from IT (labeled as mod): when no LH activation is present, a neuron can be activated solely by its excitatory inputs from IT; when LH is activated, inputs from IT do not drive the cell response. Such a non-linear interaction between different inputs may be me-

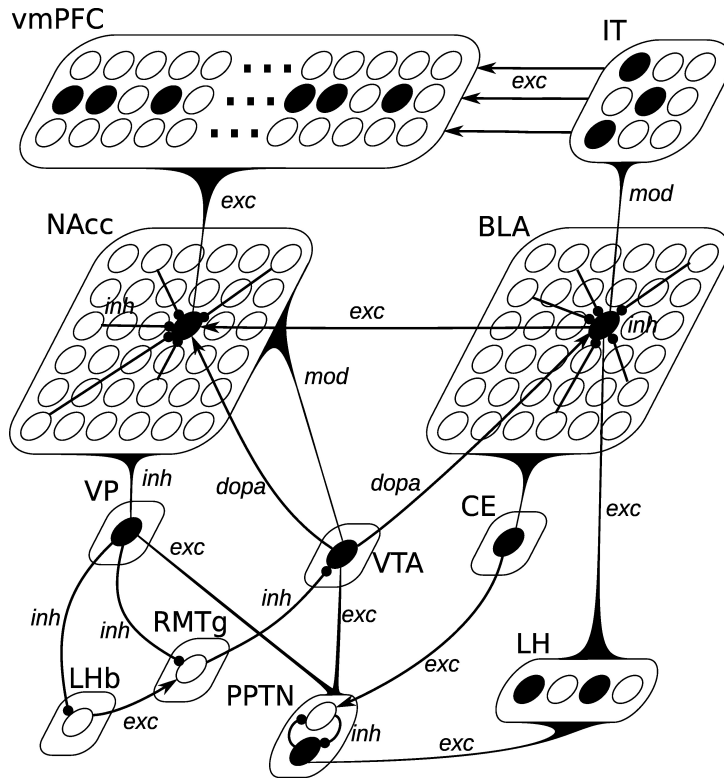


Figure 5.3: Neural network description of the model. Pointed arrows represent excitatory or dopaminergic synapses, while rounded arrows represent inhibitory synapses. The black curved triangles represent connections from all units of a given population to a single cell. The type of the connection (exc, mod, inh, dopa) is added next to the arrow. Lateral inhibitory connections within BLA and NAcc are only partially represented for simplicity. BLA is composed of 36 units, whose activation is defined by Equation 5.10. Each unit receives excitatory connections from all LH units ($g_{exc}(t)$), modulated connections from all IT units ($g_{mod}(t)$), one dopaminergic connection from VTA ($g_{dopa}(t)$) and inhibitory connections from all other BLA units ($g_{inh}(t)$). Each of the 3 banks of 50 oscillators in vmPFC receives excitatory connections ($g_{exc}(t)$) from a specific cluster of 3 units in IT representing a given CS. NAcc is composed of 36 units, whose activation is defined by equation Equation 5.16. Each unit receives a single excitatory connection from BLA ($g_{exc}(t)$), excitatory connections from all units of vmPFC ($g_{mod}(t)$), one dopaminergic connection from VTA ($g_{dopa}(t)$) and inhibitory connections from all other NAcc units ($g_{inh}(t)$). The other populations are composed of single units, integrating excitatory or inhibitory inputs.

5 Timing and expectation of reward

diated through the somatostatin-containing interneurons in BLA, which are able to suppress excitatory inputs to pyramidal cell distal dendrites (presumably from the cortex), but let them react to the inputs from LH (Muller et al., 2007). A BLA unit in this model therefore averages the behavior of pyramidal excitatory neurons, somatostatin- and parvalbumin-containing inhibitory interneurons into a single equation.

The membrane potential of each cell is driven by Equation 5.10:

$$\tau \cdot \frac{dm(t)}{dt} + m(t) = \Phi_{\tau_{\text{exc}},k}(g_{\text{exc}}(t)) + (1 - \Delta_{\Gamma}(g_{\text{exc}}(t))) \cdot \Phi_{\tau_{\text{mod}},k}(g_{\text{mod}}(t)) - g_{\text{inh}}(t) + \eta(t) \quad (5.10)$$

where $\tau = 10$ ms is the time constant of the cell, $\tau_{\text{exc}} = \tau_{\text{mod}} = 500$ ms are the integration constants for the phasic functions of inputs, $k = 0.8$ is a parameter ensuring that the cell still responds with a significant firing rate after the phasic component is processed, $\Gamma = 0.1$ is a threshold on the excitatory inputs ensuring that modulated inputs from IT can only drive the cell's activity when the input from LH is absent. The effect of this complex equation will be explained with more details in Section 5.3.1.

CE is composed of a single unit, receiving excitatory inputs from all BLA units. Its membrane potential is driven by Equation 5.9, with $\tau = 10$ ms. As only one unit is active at a time in BLA because of lateral inhibition, CE simply copies activity in BLA, regardless the CS-US association.

Learning occurs in BLA for three types of connections: the excitatory input from LH, the modulated input from IT and the inhibitory lateral connections between the BLA neurons. The learning procedure is composed of two phases: in the sensitization phase, the US are presented alone, without any CS. This allows BLA to learn to represent each US by a single neuron. In the conditioning phase, learning in the LH \rightarrow BLA pathway is reduced. This represents the fact that the formation of food reward representations in BLA is a much slower process than the conditioning sessions.

Excitatory connections from LH to BLA are learned with a dopamine-modulated covariance-based learning, with the addition of a homeostatic mechanism to ensure the weights do not increase infinitely. The evolution of these weights is described by Equation 5.11:

$$\epsilon \cdot \frac{dw_{i,j}(t)}{dt} = K \cdot \Phi_{\tau_{\text{dopa}},k}(g_{\text{DA}}(t)) \cdot \text{OR}(r_{\text{pre}}^i(t) - \bar{r}_{\text{pre}}(t), r_{\text{post}}^j(t) - \bar{r}_{\text{post}}(t)) - \alpha^j(t) \cdot r_{\text{post}}^j(t)^2 \cdot w_{i,j}(t) \quad (5.11)$$

with $\epsilon = 100$ in the sensitization phase and 10000 in the conditioning phase, $K = 10$, $\tau_{\text{dopa}} = 100$ ms, $k = 1$. In the first term of the equation, the covariance term is modulated by a value depending on the dopaminergic activity in VTA. This allows DA extracellular levels to influence the induction of LTP in BLA, as experimentally observed (Bissière et al., 2003). It is

filtered through the phasic function $\Phi_{\tau_{DA},k}(g_{\text{dopa}}(t))$ with $k = 1$, so that DA-mediated learning only takes temporarily place when DA is significantly above its baseline, i.e. during a phasic burst of activation.

This first term also differs from the covariance learning rule described by Equation 5.8, as it uses a $\text{OR}(x, y)$ function, being $\text{OR}(x, y) = x \cdot y$ if $x > 0$ or $y > 0$ and $\text{OR}(x, y) = 0$ if both $x < 0$ and $y < 0$. If both cells are significantly more activated than their respective population, the term is positive and LTP is engaged. If only one cell is significantly active (either pre- or post-synaptic), the term is negative and LTD appears (homo- or hetero-synaptic LTD, respectively). This simple behavior allows to develop a high selectivity for specific patterns in the presynaptic population. In the case where both cells are inactive ($r_{\text{pre}}^i(t) < \bar{r}_{\text{pre}}(t)$ and $r_{\text{post}}^j(t) < \bar{r}_{\text{post}}(t)$), the covariance term would be positive but we set it artificially to 0, in order to avoid that silent neurons build up strong connections.

The second term of the learning rule implements a regularization term derived from the Oja learning rule (Oja, 1982) ensuring that the postsynaptic activity does not increase indefinitely during learning (Schroll et al., 2012; Vitay and Hamker, 2010). This mechanism implements homeostatic plasticity whose role is to keep neurons in an energetically efficient mode (Turriano, 2008). As formulated in Equation 5.12, the regularization term $\alpha(t)$ becomes positive whenever the postsynaptic neuron fires above a certain threshold, thereby down-scaling the most active connections to this neuron:

$$\tau_{\alpha} \frac{d\alpha^j(t)}{dt} + \alpha^j(t) = (r_{\text{post}}^j(t) - r_{\text{max}})^+ \quad (5.12)$$

$r_{\text{max}} = 1$ being the postsynaptic firing rate above which regularization is engaged.

The modulated projection from IT to BLA follows a different learning rule: its principle is that this projection should learn to activate a BLA neuron with the same strength as the corresponding US. Learning is also modulated by dopamine release, as described by Equation 5.13:

$$\epsilon \cdot \frac{dw_{i,j}(t)}{dt} = \Delta_{\Gamma_{\text{dopa}}} (g_{\text{dopa}}^j(t)) \cdot (r_{\text{pre}}^i(t) - \bar{r}_{\text{pre}}(t)) \cdot (r_{\text{post}}^j(t) - \bar{r}_{\text{post}}(t)) \cdot (g_{\text{exc}}^j(t) - g_{\text{mod}}^j(t))^+ \quad (5.13)$$

with $\Gamma_{\text{dopa}} = 0.3$ being a threshold on VTA activity. The term $(g_{\text{exc}}^j(t) - g_{\text{mod}}^j(t))^+$ ensures that the modulated projections stop learning whenever their net effect on a postsynaptic neuron exceeds the one of the excitatory projection from LH during DA bursts.

Lateral inhibitory connections between BLA cells are learned according to the covariance-based learning rule described in Equation 5.8, forcing competition between the cells and ensuring that only one BLA cell is active for a single stimulus.

Pedunculopontine nucleus

PPTN is involved in generating phasic DA bursts in VTA for both reward-predicting cues and rewards through direct glutamatergic projections (Pan et al., 2005). Two different populations of PPTN neurons signal CS- and US-related signals to VTA (Kobayashi and Okada, 2007). In the model, PPTN is therefore composed of two units, one receiving US information from LH, the other CS information from CE, as depicted on Figure 5.3. These two neurons are moreover inhibiting each other, so that only one is active at a given time. The dynamics of these neurons are described by the same Equation 5.14, the only difference being the origin of the excitatory information:

$$\tau \cdot \frac{dm(t)}{dt} + m(t) = \Phi_{\tau_{\text{exc}}, k}(g_{\text{exc}}(t)) - g_{\text{inh}}(t) + \eta(t) \quad (5.14)$$

with $\tau = 10$ ms, $\tau_{\text{exc}} = 50$ ms and $k = 1$.

Ventromedial prefrontal cortex

As in the Striatal-beat frequency model (Matell and Meck, 2004), we model the cortical inputs to NAcc by a bank of oscillators synchronized at CS onset. Each CS is represented by a group of 50 units oscillating at various frequencies between 2 and 8 Hz. Indeed, enhanced top-down synchrony in the extended theta band has been observed between vmPFC and NAcc during reward anticipation (Cohen et al., 2012).

As three CS are used in the experiments presented in this article, there are three banks of 50 units, each activated by the corresponding cluster in IT. When the sum of excitatory inputs exceeds a given threshold $T_{\text{start}} = 0.8$, the current time t of the simulation is stored in the variable t_0 , and the membrane potential of each unit varies according to the Equation 5.15:

$$\tau \cdot \frac{dm(t)}{dt} + m(t) = \frac{1 + \sin(2\pi \cdot f \cdot (t - t_0) + \varphi)}{2} \quad (5.15)$$

with $\tau = 1$ ms, f the frequency of the oscillator randomly chosen at the beginning of the simulation in the range $[2, 8]$ (uniform distribution) and φ the phase of the oscillator randomly chosen in the range $[0, \pi]$. When the excitatory input falls below a threshold $T_{\text{stop}} = 0.2$, the membrane potential is set to 0. Contrary to the rest of the network, this mechanism is not biologically plausible, but it abstracts the behavior of a coupled network of excitatory and inhibitory neurons, all activated by CS onset and interacting with different synaptic strengths and delays.

Nucleus accumbens

As described by Figure 5.3, NAcc is composed of 36 units, integrating excitatory inputs from BLA with a one-to-one pattern (each NAcc neuron receives a connection from only one neuron in BLA), excitatory inputs from vmPFC (all-to-all), dopaminergic inputs from VTA and lateral inhibitory connections forcing competition between NAcc cells. Their membrane potential can be either in a hyperpolarized *down-state* or in a depolarized *up-state*, depending on several factors: 1) spontaneous transition from the down-state to the up-state have been described, exhibiting rhythmic delta-frequency (0.5-2Hz) activities in freely moving rats (Leung and Yim, 1993); 2) Phasic DA release from VTA can bring NAcc neurons in the up-state (Goto and Grace, 2005; Gruber et al., 2003); 3) Massive input from the prefrontal cortex (together with hippocampal input, not modeled here) can also force this transition (McGinty and Grace, 2009).

Consequently, each unit of NAcc has an additional input variable $s(t)$ describing its current state, taking the value -0.9 in the down-state and -0.4 in the up-state. Its effect is that the neuron can more easily have a non-zero firing rate in the up-state than in the down-state. The membrane potential of each NAcc cell evolves according to the Equation 5.16:

$$\tau \cdot \frac{dm(t)}{dt} + m(t) = g_{\text{exc}}(t) - g_{\text{inh}}(t) + g_{\text{dopa}}(t) + s(t) + \eta(t) \quad (5.16)$$

with $\tau = 10$ ms. The corresponding firing rate is restricted to the range $[0, 1.1]$. Transitions between the two states are followed by another variable $s_{\text{time}}(t)$, which integrates $s(t)$ over time, as described by the Equation 5.17:

$$\tau \cdot \frac{ds_{\text{time}}(t)}{dt} + s_{\text{time}}(t) = s(t) \quad (5.17)$$

with $\tau = 450$ ms. The role of the variable $s_{\text{time}}(t)$ is to ensure spontaneous transitions between the up- and down-states in the absence of external inputs or dopaminergic activation. Transitions from the down-state to the up-state are provoked by one of the following events:

- The activity of VTA exceeds a threshold $\Gamma_{\text{dopa}} = 0.3$;
- Excitatory inputs $g_{\text{exc}}(t)$ exceed the threshold $\Gamma_{\text{glut}} = 1$;
- The variable $s_{\text{time}}(t)$ exceeds the threshold $\Gamma_{\text{up}} = -0.45$.

Transitions from the up-state to the down-state are provoked by the combination of these two conditions:

- The activity of VTA is below the threshold $\Gamma_{\text{dopa}} = 0.3$;
- The variable $s_{\text{time}}(t)$ is below the threshold $\Gamma_{\text{down}} = -0.85$.

5 Timing and expectation of reward

The role of the variable $s_{\text{time}}(t)$ is therefore to ensure spontaneous transitions from the down-state to the up-state, regardless other inputs. It also ensures that the NAcc cell stays long enough in the up-state before going back to the down-state when the other inputs fade away.

The mechanism proposed to exhibit up- and down-state fluctuations in our model of NAcc is a phenomenological abstraction of the underlying biological components, sufficient to reproduce some of their functional properties. A more detailed modeling approach is needed to better describe and understand the observed patterns in the context of temporal prediction. It could rely on existing biophysically-detailed models of striatal spiny neurons, studying the effects on membrane bistability of slow and fast potassium currents (Gruber et al., 2003), NMDA/AMPA receptors ratio (Wolf et al., 2005) or D1-receptor activation (Humphries et al., 2009), for example.

Excitatory inputs from vmPFC are learned using the same dopamine-modulated learning rule as the LH \rightarrow BLA projection, described by Equation 5.11 and Equation 5.12, with $\epsilon = 50$, $K = 5$, $\tau_{\text{dopa}} = 10 \text{ ms}$, $k = 1$, $\tau_{\alpha} = 10 \text{ ms}$ and $r_{\text{max}} = 1$. This three-factors rule covers some known effects of dopamine on corticostriatal learning (Calabresi et al., 2007; Reynolds and Wickens, 2002; Shen et al., 2008): phasic DA release potentiates learning; LTP requires both DA release, presynaptic activity and postsynaptic depolarization; strong presynaptic activation when the postsynaptic cell is in the down-state leads to LTD. The third condition of the learning rule, called heterosynaptic LTD where only the post-synaptic cell is active but not the pre-synaptic one, has not been observed in the striatum but in the hippocampus (Doyere et al., 1997). However, low-frequency stimulation at 1 Hz engage LTD at corticostriatal synapses (Fino et al., 2005), so such a mechanism can not be ruled out. The known influence of dopamine depletion on corticostriatal learning is not used in this model.

τ_{α} is set very low, restricting learning to the early phase of the dopaminergic burst of VTA activity. The weights between vmPFC and NAcc are allowed to become negative ($w_{\text{min}} = -0.2$) to reflect the role of accumbal interneurons (TANs and GABAergic) in timing processes (Apicella et al., 2009; Coull et al., 2011). This particularity is essential for the adequate temporal response of NAcc neurons. Inhibitory lateral connections between NAcc cells are learned according to the covariance-based learning rule described by Equation 5.8.

Ventral Pallidum

During classical conditioning, VP cells are excited by large rewards and the cues predicting them, but are inhibited by small rewards (Tindell et al., 2004). While the major source of inhibition is clearly NAcc, the source of excitation is still unknown. Based on known anatomical connections, we hypothesize that this phasic excitation is transmitted by PPTN (Hallanger and Wainer, 1988). However, when a reward is fully predicted and delivered, NAcc is activated and cancels the excitation provided by PPTN. We propose a mechanism where VP is inhibited by NAcc activation unless excitatory inputs from PPTN are present. This shunting mechanism is described by Equation 5.18 governing the membrane potential of the single unit in VP:

$$\tau \cdot \frac{dm(t)}{dt} + m(t) = g_{\text{exc}}(t) - \Delta_{\Gamma}(g_{\text{exc}}(t)) \cdot g_{\text{inh}}(t) + B + \eta(t) \quad (5.18)$$

where $\tau = 10$ ms, $B = 0.5$ is the baseline activity of the VP neuron and $\Gamma = 0.1$ is a threshold on excitatory inputs. The inhibitory projection from NAcc is learned according to the thresholded Hebbian learning rule described by the Equation 5.7.

Lateral Habenula

LHb is activated by aversive stimuli and reward omission (Hikosaka et al., 2008; Hong et al., 2011). In this model, signaling of reward omission is provoked by disinhibition from VP: when VP is inhibited by NAcc at the expected time of reward delivery, it stops inhibiting LHb and allows it to fire. As the source of excitatory inputs to LHb is still not clear, we simply consider in this model that the single LHb cell has a very high baseline activity, which is normally cancelled by the tonic inhibition of VP, as expressed by Equation 5.19:

$$\tau \cdot \frac{dm(t)}{dt} + m(t) = -g_{\text{inh}}(t) + B + \eta(t) \quad (5.19)$$

with $\tau = 10$ ms and $B = 1$.

Rostromedial tegmental nucleus

While most RMTg neurons are activated by aversive events, some also respond to reward omission. They are inhibited by rewards and reward-predicting stimuli (Jhou et al., 2009). The excitation at reward omission has been shown to come from LHb glutamatergic inputs (Balcita-Pedicino et al., 2011; Hong et al., 2011). In this model, the single unit of RMTg is under the tonic inhibition from VP (Jhou et al., 2009), and can become activated when excitatory inputs from LHb are present, as formulated by the Equation 5.20:

$$\tau \cdot \frac{dm(t)}{dt} + m(t) = g_{\text{exc}}(t) - g_{\text{inh}}(t) + \eta(t) \quad (5.20)$$

with $\tau = 10$ ms.

Ventral tegmental area

The final stage of the model is a single dopaminergic unit in VTA. It receives excitatory inputs from PPTN, inhibitory inputs from RMTg and modulatory inhibitory inputs from NAcc. The excitatory inputs can progressively be canceled by the modulatory inputs, as the US becomes

5 Timing and expectation of reward

temporally predictable by NAcc. Additionally, RMTg inputs can provoke a prolonged inhibition of the VTA cell below baseline if no reward is present. This is reflected by the Equation 5.21:

$$\tau \cdot \frac{dm(t)}{dt} + m(t) = g_{\text{exc}}(t) * (1 - \Phi_{\tau_{\text{mod}},k}(g_{\text{mod}}(t))) - (1 - \Delta_{\Gamma}(g_{\text{exc}}(t))) \cdot \Phi_{\tau_{\text{inh}},k}(g_{\text{inh}}(t)) + B + \eta \quad (5.21)$$

with $\tau = 10$ ms, $\tau_{\text{mod}} = 300$ ms, $k = 1$, $\Gamma = 0.1$, $\tau_{\text{inh}} = 30$ ms and $B = 0.2$. Modulatory inputs from NAcc are learned according to the learning rule defined in Equation 5.7}.

5.3 Results

Most experiments in this section concern the concurrent learning of the three CS-US associations described in Table 5.1. The learning procedure is split into two phases: the sensitization phase, where each US is presented alone for 10 trials, and the conditioning phase, where the CS and US are presented together for 15 trials. The three CS-US associations are intermingled in ascending order for simplicity, but a randomized order would not change the results. The organization of each trial is described in Section 5.2.2.1.

5.3.1 CS-US associations in the amygdala

Figure 5.4 shows the firing rate of single BLA cells during the first (top row) and fifteenth (bottom row) trials of the conditioning phase, for each of the three CS-US associations. After the sensitization phase, only one cell in BLA is selective for each US because of the increased competition induced by antihebbian learning in the lateral connections within BLA. The activity of these US-specific neurons only is displayed, the other cells having a firing rate close to 0.

During the first conditioning trial, each BLA cell is activated only at reward delivery, with an amplitude proportional to the magnitude of the US. It reaches a peak shortly after US onset and slowly decreases to a small baseline because of the phasic integration of LH inputs described in Equation 5.10. During the late conditioning trial, the same cells are activated by the onset of the corresponding CS. Their firing rate also reaches a peak shortly after CS onset, with a magnitude proportional to the reward magnitude (see Section 5.3.4 for further discussion) and slowly decays to around 20% of their peak amplitude, due to the temporal integration of IT inputs in Equation 5.10. However, these cells are still phasically excited by the delivery of the predicted reward.

This behavior of single BLA cells during conditioning is in agreement with the known dependency of BLA activity on reward magnitude (Bermudez and Schultz, 2010) as well as with the observed firing rate of individual BLA neurons for both CS and US (Maren and Quirk, 2004; Ono et al., 1995). As CE simply sums up BLA activity in our model, the response profile in CE is

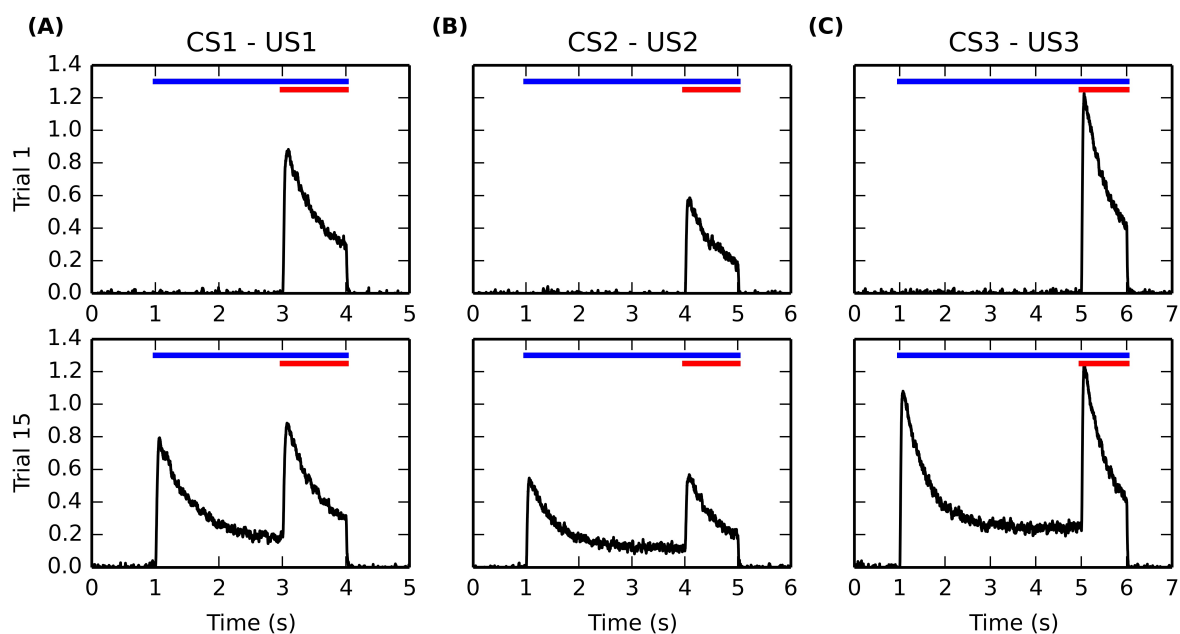


Figure 5.4: Timecourse of the activity of different BLA cells before and after conditioning. Activities for the CS1-US1, CS2-US2 and CS3-US3 associations are represented from left to right in panels **(A)**, **(B)** and **(C)**, respectively. For each figure, the horizontal blue line represents the presentation of the CS, while the red line represents the presentation of the US. The top row shows the evolution of the firing rate of a single BLA neuron over time during the first trial of conditioning. Because of the sensitization phase and the lateral inhibition in BLA, there is only one cell in the population which represents each US. During the first trial, this cell gets maximally activated at the time of reward delivery (3, 4 and 5 seconds after the start of the trial, respectively), and its firing rate decreases because of the adaptation of excitatory inputs in BLA, before returning to baseline when the US is removed after 1 second. All other cells in BLA are not activated. The bottom row shows the activity of the same cells during the fifteenth trial of conditioning. They now show an increase of activity when the CS appears (1 second after the start of the trial), reaching a maximum of similar amplitude as the response evoked by the US, and slowly decreasing to a baseline of about 20% of this maximal activity. When the reward is delivered, they increase their firing rate similarly as in the first trial.

5 Timing and expectation of reward

similar during conditioning, although not specific to the CS-US association. This means that the $CE \rightarrow PPTN \rightarrow VTA$ pathway is able to signal the onset of specific reward-predicting cues to VTA and generate the corresponding phasic burst, as observed experimentally (Fudge and Haber, 2000; Lokwan et al., 1999).

5.3.2 Timecourse of activity in VTA

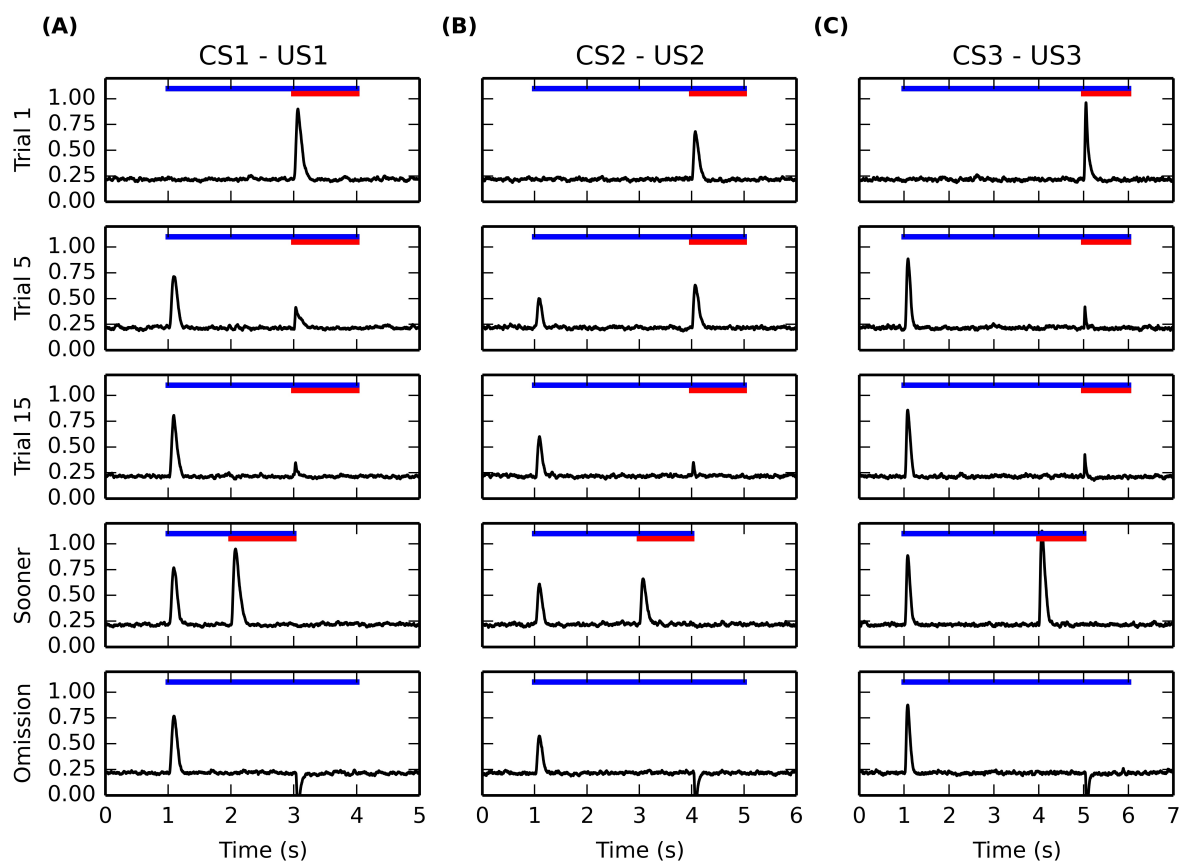


Figure 5.5: Timecourse of the activity of the VTA cell during conditioning. The activity for the three CS-US associations is displayed from left to right in panels (A), (B) and (C), respectively. For each figure, the horizontal blue line represents the presentation of the CS, while the red line represents the presentation of the US. The first row represents the activity of VTA during the first trial of conditioning, the second row during the fifth trial, the third during the fifteenth trial. They show a progressive reduction of the amplitude of the US-related burst, while the CS-related burst appears early in learning. The fourth row shows the activity of the VTA cell when the reward is delivered one second earlier than previously associated. It shows that the VTA cell responds to rewards delivered earlier with the same activation as for unpredicted rewards. The fifth row shows omission trials: the CS is presented normally, but the US is omitted. The VTA cell shows a phasic pause in firing at the time when reward was expected.

Figure 5.5 shows the temporal evolution of VTA activity during several conditioning trials for the three CS-US associations. The first row shows its activity during the first conditioning trial.

As expected, the VTA cell only fires transiently at reward delivery, with an amplitude proportional to the reward magnitude. This phasic excitation is provoked by the LH \rightarrow PPTN \rightarrow VTA pathway.

The second and third rows show VTA activity during the fifth and fifteenth conditioning trials for each association. The DA cell shows very early in learning a phasic burst of activity at CS onset. In parallel, the amplitude of the US-related burst progressively decreases until an almost complete cancellation at the fifteenth trial. This pattern of evolution is in accordance of the observations of Pan and Hyland (2005) showing that the CS- and US-related bursts of DA activation coexist in the early phases of training. Simple disconnection experiments show that the CS-related phasic bursts are dependent on the CE \rightarrow PPTN \rightarrow VTA pathway, while the cancellation of the US-related bursts is dependent on the modulatory projection from NAcc to VTA.

After 15 conditioning trials for each association have been executed, two additional trials are performed to test the functional properties of the model. The first additional trial (fourth row of Figure 5.5) consists in early delivery of reward: the US previously paired with the CS is presented one second earlier than usual (i.e. 1s after CS onset instead of 2s for the CS1-US1 association, 2s for CS2-US2 and 3s for CS3-US3). The CS presentation stops with the end of the US. In this case the VTA cell reacts phasically to reward delivery with the same amplitude as for an unpredicted reward, instead of the diminished burst observed when the reward is presented at the expected time. This is in accordance with the experimental findings of Hollerman and Schultz (1998).

In the second type of additional trial (fifth row of Figure 5.5), each CS is presented normally but the US is omitted. Shortly after the expected delivery time (around 50ms), the VTA cell receives a strong phasic inhibition bringing its firing rate to 0 for a prolonged period of time. This activation dip is provoked by the NAcc \rightarrow VP \rightarrow LHb \rightarrow RMTg \rightarrow VTA pathway. This behavior is in accordance with the reward-prediction error interpretation of VTA activity during conditioning (Fiorillo et al., 2003; Schultz et al., 1997).

5.3.3 Evolution of VTA activity during conditioning

In this section, we take a closer look at the evolution of phasic activities in VTA during the conditioning process. Figure 5.6 shows the evolution of US- and CS-related activation in BLA over the 15 conditioning trials, for each of the three associations. The amplitude of the CS-related (in blue) and US-related (in red) bursts is computed by taking the maximal firing rate of the VTA cell in a small time window (± 100 ms) around CS and US onsets, respectively.

Panels (A) and (C) (corresponding to rewards of magnitude 0.8 and 1.0, respectively) show that the CS-related bursts, initially nonexistent as the baseline activity of VTA is 0.2, quickly rise in a few trials to reach up a limit dependent on the reward magnitude. The US-related bursts show the opposite pattern: the amplitude is initially dependent on the reward magnitude, but

5 Timing and expectation of reward

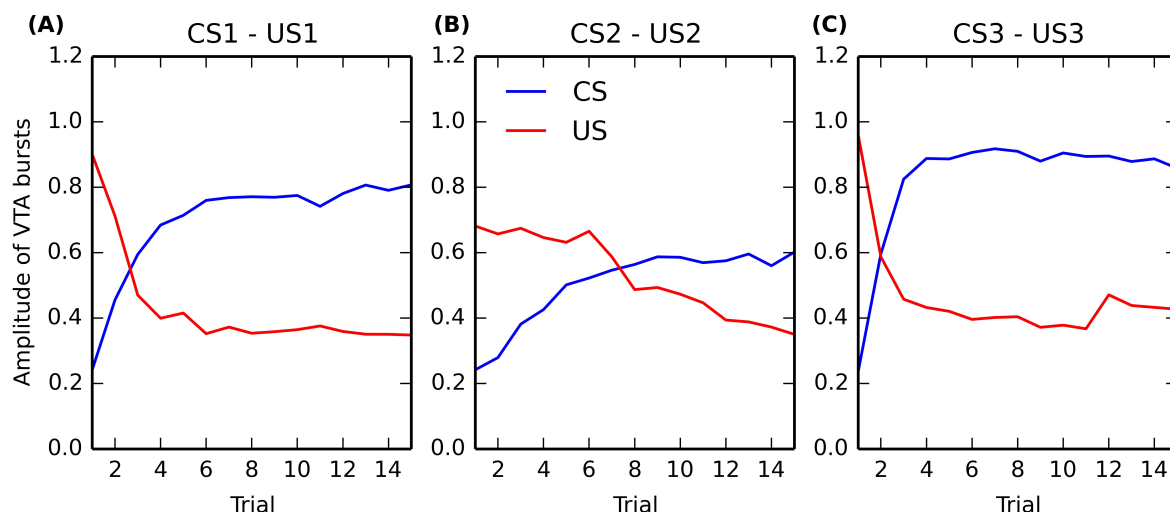


Figure 5.6: Evolution of the maximal activity in VTA during conditioning. For each of the three associations (panels **(A)**, **(B)** and **(C)**, respectively), the maximal activity of the VTA cell at CS onset (in blue) and at reward delivery (in red) is plotted for each trial of the conditioning phase. These values are computed by taking the maximum value of the firing rate of the VTA cell in a small time window (± 100 ms) around CS onset and reward delivery. The panels show the relative speed at which the CS-related bursts appear and the one at which the US-related bursts are canceled.

is progressively decreases to a value close to the VTA baseline. One can observe that the cancellation is not total, the maximal value of US-related bursts being between 0.3 and 0.4, while the baseline activity is 0.2. However the duration of the phasic is also reduced from approximately 200ms for unpredicted rewards to 50ms for fully predicted rewards, so the total amount of dopamine released can be considered relatively low. This aspect will be discussed in Section 5.4.2.

Panel **(B)**, corresponding to a reward magnitude of 0.5, shows a different behavior. While the CS-related burst still increases to reach a maximum equal to the initial US-related burst (although more slowly), the cancellation of the US is both slower and not total. This suggests that reward magnitude influences conditioned responses in VTA in a non-linear manner. This will be further investigated in the following section. Altogether, the results show that the cancellation of the US-related VTA activation happens well after the appearance of CS-related bursts, what is consistent with the experimental data (Pan and Hyland, 2005).

5.3.4 Influence of reward magnitude on conditioning

In order to study the influence of reward magnitude on VTA activity, we modified the conditioning procedure. In this section, only one CS-US association (CS1-US1, with an interval of 2 seconds between the CS and US) is learned by the network, but the reward magnitude is varied linearly between 0 and 1 instead of the previous value 0.8. For each value of the reward magnitude, a different network performs the sensitization and conditioning tasks for this particular

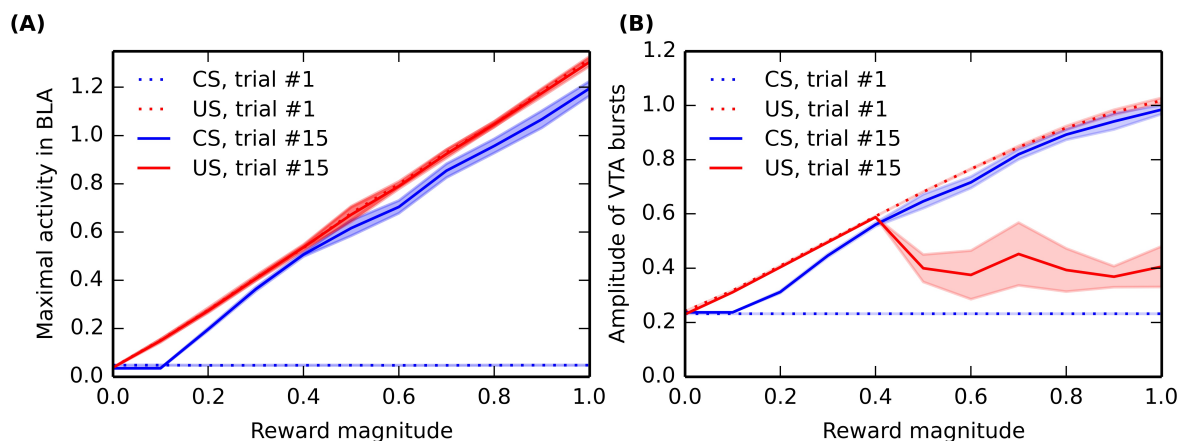


Figure 5.7: Dependency of the activity in BLA and VTA on reward magnitude. Panel (A) shows the maximal firing rate in BLA around CS-onset and reward delivery during the first and last trial of conditioning, for different reward magnitudes. For each value of the reward magnitude, the CS1-US1 association is presented 15 times, and the maximal activity in BLA around CS-onset (between 900 and 1100ms after the start of each trial) and reward delivery (between 3900 and 4100ms after the start of the trial) is recorded. The experiment is repeated 10 times (without different initial values), and the mean (solid line) and standard deviation (colored area) of these measurements are plotted. The blue dotted line shows the maximal activity at CS-onset during the first trial, which does not depend on reward magnitude, as no learning has taken place yet. The red dotted line shows the maximal activity at reward delivery during the first trial, which is proportional to the reward magnitude because of learning in the LH \rightarrow BLA projection during the sensitization phase. For the last trial of conditioning, the blue and red solid lines show the dependency on reward magnitude of the maximal activity in BLA at CS onset and reward delivery, respectively. While the US-related response is proportional to the reward, the CS-related activity only appears for reward magnitudes bigger than 0.1. Panel (B) shows the dependency on reward magnitude of the VTA bursts in the same conditions (blue dotted = CS onset at trial 1, red dotted = US delivery at trial 1, blue solid = CS onset at trial 15, red solid = US delivery at trial 15). While there are no CS-related bursts during trial 1, the US-related burst is proportional to reward magnitude. A similar relationship can be observed for the CS-related burst at the end of learning. However the US-related burst after learning shows a different pattern: small rewards (magnitude smaller than 0.4) elicit burst proportionally to their magnitude, but bigger rewards elicit strongly attenuated bursts, showing that the cancellation of US-related bursts is dependent on reward magnitude.

5 Timing and expectation of reward

association. Activities in BLA and VTA are recorded during the first and fifteenth conditioning trials, and the maximal activity of VTA and BLA cells at CS and US onsets (computed within a time window of ± 100 ms) is shown on Figure 5.7, averaged for 10 different networks. Figure 5.7 A shows the dependency of US- and CS-related activation in BLA on reward magnitude, while Figure 5.7 B shows the reward-magnitude dependency of VTA bursts.

During the first trial of conditioning, there is logically no CS-related activity in BLA and VTA (blue dotted line), regardless the reward magnitude, as conditioning has not taken place yet. The US-related activity (red dotted line) shows a linear dependency on reward magnitude in both VTA and BLA. This is explained by the linear encoding of reward magnitude in LH: a more precise model of food-related activation in LH may change this property.

During the last trial of conditioning, the CS elicits strong phasic activity in both BLA and VTA (blue solid line), which is roughly proportional to the reward magnitude: additive noise plays an important role in the learning dynamics of the model, what explains that different networks may exhibit slightly different results. This is in accordance with the observation that CS-elicited DA bursts increase monotonically with the magnitude of expected rewards (Tobler et al., 2005).

The situation is more contrasted regarding the US-related activation after conditioning (red solid line): while BLA still phasically responds linearly to the US magnitude (see also Figure 5.4), the cancellation of reward-delivery bursts in VTA only occurs if the reward magnitude is high enough (above 0.4). This cancellation is dependent on learning in NAcc, which is itself dependent on DA release by VTA. Small rewards do not provoke sufficiently high VTA bursts to modulate striatal processing and learning. While there is no direct evidence of such an effect of reward magnitude on US cancellation, this effect is in agreement with the known influence of reinforcer magnitude on the emergence of conditioned responding (Morris and Bouton, 2006) or peak-interval tasks (Ludvig et al., 2007), which are dependent on learning in the striatum.

5.3.5 Timing mechanism in NAcc

An important functional aspect of the model is the inducement of dips in VTA when a predicted reward is omitted. It relies on the ability of specific NAcc cells to learn the CS-US interval duration based on inputs from the synchronized oscillators in vmPFC, gated by the dopaminergic bursts of VTA.

Figure 5.8 shows the evolution of several internal variables of one NAcc cell during reward omission. This cell is selective for the US2 because of the corresponding input from BLA. After successful learning of the CS2-US2 association (15 trials), CS2 is presented alone while we record the temporal evolution of 1) the membrane potential of this cell (governed by Equation 5.16, red line), 2) the weighted sum of excitatory inputs from vmPFC (blue line) and 3) its up- or down-state $s(t)$ (green line). For simplicity, its firing rate is not depicted, as it is only the positive part of the membrane potential.

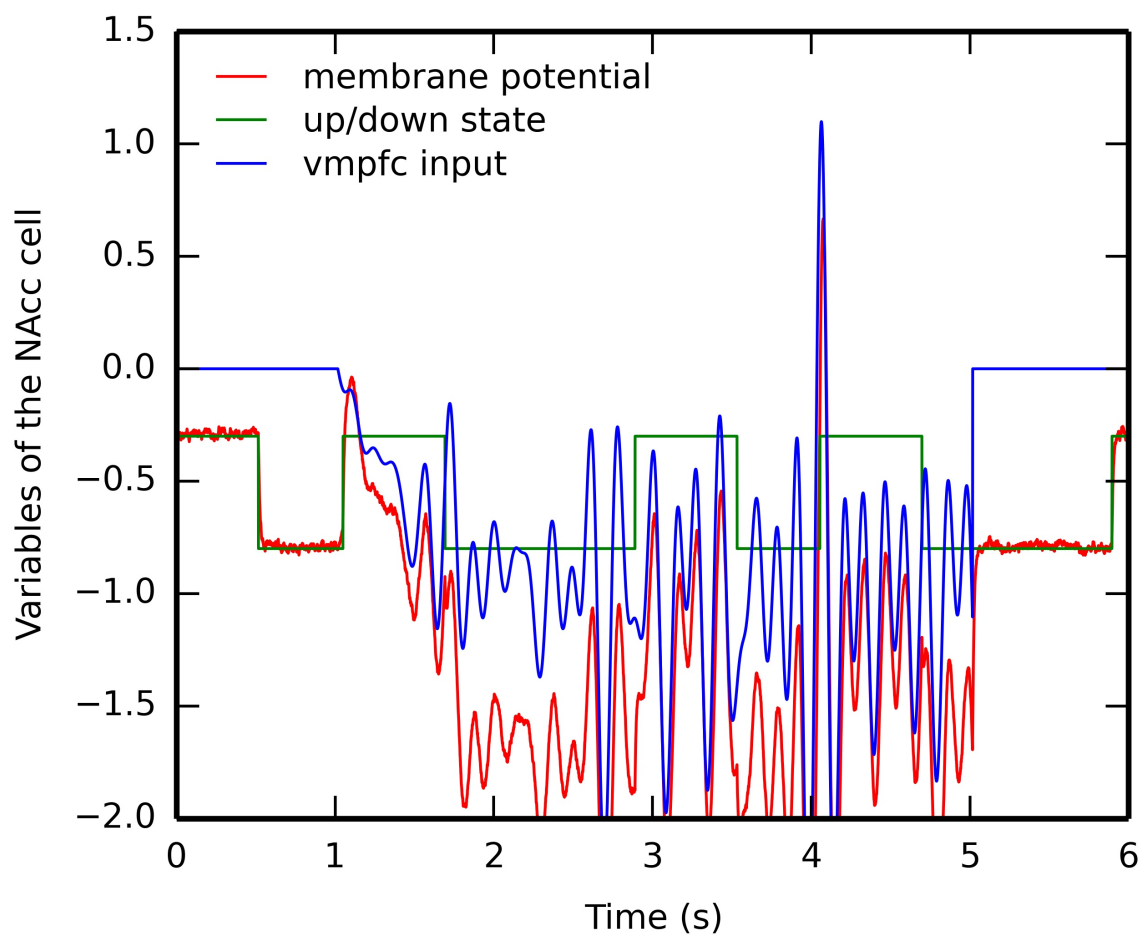


Figure 5.8: Timecourse of the internal variables of a single NAcc neuron during a reward omission trial. After the conditioning phase, CS2 is presented alone. The NAcc neuron which was selective for US2 during conditioning is recorded: its membrane potential $m(t)$ in red, the weighted sum of excitatory inputs from vmPFC in blue and its up- or down-state $s(t)$ in green. The firing rate of the neuron is the positive part of the membrane potential: the firing rate becomes only non-zero shortly at the time where reward is expected but omitted.

When the CS appears one second after the start of the trial, the CS-evoked VTA burst brings the cell into the up-state, while the cortical oscillators start influencing the membrane potential. However, this excitation is not sufficient to bring the membrane potential above the threshold and activate the cell. During the delay period, the cell switches between down- and up-states based on the internal dynamics of the variable $s_{\text{time}}(t)$ (Equation 5.17). The sum of inputs from vmPFC oscillate during this period, but is never strong enough to activate the cell. However, at the time when the US is expected (4 seconds after the beginning of the trial), these inputs become able to bring the cell into the up-state, what results in a membrane potential well above threshold and provokes a short burst of the firing rate, although the US is not delivered.

This mechanism is very similar to the Striatal-Beat Frequency model proposed by Matell and Meck (2004), although based on a different implementation (different number of cortical oscillators, different frequency range and different learning rule). The weighted sum of cortical inputs, which peaks for the cortical pattern describing the learned interval, fluctuates a lot during the delay period. In particular, there are several peaks during the delay period corresponding to different harmonics ($\frac{1}{2}, \frac{1}{3} \dots$). As suggested in (Matell and Meck, 2004), the up- and down-states are necessary to avoid spurious activation of NAcc during this period, what would lead to unwanted VTA dips, especially at the beginning of learning. In the early conditioning trials, the vmPFC input is too weak to bring the NAcc cell into the up-state, which is only dependent on phasic DA bursts at reward delivery. As in the Striatal-Beat Frequency, we do not precisely model how the cortical oscillators could be synchronized at CS onset: it is a simple threshold on visual inputs from IT. A more detailed model is necessary to generate these oscillations, perhaps through the opening of a vmPFC \rightarrow ventral BG \rightarrow medial thalamus \rightarrow vmPFC loop, gated by the VTA burst at CS onset.

5.3.6 Acquisition rate of temporal prediction

In order to study the speed at which the CS-US interval is learned in NAcc, we designed a different conditioning schedule. After sensitization to the three US, the 15 conditioning trials per association are alternated with omission trials, i.e. each CS-US trial is immediately followed by the CS alone. All learning rules are disabled during these omission trials, as we only want to use the CS as a probe to measure the acquisition rate: we want to study what would happen if the reward were omitted earlier in the conditioning process.

Figure 5.9 shows the maximal activity in NAcc (blue line) and the minimal activity in VTA (red line) during these omission trials for each CS-US association ((A), (B) and (C)). One can observe that NAcc becomes quickly able to react for an omitted reward (after only 2 conditioning trials for CS3, 3 for CS1 and 7 for CS2). The speed of learning is therefore dependent on reward magnitude, what is due to the dopaminergic modulation of cortico-striatal learning: smaller rewards generate smaller VTA bursts, inducing less LTP in the NAcc. The VTA dips are directly dependent on this learning: as soon as NAcc is able to get activated for omitted rewards, the

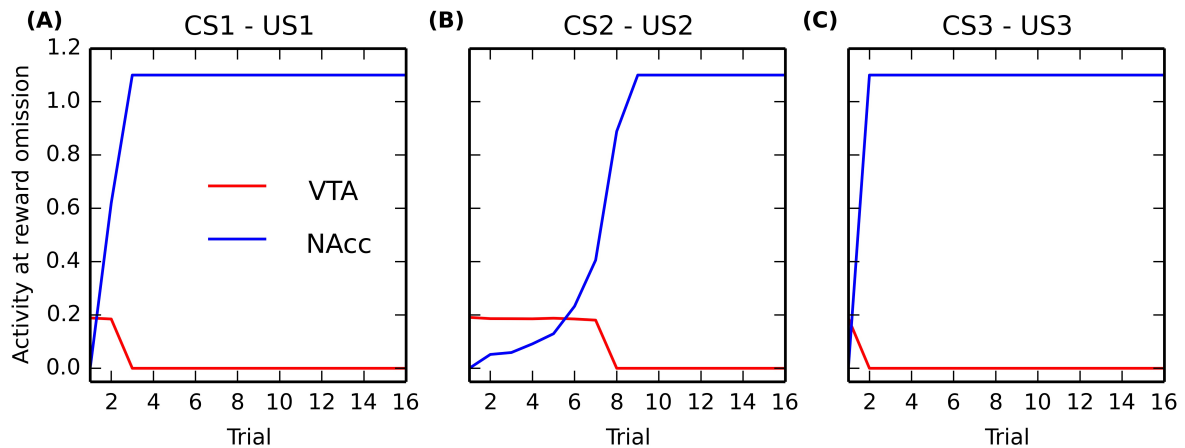


Figure 5.9: Apparition of VTA dips during conditioning. For the three CS-US associations (panels **(A)**, **(B)** and **(C)**, respectively), the panel represents what would happen in VTA (red) and NAcc (blue) if the reward were omitted directly after each conditioning trial. Learning is shut off during these omission trials. The red line shows the minimal activity in VTA during these omission trials. After the first few conditioning trials, this minimal activity is around the baseline (0.2), but quickly becomes equal to 0, denoting the appearance of the strong phasic inhibition of VTA at reward omission. The blue line shows the emergence of activity in NAcc at reward omission. The speed at which the timing prediction appears in the ventral BG depends on reward magnitude.

minimal activity in VTA at reward omission switches from the VTA baseline activity (0.2) to 0, indicating that VTA successfully signals reward omission.

This result is in accordance with experiments showing that the time interval from CS onset to US delivery is learned very rapidly at the start of training (Balsam et al., 2002). Although reward magnitude was long considered as playing only a minor role in acquisition speed during conditioning (Gallistel and Gibbon, 2000), more recent experiments showed that it influences the number of trials needed by an animal to exhibit conditioned responses during both appetitive and aversive conditioning (Morris and Bouton, 2006) and that it speeds up learning of discrimination tasks (Rose et al., 2009). In accordance with these results, our model predicts that the ability to signal negative reward-prediction errors is learned faster when the reward magnitude is high.

5.3.7 Time course of forebrain nuclei

In order to better understand how the different nuclei in the model interact during conditioning and reward omission, Figure 5.10 shows the time course of activity of several populations during the fifteenth conditioning trial of CS1-US1 (Figure 5.10 A), followed by the omission of US1 (Figure 5.10 B). The first row depicts the inputs to the networks, with the blue line showing the mean activity in the IT cluster selective for CS1 and the black line showing the mean activity of the LH neurons representing US1. As previously shown, VTA (second row) exhibits

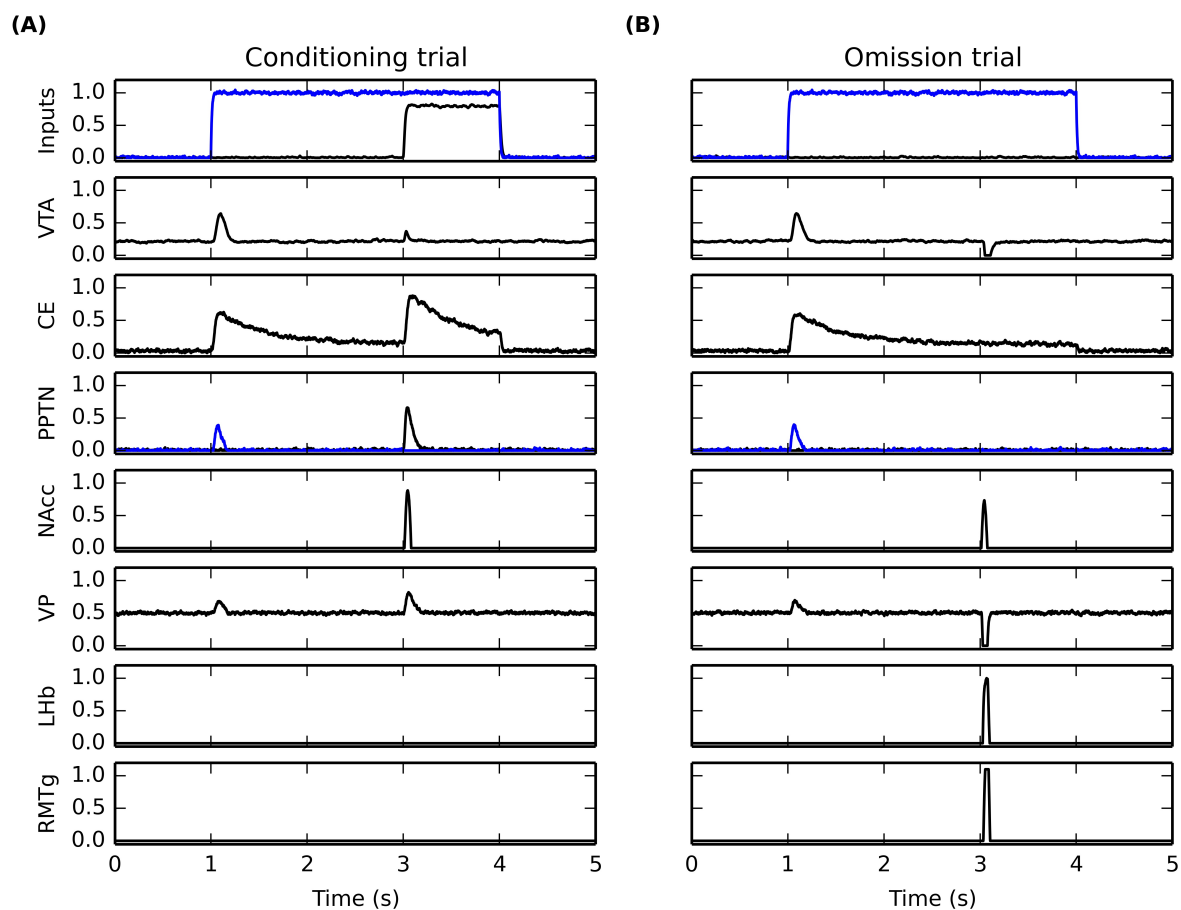


Figure 5.10: Timecourse of activity in different areas of the model. Panel **(A)** shows the activity during the last conditioning trial of the CS1-US1 association, while panel **(B)** shows what happens during reward omission after learning (CS1 alone). The first row shows the inputs to the network, with the blue line showing the mean activity in the IT cluster corresponding to CS1, while the black line shows the mean activity for the neurons of LH representing US1. The second row shows the timecourse of the VTA cell during these trials, similar to what is shown on Figure 5.5. The third row shows activity in CE, which matches the already observed timecourse in BLA during conditioning on Figure 5.4. The fourth row depicts the timecourse of activity in PPTN, with the blue line showing the unit responding to CS onset (with inputs from CE) and the black the one responsive to the US (with inputs from LH). The fourth, fifth, sixth, seventh and eighth rows depict the maximal activity in NAcc, VP, LHb and RMTg, respectively. Please refer to the text for how these activations relate to each other.

a phasic burst at CS onset on both trials, but barely reacts after learning when the reward is delivered, while it is strongly inhibited when the reward is omitted. The CS-driven burst is due to associative learning in the amygdala, what is reflected in the activity of the CE unit (third row). The transient activation of CE excites the CS-selective population in PPTN (fourth row, in blue), which in turn generates the phasic VTA burst and excites VP (sixth row). The excitation of VP increases the inhibition on LHb (seventh row) and RMTg (eighth row), which therefore remain silent.

When the reward is delivered (Figure 5.10 A), LH activates directly the US-selective population of PPTN (fourth row, in black), but also the amygdala (reflected in the excitation of CE). However, the strong competition between the CS- and US-related populations of PPTN results in the phasic activation of the US group only (as it receives LH inputs slightly before the CS group gets activated by CE, which is a disynaptic pathway and therefore slower). The US group of PPTN activates VTA and VP similarly. At the same time, NAcc gets activated by the reward delivery, through its inputs from BLA and vmPFC, in conjunction with the phasic VTA burst bringing the cell into the up-state. NAcc is then able to cancel the VTA burst through its direct modulatory projection. NAcc also inhibits strongly VP, but this inhibition is canceled by the excitatory projection from PPTN to VP. VP therefore keeps inhibiting LHb and RMTg, and no VTA dip is observed.

When the reward is omitted (Figure 5.10 B), PPTN does not receive inputs from LH or CE. The activation of NAcc at the expected time of reward delivery is now able to inhibit strongly VP, what releases LHb and RMTg from its strong tonic inhibition. LHb becomes transiently activated, exciting RMTg which can provoke a complete pause in VTA firing.

Although not directly comparable to recorded firing rates, the displayed time courses are in agreement with several observations, such as the activation of two different populations of PPTN neurons for reward-predictive cues and rewards (Pan et al., 2005), the activation at reward omission of LHb (Hikosaka et al., 2008; Hong et al., 2011) and RMTg (Jhou et al., 2009), or the activation of VP for large reward-predicting cues and rewards (Smith et al., 2009; Tindell et al., 2004). VP is also inhibited at reward omission, what is consistent with the observed inhibition of some VP cells when small rewards is received during a session where larger rewards are available (Tachibana and Hikosaka, 2012).

5.4 Discussion

We have proposed a neuro-computational model of the afferent system to the dopaminergic area VTA, which is able to reproduce several observations on VTA's behavior during appetitive conditioning: progressive appearance of phasic bursts of activity at CS onset, progressive diminution of the amplitude of the phasic bursts elicited by primary rewards, strong phasic inhibition at the time when reward is expected but not delivered (Fiorillo et al., 2003; Pan and Hyland, 2005; Schultz et al., 1997). Cancellation of US-related bursts and inhibition at reward omission

5 *Timing and expectation of reward*

both rely on learning of the duration of the CS-US interval in the NAcc, which influences VTA either directly or through the output structures of the ventral BG. This is in accordance with experiments showing that rewards delivered earlier than expected provoke a very high amplitude VTA burst which would have been canceled if delivered at the learned time (Hollerman and Schultz, 1998). Furthermore, the model reproduces the dependency on reward magnitude of the activities in BLA (Bermudez and Schultz, 2010) and VTA (Tobler et al., 2005).

There are several aspects of reward processing and dopaminergic activity which are not covered by this model: the model is limited in its current form to classical conditioning and does not specifically address instrumental conditioning or goal-directed learning. However, Pavlovian-to-Instrumental transfer of learning, which is known to be particularly dependent on NAcc, is thought to be a critical component of goal-directed learning (Cardinal et al., 2002; Corbit and Balleine, 2011) and the proposed model is a first step towards understanding these processes. Consequently, the model does not incorporate yet the known effects of the tonic component of VTA activity, which is thought to modulate motivation and engage reward-directed behaviors (Daw et al., 2006; Niv et al., 2007), and focuses only on the phasic components of VTA activity.

Three dimensions are particularly relevant in reward processing: reward magnitude, reward probability and time, with NAcc having been shown crucial in the adequate response to each of these dimensions (Stopper and Floresco, 2011). The proposed model focuses on reward-magnitude and time, leaving reward probability to further work. Manipulating reward probability will require to investigate the effect of VTA dips on learning in BLA and NAcc, with the extreme end of the spectrum being extinction of conditioning (Tye et al., 2010).

Within these validity boundaries, the model is able to make several testable predictions, among which the fact that VTA dips should only appear for sufficiently big rewards, or that the number of trials needed to observe US-related burst cancellation should be proportional to reward magnitude. It also predicts that at least a subpopulation of NAcc (presumably in the shell part) should be activated by reward omission. This prediction will be further discussed in the rest of the section.

From the neuro-computational point of view, the model is fully autonomous: it only learns from the relative timecourse of CS and US inputs. Apart from the distinction between the sensitization and conditioning phases, no additional mechanism such as a central executive is required to control learning in any of its populations. It relies only on the numerical integration of a set of interdependent dynamical equations, in conjunction with sensory inputs. Moreover, the neural mechanisms employed provide scalability, as multiple CS-US associations can be learned in parallel, depending on the number of neurons in BLA and NAcc. Future work will address its integration on a neurorobotical platform with realistic inputs.

5.4.1 Relation to other work

Early implementations of the TD algorithm used a unitary backward chaining mechanism using serial-compound temporal representations of the CS, where the value of the reward is progressively transferred to the previous time step (or state), until it corresponds to CS onset (Montague et al., 1996; Schultz et al., 1997; Suri and Schultz, 1999). For each time step of the conditioning sequence, DA represents a reward prediction error, i.e. the discrepancy between the amount of predicted reward and the actually received reward. Unless very long eligibility traces are used, TD predicts that DA bursts will gradually shift backwards in time from reward delivery to CS onset, what is not observed experimentally (Pan and Hyland, 2005). This also implies that the mechanism should work for any higher-order conditioning task, transferring the phasic burst to the earliest predictor of reward. In practice, only second-order conditioning has been observed, as noted in (Hazy et al., 2010). It however explains phenomenologically many aspects of DA activity during conditioning and has been used with great success in action-selection and decision-making frameworks as long as the action space is not too large, but its mapping on brain structures is problematic.

Ludvig et al. (2008) introduced an alternative temporal representation of the stimuli for the TD(λ) algorithm. A set of overlapping temporal basis functions is used to filter out an exponentially decreasing trace of the stimuli (both CS and US) and provide a coarse coding of the time elapsed since stimulus onset. The output of this microstimuli representation gradually becomes weaker and coarser as time goes. Using these representations as inputs, the TD(λ) algorithm is able to learn a reward-prediction error signal, gradually responding positively to the CS while cancelling its response to the US. If the US is omitted, it exhibits a negative reward-prediction error, although much weaker than previous versions of TD. If the reward is delivered earlier than expected, it responds maximally to it but shows only a very small dip at the expected time, without the need for an explicit reset of the temporal representations (see below for a discussion). A later extension of this model (Ludvig et al., 2009) incorporated an additional array of microstimuli signaling the presence of a stimulus in addition to its trace and was able to better explain the functional difference between delay and trace conditioning, as well as to make interesting predictions about the role of the hippocampus in trace conditioning.

The model of Rivest et al. (2010; Rivest et al., 2013) used an interesting approach to provide a temporal representation of the stimuli to the TD(λ) algorithm: a LSTM network (Hochreiter and Schmidhuber, 1997) is used to learn a temporal representation of both CS and US based only on stimulus onset and the reward-prediction error signal. A LSTM network is composed of recurrent memory blocks, each integrating its inputs depending on an adaptive gating function. This allows to learn to represent the CS by ramping functions peaking just before US delivery, allowing the TD(λ) to access an adaptively timed representation of the stimulus. This model exhibits all the expected temporal properties of the DA signal in both delay and trace conditioning without any explicit representation of the task. Although needing an unrealistic number of trials to converge and having a significant error rate, this model builds an interesting bridge between reward-prediction, timing and working memory processes.

5 Timing and expectation of reward

The proposed model shares more assumptions with the dual-pathway models. The model of Brown et al. (1999), later extended by Tan and Bullock (2008), has been a very important step in overcoming the problems of TD, and many of its assumptions still hold true. It similarly considers that rewards provoke DA bursts (although in SNc rather than VTA, but this is more a labeling issue) through the LH → PPTN → SNc pathway. Reward-predicting cues progressively elicit burst firing through the NAcc → VP → PPTN → SNc pathway, while the striosomes of NAcc learn to generate lagged, adaptively timed signals inhibiting SNc at the time when reward is expected. The comparison between the predicted and received rewards occurs directly at the level of the dopaminergic cells, while it occurs in VP in our model, providing an explanation for the role of LHb and RMTg in reward omission. Moreover, this model hypothesizes a common NAcc → SNc pathway for both US-related burst cancellation and dips at reward omission, while they are functionally separated in our model. The major problem with the model of Brown et al. (1999) and Tan and Bullock (2008) in our view is the mechanism underlying the adaptively timed inhibitory learning in the striosomes of NAcc. The proposed intracellular spectral timing mechanism (Fiala et al., 1996; Grossberg and Schmajuk, 1989), relying on mGLUR1-mediated delayed Ca^{2+} spikes with distinct time constants for each striosomal cell, indeed allows to learn specific duration in conjunction with DA bursts, but the maximal interval learnable by this mechanism is equal to the longest delayed spike possible, what is likely to lie in the sub-second range as in the cerebellum (Fiala et al., 1996). For the supra-second range, network-based oscillatory mechanisms such as the striatal-beat frequency model are more likely to be sufficiently efficient and robust to learn such delays (Coull et al., 2011).

The model called PVLV (Primary-Value and Learned-Value) initially proposed by O'Reilly et al. (2007) and refined in Hazy et al. (2010) builds up on these ideas. The primary value (PV, the value of the reward itself) and the learned value (LV, the value of the reward-predicting cue) during conditioning are computed by two different afferent systems to VTA, both with an excitatory and an inhibitory component. The excitatory PV system PVe signals reward delivery to VTA through a direct connection from LH to VTA, although a relay through PPTN would perform the same function as in our model. The excitatory LV system LVe learns to generate DA bursts at CS onset, through a direct projection from CE to VTA: as in our model, the amygdala learns to associate a sustained representation of the CS to the delivery of reward when the US-related burst (or dip) occurs. The inhibitory PV system PVi, composed of the striosomal neurons in NAcc, learns to cancel progressively US-related bursts, but in an almost time-independent manner: they use a ramping function activated by CS onset and peaking at reward delivery that modulates the reward prediction. The origin of such a signal is putatively in the cerebellum, but no details are provided on how such a signal could be adapted to different CS-US durations. Moreover, this implies that rewards given earlier than expected would still provoke attenuated DA bursts. Last, the inhibitory LV system LVi, also in the striosomes of NAcc, slowly learns to cancel CS-related bursts in order to avoid over-learning in auto-shaping experiments (where the CS becomes an incentive to action, what is not covered by our model). The main issue with this model is that timing mechanisms are only phenomenologically incorporated, what may be due to the fact that the equations governing neuronal activation and learning are discretized with

a time step of 1 second, instead of 1 millisecond in the model of Brown et al. (1999) or ours. However, this model explains several aspects of conditioning, including acquisition, extinction, blocking, overshadowing, conditioned inhibition and second-order conditioning. Furthermore, it has been successfully integrated into a wider functional model of working memory including the prefrontal cortex and the dorsal BG (O'Reilly and Frank, 2006).

Together with an extensive review of the functional and electrophysiological properties of the ventral basal ganglia, Humphries and Prescott (2010) propose a neuro-computational model of how a specific subcircuit of the ventral BG, involving the shell part of NAcc (which integrates cortical, amygdalar and hippocampal inputs) and some part of VP, can selectively produce either bursts or dips in VTA, depending on the relative balance between the direct pathway (arising from NAcc cells carrying D1 receptors and projecting directly on VTA) and the indirect pathway (with NAcc neurons carrying both D1 and D2 receptors and projecting mainly on VP). In this framework, the prediction of a reward activates the direct pathway, what can either reduce the bursting amplitude or produce a dip in VTA, while the actual receipt of that reward activates the indirect pathway, canceling the influence of the direct pathway and allowing VTA bursts. While being more precise than our model on the functional role of NAcc cell subtypes, this model is limited to bursts or dips occurring at reward delivery (or at the time when reward is expected), but does not address the case of reward-predicting stimuli nor the issue of timing. This model has nevertheless the advantage of being understood equally well in the reward-prediction error framework of DA activity and in the action-outcome repertoire framework, which proposes that DA bursts primarily help associating an action with its delayed consequences (Redgrave et al., 2008).

Chorley and Seth (2011) proposed a dual-pathway model incorporating some concepts of the striatal-beat frequency model. It is composed of several populations of spiking point-neurons, subject to synaptic plasticity using a dopamine-modulated spike-timing dependent plasticity (STDP) learning rule (Izhikevich, 2007). In this model, the sensory representation of the US initially activates the DA population through an excitatory relay (either the subthalamic nucleus (STN) or the superior colliculus). The corresponding DA burst enables STDP learning between the sustained sensory representation of the CS and STN, what leads to a progressive bursting behavior in VTA at CS onset. In parallel, the inhibitory pathway to VTA, involving the prefrontal cortex and the striatum, learns to progressively cancel the US-related burst and, if reward is omitted, to strongly inhibit the VTA population. The mechanism for learning the CS-US interval is similar to the striatal-beat frequency hypothesis: CS onset activates a pre-recorded sequence of spikes in the prefrontal cortex (identical in each trial) and the striatum learns to react phasically to the precise pattern corresponding to the elapsed duration at US onset. This pre-recorded sequence of spikes is functionally equivalent to a set of neural oscillators synchronized at CS onset and expressing reproducible patterns at the population level. Oprisan and Buhusi (2011) investigated a similar mechanism using Morris-Lecar neurons and showed that even noisy oscillators, with variable inter-spike intervals, are able to produce a population code for the elapsed duration since CS onset which can be detected by striatal coincidence detectors. The model of Chorley and Seth (2011) is an elegant mechanism describing the evolution

of DA bursts during conditioning as well as for earlier delivery of reward or reward omission. It does not however map very precisely on the brain's architecture, nor take the effect of reward magnitude into account.

5.4.2 Biological plausibility

The structure of the proposed model is derived from known anatomical connections, and the used neural mechanisms are consistent with experimental data, either at the cellular or population level. It provides a minimal description of the network involved in controlling VTA activity during classical conditioning, with respect to a limited set of observations. However, there exists a certain number of other brain areas which are directly or indirectly involved in this process. Similarly, alternative mechanisms, especially for timing, might replace or complement the proposed ones. The purpose of this section is to discuss alternatives to the current assumptions.

One key assumption in the model is that there exists a subgroup of NAcc neurons, presumably in the striosomes (group of striatal neurons that project directly on SNc or VTA), which get activated at reward omission. The previously reviewed dual-pathway models also share this assumption, and justify it by observations that some cells in the ventral striatum display a ramping activity pattern, with firing rates almost linearly increasing from CS onset and peaking at the time when reward is expected (Deadwyler et al., 2004; Schultz et al., 1992). This indicates that the CS-US interval duration is indeed learned by NAcc cells, but raises the question of how such a ramping signal can be transformed into a phasic inhibition after reward is expected: direct inhibition of VTA by such ramping cells in NAcc should progressively reduce VTA firing as the time since CS onset increases, which is obviously not the case. Is there a still undiscovered group of NAcc cells firing only at reward delivery/omission, or do these ramping activities play a more complex role in the timing of CS-US intervals during conditioning? In the striatum, some cholinergic TAN interneurons show complex patterns (either excitation or inhibition) at reward omission (Apicella et al., 2009). As these cholinergic interneurons can disinhibit MSNs through the modulation of fast-spiking inhibitory interneurons and bring them in the up-state (Coull et al., 2011), it may provide a mechanism for the phasic activation of a subgroup of NAcc cells at reward omission. A more detailed model of the internal circuitry of NAcc is obviously needed.

Alternatively, ramping activities in the NAcc during the CS-US interval might complement or even replace such mechanisms. Such ramping activities have been also observed in the thalamus (Komura et al., 2001) and prefrontal cortex (Reutimann et al., 2004), with the slope of the ramp being proportional to the duration. This suggests that a cortex - ventral basal ganglia - thalamus loop might be a good candidate to actually learn the CS-US interval duration with climbing activities, modulated by the dopamine level. Based on this idea, many models have been proposed for interval timing using neural integration or drift-diffusion models (Durstewitz, 2004; Luzardo et al., 2013; Simen et al., 2011). The model of (Rivest et al., 2010; Rivest et al.,

2013) is a good example of such a mechanism. However, how the maximal activity reached by such ramps is transformed into a precisely-timed phasic signal at reward omission still raises difficult technical questions, such as the effect of noise on the precision of neural integration, especially for long intervals, or the plausibility of the learning mechanisms.

In comparison to the other dual-pathway models, our model is to our knowledge the first to explicitly incorporate distinct origins for the cancellation of US-related bursts and for the dips at reward omission, although the idea was already proposed in (Hazy et al., 2010) as a functional interpretation of the inhibitory component of the PV system PV_i. As the authors noted, cancellation of a US-related burst must derive from an inhibitory signal occurring slightly in advance from the receipt of reward in order to be efficient, while the dips associated with omitted rewards occur clearly after the expected time, and the duration of these dips extends significantly longer than the corresponding bursts. They state that the first component is likely to be implemented by the direct inhibitory projection of NAcc on VTA, while the second results from a disinhibition of LHb by NAcc through a relay on VP, but the learning site of the CS-US duration is NAcc in both cases. This interpretation is consistent with our model. The question that arises is whether distinct subpopulations of NAcc participate in these two mechanisms: do the striosomes directly projecting to VTA exhibit ramping activity, thus being able to cancel US-related bursts in advance, while the matrix neurons, projecting to VP and therefore to the LHb/RMTg complex, exhibit a more phasic behavior and get activated only at reward delivery or omission, as predicted by the striatal-beat frequency model?

As observed experimentally (Fiorillo et al., 2008), the cancellation of the US-related bursts becomes weaker when the CS-US interval increases. We are not aware of any study reporting a similar effect of the interval duration on dips at reward omission. If not, this may support the idea that two different mechanisms govern the two types of inhibition: neural integration becomes less precise when the duration increases, as it becomes more difficult to detect when the maximum of the slope is attained, while coincidence detectors are more robust, provided that the oscillators are not too noisy (Matell and Meck, 2004; Oprisan and Buhusi, 2011).

An open issue with the coincidence detectors hypothesis is that corticostriatal learning is potentiated by DA bursts at reward delivery. Typical bursts in VTA are relatively long (150 to 200 ms), what implies that cortical oscillators with a frequency superior to 5 or 6 Hz can show a full period during the burst. In the model, the parameter $\tau_{\text{dopa}} = 10$ ms representing the time constant of the phasic effect of DA on corticostriatal learning (Equation 5.11) was artificially set to a very fast value to ensure that learning occurs at the very beginning of the burst. Slower values led to the situation where NAcc could only predict the occurrence of reward delivery at the end of the burst, what arrives too late to effectively cancel the burst. In the model of (Chorley and Seth, 2011), bursting behavior occurs in a time window of 50 ms, which, coupled to the precise timing properties of STDP when compared to Hebbian learning rules, allows a very sharp learning of the time elapsed since CS onset. How can very high oscillation frequencies (the original Striatal-Beat Frequency model uses oscillators in the delta range 8 to 13 Hz) accommodate with such large DA bursts is still an unresolved question.

5 Timing and expectation of reward

In Section 5.3.2, the earlier delivery of a reward lead to a VTA burst of the same amplitude as an expected reward, but not to a dip at the expected time, as observed experimentally (Hollerman and Schultz, 1998). This is only because the CS representation stops when the US disappears. If the CS were maintained for a longer duration, such a dip would in fact be observed as the oscillators in vmPFC would still signal the elapsed duration. There is a need for a reset mechanism stopping the oscillators at reward delivery. A possible pathway would involve a closed-loop between vmPFC and the ventral BG, with the inhibitory projection from VP on the mediodorsal nucleus of the thalamus (MD) being able to stop thalamo-cortical oscillations between MD and vmPFC at reward delivery. The problem of resetting temporal representations after reward delivery is common to many models (see Daw et al. (2006) for a review), at the notable exception of the model of Ludvig et al. (2008).

Although successfully reproducing the known effects of reward magnitude on DA activity, the proposed model does not investigate the case where less reward than expected, instead of no reward at all. Experimentally, VP gets activated by large rewards and inhibited by small ones (Tachibana and Hikosaka, 2012), while LHb shows the opposite pattern (Hikosaka et al., 2008). Based on the current model, we propose that the comparison between predicted and received reward may be computed in VP through the competition between inhibitory inputs from NAcc and excitatory inputs from PPTN and is further transmitted to VTA either directly or through disinhibition of LHb and RMTg. A further refinement of the model in these areas may also shed some light on the influence of aversive stimuli, which are able to activate the lateral habenula and produce DA dips (Matsumoto and Hikosaka, 2007) but also to generate bursts in some subpopulations of VTA (Brischoux et al., 2009; Lammel et al., 2012).

The subthalamic nucleus (STN) has been left out of the model, although it is part of the ventral BG. Like NAcc, its medial part receives cortical inputs from the medial prefrontal cortex, but it projects excitatorily on the part of VP receiving connections from the core of NAcc. It has been shown to encode both reward magnitude, reward expectation and errors (Darbaky et al., 2005; Lardeux et al., 2009) and is important for Pavlovian-to-Instrumental transfer of learning (Winstanley et al., 2005). STN may signal the motivational value of stimuli to VP, complementing the information received from PPTN. Future extension of this model to instrumental learning will have to investigate the role of STN more deeply.

Similarly, the cerebellum is a very important player in aversive conditioning, as in the eyeblink conditioning paradigm (Christian and Thompson, 2003; Thompson and Steinmetz, 2009). It has been left out of the model as its involvement in appetitive conditioning is still unknown. However, it is now acknowledged that the cerebellum and the basal ganglia communicate more with each other than initially thought: in particular, the cerebellum projects on thalamic nuclei which directly contact the striatum, especially the D2-type neurons of the indirect pathway (Bostan and Strick, 2010). How the BG and the cerebellum cooperate during conditioning still has to be explored.

The role of the ventral striatum in timing processes is also subject to debate. Several studies have shown that NAcc plays no important role in the timing of instrumental responding (Gal-

tress and Kirkpatrick, 2010; Meck, 2006), contrarily to the timing of Pavlovian responses (Singh et al., 2011). However, both processes are interrelated, as they both rely on dopaminergic activation, while NAcc is considered as a crucial site for Pavlovian-to-Instrumental transfer of learning (Corbit and Balleine, 2011). The Striatal-Beat Frequency model was initially proposed for the timing of instrumental responses, and identified the dorsal striatum as a potential substrate for the coincidence detection. Are two sites of temporal learning really needed for such interdependent processes? Kirkpatrick (2013) proposed a functional model of the interactions of timing and prediction error learning, where NAcc and BLA cooperate to compute the reward value, while the timing of the association itself is learned in the dorsal BG and transmitted to the DA system through its output GPi (internal segment of the globus pallidus). Indeed, the border regions of GPi, which is usually considered as composed of GABAergic neurons projecting to the thalamus, have been shown to send an excitatory projection on LHb, what can in turn produce DA dips (Hong and Hikosaka, 2008). These LHb-projecting neurons in GPi exhibit a negative reward-prediction error pattern, excited by reward omission and inhibited by large rewards, which is similar to the one in LHb but occurs slightly in advance. These border regions of GPi receive projections from both the dorsal and ventral striatum, so it is possible that both the dorsal and ventral parts of the BG cooperate to learn the temporal properties of both action-outcome and stimulus-reward associations.

The proposed model is also rather conservative regarding the role of the amygdala in timing: given that the amygdala is a key structure in acquiring, processing and storing Pavlovian associations and that timing is a fundamental component of conditioning, there should be some neural correlates of temporal processing in the amygdala. Several lines of evidence indeed suggests such an involvement, as reviewed in (Díaz-Mataix et al., 2013). In particular, a subgroup of neurons in BLA exhibits a strong change in firing rate at the time when the US is expected but not delivered (Belova et al., 2007), while some others show anticipatory activity for the reward, proportional to the instantaneous reward delivery probability (Bermudez and Schultz, 2010). This phenomenon might be particularly relevant for extinction, where the prolonged absence of the US should decrease the conditioning strength associated to the CS (Tye et al., 2010). The question is now from where does this timing information come from. Is it only signaled by the dopaminergic projection from VTA to BLA, which is able to modulate both firing and learning in BLA, or do other structures such as the hippocampus or vmPFC play a role?

In our model, the CS-related bursts in VTA arise from the BLA \rightarrow CE \rightarrow PPTN pathway, both during and after learning. However, CE has been shown to be important for learning but not expressing approach to appetitive cues (Groshek et al., 2005; McDannald et al., 2004). One possibility is that associations learned in the amygdala are progressively transferred to the orbitofrontal or ventromedial prefrontal cortices, which are known to project excitatorily onto VTA (Geisler et al., 2007). It is indeed known that frontal-amygdalar interactions are necessary for the formation and use of expectancies of reinforcers in the guidance of goal-directed behavior (Holland and Gallagher, 2004). It is therefore possible that the value associated to a reward is first associated to the sensory features of the predicting CS in the amygdala (what can initially generate CS-related bursts) but that the prefrontal cortex progressively learns to compute

5 *Timing and expectation of reward*

the motivational value of the CS and activate the dopaminergic system with this information. The known inhibitory projection from the medial prefrontal cortex to BLA might provide a direct mechanism to implement this transfer of responsibility (Carmichael and Price, 1995), while NAcc is at a central position to control their interplay (O'Donnell and Grace, 1995).

5.4.3 Conclusion

We have proposed a neuro-computational model linking reward processing to timing processes by focusing on the observed activity patterns of dopaminergic neurons during Pavlovian conditioning. We isolated a group of brain areas involved in the different aspects of appetitive conditioning and built a network using known anatomical connections. The resulting neural network model reproduces several experimental observations, while providing a robust mechanism for classical conditioning which can be implemented on a robotical platform. Its structure provides a first step toward building biologically realistic models of instrumental responding by understanding how the dopaminergic signal can be generated. Future extensions of this model, especially by focusing on the ventral BG and the crucial role of NAcc, will allow to learn the motivational value of different stimuli by transferring the value of an outcome to the action associated to the stimulus. They will ultimately allow to study the neural substrates of goal-directed behavior and their relationship with neuromodulators such as dopamine.

Disclosure/Conflict-of-Interest Statement

The authors declare that the research was conducted in the absence of any commercial or financial relationships that could be construed as a potential conflict of interest.

Acknowledgement

The authors are partially funded by the Deutsche Forschungsgemeinschaft (DFG) grant HA2630/4-2 and clinical research group DFG HA2630/7-1.

6 ANNarchy: a code generation approach to neural simulations on parallel hardware

Abstract

Many modern neural simulators focus on the simulation of networks of spiking neurons on parallel hardware. Another important framework in computational neuroscience, rate-coded neural networks, is mostly difficult or impossible to implement using these simulators. We present here the ANNarchy (Artificial Neural Networks architect) neural simulator, which allows to easily define and simulate rate-coded and spiking networks, as well as combinations of both. The interface in Python has been designed to be close to the PyNN interface, while the definition of neuron and synapse models can be specified using an equation-oriented mathematical description similar to the Brian neural simulator. This information is used to generate C++ code that will efficiently perform the simulation on the chosen parallel hardware (multi-core system or graphical processing unit). Several numerical methods are available to transform ordinary differential equations into an efficient C++ code. We compare the parallel performance of the simulator to existing solutions.

6.1 Introduction

The efficiency and flexibility of neural simulators becomes increasingly important as the size and complexity of the models studied in computational neuroscience grows. Most recent efforts focus on spiking neurons, either of the integrate-and-fire or Hodgkin-Huxley type (see Brette et al., 2007 for a review). The most well-known examples include Brian (Goodman and Brette, 2008; Stimberg et al., 2014), NEST (Gewaltig and Diesmann, 2007), NEURON (Hines and Carnevale, 1997), GENESIS (Bower and Beeman, 2007), Nengo (Bekolay et al., 2014) or Aurnyn (Zenke and Gerstner, 2014). These neural simulators focus on the parallel simulation of neural networks on shared memory systems (multi-core or multi-processor) or distributed systems (clusters) using either OpenMP (open multi-processing) or MPI (message parsing interface). Recent work address the use of general-purpose graphical processing cards (GPU) through the CUDA or OpenCL frameworks (see Brette and Goodman, 2012 for a review). The neural simulators GeNN¹, NCS (Thibeault et al., 2011), NeMo (Fidjeland et al., 2009) and CARLsim (Carlson et

¹The GeNN project, <http://sourceforge.net/projects/genn/>

al., 2014) provide in particular support for the simulation of spiking and compartmental models on single or multiple GPU architectures.

A common approach to most of these neural simulators is to provide an extensive library of neuron and synapse models which are optimized in a low-level language for a particular computer architecture. These models are combined to form the required network by using a high-level interface, such as a specific scripting language (as in NEST or NEURON) or an interpreted programming language (e.g. Python). As these interfaces are simulator-specific, the PyNN interface has been designed to provide a common Python interface to multiple neural simulators, allowing a better exchange of models between researchers (Davison et al., 2008). The main drawback of this approach is that a user is limited to the neuron and synapse models provided by the simulator: if one wants to even marginally modify the equations of a model, one has to write a plugin in a low-level language without breaking the performance of the simulator. This can be particularly tedious, especially for CUDA code on GPUs.

A notable exception is the Brian simulator, which allows the user to completely define the neuron and synapse models using a simple mathematical description of the corresponding equations. Brian uses a code generation approach to transform these descriptions into executable code (Goodman, 2010), allowing the user to implement any kind of neuron or synapse model. The first version of Brian executes the code in Python directly (although some code portions can be generated in a lower-level language) using vectorized computations (Brette and Goodman, 2011), making the simulation relatively slow and impossible to run in parallel on shared memory systems. The second version in development (Brian 2, Stimberg et al., 2014) proposes a complete code generation approach where the simulation can be implemented in different languages or parallel frameworks. This approach is promising as it combines flexibility in model design with efficient and parallel simulation performance.

Rate-coded networks, however, do not benefit much from the advances of spiking simulators. Rate-coded neurons do not communicate through discrete spike events but through instantaneous firing rates (real values computed at each step of the simulation). Rate-coded simulators are either restricted to classical neural networks (static neurons learning with the backpropagation algorithm) or optimized for particular structures such as convolutional networks. To our knowledge, no rate-coded simulator provides a flexibility similar to what Brian proposes. The Emergent simulator (Aisa et al., 2008) provides some features - including parallel computing - and is used in a number of models in computational neuroscience (e.g. O'Reilly and Frank, 2006) but is restricted to a set of neuron and synapse models provided by the Leabra library. Topographica (Bednar, 2009) and CNS (Cortical Network Simulator, Mutch et al., 2010) primarily focus on convolutional networks. DANA (Distributed, Asynchronous, Numerical and Adaptive computing framework, Rougier and Fix, 2012) is a generic solver for distributed equations which can flexibly simulate dynamical rate-coded networks, but it does not address parallel computing yet.

Rate-coded networks are nevertheless an important paradigm in computational neuroscience, as they allow to model complex structures and dynamics with a smaller computational foot-

print than spiking networks. Each unit of a rate-coded network can model the dynamics of several biological neurons, so a rate-coded network typically requires less units to perform a function than a functionally equivalent spiking network. The rate-coded domain also benefits from a wide range of biologically realistic learning rules - such as the Bienenstock-Cooper-Munro (BCM) rule (Bienenstock et al., 1982) or the Oja learning rule (Oja, 1982). Synaptic plasticity in spiking networks, including spike-timing dependency plasticity (STDP), is an active research field and the current implementations can be hard to parameterize. Except in cases where synchronization mechanisms take place or where precise predictions at the single-cell level are required, rate-coded networks can provide a valid approximation of the brain's dynamics at the functional level, see for example models of reinforcement learning in the basal ganglia (Dranias et al., 2008; O'Reilly and Frank, 2006; Schroll et al., 2014), models of visual attention (Beuth and Hamker, 2015; Zirnsak et al., 2011) or models of gain normalization (Carandini and Heeger, 2012).

Another reason why rate-coded networks should not be neglected by neural simulators is that advances in computational neuroscience allow to aim at complete functional models of the brain which could be implemented in simulated agents or robots (e.g. Eliasmith et al., 2012). However, spiking networks may not yet be able to perform all the required functions, especially when in a learning context. Hybrid architectures, combining rate-coded and spiking parts, may prove very useful to achieve this goal. We consider there is a need for a parallel neural simulator which should: 1) be flexible for the definition of neuron and synapse models, 2) allow the definition of rate-coded, spiking and hybrid networks, 3) be computationally efficient on CPU- and GPU-based hardware and 4) be easy to interface with external programs or devices (such as robots).

This article presents the neural simulator ANNarchy (Artificial Neural Networks architect) which allows to simulate rate-coded, spiking as well as hybrid neural networks. It proposes a high-level interface in Python directly inspired from PyNN for the global structure and Brian for the definition of neuron and synapse models. It uses a C++ code generation approach to perform the simulation in order to avoid the costs of an interpreted language such as Python. Furthermore, rate-coded and spiking networks raise different problems for parallelization (Dinkelbach et al., 2012), so code generation ensures the required computations are adapted to the parallel framework. ANNarchy is released under the version 2 of the GNU Public License. Its source code and documentation² are freely available.

²<http://bitbucket.org/annarchy/annarchy> and <http://annarchy.readthedocs.org>

6.2 Interface of the simulator

6.2.1 Structure of a network

The interface of ANNarchy focuses on the definition of populations of neurons and their interconnection through projections. Populations are defined as homogeneous sets of identical neurons, while projections gather all synapses formed between the neurons of the pre-synaptic population and the ones of the post-synaptic population. Each projection is associated to a target name (e.g. 'exc' for excitatory synapses and 'inh' for inhibitory ones). This allows the post-synaptic neurons receiving these synapses to integrate them differently, for example to implement modulatory effects. The target can represent the excitatory/inhibitory nature, the corresponding neurotransmitter ('ampa', 'nmda', 'gaba') or even the functional role of a synapse ('feedforward', 'feedback').

```

from ANNarchy import *
# Create the populations of Izhikevich neurons
P = Population(geometry=1000, neuron=Izhikevich)
PE = P[:800] ; PI = P[800:]
re = np.random.random(800) ; ri = np.random.random(200)
PE.noise = 5.0 ; PI.noise = 2.0
PE.a = 0.02 ; PI.a = 0.02 + 0.08*ri
PE.b = 0.2 ; PI.b = 0.25 - 0.05*ri
PE.c = -65.0 + 15.0*re**2 ; PI.c = -65.0
PE.d = 8.0 - 6.0*re**2 ; PI.d = 2.0
P.v = -65.0 ; P.v_thresh = 30.0
P.u = P.v * P.b
# Create the projections
exc_proj = Projection(PE, P, 'exc')
exc_proj.connect_all_to_all(weights=Uniform(0.0, 0.5))
inh_proj = Projection(PI, P, 'inh')
inh_proj.connect_all_to_all(weights=Uniform(0.0, 1.0))
# Generate and compile the C++ code
compile()
# Simulate for 1 second
simulate(1000.0)

```

Figure 6.1: ANNarchy script reproducing the pulse-coupled spiking network described in Izhikevich (2003). A population of 1000 Izhikevich neurons is created and split into subsets of 800 excitatory and 200 inhibitory neurons. The different parameters of the Izhikevich neuron are then initialized through attributes of the two populations. a , b , c and d are dimensionless parameters, noise is a multiplicative factor on the random variable $\text{Normal}(0., 1.)$ drawn each step from the standard normal distribution $\mathcal{N}(0, 1)$, v_thresh is the spiking threshold of the neurons and τ is the time constant in milliseconds of the membrane conductances. The network is fully connected, with weight values initialized randomly using uniform distributions whose range depend on the pre-synaptic population. The source code for the network is then generated, compiled and simulated for 1000 milliseconds.

Figure 6.1 shows a simple example implementing the pulse-coupled spiking network proposed by Izhikevich (2003). It creates a population of 1000 Izhikevich neurons and splits it into two subsets of 800 excitatory and 200 inhibitory neurons each. These neurons are reciprocally con-

nected with each other (all-to-all connection pattern) through excitatory and inhibitory synapses. Such a pulse-coupled network exhibits oscillating pattern at various frequencies, depending on the strength of the connections. The example uses Izhikevich neurons, which are defined by Equation 6.1:

$$\begin{aligned}
 I(t) &= g_{\text{exc}}(t) - g_{\text{inh}}(t) + n \cdot \chi \\
 \frac{dv(t)}{dt} &= 0.04 \cdot v(t)^2 + 5 \cdot v(t) + 140 - u(t) + I(t) \\
 \frac{du(t)}{dt} &= a \cdot (b \cdot v(t) - u(t)) \\
 \text{if } v(t) > v_{\text{thresh}} &: v(t) = c \quad \text{and} \quad u(t) += d
 \end{aligned} \tag{6.1}$$

with $I(t)$ being the total input current to a neuron at time t , $g_{\text{exc}}(t)$ (resp. $g_{\text{inh}}(t)$) the total current injected by excitatory (resp. inhibitory) synapses, $v(t)$ the membrane potential and $u(t)$ a recovery variable. χ is an additive random variable following a standard normal distribution and n a multiplicative factor. When the membrane potential $v(t)$ exceeds a threshold v_{thresh} , a spike is emitted, the membrane potential is reset and the recovery variable is incremented. a , b , c and d are dimensionless parameters specifying the dynamics of the neuron type.

Populations are defined by three fields: 1) the geometry, which can represent either the total number of neurons (a single integer) or a multi-dimensional structure (tuple) similar to the shape of a Numpy array (Walt et al., 2011); 2) the type of neuron used in the population (either a pre-defined neuron model or one defined by the user, see Section 6.2.3 and Section 6.2.4) and 3) an optional unique name allowing to access the population globally. Defining a multi-dimensional geometry is primarily useful for visualization purposes and when defining distance-dependent connection patterns between two populations, but the internal data is arranged in one-dimensional arrays (see Section 6.3.1).

Once the populations are created, the value of each parameter and variable can be directly set using population attributes, by providing either a single value (which will be the same for all neurons) or lists/Numpy arrays of the same size/shape as the population. Like many other simulators, but unlike Brian, parameters and variables use implicit physical units: except for time which is expressed in milliseconds, the user must decide if the value of a variable represents volts or millivolts, for example. Brian uses explicit physical units, which allows to ensure consistency between the parameters. The neurons of a population can be accessed either individually or in subsets (similar to the PopulationViews of PyNN), allowing a finer control over the parameter values. Subsets use the slice notation of NumPy.

Projections are defined by four values: 1) the pre-synaptic population, 2) the post-synaptic population, 3) the associated target (e.g. "exc" or "inh") and 4) optionally the synapse type. Subsets of a population can also be used to create the projection. A connecting method has to be applied on the projection in order to create the synapses using a pre-defined scheme and

initialize the corresponding weights and delays. The network is here fully connected, using the `connect_all_to_all()` method. Several methods are provided by the simulator (all-to-all, one-to-one, distance-dependent, probabilistic...) but the user can also define its own connection patterns in Python, or load connection matrices from a file. Compatibility with the *Connection Set Algebra* proposed by Djurfeldt (2012) is currently under development.

Once the populations and projections are defined and initialized, the corresponding C++ code has to be generated and compiled by calling the `compile()` method. If the network structure has not changed since the last execution of the script, compilation is skipped. The C++ structures storing the parameters and variables of the populations and projections are then initialized with the values previously defined. The network can be then simulated for a certain duration in milliseconds. The values of all population/projection attributes can be read and modified at any point between two calls to `simulate()`, allowing an easy definition of complex experimental protocols.

This simple script outlines the high-level interface necessary to create a network: in its most simple form, all implementation details (including the neuron/synapse models) are hidden to the user. At this level, there is also no distinction between rate-coded and spiking networks. This distinction only appears when defining or using neuron and synapse models.

6.2.2 Equation-oriented description

Neuron and synapse models are described using an equation-oriented approach, where each equation is expressed by a simple textual description. The goal of the syntax is to provide a high flexibility to the user while being close to natural mathematical descriptions (Stimberg et al., 2014). Our equation-oriented syntax has been designed to be close to the Brian syntax (Goodman and Brette, 2008), although some differences had to be introduced to take into account the semantic difference between rate-coded and spiking neurons.

The syntax chosen for the equations ruling each variable allows to describe most common mathematical operations. Each variable has to be described by an equation, either regular or differential. For the moment, ANNarchy only supports first-order ordinary differential equations (ODE). For regular equations, the left side must hold only the name of the variable which will be updated (e.g. $a = b + c$). The available operators are assignment ($=$) and the different augmented assignments ($+=$, $-=$, $*=$, $/=$). For ODEs, the left term can be more complex ($\tau \cdot dv/dt + v = E$ is the same as $dv/dt = (E - v)/\tau$), but only the assignment operator is allowed. The right term can use single operations ($+$, $-$, $*$, $/$) or power functions (y^d) of other parameters or variables. Different mathematical functions are available (given they exist in the C math library), for example `cos`, `sin`, `exp`, `log`...

Conditional statements (if/then/else) can be useful for some rate-coded neurons, although they are classically avoided in spiking neurons. They follow a Python-like syntax using the `if` and

else keywords and `:` as a separator. The rectifier transfer function can for example be implemented like this:

```
r = if v > 0.0: v else: 0.0
```

with `r` being the output of a neuron and `v` its net activation. The condition can use any parameters or variable of the neuron or synapse. All relational operators are available (`<`, `>`, `<=`, `>=`, `==`, `!=...`), and they can be combined using the `and` and `or` logical operators. Conditional statements can be nested.

6.2.3 Rate-coded neurons and synapses

```
a) # Noisy leaky-integrator rate-coded neuron
LeakyNeuron = Neuron(
    parameters = """
        tau = 10.0 : population
        B = 0.0
    """,
    equations = """
        tau * dr/dt + r = B + sum(exc)
        + Uniform(-1.0, 1.0) : init=1.0, min=0.0
    """
)

b) # IBCM learning rule
IBCM = Synapse(
    parameters = """
        tau = 2000.0 : postsynaptic
    """,
    equations = """
        tau * dtheta/dt + theta = post.r^2 : postsynaptic
        dw/dt = post.r * (post.r - theta) * pre.r : min=0.0
    """
)
```

Figure 6.2: Examples of rate-coded neuron and synapse definitions. a) Noisy leaky-integrator rate-coded neuron. It defines a global parameter `tau` for the time constant and a local one `B` for the baseline firing rate. The evolution of the firing rate `r` over time is rules by an ODE integrating the weighted sum of excitatory inputs `sum(exc)` and the baseline. The random variable is defined by the `Uniform(-1.0, 1.0)` term, so that a value is taken from the uniform range $[-1, 1]$ at each time step and for each neuron. The initial value at $t = 0$ of `r` is set to 1.0 through the `init` flag and the minimal value of `r` is set to zero. b) Rate-coded synapse implementing the IBCM learning rule. It defines a global parameter `tau`, which is used to compute the sliding temporal mean of the square of the post-synaptic firing rate in the variable `theta`. This variable has the flag `postsynaptic`, as it needs to be computed only once per post-synaptic neuron. The connection weights `w` are then updated according to the IBCM rule and limited to positive values through the `min=0.0` flag.

Rate-coded neurons

The definition of a rate-coded neuron model is done by instantiating a Neuron object, with arguments specifying the parameters and variables of the neuron. Let us consider a simple noisy leaky-integrator rate-coded neuron:

$$\tau \cdot \frac{dr(t)}{dt} + r(t) = \sum_{i=1}^N w_i \cdot r_i(t) + B(t) + u(-1, 1) \quad (6.2)$$

where $r(t)$ is the instantaneous firing rate of the neuron at time t , τ its time constant, $B(t)$ its baseline firing rate (which can change over time), $u(-1, 1)$ a random variable taken at each time t in the uniform range $[-1, 1]$ in order to add noise and $\sum_{i=1}^N w_i \cdot r_i$ represents the weighted sum of excitatory inputs to a particular neuron. Figure 6.2 a shows a possible implementation of such a neuron in ANNarchy.

The first argument `parameters` is a string or multi-line string defining two parameters: `tau`, the time constant of the neuron, initialized to 10 milliseconds, and `B`, the baseline firing rate, initialized to 0. Parameter definitions can be placed on different lines or separated by semicolons. Once a population is created, these parameters are accessible and modifiable through population attributes. Various flags can be set after the `:` symbol. In this example, the flag `population` tells the code generator that the value of `tau` will be shared by all neurons of a population, so it only needs to store one value. It is also possible to specify the type of the parameter: parameters (and variables) are by default represented by double precision floating-point values. The `int` and `bool` flags change the type of the attribute to integer or boolean, if needed.

The second argument `equations` defines the variables of the neuron, whose value will evolve with time during the simulation. The number of variables defined in the model is unlimited, but at least one of them should be named `r`, as this is the default variable used by post-synaptic neurons to compute their weighted sum of inputs. The code corresponding to Equation 6.2 is straightforward. The temporal derivative of $r(t)$ is symbolized by the term dr/dt . The random variable $u(-1, 1)$ is generated by the term `Uniform(-1.0, 1.0)`, where -1.0 and 1.0 are the bounds of the uniform range. Different distributions can be used in an equation, including the normal, log-normal, exponential and gamma distributions. The weighted sum of excitatory inputs is represented by `sum(exc)`, which sums over all projections possibly reaching a particular neuron the product between the connection weight `w` and the firing rate of the pre-synaptic neuron `r`. The term `exc` corresponds to the target name defined when creating the projections. By default, this ODE will be solved using the explicit (forward) Euler method, but other methods are available, see Section 6.3.4. The flag `init` defines the initial value of the variable for all neurons and `min` defines a lower bound for the variable (if `r` is negative after an update, it will be set to 0), as the firing rate `r` is usually ensured positive in rate-coded networks. The `max` flag is also available.

Rate-coded synapses

When the pre-synaptic population of a projection is rate-coded, the synapses of the projection are assumed to be also rate-coded. A synapse is represented by a fixed connection weight (or synaptic efficiency) named w and a delay in synaptic transmission d (in milliseconds). Each synapse will participate in the weighted sum of inputs of the post-synaptic neuron with $w(t) * r(t - d)$, where $r(t - d)$ is the firing rate of the pre-synaptic neuron at time $t - d$. Synaptic delays in a network must be a multiple of the fixed integration step dt (see Section 6.3.4), but each synapse of a projection can define a different delay. The minimal delay is dt , as neurons can only access the value of variables computed at the previous time step (synchronous computation). Note that the Brian simulator can simulate rate-coded synapses, but only without delay.

In a learning context, connection weights evolve with time according to a variety of learning rules (Dayan and Abbott, 2001). Synapse models can be created to override the default behavior and implement synaptic plasticity or non-linear transmission. Figure 6.2 b shows a possible implementation of the IBCM learning rule (Intrator and Cooper form of the BCM rule) (Intrator and Cooper, 1992). It is a Hebb-like product of the pre-synaptic firing rate and a quadratic function of the post-synaptic firing rate. The quadratic function uses a dynamical threshold $\theta(t)$ which is defined as the expectation of the square of the post-synaptic firing rate:

$$\begin{aligned} \theta(t) &= E(y^2(t)) \\ \frac{dw(t)}{dt} &= y(t) \cdot (y(t) - \theta(t)) \cdot x(t) \end{aligned} \tag{6.3}$$

where $x(t)$ is the pre-synaptic firing rate, $y(t)$ the post-synaptic one, $w(t)$ the connection weight and $\theta(t)$ is defined as the moving average of $y^2(t)$ through the $E()$ expectation operator. In the code displayed on Figure 6.2 b, the moving average is calculated using a first-order ODE integrating the square of the post-synaptic firing rate, with a time constant τ of 2 seconds by default. Pre- and post-synaptic neural variables (usually the firing rate r , but any other variable can be used) can be accessed by prefixing the variable name by `pre.` and `post.`, respectively.

The update rule for the weight w is simply derived from Equation 6.3 using these conventions. `theta` is a post-synaptic variable, as it only depends on the post-synaptic neural activity. It would therefore be a waste of resources to compute it for each synapse: once per post-synaptic neuron is enough. The equation for `theta` (as well as the corresponding parameter `tau`) is associated with the flag `postsynaptic`, which has a similar meaning as `population` for a neuron: the global variable will be updated only once per post-synaptic neuron. The variable w is local to a synapse, so the flag should not be set. Instead, `min=0.` is used to ensure that the weight will not become negative over time.

In a rate-coded neuron model, the term `sum(exc)` represents by default the weighted sum of excitatory inputs to this neuron. It is possible to change this behavior in the synapse definition by adding a `psp` argument to the synapse definition, whose default value is `"w * pre.r"`. Non-linear synapses, where for example $w_i \cdot \log(r_i)$ should be summed over all synapses instead of $w_i \cdot r_i$, can be implemented by setting `psp = "w * log(pre.r)"`. The summation operation can also be changed, by defining the operator argument, whose default value is `"sum"`. If `"max"`, `"min"` or `"mean"` is used, the maximal (resp. minimal or mean) value of `psp` is calculated over all synapses associated to the target `exc` will be returned by `sum(exc)`. This is particularly useful for pooling operations, which are used for example in hierarchical visual processing (Hamker, 2004b; Riesenhuber and Poggio, 1999).

6.2.4 Spiking neurons and synapses

Spiking neurons

Integrate-and-fire neurons (IF) describe the temporal evolution of the membrane potential $v(t)$ through a system of first-order ODEs. When the membrane potential exceeds a given threshold, a spike is emitted and the value of the different neural variables is clamped to a reset value for a certain duration called the refractory period. The condition for spike emission as well as the reset and refractory behaviors have to be explicitly defined in addition to the internal dynamics. More complex spiking neurons such as the Hodgkin-Huxley neuron model have their own dynamics for the reset and refractory mechanisms. Figure 6.3 a shows a possible implementation of the Izhikevich neuron described by Equation 6.1.

As for rate-coded neurons, the argument `parameters` describes the different parameters of the neuron model: `a`, `b`, `c` and `d` are dimension-less parameters, `v_thresh` is the spiking threshold, `noise` is a multiplying factor on the noise random variable and `tau` is the time constant in milliseconds of the conductances. The argument `equations` describes the evolution of the three variables `I`, `v` and `u` of Equation 6.1. `Normal(0., 1.)` is a random variable taken from the standard normal distribution. `g_exc` and `g_inh` represent the total excitatory and inhibitory currents or conductances generated by incoming pre-synaptic spikes. They are the equivalent for spiking neurons of `sum(exc)` and `sum(inh)` for rate-coded neurons. The syntax `g_target` is different from the rate-coded case because they have a different behavior: while `sum(target)` is computed at every time step of the simulation by summing pre-synaptic activity, `g_target` is event-driven. Every time a pre-synaptic spike arrives to a neuron, the corresponding conductance is increased from a value corresponding to the weight (or efficiency) `w` of the synapse. If no spike arrives, the conductance evolves with its own dynamics, independently from inputs.

The default behavior for conductances is governed by instantaneous synapses: once all the incoming spikes have been summed, the total conductance is reset to 0 for the next time step. More realistic models use exponentially decreasing or alpha (double exponential) functions to model the dynamics of the conductance. The example of Figure 6.3 a uses exponentially

6.2 Interface of the simulator

```

a) # Izhikevich spiking neuron
Izhikevich = Neuron(
  parameters = """
    a = 0.2 ; b = 0.2
    c = -65.0 ; d = 2.0
    v_thresh = 30.0
    noise = 0.0
    tau = 5.0
  """,
  equations = """
    I = g_exc - g_inh + noise * Normal(0.0, 1.0)
    dv/dt = 0.04*v^2 + 5*v + 140 - u + I : init=-65.0
    du/dt = a * (b*v - u) : init=-14.0
    tau * dg_exc/dt = - g_exc
    tau * dg_inh/dt = - g_inh
  """,
  spike = "v > v_thresh",
  reset = "v = c ; u += d",
  refractory = 2.0
)

b) # Short-term plasticity synapse
STP = Synapse(
  parameters = """
    tau_rec = 100.0
    tau_facil = 0.01
    U = 0.5
  """,
  equations = """
    dx/dt = (1 - x)/tau_rec : init = 1.0, event-driven
    du/dt = (U - u)/tau_facil : init = 0.5, event-driven
  """,
  pre_spike="""
    g_target += w * u * x
    x *= (1 - u)
    u += U * (1 - u)
  """,
)

c) # STDP learning rule
STDP = Synapse(
  parameters="""
    tau_plus = 20.0 : postsynaptic
    tau_minus = 20.0 : postsynaptic
    A_plus = 0.01 : postsynaptic
    A_minus = 0.01 : postsynaptic
    w_max = 1.0 : postsynaptic
  """,
  equations = """
    tau_plus * dApre/dt = -Apre : event-driven
    tau_minus * dApost/dt = -Apost : event-driven
  """,
  pre_spike="""
    g_target += w
    Apre += A_plus * w_max
    w = clip(w - Apost, 0.0 , w_max)
  """,
  post_spike="""
    Apost += A_minus * w_max
    w = clip(w + Apre, 0.0 , w_max)
  """,
)

d) # NMDA non-linear synapse
NMDA = Synapse(
  parameters = """
    tau = 10.0 : postsynaptic
  """,
  equations = """
    tau * dx/dt = -x
    tau * dg/dt = -g + x * (1 - g)
  """,
  pre_spike = "x += w",
  psp = "g"
)

```

Figure 6.3: Examples of spiking neuron and synapse definitions. a) Izhikevich neuron. The parameters and equations fields follow the same principles as for rate-coded neurons. The variable I gathers the inputs to the neuron, namely the sum of the excitatory g_exc and inhibitory g_inh input currents and a constant current i_offset . The membrane potential v and the recovery variable u are updated according to the desired dynamics, with initial values specified with the `init` keyword. The spike field defines the condition for emitting a spike, here when the membrane potential v exceeds the threshold v_thresh . The reset field specifies the modifications happening after a spike is emitted. Here the membrane potential is clamped to the value c and the recovery variable u is incremented by d . The refractory period is determined by the refractory field, here 2 milliseconds. b) Short-term plasticity (STP) synapse. For this synapse, the increment of the post-synaptic conductance g_target when a pre-synaptic spike arrives depends not only on the synaptic efficiency w , but also on the value of variables internal to the synapse x and u . These are updated through two mechanisms: the equations field specifies their exponentially-decreasing dynamics, while the `pre_spike` defines their increments when a pre-synaptic spike arrives at the synapse. However, the integration of the corresponding ODEs is event-driven through the use of the `event-driven` flag: when a pre- or post-synaptic spikes occurs, the new value of these variables is directly computed using the analytical solution of the ODE. This can speed up the simulation if the number of spiking events is low. c) Spike-timing dependent plasticity (STDP) synapse. For this synapse, the post-synaptic conductance is increased by w after a pre-synaptic spike is received, but the synaptic efficiency is adapted depending on two internal variables $Apre$ and $Apost$. The `pre_spike` field states what should happen when a pre-synaptic spike arrives at the synapse, while the `post_spike` field describes the changes occurring when the post-synaptic neuron fires. The variables $Apre$ and $Apost$ are integrated in an event-driven manner. The `clip()` function is used to maintain w in the range $[0, w_max]$. d) NMDA non-linear synapse. This synapse does not transmit information to the post-synaptic neuron in an event-driven manner. Rather, the synaptic variable g is summed at each time step by the post-synaptic neuron, as for rate-coded networks. This is specified by the `psp` field

decreasing synapses, by specifying a linear first-order ODE for the conductances g_{exc} and g_{inh} . If no spike arrives for a certain duration, the conductances will progressively decay back to 0, with a time constant defined by the parameter τ .

Two other arguments of the Neuron object have to be defined: `spike` defines the spiking condition, i.e. the condition that must be satisfied in order to emit a spike (typically when the membrane potential exceeds a given threshold); `reset` describes what should happen after a spike is emitted. The spiking condition has to be a boolean expression; it can depend on any parameter or variable, possibly combined through the logical operators `and` and `or`. The reset statement forces some neural variables to take predefined values after a spike is emitted: here the membrane potential is clamped to a reset value c and the recovery variable is incremented by d .

Spiking neurons can also define a refractory period, during which the ODEs are not evaluated (i.e. the membrane potential stays at its reset value), except for the conductances g_{exc} and g_{inh} . This corresponds to the hyper-polarized state of a neuron after spike emission, where no spike can be further emitted. The duration of this refractory period is set through the `refractory` argument, which takes here a constant value of 2 milliseconds, but the name of a parameter or variable can be given, allowing for dynamical refractory period: for example, the refractory period can be progressively increased if the firing rate becomes too high.

As shown in Stimberg et al. (2014), the five arguments `parameters`, `equations`, `spike`, `reset` and `refractory` are sufficient to describe the dynamics of most point-spiking neurons, including IF and Hodgkin-Huxley models, and are directly related to the Brian syntax (although `parameters` is implicit in Brian). They are not well suited to describe multi-compartment models, which are the main focus of simulators such as NEURON or GENESIS. However, Brian 2 introduces support for this kind of models.

Event-driven synaptic transmission

Synaptic behavior in spiking networks is also different from rate-coded networks, and requires additional description. The basic type of synapses is the linear synapse, where synaptic transmission is event-driven: when the pre-synaptic neuron emits a spike, it increases the corresponding post-synaptic conductance by a given value (generally the synaptic efficiency w). If no spike occurs, the synapse does not need to transmit any information: the dynamics of conductances are already defined at the post-synaptic neuron level. As in Brian, a spiking synapse can therefore define two additional arguments: `pre_spike` which specifies what should happen when a pre-synaptic spike arrives at the synapse (potentially after a given delay) and `post_spike` when the post-synaptic neuron emits a spike. The default linear synapse only defines `pre_spike` with the value $g_{target} += w$. g_{target} is a generic name for the conductance associated to the synapse. Depending on the target of the projection, g_{target} will be replaced by g_{exc} or g_{inh} , for example. The underlying idea is that the same synapse type can be used in different projections, regardless of their target.

Some event-driven synapse models modify the post-synaptic conductance with a value depending on specific synaptic variables. This is for example the case in short-term plasticity (STP) synapses (Markram et al., 1998), where the increment of the post-synaptic conductance depends on the history of the synapse. Frequent stimulation of a facilitating synapse leads to an increased influence on the post-synaptic neuron, while depressing synapses show the opposite effect. A possible model of STP synapses uses two internal variables $u(t)$ and $x(t)$, which evolve continuously according to linear ODEs:

$$\begin{aligned}\tau_{\text{rec}} \cdot \frac{dx(t)}{dt} &= 1 - x(t) \\ \tau_{\text{facil}} \cdot \frac{du(t)}{dt} &= U - u(t)\end{aligned}\tag{6.4}$$

When a pre-synaptic spike arrives at the synapse, the post-synaptic conductance should be incremented with $w(t) \cdot u(t) \cdot x(t)$, while the synaptic variables should be modified according to:

$$\begin{aligned}x(t) &\leftarrow x(t) \cdot (1 - u(t)) \\ u(t) &\leftarrow u(t) + U \cdot (1 - u(t))\end{aligned}\tag{6.5}$$

Figure 6.3 b shows an implementation of a synapse with short-term plasticity. The parameters are `tau_rec`, `tau_facil` and `U`, which define the dynamics of the synapse and whether it is facilitating or depressing. The two variables `u` and `x` directly relate to Equation 6.4. The `pre_spike` argument defines what should be modified when the pre-synaptic spike occurs: `g_target` should be incremented with `w*u*x` instead of `w` by default, and `u` and `x` are modified according to Equation 6.5.

The equations for `u` and `x` use the flag `event-driven`. As explained later in Section 6.3.4, this defines the numerical method used to integrate the ODE. Here both variables are defined by first-order linear ODEs, so their current value can be directly calculated whenever a pre- or post-synaptic spike occurs, based on the time elapsed since the last event (exponentially decreasing function of time). This can spare a lot of computations if the number of spikes in the network is not very high.

An event-driven synapse does not need to rely only on spike times for its dynamics. As for rate-coded synapses, it can access pre- and post-synaptic variables during updates: the pre- (resp. post-) synaptic membrane potential is accessed with `pre.v` (resp. `post.v`). Pre-synaptic variables are delayed if necessary. However, only the post-synaptic conductance `g_target` can be modified by a synapse, contrary to Brian 2.

Synaptic plasticity

Synaptic plasticity can also be described using event-driven mechanisms: the weight w of a synapse usually only needs to be updated when a pre- or post-synaptic spike occurs. Most biologically-realistic synaptic plasticity mechanisms in spiking networks indeed derive from the *spike timing dependent plasticity (STDP) rule* (Gerstner et al., 1996; Markram et al., 1997). Although many different implementations exist, there is an online version of STDP which is event-driven (Song et al., 2000). With this rule, each synapse integrates two variables $A_{\text{pre}}(t)$ and $A_{\text{post}}(t)$ which represent traces of the pre- and post-synaptic spikes, respectively. Between two spikes, they follow linear first-order ODEs:

$$\begin{aligned}\tau_+ \cdot \frac{dA_{\text{pre}}(t)}{dt} &= -A_{\text{pre}}(t) \\ \tau_- \cdot \frac{dA_{\text{post}}(t)}{dt} &= -A_{\text{post}}(t)\end{aligned}\tag{6.6}$$

When a pre-synaptic spike occurs, the pre-synaptic trace $A_{\text{pre}}(t)$ is incremented by a fixed value, and at the same time the post-synaptic trace $A_{\text{post}}(t)$ is subtracted from the synaptic efficiency $w(t)$, allowing long-term depression (LTD):

$$\begin{aligned}A_{\text{pre}}(t) &\leftarrow A_{\text{pre}}(t) + A_+ \cdot w_{\text{max}} \\ w(t) &\leftarrow w(t) - A_{\text{post}}(t)\end{aligned}\tag{6.7}$$

with w_{max} being the maximal value allowed for the weight. When a post-synaptic spike occurs, the post-synaptic trace is incremented, and the synaptic efficiency $w(t)$ is increased from the pre-synaptic trace, allowing long-term potentiation (LTP):

$$\begin{aligned}A_{\text{post}}(t) &\leftarrow A_{\text{post}}(t) + A_- \cdot w_{\text{max}} \\ w(t) &\leftarrow w(t) + A_{\text{pre}}(t)\end{aligned}\tag{6.8}$$

Figure 6.3 c shows a possible implementation of this STDP plasticity rule. The equations for A_{pre} and A_{post} can be integrated with an event-driven method, as their value is only required when a pre- or post-synaptic spike occurs. Synaptic transmission is linear, so `pre_spike` defines `g_target += w`. The increments in `pre_spike` and `post_spike` follow Equation 6.7 and Equation 6.8, while the weight w is clipped between 0 and w_{max} by using the `clip` function. An alternative implementation could have used the `min` and `max` flags instead of the `clip` function, as w is a variable of the synapse.

Continuous synaptic transmission

In some cases, synaptic transmission cannot be described in an event-driven framework. Synapses using the NMDA neurotransmitter are for example often modeled as non-linear synapses (Wang, 2002). These synapses require the post-synaptic conductance to be a sum of synapse-specific variables, as for rate-coded neurons, and not simply incremented when a pre-synaptic spike occurs. This is similar to the summed flag of Brian 2. NMDA synapses can be represented by two variables $x(t)$ and $g(t)$ following first-order ODEs:

$$\begin{aligned}\tau \cdot \frac{dx(t)}{dt} &= -x(t) \\ \tau \cdot \frac{dg(t)}{dt} &= -g(t) + x(t) \cdot (1 - g(t))\end{aligned}\tag{6.9}$$

When a pre-synaptic spike occurs, $x(t)$ is incremented by the weight $w(t)$. However, it does not directly influence the post-synaptic neuron, as the output of a synapse is the signal $g(t)$. The post-synaptic conductance is defined at each time t as the sum over all synapses of the same type of their variable $g(t)$:

$$g_{\text{exc}}(t) = \sum_{i=1}^{N_{\text{exc}}} g_i(t)$$

Figure 6.3 d shows a possible implementation of such a non-linear NMDA synapse. The main difference with the previous models is that it defines a psp argument which means that the post-synaptic conductance should be summed over this value (g in this case) at every time step. It is therefore not possible to use the event-driven scheme for such non-linear synapses. The psp argument can access any synaptic variable, as well as any pre- or post-synaptic variable. For example, it can be used for gap junctions (also called electrical synapses) which do not exchange spikes but directly a function of the pre- and post-synaptic membrane potentials.

6.2.5 Additional features

Standard neurons and synapses

Although the definition of neuron and synapse types is rather simple, the library provides a set of predefined models which can be used directly when creating populations and projections. Spiking neuron models are conveniently standardized, especially since the introduction of the PyNN interface (Davison et al., 2008). Using the PyNN nomenclature for the model names and parameters, ANNarchy provides the main neuron models common to most neural simulators: simple integrate-and-fire neuron, using either exponentially-decaying or alpha-shaped conductances or currents (IF_curr_exp, IF_cond_exp,

IF_curr_alpha, IF_cond_alpha), adaptive integrate-and-fire neurons (Izhikevich, EIF_cond_alpha_isfa_ista, EIF_cond_exp_isfa_ista) or Hodgkin-Huxley neurons (HH_cond_exp). Synapse models include short-term plasticity (STP) and spike-timing dependent plasticity (STDP). Each model is associated with a docstring describing completely the parameters and equations, allowing to easily create a new derivative model. Rate-coded neuron models are less standardized than spiking ones. The library only provides a generic leaky-integrator neuron similar to Equation 6.2. Rate-coded synapses include the Hebbian learning rule (Hebb), the Oja learning rule (Oja) and the IBCM learning rule described by Equation 6.3 (IBCM). The available rate-coded models will be extended in future versions.

Specific populations

Specific populations are available to provide functions which are difficult or unnecessarily complicated to implement with single neuron models. The `PoissonPopulation` class allows to directly create a population of spiking neurons whose spikes are generated from a Poisson distribution. The rate underlying the distribution can be a single value or one value per neuron (homogeneous Poisson process, as the rate for each neuron is constant), or a string expression defining the evolution of rate over time (e.g. `'1 + sin(2*pi*t)'`, heterogenous Poisson process). The `SpikeArray` class allows to create a population and to specify for each neuron the exact times at which they will emit a spike. These spiking times can be modified between two simulations using attributes.

The `ImagePopulation` class allows to represent images through the firing rates of a rate-coded population with the same geometry as the image (two-dimensional for grayscale, three for colored images, the last dimension representing the R, G and B components). Firing rates are normalized between 0 and 1. It relies on the Python Imaging Library (PIL), which allows the use of many file formats, including JPEG. Similarly, the `VideoPopulation` class allows to grab image streams from webcams and use them as firing rates of a population. It relies on the OpenCV 2.x C++ library to access the desired hardware. Grabbing images has to be explicitly called by the user between two simulations.

Hybrid networks

Apart from the neuron and synapse definitions, there is no difference in the interface between rate-coded and spiking networks: populations and projections behave the same regardless of the framework. It then becomes possible to create hybrid networks, composed of rate-coded and spiking populations interacting with each other. Interaction between the two types of neurons is achieved by introducing specific populations and projections to perform the conversion.

Converting a rate-coded population into a spiking one is straightforward: the output r of the rate-coded population is interpreted as an instantaneous firing rate in Hz and used to generate

spikes according to a Poisson distribution. The abovementioned `PoissonPopulation` object accepts a `target` argument, stating that the rate of each Poisson neuron is determined by its weighted sum of inputs:

```
pop1 = Population(1, Neuron(equations="r = 1 + sin(2*pi*t)"))
pop2 = PoissonPopulation(100, target='exc')
proj = Projection(pop1, pop2, 'exc')
proj.connect_all_to_all(1.0)
```

The connectivity matrix can have any form, but in the most simple case one single rate-coded neuron should determine the firing rate of a group of spiking neurons (one-to-many pattern). The weight of the connection determines the scaling: a weight of 1.0 means that a pre-synaptic rate of 1.0 will generate Poisson spike trains at 1 Hz. With a weight of 100.0, the train would be at 100 Hz. Other distributions than Poisson will be added in future versions.

Converting a spiking population into a rate-coded one is a much more difficult problem. Estimating neural firing rates from single spike trains instead of averaging over multiple trials is an open issue in neuroscience (Cunningham et al., 2009). The main methods include peri-stimulus time histograms (PSTH, Gerstein and Kiang (1960)), smoothing kernels (Nawrot et al., 1999), Kalman filters (Wu et al., 2004) or Bayesian estimation (Shimokawa and Shinomoto, 2009). All these methods are biased and can only infer firing frequencies in a particular bandwidth. Here, the problem is even more difficult as it has to be performed online during the simulation: in the interval between two spikes of the same neuron, it is not possible to predict the real instantaneous firing rate of the neuron, as future incoming spikes are still unknown.

ANNarchy provides a simple method to infer online the firing rate of a spiking population, using the assumption that a rate-coded neuron usually represents a large group of spiking neurons. The two populations are connected with a specific projection object `DecodingProjection` and a many-to-one pattern. For example, a single rate-coded neuron could decode the firing rate of a population of 1000 Poisson neurons:

```
pop1 = PoissonPopulation(1000, rates=100.0)
pop2 = Population(1, Neuron(equations="r=sum(exc)"))
proj = DecodingProjection(pop1, pop2, 'exc', window=10.0)
proj.connect_all_to_all(1.0)
```

The input `sum(target)` of a post-synaptic neuron at time t is a weighted sum of all spikes received during a sliding window of duration T (defined by the argument `window`), normalized by the total number of synapses to this neuron:

$$\text{sum(target)}(t) = \frac{\text{Weighted sum of spikes received in } [t - T, t]}{T * \text{Number of incoming synapses}}$$

It approximates the mean firing rate in the pre-synaptic population during the last T milliseconds. By default, T is equal to the simulation step dt , but the decoded rate may be fluctuating

if the number of pre-synaptic neurons is too small. One should either increase T or apply a low-pass filter to `sum(target)` in the post-synaptic neuron. The weights of the projection can be used to scale the output firing rate: by default, an input firing rate at 1 Hz leads to `sum(target)=1.0`.

Figure 6.4 illustrates the use of hybrid networks. A single rate-coded neuron is used to activate a population of 1000 Poisson neuron with a firing rate increasing every 250 ms (0, 10, 50 and 100 Hz). Figure 6.4 a shows a raster plot of the spikes emitted by the Poisson population. Figure 6.4 b shows the original (blue) and decoded (green) firing rate, for a single rate-coded neuron connected to all 1000 Poisson neurons. The projection uses a sliding window of 10 ms to smoothen the rate. The decoded firing rate follows the original one, but with a small variance due to the stochastic nature of the Poisson spike trains, and with a small temporal lag corresponding to the sliding window: when the firing rate suddenly increases, it takes approximately T milliseconds to completely reflect the change.

Figure 6.4 c shows the effect of the number of connected neurons on the precision of the decoding. For the three stimulations at 10, 50 and 100 Hz, we measure the mean of the normalized error between the decoded firing rate $r(t)$ and its target value $F \in [10, 50, 100]$: $\epsilon = \frac{1}{250} \int_{t=0}^{250} \frac{|r(t)-F|}{F} dt$ for post-synaptic neurons receiving 1 to 1000 inputs from the Poisson population. Unsurprisingly, the more inputs are used for decoding, the better is the precision. The sliding window method is also more precise at high frequencies, as more spikes can be used to estimate the firing rate. The remaining error for a high number of neurons is mostly due to the temporal lag of the integration. The script allowing to reproduce Figure 6.4 is given in the Supplementary Material.

Weight sharing and convolution operations

Regular projections instantiate a set of connection weights per post-synaptic neuron. This can be a waste of resources when the weights are identical for each neuron, the only difference being the coordinates of the corresponding neurons in the pre-synaptic population, as it is the case in convolutional networks (Lecun et al., 1998) or image filtering. Such convolution operations can be implemented by creating a `SharedProjection` instead of a `Projection` and calling the `convolve()` connector method:

```
proj = SharedProjection(pre=pop1, post=pop2, target='exc')
proj.convolve(weights=kernel)
```

The generated code depends on the respective geometry of the pre- and post-synaptic populations, as well as on the weights kernel. If they all have the same number of dimensions (for example two-dimensional), a regular convolution will be performed:

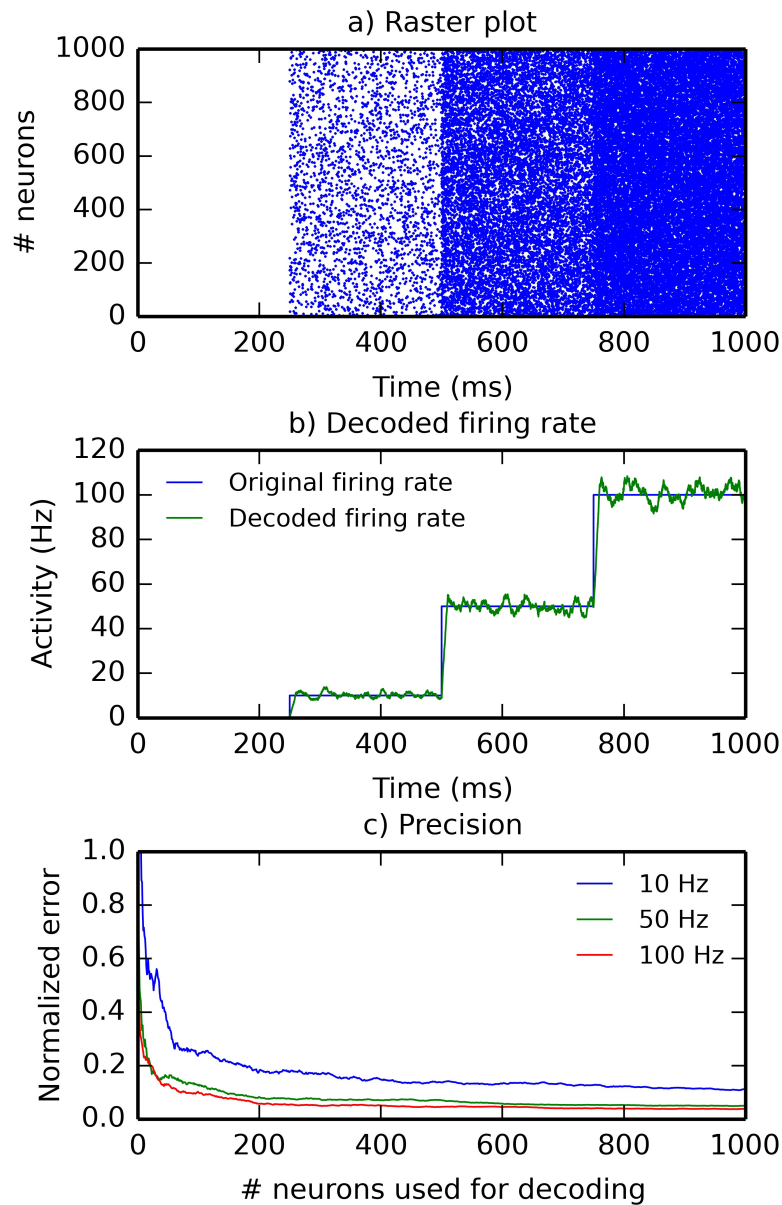


Figure 6.4: Example of an hybrid network encoding a rate-coded population into a spiking population (PoissonPopulation) and decoded back to the rate-coded domain (DecodingProjection). The script for this plot is provided in the Supplementary Material. a) Raster plot of the spiking population reacting to step-wise inputs for 1 second. Each step lasts 250 ms (0, 10, 50 and 100 Hz). b) Firing rate of a single rate-coded neuron decoding the corresponding spiking neuron. The blue line shows the firing rate in the input population and the green line shows the decoded firing rate. It follows the original firing rate with some noise due to the stochastic nature of the spike trains and some delay due to the integration window. c) Relative decoding error ($\epsilon = \frac{1}{250} \int_{t=0}^{250} \frac{|r(t)-F|}{F} dt$) depending on the number of spiking neurons used for decoding, for different input firing rates (10, 50 and 100 Hz). For small number of neurons, the decoding error is high as individual spike trains are stochastic. When the number of neurons is increased (over 200), the decoding error is reduced. Decoding is relatively more precise at high frequencies than at low ones.

$$\text{sum}_{\text{exc}}(x, y) = \sum_{i=-d_i}^{d_i} \sum_{j=-d_j}^{d_j} W(i, j) \cdot \text{pre.r}(x - i, y - j)$$

with (d_i, d_j) representing the extent of the weights kernel W . If the pre- and post-populations do not have the same number of neurons in each dimension (for example $200 * 200$ and $100 * 100$, corresponding to a sub-sampling ratio of 2), the mapping between the coordinates of the post-synaptic neurons and the center of the corresponding pre-synaptic region is automatically computed, but this can be overwritten.

The convolution operation can also be performed in parallel over a specific dimension of the pre-synaptic population. For example, if the last dimension of the population represents the RGB color channels of an image, the first two being the width and height, a two-dimensional filter can be applied on each color channel separately. The post-synaptic population has then three dimensions too. It is also possible to apply a bank of filters on the pre-synaptic population (e.g. edge detection with different orientations), leading to a post-synaptic population with one additional dimension (feature map).

Pooling (e.g. max-pooling) can also be implemented using a shared projection. The operation must be specified when creating the projection, before calling the pooling connector method:

```
proj = SharedProjection(pre=pop1, post=pop2, target='exc', operation='max')
proj.pooling()
```

Each post-synaptic neuron will be associated to a region of the pre-synaptic population and will extract the maximal firing rate in this region, without defining any weight. For example, if the two populations are $200 * 200$ and $100 * 100$, each post-synaptic neuron covers a $2 * 2$ area. The extent of the region is automatically computed based on the respective geometries, but this can be overwritten. The operation can be changed to the minimal or mean firing rate in the region ('min' and 'mean'). Weight sharing is for the moment only possible for rate-coded networks and learning is disabled. This will be improved in future versions.

Recording of variables

All neural and synaptic variables (defined in the equations argument of a neuron or synapse) can be recorded during a simulation. Populations (or subsets of a population) and projections can be associated to a `Monitor` object together with a list of variable names. A frequency of recording can also be defined, e.g. once every 10 ms. In the following calls to `simulate()`, the value of these variables for all neurons/synapses will be internally appended to a vector until `get()` is called, which returns a matrix containing the recorded values and empties the recording vectors. Recording can be stopped, paused and resumed using methods of `Monitor`.

The advantage of this recording method is that the user is not bound to a specific file format: the returned values are a dictionary of Numpy arrays (one per variable) which can be directly manipulated or saved into a file. The drawback is that the available RAM can quickly be filled, especially when recording synaptic variables such as weights. It is the user's responsibility to record only the necessary periods of the simulation (using pause/resume) and to save intermediary results regularly.

Conditional simulations

By default, `simulate()` runs the simulation for a fixed duration. In some cases it may be useful to simulate until a criterion is reached, for example when the maximal firing rate in a population crosses a threshold, or a neuron has emitted a certain number of spikes. This can be used to run conditional simulations, e.g. the network has made a decision and we need to perform the corresponding action. Each population accepts a `stop_condition` argument, which states the condition that must be true to stop the simulation. In the following example, the simulation would be stopped when one or more neurons of the population have a firing rate `r` higher than 1:

```
pop1 = Population( ... , stop_condition = "r > 1.0")
```

The stop condition can use any neural parameter or variable, and can combine several boolean predicates using the `and`, `or` and `not` operators. If the simulation should be stopped when the condition is true for all neurons, not just any of them, the `: all` flag can be appended to the condition. The simulation can then be run with the `simulate_until()` method, which accepts a maximal duration for the simulation (if the criteria is never met) and a (list of) population(s) whose criteria should be checked.

Structural plasticity

The number of synapses in a network is determined at the time when projections are created and is usually constant during the simulation. Some networks require to dynamically add or remove synapses between neurons during the simulation, a mechanism called *structural plasticity* (Butz et al., 2009). Projections define `create_synapse()` and `prune_synapse()` methods which allow to dynamically create or delete synapses between any pair of neurons. These functions are called from Python, so the user has to regularly stop the simulation and check if the conditions for creating or deleting a synapse are met, depending on some neural or synaptic variable or randomly. If the structural plasticity mechanism is applied frequently, it will slow down the simulation because of the constant switches between Python and C++.

Alternatively, simple rules for the creation or deletion of a synapse can be passed to the definition of the synapse model. The `pruning` argument takes a simple boolean expression which, when true, will lead to the online deletion of the synapse. Oppositely, the `creating` argument

defines a binary condition which leads to the creation of a synapse if it does not exist yet. Creation or deletion can be made probabilistic by passing the flag `proba` after the rule. The weight and delay of created synapses can also be specified.

In the following example, each synapse updates an age variable which is incremented at each simulation step, but is reset to 0 when both pre- and post-synaptic neurons are simultaneously active. When the age of a synapse exceeds a given threshold, the synapse is pruned with a probability of 0.5. Similarly, a synapse can be created when two unconnected neurons are strongly active at the same time.

```
StructuralPlasticity = Synapse(
  parameters = "max_age = 1000.0 : postsynaptic",
  equations = "age = if pre.r * post.r > 0.9: 0.0 else: age + dt",
  pruning = "age > max_age : proba=0.5",
  creating = "pre.r * post.r > 0.9 : proba=0.5, w=0.5"
)
```

Creation and pruning of synapses have to be explicitly started with `start_creating()` and `start_pruning()` methods, which also accept a period argument defining how often the structural plasticity conditions will be checked (by default at every time step, which is computationally inefficient and probably unnecessary in most cases). Structural plasticity is available for spiking networks, but creating and pruning can not be linked to events such as the emission of a spike: it must rely on continuous variables.

Reporting

As noted by Stimberg et al. (2014), the equation-based representation of neural networks allows the automatic documentation of models. Parameters are known, equations can be parsed to \LaTeX mathematical code, and the structure of the network is simply defined in terms of populations and projections. User-defined neuron or synapse models can be documented by adding a name and a detailed text description of its behavior. Calling the `report()` method will generate a complete \LaTeX file, organized in tables as suggested by Nordlie et al. (2009). It contains a summary of the network, a list of all the populations (including their size and the neuron model), a list of all the projections with a description of the connectivity and the synapse model, a textual description of each neuron and synapse models used in the network (with the parsed equations) and finally the initial value of the parameters used in each population and projection. The generated file still requires some editing before being published, but it should ease the modeler's work.

6.3 Code generation

The approach chosen for the neural simulator is based on a complete code generation mechanism. As noted in Goodman (2010), code generation allows to couple the flexibility of a high-level language (here Python) with the speed and hardware specificities of a low-level language (C++). This approach is used in Brian to speed up some code portions and is further extended in Brian 2 where a complete C++ code for the network can be optionally generated at runtime (`cpp_standalone` mode, Stimberg et al., 2014). ANNarchy relies entirely on this concept, by generating and compiling a shared C++ library during the call to `compile()`. Only this library will hold the data representing the model. The library is then imported by the Python script which transfers the initial value of all parameters and variables and starts the simulation. The Python script has only an indirect access to the C++ data and possible recordings through Cython wrappings. Cython is a Python-like compiled language allowing to execute instructions at C-speed and to access C or C++ data structures and methods (Behnel et al., 2009). Cython was for example used to create maintainable bindings to NEST (Zaytsev and Morrison, 2014).

The main advantage of a complete code generation in comparison to a simple interface to a low-level simulator [as in PyNest; Eppler et al. (2008)] is that it allows to optimize the execution regarding the structure of the network. For example, if the model does not use delays in synaptic transmission (which require to implement queues for the output variables), or if no structural plasticity mechanism is involved (requiring more flexible data structures for the synapses), the corresponding code is not generated, reducing the complexity of the code and avoiding unnecessary overhead. Furthermore, the code can be adapted to the parallel computing platform, either a shared memory system with OpenMP (the parallel strategy can be different depending on whether 4 or 256 cores are available) or a graphical processing unit with CUDA (depending on its model or version). A drawback is that the structure of the network cannot be changed after the call to `compile()`: no population or projection can be added, or equations modified. The only changes possible are parameter or variable values, as well as the dynamical addition or suppression of synapses in case of structural plasticity.

6.3.1 Internal representation of data

Each population and projection is represented by a C++ structure storing each attribute, either a parameter or a variable. Their name is easily extracted from the `parameters` and `equations` arguments to the neuron model: they are alone on the left side of the equation, except for ODEs where it is surrounded by `d` and `/dt`. Local attributes of a population are represented by a standard C++ vector with as many elements as neurons in the population while global ones (annotated by the `population` flag) are represented by a single value. Indexing is simple because all neurons have the same attributes.

For projections, the data representation depends on the platform: on shared memory systems with openMP, local attributes are represented by a vector of vectors, one per post-synaptic neu-

ron receiving connections. Each of these vectors represents all synapses reaching this post-synaptic neuron (they can have different sizes). The connectivity matrix is therefore stored as a list of lists (LIL) structure in order to associate each value to the corresponding synapse. On graphical cards with CUDA, the connectivity is stored in the compressed sparse row (CSR) format, where the values of each attribute are flattened into a single vector and a list of row pointers allow to attribute portions of this array to a single post-synaptic neuron (see Brette and Goodman, 2011 for a review). These different data structures lead to a better parallel performance: CSR representations ensure a *coalesced* access to the attributes (i.e. the data is contiguous in memory), which is a strong condition for GPU computations to be efficient (Brette and Goodman, 2012), while the LIL structure allows a faster distribution of the data to the different OpenMP threads (Dinkelbach et al., 2012). LIL and CSR representations have similar memory requirements, but LIL is more adapted to the dynamical addition or suppression of synapses: structural plasticity is very inefficient on the GPU platform and is currently disabled.

The ability to adapt the data structures to the hardware is a clear advantage of the code generation approach, especially when the number and type of attributes is *a priori* unknown. These data structures can furthermore be easily exported to the Python namespace through the generation of Cython bindings, so the choice of the data structure is transparent to the user.

6.3.2 Simulation steps

ANNarchy performs the simulation with an equidistant time grid, where the integration step size dt is fixed for all equations. Although this scheme is natural for rate-coded networks, it can have a negative influence on spiking networks because of the forced alignment of spike times on this grid (Morrison et al., 2007). Brian also allows the use of different clocks for different parts of the model, which is currently impossible in ANNarchy. Future versions will address this issue.

Each simulation step is composed of several successive computational processes, which are mainly common to spiking and rate-coded networks:

1. *Propagation*: the results of the previous simulation step is propagated in the network. For rate-coded projections, the weighted sum of pre-synaptic firing rates is accumulated in the post-synaptic population. For spiking projections, the post-synaptic conductances are increased from the synaptic weight (or any other value defined in the `pre_spike` argument of the synapse) if the corresponding pre-synaptic neuron has emitted a spike. The variable updates defined in `pre_spike` are also processed if they exist (e.g. in the STDP rule). In both cases, if delays in synaptic transmission are defined, these operations are performed on the value of these variables at the corresponding time.
2. *Neural update*: the variables of each population are updated according to their definition in the `equations` argument of the neuron model. For spiking populations, the spiking

condition is then evaluated. If the condition is met, the rank of the neuron is appended to a vector, the reset statement is evaluated and the neuron is possibly put into a refractory state. However, if a spiking neuron is in the refractory state, only the ODEs corresponding to the conductances are updated until the refractory period has elapsed, so no spike can be emitted.

3. *Delayed outputs*: before the simulation starts, each population computes the maximal delay in synaptic transmission required by outgoing projections and instantiates a double-ended queue of the adequate size. In this step, the new value of the output variable (firing rate or spike) is appended to the queue while the oldest value is removed.
4. *Synaptic updates*: the variables of each projection (if any) are updated, including synaptic plasticity.
5. *Post-synaptic events*: for each spiking projection where a post-synaptic neuron has emitted a spike, the `post_spike` statement is evaluated for all synapses reaching this neuron.
6. *Structural plasticity*: if structural plasticity is defined, the addition/suppression of synapses is evaluated.
7. *Recording*: each neural or synaptic variable is associated with a boolean flag which enables the recording of the variable with a given period. When the criterion is met, the value of the variable is appended to a vector.

Finally, the internal time t is incremented. These steps are all performed sequentially to ensure the correctness of the simulation. Parallel computations only occur within each of these steps if possible. The only difference between rate-coded and spiking networks are the `pre_spike` and `post_spike` statements, as well as the spike emission mechanism. This common structure allows hybrid networks to be simulated.

6.3.3 Mathematical parser

The different mechanisms described above are based on the equations defined at the neural or synaptic level. As the simulation is performed in C++, the computations are not vectorized, so an update rule for the variable has to be defined for each neuron of a population or each synapse of a projection. The transformation between the mathematical equation and the corresponding C++ code snippet is performed through the use of the Sympy library (Joyner et al., 2012) coupled with regular expressions.

The first step in the analysis of a neuron or synapse model is to determine with regular expressions the list of parameters and variables (by analysing the left side of the equation), their locality (presence of `population` or `postsynaptic` in the flags), their type (int, float or bool), bounds (min and max), initial value (init) and eventually the associated numerical method. The value of each parameter (e.g. `tau = 10.0`) is stored in a temporary dictionary which will be transferred to the C++ library when it is instantiated.

For each variable, the equation is first manipulated to extract non-standard vocabulary. For example, the weighted sum in a rate-coded neuron ($\text{sum}(\text{exc})$) is extracted and replaced by a temporary variable name ($_sum_exc_$). The same is done for random number distributions ($\text{Uniform}(0, 1)$ is replaced by $_rand_$) and global operations ($\text{mean}(\text{pre}.r)$ by $_mean_pre_r$). Conditional statements ($\text{if } A: B \text{ else: } C$) are also extracted and each of the three terms are recursively analyzed. These temporary variables are added to the list of parameters and variables of the model.

This list allows to build a dictionary where the correspondence between the name of an attribute and its C++ equivalent is calculated. Each attribute belongs to a C++ structure representing a population or projection, so the name of the attribute must be prepended by the instance of the structure: $\text{pop}\%(\text{id})\text{s}$. for populations, $\text{proj}\%(\text{id})\text{s}$. for projections, where $\%(\text{id})\text{s}$ will be replaced by the ID of the population or projection when the complete code is generated. As the update will be performed in a loop over all neurons or synapses, the index of the neuron in its population ($[i]$) or of the synapse in the projection ($[i][j]$ for the LIL structure) is appended to this name. For example, the firing rate r of a neuron is represented by $\text{pop}\%(\text{id})\text{s}.r[i]$ while the weight of a synapse becomes $(\text{proj}\%(\text{id})\text{s}.w[i][j])$.

Once the dictionary is built, Sympy is able to directly generate the C++ code equivalent to each side of the equation: constants (such as numbers) and functions of the C math library are automatically recognized and correctly translated. The temporary variables introduced for the weighted sums or random distributions are finally replaced by the adequate code thanks to regular expressions. As an example, the following equation for a neuron:

$$r = \text{sum}(\text{exc}) + B + \cos(2*\text{pi}*t)$$

with B being a global parameter and t the current time in milliseconds, leads to the following code:

$$\text{pop}\%(\text{id})\text{s}.r[i] = \text{pop}\%(\text{id})\text{s}.sum_exc[i] + \text{pop}\%(\text{id})\text{s}.B + \cos(2.0*M_PI*\text{double}(t)*dt))$$

6.3.4 Numerical methods

A special case has to be made for ODEs, as the desired numerical method will influence the resulting C++ code. Additionally, a neuron or synapse can be described by a set of coupled ODEs, so the code generation must be performed globally depending on the numerical method. We retained an approach similar to the one described in Stimberg et al. (2014), except that we do not explicitly generate an abstract code representation of the equations, but rather directly manipulate Sympy symbols.

To illustrate how the numerical methods are applied, we take the example of a simple spiking neuron defined by Equation 6.10, but the principle is similar for synapses or rate-coded models, regardless of the number of ODEs.

$$\begin{aligned}\tau \cdot \frac{dv(t)}{dt} + v(t) &= g_{\text{exc}}(t) - u(t) \\ \tau \cdot \frac{du(t)}{dt} + u(t) &= v(t)\end{aligned}\tag{6.10}$$

Such a neuron could be represented by the following description:

```
tau * dv/dt + v = g_exc - u
tau * du/dt + u = v
```

with tau being a global parameter of the population. The problem to be addressed by the numerical method is to find the next value of the variables v and u based on the value they had at the previous time step and the current value of the conductance g_exc. Figure 6.5 shows the code generated for these equations by the different available numerical methods (explicit, implicit, exponential and midpoint).

Explicit Euler

The explicit (or forward) Euler method evaluates the gradients dv/dt and du/dt at the current time t . In the textual representations of the equations, dv and du are simply replaced by two new variables `_v` and `_u`, and the system of equations is solved and simplified to find the value of these increments as a function of v, u, tau and g_exc. Here, the problem is simple because `_v` and `_u` are present only once per equation: the equations are not coupled. The increments are translated into a C++ code snippet using the same dictionary-based approach as for regular equations, and the increments are then added to the previous value of v and u.

Implicit Euler

The implicit (or backward) Euler method evaluates the gradients dv/dt and du/dt at the next time $t + dt$. dv and du are replaced by `_v - v` and `_u - u`, where `_v` and `_u` represent the next value of the variables, and all occurrences of v and u are replaced by `_v` and `_u`. This leads to a system of two linear equations with two variables, which is solved using the Sympy linear solver. Contrary to the explicit method, the equations are coupled, and the solver will only succeed if the equations are linear in v and u. The parser will return an error if not. Once the solution is found, we subtract v and u to `_v` and `_u` and simplify the equation in order to find the increment that will be added to the previous value of the variables.

```

// 1. Explicit Euler method
double _v = dt*(pop0.g_exc[i]-pop0.u[i]-pop0.v[i])/pop0.tau;
double _u = dt*(-pop0.u[i]+pop0.v[i])/pop0.tau;
pop0.v[i] += _v ;
pop0.u[i] += _u ;

// 2. Implicit Euler method
double _v = (dt + pop0.tau)*(dt*(pop0.g_exc[i]-pop0.u[i]
    + pop0.v[i])+pop0.tau*pop0.v[i])
    / (pow(dt,2)+pow(dt+pop0.tau,2));
double _u = (dt*(dt*pop0.g_exc[i]+dt*pop0.v[i]
    + pop0.tau*pop0.v[i])+pop0.u[i]*pow(dt+pop0.tau,2))
    / (pow(dt,2)+pow(dt+pop0.tau,2));
pop0.v[i] += _v;
pop0.u[i] += _u;

// 3. Exponential Euler method
double _v = (1.0-exp(-dt/pop0.tau))
    *(pop0.g_exc[i]-pop0.u[i]-pop0.v[i]);
double _u = (1.0-exp(-dt/pop0.tau))*(pop0.v[i]-pop0.u[i]);
pop0.v[i] += _v ;
pop0.u[i] += _u ;

// 4. Midpoint method
double _k_v = (pop0.g_exc[i]-pop0.u[i]-pop0.v[i])/pop0.tau;
double _k_u = (-pop0.u[i]+pop0.v[i])/pop0.tau;
double _v = (- (pop0.u[i]+0.5*dt*_k_u ) - (pop0.v[i]+0.5*dt*_k_v)
    +pop0.g_exc[i])/pop0.tau;
double _u = (- (pop0.u[i]+0.5*dt*_k_u ) + (pop0.v[i]+0.5*dt*_k_v))
    /pop0.tau;
pop0.v[i] += dt*_v ;
pop0.u[i] += dt*_u ;

```

Figure 6.5: Example of code generated for Equation 6.10 using different numerical methods: 1. Explicit Euler, 2. Implicit Euler, 3. Exponential Euler, 4. Midpoint (Runge-Kutta method of order 2). `pop0` is a C++ structure holding the different attributes of the population: the vectors `v` and `u` for the two variables, the vector `g_exc` for the excitatory inputs and the double value `tau` for the time constant. All methods compute first the increments `_v` and `_u` before adding them to `v` and `u`, in order to make sure the update rules use the previous values of these variables. The number of elementary operations differs from one method to another, increasing the simulation runtime, but the numerical precision and stability of the more complex methods might be required in some cases.

Exponential Euler

The exponential Euler method is a special forward method which has the smallest numerical error on uncoupled linear first-order ODEs. The first step is to canonize each equation in the form $\tau \cdot \frac{dx(t)}{dt} + x(t) = A(t)$, with τ being the time constant of the variable and $A(t)$ its steady state. Here the equations are already in this form, but a conductance-based neuron with the equation $\tau \cdot dv/dt + v = g_{exc} \cdot (E - v)$ would have an equivalent time constant of $\tau / (1 + g_{exc})$ and a steady state of $g_{exc} \cdot E / (1 + g_{exc})$. Once these equivalent time constants and steady states are identified and simplified for each equation, the increments can be directly obtained through:

$$x(t + dt) = x(t) + (1 - \exp(-\frac{dt}{\tau})) \cdot (A(t) - x(t))$$

Midpoint

The midpoint method is a Runge-Kutta method of order 2, described in Stimberg et al. (2014). It evaluates successively the gradient at t and in the middle of the interval $[t, t + dt]$. The gradient at t is evaluated using the same mechanism as in the explicit Euler method and stored in the variables `_k_v` and `_k_u`. These variables allow to estimate the value of v and u by $v + dt/2 \cdot _k_v$ and $u + dt/2 \cdot _k_u$, respectively. The equations are again manipulated, by replacing all occurrences of v and u by their estimates at $t + dt/2$ and finding the corresponding increment using the explicit Euler method. This method has a much smaller numerical error and is more stable than the explicit or implicit methods, but requires more computations during the simulation, as the gradient is evaluated twice.

Event-driven integration

This method is only available for spiking synapses, if the ODEs are linear (which is the case for the online STDP rule). For this method, the equations are not evaluated at each time step, but only when a pre- or post-synaptic spike occurs for a synapse. The new value of the variables is then computed exactly, using the time elapsed since the last event. Event-driven integration is not yet available for neural equations, as it requires to predict the occurrence of the next spike. Future versions of ANNarchy will address this mechanism. However, it may only speed simulations up if the network is small and does not generate too many spikes per step (Brette et al., 2007; Morrison et al., 2007).

6.3.5 OpenMP and CUDA code generation

Once the structure of network is known and all equations have been analyzed, the C++ code corresponding to the simulation can be generated depending on the desired parallel framework.

```

a) Neuron model
neuron = Neuron(
    parameters = "tau = 10.0 : population",
    equations = "tau*dr/dt + r = sum(exc) : min=0.0"
)

b) OpenMP framework (ANNarchy.cpp)
// Updating the local variables of population 0
#pragma omp parallel for
for(int i = 0; i < 1000; i++)
{
    double _r = dt*(pop0._sum_exc[i]-pop0.r[i])/pop0.tau;
    pop0.r[i] += _r ;
    if(pop0.r[i] < 0.0)
        pop0.r[i] = 0.0;
}

c) CUDA framework (ANNarchy.cu)
// Updating the local variables of population 0
cuPop0_step<<<nb, __pop0__, 0, stream>>>(dt,
    pop0.gpu_sum_exc,
    pop0.gpu_r,
    pop0.tau );

// gpu device kernel for population 0
__global__ void cuPop0_step(double dt,
    double* _sum_exc, double* r, double tau)
{
    int i = threadIdx.x + blockIdx.x*blockDim.x;
    if ( i < 1000 ) {
        double _r = dt*(_sum_exc[i] - r[i])/tau;
        r[i] += _r ;
        if(r[i] < 0.0)
            r[i] = 0.0;
    }
}

```

Figure 6.6: Code generated for a single population pop_0 of 1000 identical neurons. a) Neuron model used for code generation: a global parameter τ and a local variable r following a linear ODE and limited to positive values. b) Code generated for the OpenMP framework. The code is pasted into the main C++ code `ANNarchy.cpp` and called at each step. It iterates over the 1000 neurons of the population and updates their firing rate depending on the corresponding code snippet. It operates directly on the data contained in the structure `pop0`. A simple `#pragma` statement allows parallel processing over the available threads. c) Code generated for the CUDA framework. The code is pasted into the specific `ANNarchy.cu` file. A copy of the vectors `_sum_exc` and `r` (prefixed by `gpu`) is sent to the device (GPU) through the call to `cuPop0_step` by the host (CPU). The code inside `cuPop0_step` is executed in parallel on the device for the 1000 neurons and updates the array corresponding to `r`. This copy of `r` is transferred back to the CPU at the end of the simulation block for analysis in Python. Note that the parser can be configured to not generate the struct prefixes as for the OpenMP backend.

Each simulation step described in Section 6.3.2 leads to the generation of a code portion for the corresponding populations and projections which is then integrated into the main simulation code. Figure 6.6 shows an example of a code portion for the update of the neural variables of a population `pop0` whose 1000 neurons are defined by the neuron model described on Figure 6.6 a. It defines a global parameter `tau` and the firing rate `r` is defined by the ODE $\tau \cdot dr/dt = \text{sum}(\text{exc}) - r$, limited to positive values with the flag `min=0.0`. The OpenMP implementation on Figure 6.6 b is in this case simple: the code snippet corresponding to the ODE (here using the explicit Euler method) is integrated into a for-loop over the 1000 neurons, where the value of each element in the corresponding vector is updated sequentially. The parallel execution of this loop over the available cores is ensured through the addition of an OpenMP `#pragma` statement. The complete code is pasted in a standard C++ file called `ANNarchy.cpp` and compiled using `g++` on Linux or `clang++` on MacOS X.

The code generated for the same population in the CUDA framework is more complex, as shown on Figure 6.6 c. The instructions executed on the GPU have to be compiled with the NVIDIA compiler `nvcc`, so the code is generated in a special file called `ANNarchy.cu`. CUDA code generally consists of two sections: one is intended to run on the CPU (host code) while the other (flagged with the keywords `__global__` or `__device__`) will be executed on the GPU (device code). At the beginning of the simulation, the vectors holding population and projection data are transferred to the GPU using the CUDA method `cudaMemcpy()`. The CUDA object will work on these copies during the whole simulation and they will be transferred back to the host at the end, allowing the Python script to analyze the results. An exception is during the recording of variables: the arrays to be recorded are transferred to the host at each time step, as the amount of memory is usually limited on GPUs.

Figure 6.6 c shows the corresponding host and device code portions: the host code simply calls the device method with a copy of the necessary data. The device code updates the passed variables in parallel according to the desired numerical method. The same mechanism is used for all steps of the simulation. The weighted sum of inputs is for example executed in parallel over blocks of post-synaptic neurons with OpenMP. In contrast, parallel reduction is used in the CUDA implementation, as it leads to better performance (Dinkelbach et al., 2012). The main advantage of this code generation approach is that only the required steps are generated: spike-only mechanisms are skipped for rate-coded networks, as well as mechanisms for synaptic delays or structural plasticity if the network does not define them. This allows to minimize the code overhead and improves the readability of the generated code.

6.4 Benchmarks

We here report the parallel performance of the neural simulator but do not attempt to study it in all details. It is planned to issue future releases of ANNarchy, most improvements concerning

the parallel performance. Nevertheless, we want to highlight that code generation already allows to obtain a parallel performance comparable to most specialized simulators. The OpenMP tests are performed on a Linux machine with 2 Intel XEON X5675 at 3 GHz (12 physical cores in total, with hyperthreading disabled) and 12 GB RAM. The CUDA tests are performed on a Linux machine with 2 Intel XEON E5-2650 at 2.6 GHz, 128 GB RAM and a NVIDIA Tesla K20m graphical card. The simulation times are measured and averaged over 10 different trials with the same initial conditions (standard deviations are omitted as they are negligible in all cases). All scripts used in this section are provided in the Supplementary Material.

Rate-coded benchmark

To test the parallel performance of rate-coded networks, we used a simple network of two populations composed of $N = 1000$ (resp. 4000) neuron each, connected with a all-to-all projection representing 1 (resp. 16) million connections. Each neuron is a simple leaky-integrator of excitatory inputs with a firing rate defined by the ODE $\tau \cdot dr/dt + r = \text{sum}(\text{exc})$, τ being a global parameter of the population. Unlike spiking networks, the simulation time of a rate-coded network does not depend on the activity in the network and the summation of inputs for all-to-all connectivity patterns hugely overcomes the update of neural variables (Dinkelbach et al., 2012), so such a simple network is sufficient to exhibit the parallel performance of the simulation. As outlined in the introduction, we are not aware of parallel simulators of rate-coded networks which could simply implement this network, so we only present in Figure 6.7 the speed-up ratio of the simulation time when using 1 to 12 threads with OpenMP or when using CUDA as the simulation backend. The single-threaded implementation is performed without the OpenMP primitives, so it avoids the small sequential overhead of OpenMP. The CUDA implementation uses the default configuration used by ANNarchy (32 threads for the neural variables updates, 192 threads for the weighted sums), but this can be changed by the user.

The network with 1000 neurons in each population shows a fairly efficient scaling behavior, while the network with 4000 neurons quickly saturates to a speed-up of approximately 2.9. This can be explained by the fact that the connectivity matrix with 16 million synapses (each connection weight being represented by a double floating-point value) cannot fit into the cache, so we have a memory-bound problem where memory transfers between the RAM and the processor limit the efficiency of the parallel implementation on shared-memory systems. This limitation is well-known for this kind of operation, especially because of the LIL structure used for the connectivity matrix. We chose this structure as it allows easier modification through structural plasticity mechanisms and internal tests showed that a CSR structure does not improve much the performance. We will investigate further the influence of data structures on parallel performance. The main operation performed here is a matrix-vector multiplication. The strategy to efficiently parallelize this operation depends on the sparseness of the connectivity matrix. Depending on this type, there are multiple methods available, including single-instruction-multiple-data operations (SIMD), cache blocking, loop unrolling, prefetching and autotuning (Kelefouras et al., 2015; Williams et al., 2007). Thanks to the code generation approach used in ANNarchy,

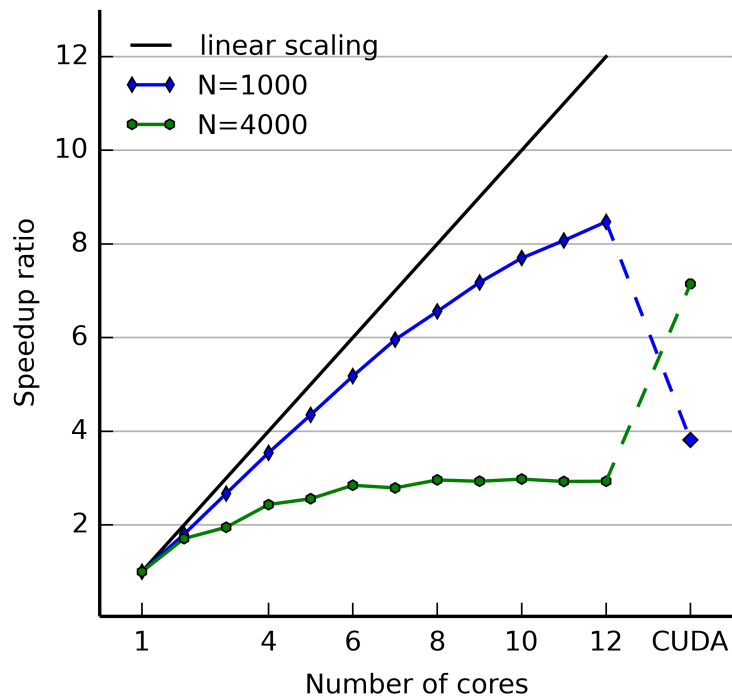


Figure 6.7: Speedup ratio obtained by ANNarchy for a fully connected rate-coded network composed of two populations of 1000 (resp. 4000) neurons each. The speedup ratio is defined by the ratio between the execution time (measured for a simulation of 1 second) of the single-threaded implementation and the one measured when using T threads. The single-threaded implementation does not use OpenMP nor CUDA primitives. For the OpenMP implementation, the number of threads is varied between 2 and 12. For the CUDA implementation, the default configuration of ANNarchy (32 threads for the neural variables updates, 192 threads for the weighted sums) is used. The CUDA implementation is run on a different machine for technical reasons, so the single-threaded baseline measured on this machine differs from the one used for OpenMP. Nevertheless, only the scaling ratio is interesting here, not the absolute execution times. The black line denotes the ideal linear scaling, the blue line the scaling of the network with 1000 neurons, the green one the scaling for 4000 neurons. With OpenMP, the scaling for 1000 neurons is slightly sub-optimal, while the one for 4000 neurons saturates quickly at a ratio of 2.9. The situation is reversed with CUDA: the network with 1000 neurons only achieves a speedup ratio of 3.8, while the network with 4000 neurons achieves a ratio of 7.15.

we will be able in future versions to implement these improvements depending on the known connectivity before compilation.

The situation is reversed for the CUDA implementation: the network with 1000 neurons is speeded up by a factor 3.8, while the network with 4000 neurons obtains a speedup of 7.15, more than three times the maximal speedup obtained with OpenMP. This confirms our previous work showing that rate-coded networks with a relatively small number of connections might benefit more from a CPU-based implementation, while networks with many connections should be run on a GPU (Dinkelbach et al., 2012).

Spiking benchmark

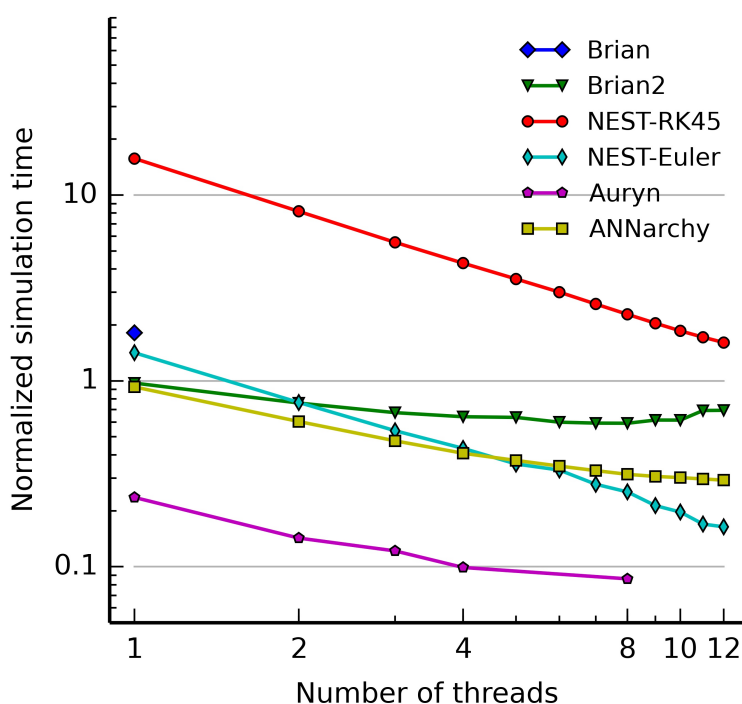


Figure 6.8: Comparison of the simulation times of different simulators depending on the number of threads on a shared-memory system. The parallel performance of the simulators Brian (version 1.4.1), Brian 2 (version 2.0b3), NEST (with Python bindings, version 2.4.2), Aurnyn (version 0.4.1) and ANNarchy (version 4.4.0) are investigated up to 12 threads. Two versions of NEST are used: one using the Runge-Kutta-Fehlberg 4(5) method (noted NEST-RK45), and a patched version using the explicit Euler method (NEST-Euler). The simulation times are normalized to show the real-time ratio: a normalized time of 1 means that simulating the network for one second takes exactly one second of computer time (simulations are run for 10 seconds). Both axes use a logarithmic scale. Brian only allows single-threaded simulations. Brian 2, NEST and ANNarchy use OpenMP, while Aurnyn uses MPI (openMPI 1.4.3). Aurnyn only allows a number of processes which is a multiple of 2. The single-threaded version of ANNarchy compares well to other neural simulators, but its scaling properties are not optimal compared to NEST.

For spiking networks, we compare the parallel performance of ANNarchy with other neural simulators on the COBA benchmark proposed in Brette et al. (2007) and based on the model of Vogels and Abbott (2005). The network is composed of 4000 integrate-and-fire neurons (3200 excitatory and 800 inhibitory) using exponentially-decreasing conductance-based synapses:

$$\begin{aligned}
 C \cdot \frac{dv(t)}{dt} &= g_L \cdot (E_L - v(t)) + g_e(t) \cdot (E_e - v(t)) + g_i(t) \cdot (E_i - v(t)) + I \\
 \tau_e \cdot \frac{dg_e(t)}{dt} &= -g_e(t) \\
 \tau_i \cdot \frac{dg_i(t)}{dt} &= -g_i(t)
 \end{aligned}
 \tag{6.11}$$

All neurons are randomly connected with a probability of 0.02. We implemented this benchmark on ANNarchy (version 4.4.0), Brian (version 1.4.1), Brian 2 (version 2.0b3), NEST (with Python bindings, version 2.4.2) and Auryn (version 0.4.1). As noted in Zenke and Gerstner (2014), NEST uses by default the precise but very expensive Runge-Kutta-Fehlberg 4(5) (RK45) numerical method, while Brian and Auryn use the faster explicit Euler method. We therefore also applied the patch provided by Zenke and Gerstner (2014) to force NEST to use the Euler method (noted NEST-Euler as opposed to NEST-RK45). The Auryn simulator was modified to use synaptic delays of 0.1 ms. The code for Brian 2 uses the `cpp_standalone` mode to generate efficient C++ code and OpenMP parallel processing. All simulations were run using the same parameters, random number generator seeds (for the initial values of the membrane potential) and connectivity matrix (generated as a Scipy sparse matrix and loaded into the different simulators). The ANNarchy and Brian implementations produced exactly the same spiking patterns, while the other simulators showed only minor deviations. The time needed for 10 seconds of simulation (excluding building time) was measured using the Python time module, except for Auryn where MPI timer routines were used.

The results are shown on Figure 6.8. In agreement with the results of Zenke and Gerstner (2014), the default NEST implementation with RK45 is roughly ten times slower than the modified NEST version with explicit Euler, but both have a very good scaling behavior. In the single-threaded version, Brian 2 is much faster than Brian and comparable to ANNarchy, but its scaling behavior is not as optimal as other simulators. It should be noted that Brian 2 is still in development, so this result is only preliminary. Auryn is almost one order of magnitude faster than the other simulators and with an satisfying scaling behavior (although the number of MPI processes must be a multiple of 2). The single-threaded implementation of ANNarchy is in comparison fairly efficient, but the scaling properties could be further improved. This is mostly due to the spike propagation mechanism (increasing post-synaptic conductances when a spike is emitted), which scales poorly in comparison to the neural variable updates. Future work will investigate different implementations of this mechanism.

6.5 Discussion

We have described the core principles of the neural simulator ANNarchy. It provides a high-level interface in Python similar to PyNN to facilitate the creation of rate-coded, spike-coded or hybrid neural networks. An important set of neuron and synapse models can be implemented with an equation-oriented syntax close to the one proposed by Brian. These definitions are used to generate an entire C++ library optimized for the underlying parallel framework (OpenMP for shared memory systems, CUDA for GPU cards). Different numerical methods are available for solving the possible ODEs. Code generation allows complete control over data structures and computational methods, which leads to the execution of fine-tuned and simple code. It allows to obtain a parallel performance comparable to specialized simulators.

ANNarchy brings the flexibility of the Brian interface to rate-coded networks, while being compatible with state-of-the-art spiking simulators. Although several features and concepts for spiking networks are comparable to other simulators (especially Brian 2, Stimberg et al., 2014), ANNarchy also provides novel features to the community. Structural plasticity can be easily implemented through simple synapse-specific rules. Any neural or synaptic variable can be easily recorded during the simulation. The network can be easily interfaced to external C/C++ libraries through the Cython bindings, so images or video streams can efficiently be fed to the network, or neural activity read to control robots in real-time. Automatic reporting allows to generate complete reports in \LaTeX about the current network model, including the network structure, the equations used for the neurons and synapses, as well as the different parameters used. Brian 2 provides a similar feature as it is also based on Sympy, but only for individual equations. Some features are implemented only for rate-coded networks (such as convolution or pooling operations which do not make much sense for spiking networks), but the hybrid ability of ANNarchy allows for example to integrate convoluted rate-coded networks for vision with spiking cognitive models.

The chosen equation-oriented approach is very powerful, but has some limitations, some of which are already listed in Stimberg et al. (2014). The number of explicit neural states is limited to two for spiking neurons (active or refractory) and only one for rate-coded ones. However, the syntax allows the use of conditional statements which can modify entirely the properties of a neuron, mimicking additional states. The equation-oriented syntax is also limited in its current form to the description of point-neurons, neglecting the effects of the neurons' morphology on their properties. Such neurons would require the use of another simulator such as NEURON or GENESIS.

As Brian 2 and ANNarchy are based on the principles stated in Stimberg et al. (2014), one should highlight the main differences between the two equation-oriented interfaces for spiking networks. Brian 2 proposes a powerful mechanism to incrementally build connection matrices by accessing the underlying data structure, possibly through text-based rules. It is also possible to dynamically add and remove populations and projections between two simulations. This is currently impossible with ANNarchy: all data structures are linked to the generated library

and are only indirectly accessible in Python. Synapse definition in Brian 2 allows to modify any pre- or post-synaptic neural variable. Because of the way the code is generated, ANNarchy only allows the synapse to modify the post-synaptic conductance in addition to synaptic variables. Brian 2 allows to solve stochastic differential equations (SDE), while ANNarchy is limited for now to ODEs: one can only use random variables inside an ODE to simulate for example intracellular noise, but this is not a stochastic process. Brian 2 allows a finer control on the evolution of neural variables during the refractory period, while ANNarchy freezes all variables during this period except for the conductances. SDEs and control over variables during the refractory period will be progressively introduced in future versions. On the other hand, ANNarchy proposes a solution to structural plasticity and hetero-synaptic plasticity (through the possible use of global post-synaptic variables in a projection) which could be integrated in Brian 2. It also provides additional control over the evolution of variables, such as their initial value and the minimal or maximal value they can take over the course of a simulation.

ANNarchy will be further maintained and new features will be integrated in future releases. Learning in rate-coded networks is focused on biologically-plausible rules where all information is local to the synapse, which currently rules out methods such as backpropagation. Synaptic delays are currently only implemented between the pre-synaptic neuron and the synapse, while some plasticity models rely on an additional delay between the synapse and the soma of the post-synaptic neuron. Exact event-based integration of neural dynamics needs to be implemented (Morrison et al., 2007), as it allows to simulate faster low-firing networks of linear neurons. Additional numerical methods (such as Runge-Kutta of order 4) will be progressively introduced. Computations are limited to an equidistant time grid, as it is the easiest method for rate-coded networks. Some networks may nevertheless benefit from adaptive time steps, or of the use of different clocks in different parts of the model. This may be particularly useful for hybrid networks, as rate-coded networks often behave well with integration steps of 1 ms, while some spiking networks require at least 0.1 ms. Finally, as the chosen interface is very close to PyNN (Davison et al., 2008), we will implement a fully compatible interface so that ANNarchy can be used as an alternative simulation backend using the available standard models.

As the interface is already stable, there is room for improvement regarding the parallel performance. On CPU-based shared memory systems, the OpenMP implementation is efficient for rate-coded networks (in the limit of memory bandwidth), but the spike propagation mechanism does not scale linearly yet, introducing a strong sequential component to the simulation. This issue will be investigated in future releases: based on our experiments, simulators using array-based computations (Brian 2, ANNarchy and partially Auryn) tend to scale sub-optimally, while NEST performs better. A possible reason for this difference is linked to the object-oriented design of NEST: each thread computes individual neurons, leading to a more cache-friendly access to the variables, especially when using synaptic delays. In contrast the array-based approach share neural and synaptic data among several threads and quickly fill the cache. The opposite effect seems to be true for the update of neural variables (Zenke and Gerstner, 2014). Hybrid solutions between array-based and object-oriented implementations might lead to a better parallel performance for spiking networks.

Parallel computing on distributed memory systems is also planned. The performance of NEST on such systems suggests that this is an interesting solution for spiking networks, although it has been shown that memory transfers might impair scaling already for medium-scale spiking networks (Zenke and Gerstner, 2014). Communication costs might become a problem for rate-coded networks, as firing rates must be exchanged at each simulation step. However, if synaptic data is appropriately distributed on each node, it may increase the total available memory bandwidth, which is an important limiting factor. We are currently investigating hybrid MPI/OpenMP solutions which may minimize the communication costs through a structural analysis of the network's topology.

The generation of CUDA code for simulation on GPU platforms is still experimental and currently only available for rate-coded networks. One major issue is the choice of the correct configuration depending on the network, such as the number of threads per operation (the optimal number of threads for the summation of inputs is different from the one for the update of neural or synaptic variables). ANNarchy currently proposes a default configuration which can be overwritten by the user, but we will investigate solutions using auto-tuning of the simulation parameters (Dinkelbach et al., 2012).

Disclosure/Conflict-of-Interest Statement

The authors declare that the research was conducted in the absence of any commercial or financial relationships that could be construed as a potential conflict of interest.

Author Contributions

JV and HÜD designed and wrote the library. JV wrote primarily the article and performed the tests. FH supervised the development and participated in the writing.

Acknowledgement

The authors would like to thank Javier Baladron for useful discussions and suggestions. Parts of this work have been supported by the Deutsche Forschungsgemeinschaft (DFG) grants HA2630/4-2, GZ: INST 270/221-1 FUGG and by the European Project FP7-NBIS "Spatial Cognition" (grant no. 600785).

References

- Aisa, B., Mingus, B., and O'Reilly, R. (2008). The emergent neural modeling system. *Neural Netw.* 21, 1146–52. doi:[10.1016/j.neunet.2008.06.016](https://doi.org/10.1016/j.neunet.2008.06.016).
- Alberts, J. L., Voelcker-Rehage, C., Hallahan, K., Vitek, M., Bamzai, R., and Vitek, J. L. (2008). Bilateral subthalamic stimulation impairs cognitive-motor performance in parkinson's disease patients. *Brain* 131, 3348–3360. doi:[10.1093/brain/awn238](https://doi.org/10.1093/brain/awn238).
- Albin, R. L., and Mink, J. W. (2006). Recent advances in tourette syndrome research. *Trends Neurosci* 29, 175–182. doi:[10.1016/j.tins.2006.01.001](https://doi.org/10.1016/j.tins.2006.01.001).
- Albin, R. L., Young, A. B., and Penney, J. B. (1989). [The functional anatomy of basal ganglia disorders](#). *Trends Neurosci* 12, 366–375.
- Albus, J. S. (1971). A theory of cerebellar function. *Math Biosci*, 25–61.
- Alegret, M., Junqué, C., Valldeoriola, F., Vendrell, P., Pilleri, M., Rumià, J., et al. (2001). [Effects of bilateral subthalamic stimulation on cognitive function in parkinson disease](#). *Arch Neurol* 58, 1223–1227.
- Alexander, G. E., DeLong, M. R., and Strick, P. L. (1986). Parallel organization of functionally segregated circuits linking the basal ganglia and cortex. *Ann Rev Neurosci* 9, 357–381.
- Amari, S. (1977). Dynamics of pattern formation in lateral-inhibition type neural fields. *Biol. Cybern.* 27, 77–87. Available at: <http://www.ncbi.nlm.nih.gov/pubmed/911931>.
- Ambroggi, F., Ishikawa, A., Fields, H. L., and Nicola, S. M. (2008). Basolateral amygdala neurons facilitate reward-seeking behavior by exciting nucleus accumbens neurons. *Neuron* 59, 648–61. doi:[10.1016/j.neuron.2008.07.004](https://doi.org/10.1016/j.neuron.2008.07.004).
- Apicella, P., Deffains, M., Ravel, S., and Legallet, E. (2009). Tonically active neurons in the striatum differentiate between delivery and omission of expected reward in a probabilistic task context. *Eur. J. Neurosci.* 30, 515–26. doi:[10.1111/j.1460-9568.2009.06872.x](https://doi.org/10.1111/j.1460-9568.2009.06872.x).
- Aron, A. R., and Poldrack, R. A. (2006). Cortical and subcortical contributions to stop sig-

References

- nal response inhibition: Role of the subthalamic nucleus. *J Neurosci* 26, 2424–2433. doi:[10.1523/JNEUROSCI.4682-05.2006](https://doi.org/10.1523/JNEUROSCI.4682-05.2006).
- Ashby, F. G., Ell, S. W., Valentin, V. V., and Casale, M. B. (2005). FROST: A distributed neurocomputational model of working memory maintenance. *J Cogn Neurosci* 17, 1728–1743.
- Ashby, F. G., Ennis, J. M., and Spiering, B. J. (2007). A neurobiological theory of automaticity in perceptual categorization. *Psychol Rev* 114, 632–656. doi:[10.1037/0033-295X.114.3.632](https://doi.org/10.1037/0033-295X.114.3.632).
- Baddeley, A. D. (1986). *Working memory*. Oxford: Oxford University Press.
- Bahuguna, J., Aertsen, A., and Kumar, A. (2015). Existence and control of go/no-go decision transition threshold in the striatum. *PLoS Comput Biol* 11, e1004233. doi:[10.1371/journal.pcbi.1004233](https://doi.org/10.1371/journal.pcbi.1004233).
- Balcita-Pedicino, J. J., Omelchenko, N., Bell, R., and Sesack, S. R. (2011). The inhibitory influence of the lateral habenula on midbrain dopamine cells: ultrastructural evidence for indirect mediation via the rostromedial mesopontine tegmental nucleus. *J. Comp. Neurol.* 519, 1143–64. doi:[10.1002/cne.22561](https://doi.org/10.1002/cne.22561).
- Baldassarre, G., Mannella, F., Fiore, V. G., Redgrave, P., Gurney, K., and Mirolli, M. (2013). Intrinsically motivated action-outcome learning and goal-based action recall: A system-level bioconstrained computational model. *Neural Netw* 41, 168–187. doi:[10.1016/j.neunet.2012.09.015](https://doi.org/10.1016/j.neunet.2012.09.015).
- Balleine, B. W., and Dickinson, A. (1998). [Goal-directed instrumental action: Contingency and incentive learning and their cortical substrates](#). *Neuropharmacology* 37, 407–419.
- Balsam, P. D., Drew, M. R., and Yang, C. (2002). Timing at the Start of Associative Learning. *Learn. Motiv.* 33, 141–155. Available at: <http://www.sciencedirect.com/science/article/pii/S002396900191104X>.
- Bar-Gad, I., Morris, G., and Bergman, H. (2003). Information processing, dimensionality reduction and reinforcement learning in the basal ganglia. *Prog Neurobiol* 71, 439–473. doi:[10.1016/j.pneurobio.2003.12.001](https://doi.org/10.1016/j.pneurobio.2003.12.001).
- Barto, A., Mirolli, M., and Baldassarre, G. (2013). Novelty or surprise? *Front Psychol* 4, 907. doi:[10.3389/fpsyg.2013.00907](https://doi.org/10.3389/fpsyg.2013.00907).
- Baxter, M. G., and Murray, E. A. (2002). The amygdala and reward. *Nat. Rev. Neurosci.* 3, 563–73. doi:[10.1038/nrn875](https://doi.org/10.1038/nrn875).
- Beaulieu, C. (1993). Numerical data on neocortical neurons in adult rat, with special reference

- to the GABA population. *Brain Res* 609, 284–292.
- Bednar, J. A. (2009). Topographica: Building and Analyzing Map-Level Simulations from Python, C/C++, MATLAB, NEST, or NEURON Components. *Front. Neuroinform.* 3, 8. doi:[10.3389/neuro.11.008.2009](https://doi.org/10.3389/neuro.11.008.2009).
- Beeler, J. A., Daw, N., Frazier, C. R. M., and Zhuang, X. (2010). Tonic dopamine modulates exploitation of reward learning. *Front Behav Neurosci* 4, 170. doi:[10.3389/fnbeh.2010.00170](https://doi.org/10.3389/fnbeh.2010.00170).
- Behnel, S., Bradshaw, R. W., and Seljebotn, D. S. (2009). Cython tutorial. in *Proc. 8th python sci. conf.*, eds. G. Varoquaux, S. van der Walt, and J. Millman (Pasadena, CA USA: http://conference.scipy.org/proceedings/SciPy2009/paper_1), 4–14.
- Bekolay, T., Bergstra, J., Hunsberger, E., Dewolf, T., Stewart, T. C., Rasmussen, D., et al. (2014). Nengo: a Python tool for building large-scale functional brain models. *Front. Neuroinform.* 7, 48. doi:[10.3389/fninf.2013.00048](https://doi.org/10.3389/fninf.2013.00048).
- Belova, M. A., Paton, J. J., Morrison, S. E., and Salzman, C. D. (2007). Expectation modulates neural responses to pleasant and aversive stimuli in primate amygdala. *Neuron* 55, 970–84. doi:[10.1016/j.neuron.2007.08.004](https://doi.org/10.1016/j.neuron.2007.08.004).
- Bermudez, M. A., and Schultz, W. (2010). Reward magnitude coding in primate amygdala neurons. *J. Neurophysiol.* 104, 3424–32. doi:[10.1152/jn.00540.2010](https://doi.org/10.1152/jn.00540.2010).
- Berns, G., and Sejnowski, T. (1998). A computational model of how the basal ganglia produce sequences. *J Cogn Neurosci* 10, 108–121.
- Berridge, K. C. (2007). The debate over dopamine's role in reward: The case for incentive salience. *Psychopharmacology (Berl)* 191, 391–431. doi:[10.1007/s00213-006-0578-x](https://doi.org/10.1007/s00213-006-0578-x).
- Beuth, F., and Hamker, F. H. (2015). A mechanistic cortical microcircuit of attention for amplification, normalization and suppression. *Vision Res.* doi:[10.1016/j.visres.2015.04.004](https://doi.org/10.1016/j.visres.2015.04.004).
- Bienenstock, E. L., Cooper, L. N., and Munro, P. W. (1982). [Theory for the development of neuron selectivity: Orientation specificity and binocular interaction in visual cortex.](#) *J Neurosci* 2, 32–48.
- Bird, C. M., and Burgess, N. (2008). The hippocampus and memory: Insights from spatial processing. *Nat Rev Neurosci* 9, 182–194. doi:[10.1038/nrn2335](https://doi.org/10.1038/nrn2335).
- Bissière, S., Humeau, Y., and Lüthi, A. (2003). Dopamine gates LTP induction in lateral amygdala

References

- by suppressing feedforward inhibition. *Nat. Neurosci.* 6, 587–92. doi:[10.1038/nn1058](https://doi.org/10.1038/nn1058).
- Bolam, J. P., Hanley, J. J., Booth, P. A., and Bevan, M. D. (2000). Synaptic organisation of the basal ganglia. *J. Anat.* 196 (Pt 4, 527–42. Available at: <http://www.pubmedcentral.nih.gov/articlerender.fcgi?artid=1468095&tool=pmcentrez/&rendertype=abstract>.
- Booth, M. C., and Rolls, E. T. (1998). View-invariant representations of familiar objects by neurons in the inferior temporal visual cortex. *Cereb Cortex* 8, 510–523.
- Bostan, A. C., and Strick, P. L. (2010). The cerebellum and basal ganglia are interconnected. *Neuropsychol. Rev.* 20, 261–70. doi:[10.1007/s11065-010-9143-9](https://doi.org/10.1007/s11065-010-9143-9).
- Botvinick, M. M., Niv, Y., and Barto, A. C. (2009). Hierarchically organized behavior and its neural foundations: A reinforcement learning perspective. *Cognition* 113, 262–280. doi:[10.1016/j.cognition.2008.08.011](https://doi.org/10.1016/j.cognition.2008.08.011).
- Bourdy, R., and Barrot, M. (2012). A new control center for dopaminergic systems: pulling the VTA by the tail. *Trends Neurosci.* 35, 681–90. doi:[10.1016/j.tins.2012.06.007](https://doi.org/10.1016/j.tins.2012.06.007).
- Bower, J. M., and Beeman, D. (2007). Constructing realistic neural simulations with GENESIS. *Methods Mol. Biol.* 401, 103–25. doi:[10.1007/978-1-59745-520-6_7](https://doi.org/10.1007/978-1-59745-520-6_7).
- Braak, H., and Del Tredici, K. (2008). Cortico-basal ganglia-cortical circuitry in parkinson's disease reconsidered. *Exp Neurol* 212, 226–229. doi:[10.1016/j.expneurol.2008.04.001](https://doi.org/10.1016/j.expneurol.2008.04.001).
- Brette, R., and Goodman, D. F. M. (2011). Vectorized algorithms for spiking neural network simulation. *Neural Comput.* 23, 1503–35. doi:[10.1162/NECO_a_00123](https://doi.org/10.1162/NECO_a_00123).
- Brette, R., and Goodman, D. F. M. (2012). Simulating spiking neural networks on GPU. *Network* 23, 167–82. doi:[10.3109/0954898X.2012.730170](https://doi.org/10.3109/0954898X.2012.730170).
- Brette, R., Rudolph, M., Carnevale, T., Hines, M., Beeman, D., Bower, J. M., et al. (2007). Simulation of networks of spiking neurons: a review of tools and strategies. *J. Comput. Neurosci.* 23, 349–98. doi:[10.1007/s10827-007-0038-6](https://doi.org/10.1007/s10827-007-0038-6).
- Brischoux, F., Chakraborty, S., Brierley, D. I., and Ungless, M. A. (2009). Phasic excitation of dopamine neurons in ventral VTA by noxious stimuli. *Proc. Natl. Acad. Sci. U. S. A.* 106, 4894–9. doi:[10.1073/pnas.0811507106](https://doi.org/10.1073/pnas.0811507106).
- Bromberg-Martin, E. S., and Hikosaka, O. (2011). Lateral habenula neurons signal errors in the prediction of reward information. *Nat. Neurosci.* 14, 1209–1216. doi:[10.1038/nn.2902](https://doi.org/10.1038/nn.2902).

- Brown, J. W., Bullock, D., and Grossberg, S. (2004). How laminar frontal cortex and basal ganglia circuits interact to control planned and reactive saccades. *Neural Netw* 17, 471–510. doi:[10.1016/j.neunet.2003.08.006](https://doi.org/10.1016/j.neunet.2003.08.006).
- Brown, J., Bullock, D., and Grossberg, S. (1999). How the basal ganglia use parallel excitatory and inhibitory learning pathways to selectively respond to unexpected rewarding cues. *J. Neurosci.* 19, 10502–11. Available at: <http://www.ncbi.nlm.nih.gov/pubmed/10575046>.
- Brown, M. T. C., Tan, K. R., O'Connor, E. C., Nikonenko, I., Muller, D., and Lüscher, C. (2012). Ventral tegmental area GABA projections pause accumbal cholinergic interneurons to enhance associative learning. *Nature* 492, 452–456. doi:[10.1038/nature11657](https://doi.org/10.1038/nature11657).
- Brown, M. W., and Xiang, J. Z. (1998). Recognition memory: Neuronal substrates of the judgement of prior occurrence. *Prog Neurobiol* 55, 149–189.
- Brunel, N., and Wang, X. J. (2001). Effects of neuromodulation in a cortical network model of object working memory dominated by recurrent inhibition. *J Comput Neurosci* 11, 63–85.
- Buckley, M. J., and Gaffan, D. (1998). Perirhinal cortex ablation impairs visual object identification. *J Neurosci* 18, 2268–2275.
- Buffalo, E. A., Ramus, S. J., Squire, L. R., and Zola, S. M. (2000). Perception and recognition memory in monkeys following lesions of area TE and perirhinal cortex. *Learn Mem* 7, 375–382.
- Buffalo, E. A., Reber, P. J., and Squire, L. R. (1998). The human perirhinal cortex and recognition memory. *Hippocampus* 8, 330–339.
- Bunge, S. A., Hazeltine, E., Scanlon, M. D., Rosen, A. C., and Gabrieli, J. D. E. (2002). [Dissociable contributions of prefrontal and parietal cortices to response selection](#). *Neuroimage* 17, 1562–1571.
- Burgess, N., Barry, C., and O'Keefe, J. (2007). An oscillatory interference model of grid cell firing. *Hippocampus* 17, 801–812.
- Bussey, T. J., and Saksida, L. M. (2002). The organization of visual object representations: A connectionist model of effects of lesions in perirhinal cortex. *Eur J Neurosci* 15, 355–364.
- Butz, M., Wörgötter, F., and Ooyen, A. van (2009). Activity-dependent structural plasticity. *Brain Res. Rev.* 60, 287–305. doi:[10.1016/j.brainresrev.2008.12.023](https://doi.org/10.1016/j.brainresrev.2008.12.023).

References

- Cabanac, M. (1971). [Physiological role of pleasure](#). *Science* 173, 1103–1107.
- Calabresi, P., Mercuri, N., Stanzione, P., Stefani, A., and Bernardi, G. (1987). Intracellular studies on the dopamine-induced firing inhibition of neostriatal neurons in vitro: Evidence for D1 receptor involvement. *Neuroscience* 20, 757–771.
- Calabresi, P., Picconi, B., Tozzi, A., and Di Filippo, M. (2007). Dopamine-mediated regulation of corticostriatal synaptic plasticity. *Trends Neurosci.* 30, 211–9. doi:[10.1016/j.tins.2007.03.001](#).
- Calzavara, R., Maily, P., and Haber, S. N. (2007). Relationship between the corticostriatal terminals from areas 9 and 46, and those from area 8A, dorsal and rostral premotor cortex and area 24c: An anatomical substrate for cognition to action. *Eur J Neurosci* 26, 2005–2024. doi:[10.1111/j.1460-9568.2007.05825.x](#).
- Carandini, M., and Heeger, D. J. (2012). Normalization as a canonical neural computation. *Nat. Rev. Neurosci.* 13, 51–62. doi:[10.1038/nrn3136](#).
- Cardinal, R. N., Parkinson, J. A., Hall, J., and Everitt, B. J. (2002). Emotion and motivation: the role of the amygdala, ventral striatum, and prefrontal cortex. *Neurosci. Biobehav. Rev.* 26, 321–52. Available at: <http://www.ncbi.nlm.nih.gov/pubmed/12034134>.
- Carlson, K. D., Nageswaran, J. M., Dutt, N., and Krichmar, J. L. (2014). An efficient automated parameter tuning framework for spiking neural networks. *Front. Neurosci.* 8, 10. doi:[10.3389/fnins.2014.00010](#).
- Carmichael, S. T., and Price, J. L. (1995). Sensory and premotor connections of the orbital and medial prefrontal cortex of macaque monkeys. *J. Comp. Neurol.* 363, 642–664. doi:[10.1002/cne.903630409](#).
- Carr, D. B., and Sesack, S. R. (2000). GABA-containing neurons in the rat ventral tegmental area project to the prefrontal cortex. *Synapse* 38, 114–23. doi:[10.1002/1098-2396\(200011\)38:2<114::AID-SYN2>3.0.CO;2-R](#).
- Cepeda, C., Colwell, C. S., Itri, J. N., Chandler, S. H., and Levine, M. S. (1998). [Dopaminergic modulation of NMDA-induced whole cell currents in neostriatal neurons in slices: Contribution of calcium conductances](#). *J Neurophysiol* 79, 82–94.
- Cepeda, C., Radisavljevic, Z., Peacock, W., Levine, M. S., and Buchwald, N. A. (1992). Differential modulation by dopamine of responses evoked by excitatory amino acids in human cortex. *Synapse* 11, 330–341.

- Chadderdon, G. L., and Sporns, O. (2006). A large-scale neurocomputational model of task-oriented behavior selection and working memory in prefrontal cortex. *J Cogn Neurosci* 18, 242–257.
- Chang, C., Crottaz-Herbette, S., and Menon, V. (2007). Temporal dynamics of basal ganglia response and connectivity during verbal working memory. *Neuroimage* 34, 1253–1269. doi:[10.1016/j.neuroimage.2006.08.056](https://doi.org/10.1016/j.neuroimage.2006.08.056).
- Chang, J.-Y., Chen, L., Luo, F., Shi, L.-H., and Woodward, D. J. (2002). Neuronal responses in the frontal cortico-basal ganglia system during delayed matching-to-sample task: Ensemble recording in freely moving rats. *Exp Brain Res* 142, 67–80. doi:[10.1007/s00221-001-0918-3](https://doi.org/10.1007/s00221-001-0918-3).
- Chen, J. Y., Wang, E. A., Cepeda, C., and Levine, M. S. (2013). Dopamine imbalance in huntington's disease: A mechanism for the lack of behavioral flexibility. *Front Neurosci* 7, 114. doi:[10.3389/fnins.2013.00114](https://doi.org/10.3389/fnins.2013.00114).
- Cheng, K., Saleem, K. S., and Tanaka, K. (1997). Organization of corticostriatal and corticoamygdalar projections arising from the anterior inferotemporal area TE of the macaque monkey: a Phaseolus vulgaris leucoagglutinin study. *J. Neurosci.* 17, 7902–25. Available at: <http://www.ncbi.nlm.nih.gov/pubmed/9315910>.
- Chevalier, G., and Deniau, J. M. (1990). [Disinhibition as a basic process in the expression of striatal functions](#). *Trends Neurosci* 13, 277–280.
- Chorley, P., and Seth, A. K. (2011). Dopamine-signaled reward predictions generated by competitive excitation and inhibition in a spiking neural network model. *Front. Comput. Neurosci.* 5, 21. doi:[10.3389/fncom.2011.00021](https://doi.org/10.3389/fncom.2011.00021).
- Christian, K. M., and Thompson, R. F. (2003). Neural substrates of eyeblink conditioning: acquisition and retention. *Learn. Mem.* 10, 427–55. doi:[10.1101/lm.59603](https://doi.org/10.1101/lm.59603).
- Cohen, M. X., Bour, L., Mantione, M., Figee, M., Vink, M., Tijssen, M. A. J., et al. (2012). Top-down-directed synchrony from medial frontal cortex to nucleus accumbens during reward anticipation. *Hum Brain Mapp* 33, 246–252. doi:[10.1002/hbm.21195](https://doi.org/10.1002/hbm.21195).
- Corbit, L. H., and Balleine, B. W. (2011). The general and outcome-specific forms of Pavlovian-instrumental transfer are differentially mediated by the nucleus accumbens core and shell. *J. Neurosci.* 31, 11786–94. doi:[10.1523/JNEUROSCI.2711-11.2011](https://doi.org/10.1523/JNEUROSCI.2711-11.2011).
- Coull, J. T., Cheng, R.-K., and Meck, W. H. (2011). Neuroanatomical and neurochemical sub-

References

- strates of timing. *Neuropsychopharmacology* 36, 3–25. doi:[10.1038/npp.2010.113](https://doi.org/10.1038/npp.2010.113).
- Cowell, R. A., Bussey, T. J., and Saksida, L. M. (2006). Why does brain damage impair memory? A connectionist model of object recognition memory in perirhinal cortex. *J Neurosci* 26, 12186–12197.
- Creed, M. C., Ntamati, N. R., and Tan, K. R. (2014). VTA GABA neurons modulate specific learning behaviors through the control of dopamine and cholinergic systems. *Front. Behav. Neurosci.* 8, 8. doi:[10.3389/fnbeh.2014.00008](https://doi.org/10.3389/fnbeh.2014.00008).
- Cromwell, H. C., and Schultz, W. (2003). Effects of expectations for different reward magnitudes on neuronal activity in primate striatum. *J Neurophysiol* 89, 2823–2838. doi:[10.1152/jn.01014.2002](https://doi.org/10.1152/jn.01014.2002).
- Cunningham, J. P., Gilja, V., Ryu, S. I., and Shenoy, K. V. (2009). Methods for estimating neural firing rates, and their application to brain-machine interfaces. *Neural Netw.* 22, 1235–46. doi:[10.1016/j.neunet.2009.02.004](https://doi.org/10.1016/j.neunet.2009.02.004).
- Curtis, C., and D'Esposito, M. (2003). Persistent activity in the prefrontal cortex during working memory. *Trends Cogn Sci* 7, 415–423.
- D'Esposito, M., Cooney, J. W., Gazzaley, A., Gibbs, S. E. B., and Postle, B. R. (2006). Is the prefrontal cortex necessary for delay task performance? Evidence from lesion and FMRI data. *J Int Neuropsychol Soc* 12, 248–260. doi:[10.1017/S1355617706060322](https://doi.org/10.1017/S1355617706060322).
- Damasio, A. R. (1994). *Descartes' error: Emotion, reason and the human brain*. New York: Grosset/Putnam.
- Darbaky, Y., Baunez, C., Arecchi, P., Legallet, E., and Apicella, P. (2005). Reward-related neuronal activity in the subthalamic nucleus of the monkey. *Neuroreport* 16, 1241–4. Available at: <http://www.ncbi.nlm.nih.gov/pubmed/16012357>.
- Davison, A. P., Brüderle, D., Eppler, J., Kremkow, J., Müller, E., Pecevski, D., et al. (2008). PyNN: A Common Interface for Neuronal Network Simulators. *Front. Neuroinform.* 2, 11. doi:[10.3389/neuro.11.011.2008](https://doi.org/10.3389/neuro.11.011.2008).
- Daw, N. D., Courville, A. C., Tourtezky, D. S., and Touretzky, D. S. (2006). Representation and timing in theories of the dopamine system. *Neural Comput.* 18, 1637–77. doi:[10.1162/neco.2006.18.7.1637](https://doi.org/10.1162/neco.2006.18.7.1637).
- Daw, N. D., Niv, Y., and Dayan, P. (2005). Uncertainty-based competition between prefrontal

- and dorsolateral striatal systems for behavioral control. *Nat. Neurosci.* 8, 1704–11. doi:[10.1038/nn1560](https://doi.org/10.1038/nn1560).
- Daw, N. D., and Touretzky, D. S. (2002). Long-term reward prediction in TD models of the dopamine system. *Neural Comput* 14, 2567–2583.
- Day, J. J., and Carelli, R. M. (2007). The nucleus accumbens and Pavlovian reward learning. *Neuroscientist* 13, 148–59. doi:[10.1177/1073858406295854](https://doi.org/10.1177/1073858406295854).
- Dayan, P., and Abbott, L. F. (2001). *Theoretical Neuroscience: Computational and Mathematical Modeling of Neural Systems*. The MIT Press Available at: <http://dl.acm.org/citation.cfm?id=1205781>.
- Deadwyler, S. A., Hayashizaki, S., Cheer, J., and Hampson, R. E. (2004). Reward, memory and substance abuse: functional neuronal circuits in the nucleus accumbens. *Neurosci. Biobehav. Rev.* 27, 703–711. Available at: <http://www.sciencedirect.com/science/article/pii/S0149763403001520>.
- Deco, G., and Rolls, E. T. (2003). Attention and working memory: A dynamical model of neuronal activity in the prefrontal cortex. *Eur J Neurosci* 18, 2374–2390.
- Delgado, M. R., Li, J., Schiller, D., and Phelps, E. A. (2008). The role of the striatum in aversive learning and aversive prediction errors. *Philos. Trans. R. Soc. Lond. B. Biol. Sci.* 363, 3787–800. doi:[10.1098/rstb.2008.0161](https://doi.org/10.1098/rstb.2008.0161).
- Delgado, M. R., Miller, M. M., Inati, S., and Phelps, E. A. (2005). An fMRI study of reward-related probability learning. *Neuroimage* 24, 862–873. doi:[10.1016/j.neuroimage.2004.10.002](https://doi.org/10.1016/j.neuroimage.2004.10.002).
- DeLong, M. R. (1990). [Primate models of movement disorders of basal ganglia origin](#). *Trends Neurosci* 13, 281–285.
- DeLong, M. R., and Wichmann, T. (2007). Circuits and circuit disorders of the basal ganglia. *Arch Neurol* 64, 20–24. doi:[10.1001/archneur.64.1.20](https://doi.org/10.1001/archneur.64.1.20).
- Desimone, R., and Duncan, J. (1995). Neural mechanisms of selective visual attention. *Ann Rev Neurosci* 18, 193–222.
- Di Filippo, M., Picconi, B., Tantucci, M., Ghiglieri, V., Bagetta, V., Sgobio, C., et al. (2009). Short-term and long-term plasticity at corticostriatal synapses: Implications for learning and memory. *Behav Brain Res* 199, 108–18.

References

- Di Giovanni, G., and Shi, W.-X. (2009). Effects of scopolamine on dopamine neurons in the substantia nigra: Role of the pedunculo-pontine tegmental nucleus. *Synapse* 63, 673–680. doi:[10.1002/syn.20650](https://doi.org/10.1002/syn.20650).
- Dinkelbach, H. Ü., Vitay, J., Beuth, F., and Hamker, F. H. (2012). Comparison of GPU- and CPU-implementations of mean-firing rate neural networks on parallel hardware. *Network* 23, 212–36. doi:[10.3109/0954898X.2012.739292](https://doi.org/10.3109/0954898X.2012.739292).
- Díaz-Mataix, L., Tallot, L., and Doyère, V. (2013). The amygdala: A potential player in timing CS–US intervals. *Behav. Processes*. Available at: <http://www.sciencedirect.com/science/article/pii/S0376635713001824>.
- Djurfeldt, M. (2012). The connection-set algebra—a novel formalism for the representation of connectivity structure in neuronal network models. *Neuroinformatics* 10, 287–304. doi:[10.1007/s12021-012-9146-1](https://doi.org/10.1007/s12021-012-9146-1).
- Dormont, J. F., Condé, H., and Farin, D. (1998). The role of the pedunculo-pontine tegmental nucleus in relation to conditioned motor performance in the cat. I. Context-dependent and reinforcement-related single unit activity. *Exp. Brain Res.* 121, 401–10. Available at: <http://www.ncbi.nlm.nih.gov/pubmed/9746146>.
- Doya, K., Ishii, S., Pouget, A., and Rao, R. P. N. eds. (2006). *Bayesian brain: Probabilistic approaches to neural coding*. The MIT Press.
- Doyere, V., Srebro, B., and Laroche, S. (1997). Heterosynaptic LTD and Depotential in the Medial Perforant Path of the Dentate Gyrus in the Freely Moving Rat. *J Neurophysiol* 77, 571–578. Available at: <http://jn.physiology.org/content/77/2/571.long>.
- Doyère, V., Schafe, G. E., Sigurdsson, T., and LeDoux, J. E. (2003). Long-term potentiation in freely moving rats reveals asymmetries in thalamic and cortical inputs to the lateral amygdala. *Eur. J. Neurosci.* 17, 2703–15. Available at: <http://www.ncbi.nlm.nih.gov/pubmed/12823477>.
- Dranias, M. R., Grossberg, S., and Bullock, D. (2008). Dopaminergic and non-dopaminergic value systems in conditioning and outcome-specific revaluation. *Brain Res.* 1238, 239–87. doi:[10.1016/j.brainres.2008.07.013](https://doi.org/10.1016/j.brainres.2008.07.013).
- Dreher, J.-C., Guigon, E., and Burnod, Y. (2002). A model of prefrontal cortex dopaminergic modulation during the delayed alternation task. *J Cogn Neurosci* 14, 853–865.
- Durstewitz, D. (2004). Neural representation of interval time. *Neuroreport* 15, 745–9. Available

- at: <http://www.ncbi.nlm.nih.gov/pubmed/15073507>.
- Durstewitz, D., Kelc, M., and Güntürkün, O. (1999). A neurocomputational theory of the dopaminergic modulation of working memory functions. *J Neurosci* 19, 2807–2822.
- Durstewitz, D., Seamans, J. K., and Sejnowski, T. J. (2000). Neurocomputational models of working memory. *Nat Neurosci Supp* 3, 1184–1191.
- Eagle, D. M., Baunez, C., Hutcheson, D. M., Lehmann, O., Shah, A. P., and Robbins, T. W. (2008). Stop-signal reaction-time task performance: Role of prefrontal cortex and subthalamic nucleus. *Cereb Cortex* 18, 178–188. doi:[10.1093/cercor/bhm044](https://doi.org/10.1093/cercor/bhm044).
- Ebner, C., Schroll, H., Winther, G., Niedeggen, M., and Hamker, F. H. (2015). Open and closed cortico-subcortical loops: A neuro-computational account of access to consciousness in the distractor-induced blindness paradigm. *Conscious Cogn* 35, 295–307. doi:[10.1016/j.concog.2015.02.007](https://doi.org/10.1016/j.concog.2015.02.007).
- Ebrahimi, A., Pochet, R., and Roger, M. (1992). [Topographical organization of the projections from physiologically identified areas of the motor cortex to the striatum in the rat.](#) *Neurosci Res* 14, 39–60.
- Eliasmith, C., Stewart, T. C., Choo, X., Bekolay, T., DeWolf, T., Tang, Y., et al. (2012). A large-scale model of the functioning brain. *Science* 338, 1202–5. doi:[10.1126/science.1225266](https://doi.org/10.1126/science.1225266).
- Elliott, R., and Dolan, R. J. (1999). [Differential neural responses during performance of matching and nonmatching to sample tasks at two delay intervals.](#) *J Neurosci* 19, 5066–5073.
- Eppler, J. M., Helias, M., Muller, E., Diesmann, M., and Gewaltig, M.-O. (2008). PyNEST: A Convenient Interface to the NEST Simulator. *Front. Neuroinform.* 2, 12. doi:[10.3389/neuro.11.012.2008](https://doi.org/10.3389/neuro.11.012.2008).
- Everitt, B. J., Dickinson, A., and Robbins, T. W. (2001). [The neuropsychological basis of addictive behaviour.](#) *Brain Res Brain Res Rev* 36, 129–138.
- Eyni, Y. S., and Horvitz, J. C. (2003). Opposing roles of D1 and D2 receptors in appetitive conditioning. *J. Neurosci.* 23, 1584–7. Available at: <http://www.ncbi.nlm.nih.gov/pubmed/12629161>.
- Featherstone, R. E., and McDonald, R. J. (2004). Dorsal striatum and stimulus-response learning: Lesions of the dorsolateral, but not dorsomedial, striatum impair acquisition of a stimulus-response-based instrumental discrimination task, while sparing conditioned place preference learning. *Neuroscience* 124, 23–31. doi:[10.1016/j.neuroscience.2003.10.038](https://doi.org/10.1016/j.neuroscience.2003.10.038).

References

- Feenstra, M. G., and Botterblom, M. H. (1996). [Rapid sampling of extracellular dopamine in the rat prefrontal cortex during food consumption, handling and exposure to novelty.](#) *Brain Res* 742, 17–24.
- Feenstra, M. G., Botterblom, M. H., and Mastenbroek, S. (2000). [Dopamine and noradrenaline efflux in the prefrontal cortex in the light and dark period: Effects of novelty and handling and comparison to the nucleus accumbens.](#) *Neuroscience* 100, 741–748.
- Fiala, J. C., Grossberg, S., and Bullock, D. (1996). Metabotropic Glutamate Receptor Activation in Cerebellar Purkinje Cells as Substrate for Adaptive Timing of the Classically Conditioned Eye-Blink Response. *J. Neurosci.* 16, 3760–3774. Available at: http://www.jneurosci.org/content/16/11/3760.abstract?ijkey=697c406d79d57535ce2655e34eacf49875ac9778/&eytype2=tf/_ipsecscha.
- Fidjeland, A. K., Roesch, E. B., Shanahan, M. P., and Luk, W. (2009). NeMo: A Platform for Neural Modelling of Spiking Neurons Using GPUs. in *2009 20th IEEE int. Conf. Appl. Syst. Archit. process.* (IEEE), 137–144. doi:[10.1109/ASAP.2009.24](https://doi.org/10.1109/ASAP.2009.24).
- Fields, H. L., Hjelmstad, G. O., Margolis, E. B., and Nicola, S. M. (2007). Ventral tegmental area neurons in learned appetitive behavior and positive reinforcement. *Annu. Rev. Neurosci.* 30, 289–316. doi:[10.1146/annurev.neuro.30.051606.094341](https://doi.org/10.1146/annurev.neuro.30.051606.094341).
- Fieres, J., Schemmel, J., and Meier, K. (2008). Realizing biological spiking network models in a configurable wafer-scale hardware system. in *Neural networks, 2008. IJCNN 2008. (IEEE world congress on computational intelligence)*, 969–976. doi:[10.1109/IJCNN.2008.4633916](https://doi.org/10.1109/IJCNN.2008.4633916).
- Fino, E., Glowinski, J., and Venance, L. (2005). Bidirectional activity-dependent plasticity at corticostriatal synapses. *J. Neurosci.* 25, 11279–87. doi:[10.1523/JNEUROSCI.4476-05.2005](https://doi.org/10.1523/JNEUROSCI.4476-05.2005).
- Fiorillo, C. D., Newsome, W. T., and Schultz, W. (2008). The temporal precision of reward prediction in dopamine neurons. *Nat. Neurosci.* doi:[10.1038/nn.2159](https://doi.org/10.1038/nn.2159).
- Fiorillo, C. D., Tobler, P. N., and Schultz, W. (2003). Discrete coding of reward probability and uncertainty by dopamine neurons. *Science* 299, 1898–902. doi:[10.1126/science.1077349](https://doi.org/10.1126/science.1077349).
- Flaherty, A. W., and Graybiel, A. M. (1994). [Input-output organization of the sensorimotor striatum in the squirrel monkey.](#) *J Neurosci* 14, 599–610.
- Frank, M. J., Loughry, B., and O'Reilly, R. C. (2001). Interactions between frontal cortex and basal ganglia in working memory: A computational model. *Cogn Affect Behav Neurosci* 1, 137–160.

- Friston, K. (2010). The free-energy principle: A unified brain theory? *Nat Rev Neurosci* 11, 127–138. doi:[10.1038/nrn2787](https://doi.org/10.1038/nrn2787).
- Fudge, J. L., and Haber, S. N. (2000). The central nucleus of the amygdala projection to dopamine subpopulations in primates. *Neuroscience* 97, 479–94. Available at: <http://www.ncbi.nlm.nih.gov/pubmed/10828531>.
- Funahashi, S., Bruce, C. J., and Goldman-Rakic, P. S. (1989). Mnemonic coding of visual space in the monkey's dorsolateral prefrontal cortex. *J Neurophysiol* 61, 331–349.
- Funahashi, S., Chafee, M. V., and Goldman-Rakic, P. S. (1993). Prefrontal neuronal activity in rhesus monkeys performing a delayed anti-saccade task. *Nature* 365, 753–6. doi:[10.1038/365753a0](https://doi.org/10.1038/365753a0).
- Furtak, S. C., Wei, S.-M., Agster, K. L., and Burwell, R. D. (2007). Functional neuroanatomy of the parahippocampal region in the rat: The perirhinal and postrhinal cortices. *Hippocampus*.
- Fuster, J. M., and Alexander, G. E. (1971). Neuron activity related to short-term memory. *Science* 173, 652–654.
- Fuster, J. M., Bauer, R. H., and Jervey, J. P. (1981). [Effects of cooling inferotemporal cortex on performance of visual memory tasks](#). *Exp Neurol* 71, 398–409.
- Fuster, J. M., Bauer, R. H., and Jervey, J. P. (1985). [Functional interactions between inferotemporal and prefrontal cortex in a cognitive task](#). *Brain Res* 330, 299–307.
- Gallistel, C. R., and Gibbon, J. (2000). Time, rate, and conditioning. *Psychol. Rev.* 107, 289–344. Available at: <http://www.ncbi.nlm.nih.gov/pubmed/10789198>.
- Galtress, T., and Kirkpatrick, K. (2009). Reward value effects on timing in the peak procedure. *Learn. Motiv.* 40, 109–131. Available at: <http://www.sciencedirect.com/science/article/pii/S0023969008000258>.
- Galtress, T., and Kirkpatrick, K. (2010). The role of the nucleus accumbens core in impulsive choice, timing, and reward processing. *Behav. Neurosci.* 124, 26–43. doi:[10.1037/a0018464](https://doi.org/10.1037/a0018464).
- Galtress, T., Marshall, A. T., and Kirkpatrick, K. (2012). Motivation and timing: clues for modeling the reward system. *Behav. Processes* 90, 142–53. doi:[10.1016/j.beproc.2012.02.014](https://doi.org/10.1016/j.beproc.2012.02.014).
- Galvan, A., and Smith, Y. (2011). The primate thalamostriatal systems: Anatomical organi-

References

- zation, functional roles and possible involvement in parkinson's disease. *Basal Ganglia* 1, 179–189. doi:[10.1016/j.baga.2011.09.001](https://doi.org/10.1016/j.baga.2011.09.001).
- Geisler, S., Derst, C., Veh, R. W., and Zahm, D. S. (2007). Glutamatergic afferents of the ventral tegmental area in the rat. *J. Neurosci.* 27, 5730–43. doi:[10.1523/JNEUROSCI.0012-07.2007](https://doi.org/10.1523/JNEUROSCI.0012-07.2007).
- Geisler, S., and Wise, R. A. (2008). Functional implications of glutamatergic projections to the ventral tegmental area. *Rev. Neurosci.* 19, 227–44. Available at: <http://www.pubmedcentral.nih.gov/articlerender.fcgi?artid=2735573&tool=pmcentrez&rendertype=abstract>.
- Gerfen, C. R., Engber, T. M., Mahan, L. C., Susel, Z., Chase, T. N., Monsma, F., Jr, et al. (1990). [D1 and D2 dopamine receptor-regulated gene expression of striatonigral and striatopallidal neurons](#). *Science* 250, 1429–1432.
- Gerstein, G. L., and Kiang, N. Y. (1960). An approach to the quantitative analysis of electrophysiological data from single neurons. *Biophys. J.* 1, 15–28. Available at: <http://www.pubmedcentral.nih.gov/articlerender.fcgi?artid=1366309&tool=pmcentrez&rendertype=abstract>.
- Gerstner, W., Kempter, R., Hemmen, J. L. van, and Wagner, H. (1996). A neuronal learning rule for sub-millisecond temporal coding. *Nature* 383, 76–81. doi:[10.1038/383076a0](https://doi.org/10.1038/383076a0).
- Gewaltig, M.-O., and Diesmann, M. (2007). NEST (NEural Simulation Tool). *Scholarpedia* 2, 1430. doi:[10.4249/scholarpedia.1430](https://doi.org/10.4249/scholarpedia.1430).
- Gisiger, T., and Kerszberg, M. (2006). A model for integrating elementary neural functions into delayed-response behavior. *PLoS Comput Biol* 2, e25.
- Goldman-Rakic, P. S., Lidow, M. S., Smiley, J. F., and Williams, M. S. (1992). The anatomy of dopamine in monkey and human prefrontal cortex. *J. Neural Transm. Suppl.* 36, 163–77. Available at: <http://www.ncbi.nlm.nih.gov/pubmed/1527516>.
- Goldman-Rakic, P. S., Muly, E. C., and Williams, G. V. (2000). D1 receptors in prefrontal cells and circuits. *Brain Res Rev* 31, 295–301.
- Goodman, D. F. M. (2010). Code generation: a strategy for neural network simulators. *Neuroinformatics* 8, 183–96. doi:[10.1007/s12021-010-9082-x](https://doi.org/10.1007/s12021-010-9082-x).
- Goodman, D., and Brette, R. (2008). Brian: a simulator for spiking neural networks in python. *Front. Neuroinform.* 2, 5. doi:[10.3389/neuro.11.005.2008](https://doi.org/10.3389/neuro.11.005.2008).

- Gorelova, N., Seamans, J. K., and Yang, C. R. (2002). Mechanisms of dopamine activation of fast-spiking interneurons that exert inhibition in rat prefrontal cortex. *J Neurophysiol* 88, 3150–3166.
- Goto, Y., and Grace, A. A. (2005). Dopaminergic modulation of limbic and cortical drive of nucleus accumbens in goal-directed behavior. *Nat. Neurosci.* 8, 805–12. doi:[10.1038/nn1471](https://doi.org/10.1038/nn1471).
- Goulet, S., and Murray, E. A. (2001). Neural substrates of crossmodal association memory in monkeys: The amygdala versus the anterior rhinal cortex. *Behav Neurosci* 115, 271–284.
- Grace, A. A. (1991). Phasic versus tonic dopamine release and the modulation of dopamine system responsivity: A hypothesis for the etiology of schizophrenia. *Neuroscience* 41, 1–24.
- Groshek, F., Kerfoot, E., McKenna, V., Polackwich, A. S., Gallagher, M., and Holland, P. C. (2005). Amygdala central nucleus function is necessary for learning, but not expression, of conditioned auditory orienting. *Behav. Neurosci.* 119, 202–12. doi:[10.1037/0735-7044.119.1.202](https://doi.org/10.1037/0735-7044.119.1.202).
- Grossberg, S., and Schmajuk, N. A. (1989). Neural dynamics of adaptive timing and temporal discrimination during associative learning. *Neural Networks* 2, 79–102. Available at: <http://www.sciencedirect.com/science/article/pii/0893608089900269>.
- Gruber, A. J., Dayan, P., Gutkin, B. S., and Solla, S. A. (2006). Dopamine modulation in the basal ganglia locks the gate to working memory. *J Comput Neurosci* 20, 153–166.
- Gruber, A. J., and McDonald, R. J. (2012). Context, emotion, and the strategic pursuit of goals: Interactions among multiple brain systems controlling motivated behavior. *Front Behav Neurosci* 6, 50. doi:[10.3389/fnbeh.2012.00050](https://doi.org/10.3389/fnbeh.2012.00050).
- Gruber, A. J., Solla, S. A., Surmeier, D. J., and Houk, J. C. (2003). Modulation of striatal single units by expected reward: a spiny neuron model displaying dopamine-induced bistability. *J. Neurophysiol.* 90, 1095–114. doi:[10.1152/jn.00618.2002](https://doi.org/10.1152/jn.00618.2002).
- Guillery, R. W., and Sherman, S. M. (2002). [Thalamic relay functions and their role in corticocortical communication: Generalizations from the visual system.](#) *Neuron* 33, 163–175.
- Gulley, J. M., Kosobud, A. E. K., and Rebec, G. V. (2002). [Behavior-related modulation of substantia nigra pars reticulata neurons in rats performing a conditioned reinforcement task.](#) *Neuroscience* 111, 337–349.

References

- Gurney, K., Prescott, T. J., and Redgrave, P. (2001a). [A computational model of action selection in the basal ganglia. I. A new functional anatomy.](#) *Biol Cybern* 84, 401–410.
- Gurney, K., Prescott, T. J., and Redgrave, P. (2001b). [A computational model of action selection in the basal ganglia. II. Analysis and simulation of behaviour.](#) *Biol Cybern* 84, 411–423.
- Gutnikov, S. A., Ma, Y. Y., and Gaffan, D. (1997). [Temporo-frontal disconnection impairs visual-visual paired association learning but not configural learning in macaca monkeys.](#) *Eur J Neurosci* 9, 1524–1529.
- Haber, S. N. (2003). [The primate basal ganglia: Parallel and integrative networks.](#) *J Chem Neuroanat* 26, 317–330.
- Haber, S. N., Fudge, J. L., and McFarland, N. R. (2000). Striatonigrostriatal pathways in primates form an ascending spiral from the shell to the dorsolateral striatum. *J. Neurosci.* 20, 2369–82. Available at: <http://www.ncbi.nlm.nih.gov/pubmed/10704511>.
- Haber, S. N., and Knutson, B. (2010). The reward circuit: linking primate anatomy and human imaging. *Neuropsychopharmacology* 35, 4–26. doi:[10.1038/npp.2009.129](https://doi.org/10.1038/npp.2009.129).
- Hallanger, A. E., and Wainer, B. H. (1988). Ascending projections from the pedunculopontine tegmental nucleus and the adjacent mesopontine tegmentum in the rat. *J. Comp. Neurol.* 274, 483–515. doi:[10.1002/cne.902740403](https://doi.org/10.1002/cne.902740403).
- Hamker, F. H. (2004a). [A dynamic model of how feature cues guide spatial attention.](#) *Vision Res* 44, 501–521.
- Hamker, F. H. (2004b). Predictions of a model of spatial attention using sum- and max-pooling functions. *Neurocomputing* 56, 329–343. doi:[10.1016/j.neucom.2003.09.006](https://doi.org/10.1016/j.neucom.2003.09.006).
- Hamker, F. H. (2005a). The emergence of attention by population-based inference and its role in distributed processing and cognitive control of vision. *J Comput Vis Image Underst* 100, 64–106.
- Hamker, F. H. (2005b). The reentry hypothesis: The putative interaction of the frontal eye field, ventrolateral prefrontal cortex, and areas V4, IT for attention and eye movement. *Cereb Cortex* 15, 431–447.
- Hazy, T. E., Frank, M. J., and O'Reilly, R. C. (2010). Neural mechanisms of acquired phasic dopamine responses in learning. *Neurosci. Biobehav. Rev.* 34, 701–20. doi:[10.1016/j.neubiorev.2009.11.019](https://doi.org/10.1016/j.neubiorev.2009.11.019).

- Hebb, D. O. (1949). *The organization of behavior: A neuropsychological theory*. New York: Wiley.
- Helie, S., Chakravarthy, S., and Moustafa, A. A. (2013). Exploring the cognitive and motor functions of the basal ganglia: An integrative review of computational cognitive neuroscience models. *Front Comput Neurosci* 7, 174. doi:[10.3389/fncom.2013.00174](https://doi.org/10.3389/fncom.2013.00174).
- Hershey, T., Wu, J., Weaver, P. M., Perantie, D. C., Karimi, M., Tabbal, S. D., et al. (2008). Unilateral vs. Bilateral STN DBS effects on working memory and motor function in parkinson disease. *Exp Neurol* 210, 402–408. doi:[10.1016/j.expneurol.2007.11.011](https://doi.org/10.1016/j.expneurol.2007.11.011).
- Hikosaka, O., Sakamoto, M., and Usui, S. (1989). Functional properties of monkey caudate neurons. III. Activities related to expectation of target and reward. *J Neurophysiol* 61, 814–832.
- Hikosaka, O., Sesack, S. R., Lecourtier, L., and Shepard, P. D. (2008). Habenula: cross-road between the basal ganglia and the limbic system. *J. Neurosci.* 28, 11825–11829. doi:[10.1523/JNEUROSCI.3463-08.2008](https://doi.org/10.1523/JNEUROSCI.3463-08.2008).
- Hines, M. L., and Carnevale, N. T. (1997). The NEURON simulation environment. *Neural Comput.* 9, 1179–209. Available at: <http://www.ncbi.nlm.nih.gov/pubmed/9248061>.
- Hirata, A., and Castro-Alamancos, M. A. (2010). Neocortex network activation and deactivation states controlled by the thalamus. *J Neurophysiol* 103, 1147–1157. doi:[10.1152/jn.00955.2009](https://doi.org/10.1152/jn.00955.2009).
- Hochreiter, S., and Schmidhuber, J. (1997). Long short-term memory. *Neural Comput.* 9, 1735–80. Available at: <http://www.ncbi.nlm.nih.gov/pubmed/9377276>.
- Hodgkin, A. L., and Huxley, A. F. (1952). A quantitative description of membrane current and its application to conduction and excitation in nerve. *The Journal of physiology* 117, 500–544. doi:[10.1113/jphysiol.1952.sp004764](https://doi.org/10.1113/jphysiol.1952.sp004764).
- Holland, P. C., and Gallagher, M. (2004). Amygdala–frontal interactions and reward expectancy. *Curr. Opin. Neurobiol.* 14, 148–155. Available at: <http://www.sciencedirect.com/science/article/pii/S095943880400039X>.
- Hollerman, J. R., and Schultz, W. (1998). Dopamine neurons report an error in the temporal prediction of reward during learning. *Nat. Neurosci.* 1, 304–9. doi:[10.1038/1124](https://doi.org/10.1038/1124).
- Holroyd, C. B., and Coles, M. G. H. (2002). [The neural basis of human error processing: Reinforcement learning, dopamine, and the error-related negativity](#). *Psychol Rev* 109, 679–709.

References

- Hong, S., and Hikosaka, O. (2008). The globus pallidus sends reward-related signals to the lateral habenula. *Neuron* 60, 720–9. doi:[10.1016/j.neuron.2008.09.035](https://doi.org/10.1016/j.neuron.2008.09.035).
- Hong, S., Jhou, T. C., Smith, M., Saleem, K. S., and Hikosaka, O. (2011). Negative reward signals from the lateral habenula to dopamine neurons are mediated by rostromedial tegmental nucleus in primates. *J. Neurosci.* 31, 11457–11471. Available at: <http://www.jneurosci.org/cgi/doi/10.1523/JNEUROSCI.1384-11.2011>.
- Horel, J. A., Pytko-Joiner, D. E., Voytko, M. L., and Salsbury, K. (1987). The performance of visual tasks while segments of the inferotemporal cortex are suppressed by cold. *Behav Brain Res* 23, 29–42.
- Horvitz, J. C. (2000). Mesolimbocortical and nigrostriatal dopamine responses to salient non-reward events. *Neuroscience* 96, 651–6. Available at: <http://www.ncbi.nlm.nih.gov/pubmed/10727783>.
- Horvitz, J. C. (2009). Stimulus-response and response-outcome learning mechanisms in the striatum. *Behav Brain Res* 199, 129–140. doi:[10.1016/j.bbr.2008.12.014](https://doi.org/10.1016/j.bbr.2008.12.014).
- Houk, J. C., Adams, J. L., and Barto, A. G. (1995). “A model of how the basal ganglia generate and use neural signal that predict reinforcement,” in *Models of information processing in the basal ganglia*, eds. J. C. Houk, J. L. Davis, and D. G. Beiser (Cambridge, MA: The MIT Press).
- Huang, Y. Y., and Kandel, E. R. (1995). D1/D5 receptor agonists induce a protein synthesis-dependent late potentiation in the CA1 region of the hippocampus. *Proc Natl Acad Sci U S A* 92, 2446–2450.
- Humphries, M. D., Lepora, N., Wood, R., and Gurney, K. (2009). Capturing dopaminergic modulation and bimodal membrane behaviour of striatal medium spiny neurons in accurate, reduced models. *Front. Comput. Neurosci.* 3, 26. doi:[10.3389/neuro.10.026.2009](https://doi.org/10.3389/neuro.10.026.2009).
- Humphries, M. D., and Prescott, T. J. (2010). The ventral basal ganglia, a selection mechanism at the crossroads of space, strategy, and reward. *Prog. Neurobiol.* 90, 385–417. doi:[10.1016/j.pneurobio.2009.11.003](https://doi.org/10.1016/j.pneurobio.2009.11.003).
- Hurd, Y. L., Suzuki, M., and Sedvall, G. C. (2001). D1 and D2 dopamine receptor mRNA expression in whole hemisphere sections of the human brain. *J Chem Neuroanat* 22, 127–137.
- Ibañez-Sandoval, O., Hernández, A., Florán, B., Galarraga, E., Tapia, D., Valdiosera, R., et al. (2006). Control of the subthalamic innervation of substantia nigra pars reticulata by D1 and D2 dopamine receptors. *J Neurophysiol* 95, 1800–1811. doi:[10.1152/jn.01074.2005](https://doi.org/10.1152/jn.01074.2005).

- Ikemoto, S. (2010). Brain reward circuitry beyond the mesolimbic dopamine system: a neurobiological theory. *Neurosci Biobehav Rev* 35, 129–150. doi:[10.1016/j.neubiorev.2010.02.001](https://doi.org/10.1016/j.neubiorev.2010.02.001).
- Intrator, N., and Cooper, L. N. (1992). Objective function formulation of the BCM theory of visual cortical plasticity: Statistical connections, stability conditions. *Neural Networks* 5, 3–17. doi:[10.1016/S0893-6080\(05\)80003-6](https://doi.org/10.1016/S0893-6080(05)80003-6).
- Ishikawa, M., Mu, P., Moyer, J. T., Wolf, J. A., Quock, R. M., Davies, N. M., et al. (2009). Homeostatic synapse-driven membrane plasticity in nucleus accumbens neurons. *J Neurosci* 29, 5820–5831. doi:[10.1523/JNEUROSCI.5703-08.2009](https://doi.org/10.1523/JNEUROSCI.5703-08.2009).
- Ito, R., Robbins, T. W., McNaughton, B. L., and Everitt, B. J. (2006). Selective excitotoxic lesions of the hippocampus and basolateral amygdala have dissociable effects on appetitive cue and place conditioning based on path integration in a novel Y-maze procedure. *Eur. J. Neurosci.* 23, 3071–80. doi:[10.1111/j.1460-9568.2006.04883.x](https://doi.org/10.1111/j.1460-9568.2006.04883.x).
- Izhikevich, E. M. (2003). Simple model of spiking neurons. *IEEE Trans. Neural Netw.* 14, 1569–72. doi:[10.1109/TNN.2003.820440](https://doi.org/10.1109/TNN.2003.820440).
- Izhikevich, E. M. (2007). Solving the distal reward problem through linkage of STDP and dopamine signaling. *Cereb. Cortex* 17, 2443–52. doi:[10.1093/cercor/bhl152](https://doi.org/10.1093/cercor/bhl152).
- Izquierdo, A., Wiedholz, L. M., Millstein, R. A., Yang, R. J., Bussey, T. J., Saksida, L. M., et al. (2006). Genetic and dopaminergic modulation of reversal learning in a touchscreen-based operant procedure for mice. *Behav Brain Res* 171, 181–188. doi:[10.1016/j.bbr.2006.03.029](https://doi.org/10.1016/j.bbr.2006.03.029).
- Jhou, T. C., Fields, H. L., Baxter, M. G., Saper, C. B., and Holland, P. C. (2009). The rostromedial tegmental nucleus (RMTg), a GABAergic afferent to midbrain dopamine neurons, encodes aversive stimuli and inhibits motor responses. *Neuron* 61, 786–800. doi:[10.1016/j.neuron.2009.02.001](https://doi.org/10.1016/j.neuron.2009.02.001).
- Joel, D., Niv, Y., and Ruppin, E. (2002). Actor-critic models of the basal ganglia: New anatomical and computational perspectives. *Neur Netw* 15, 535–547.
- Joel, D., and Weiner, I. (2000). [The connections of the dopaminergic system with the striatum in rats and primates: An analysis with respect to the functional and compartmental organization of the striatum.](#) *Neuroscience* 96, 451–474.
- Jonides, J., Schumacher, E. H., Smith, E. E., Koeppe, R. A., Awh, E., Reuter-Lorenz, P. A., et al. (1998). [The role of parietal cortex in verbal working memory.](#) *J Neurosci* 18, 5026–5034.

References

- Joshua, M., Adler, A., and Bergman, H. (2009). The dynamics of dopamine in control of motor behavior. *Current Opinion in Neurobiology* 19, 615–620. doi:[10.1016/j.conb.2009.10.001](https://doi.org/10.1016/j.conb.2009.10.001).
- Joyner, D., Čertík, O., Meurer, A., and Granger, B. E. (2012). Open source computer algebra systems. *ACM Commun. Comput. Algebr.* 45, 225. doi:[10.1145/2110170.2110185](https://doi.org/10.1145/2110170.2110185).
- Judice-Daher, D. M., and Bueno, J. L. O. (2013). Lesions of the nucleus accumbens disrupt reinforcement omission effects in rats. *Behav. Brain Res.* 252, 439–43. doi:[10.1016/j.bbr.2013.06.028](https://doi.org/10.1016/j.bbr.2013.06.028).
- Kaplan, F., and Oudeyer, P.-Y. (2007). In search of the neural circuits of intrinsic motivation. *Front Neurosci* 1, 225–236. doi:[10.3389/neuro.01.1.1.017.2007](https://doi.org/10.3389/neuro.01.1.1.017.2007).
- Kelefouras, V., Kritikakou, A., Papadima, E., and Goutis, C. (2015). A methodology for speeding up matrix vector multiplication for single/multi-core architectures. *J. Supercomput.* doi:[10.1007/s11227-015-1409-9](https://doi.org/10.1007/s11227-015-1409-9).
- Keramati, M., and Gutkin, B. (2013). Imbalanced decision hierarchy in addicts emerging from drug-hijacked dopamine spiraling circuit. *PLoS ONE* 8. doi:[10.1371/journal.pone.0061489](https://doi.org/10.1371/journal.pone.0061489).
- Khamassi, M., and Humphries, M. D. (2012). Integrating cortico-limbic-basal ganglia architectures for learning model-based and model-free navigation strategies. *Front Behav Neurosci* 6, 79. doi:[10.3389/fnbeh.2012.00079](https://doi.org/10.3389/fnbeh.2012.00079).
- Kincaid, A. E., Zheng, T., and Wilson, C. J. (1998). Connectivity and convergence of single corticostriatal axons. *J Neurosci* 18, 4722–4731.
- Kirkpatrick, K. (2013). Interactions of timing and prediction error learning. *Behav. Processes.* doi:[10.1016/j.beproc.2013.08.005](https://doi.org/10.1016/j.beproc.2013.08.005).
- Kirkpatrick, K., and Church, R. M. (2000). Stimulus and temporal cues in classical conditioning. *J Exp Psychol Anim Behav Process* 26, 206–219.
- Kita, H., Tachibana, Y., Nambu, A., and Chiken, S. (2005). Balance of monosynaptic excitatory and disinhibitory responses of the globus pallidus induced after stimulation of the subthalamic nucleus in the monkey. *J Neurosci* 25, 8611–8619. doi:[10.1523/JNEUROSCI.1719-05.2005](https://doi.org/10.1523/JNEUROSCI.1719-05.2005).
- Kita, H., Tokuno, H., and Nambu, A. (1999). [Monkey globus pallidus external segment neurons projecting to the neostriatum.](#) *Neuroreport* 10, 1467–1472.

- Kleiner-Fisman, G., Herzog, J., Fisman, D. N., Tamma, F., Lyons, K. E., Pahwa, R., et al. (2006). Subthalamic nucleus deep brain stimulation: Summary and meta-analysis of outcomes. *Mov Disord* 21 Suppl 14, S290–S304. doi:[10.1002/mds.20962](https://doi.org/10.1002/mds.20962).
- Kobayashi, Y., and Okada, K.-I. (2007). Reward prediction error computation in the pedunculo-pontine tegmental nucleus neurons. *Ann. N. Y. Acad. Sci.* 1104, 310–23. doi:[10.1196/annals.1390.003](https://doi.org/10.1196/annals.1390.003).
- Koch, K. W., and Fuster, J. M. (1989). [Unit activity in monkey parietal cortex related to haptic perception and temporary memory.](#) *Exp Brain Res* 76, 292–306.
- Komura, Y., Tamura, R., Uwano, T., Nishijo, H., Kaga, K., and Ono, T. (2001). Retrospective and prospective coding for predicted reward in the sensory thalamus. *Nature* 412, 546–9. doi:[10.1038/35087595](https://doi.org/10.1038/35087595).
- Koo, J. W., Han, J.-S., and Kim, J. J. (2004). Selective neurotoxic lesions of basolateral and central nuclei of the amygdala produce differential effects on fear conditioning. *J. Neurosci.* 24, 7654–62. doi:[10.1523/JNEUROSCI.1644-04.2004](https://doi.org/10.1523/JNEUROSCI.1644-04.2004).
- Kötter, R. (1994). [Postsynaptic integration of glutamatergic and dopaminergic signals in the striatum.](#) *Prog Neurobiol* 44, 163–196.
- Krichmar, J. L. (2013). A neurobotic platform to test the influence of neuromodulatory signaling on anxious and curious behavior. *Front. Neurobot.* 7, 1. doi:[10.3389/fnbot.2013.00001](https://doi.org/10.3389/fnbot.2013.00001).
- Krueger, K. A., and Dayan, P. (2009). Flexible shaping: How learning in small steps helps. *Cognition* 110, 380–394. doi:[10.1016/j.cognition.2008.11.014](https://doi.org/10.1016/j.cognition.2008.11.014).
- Kuhn, T. S. (1962). *The structure of scientific revolutions*. 1st ed. University of Chicago Press.
- Kumar, A., Cardanobile, S., Rotter, S., and Aertsen, A. (2011). The role of inhibition in generating and controlling parkinson's disease oscillations in the basal ganglia. *Front Syst Neurosci* 5, 86. doi:[10.3389/fnsys.2011.00086](https://doi.org/10.3389/fnsys.2011.00086).
- Kurzweil, R. (2005). *The singularity is near*. New York: Viking Books.
- Lammel, S., Lim, B. K., Ran, C., Huang, K. W., Betley, M. J., Tye, K. M., et al. (2012). Input-specific control of reward and aversion in the ventral tegmental area. *Nature* 491, 212–7. doi:[10.1038/nature11527](https://doi.org/10.1038/nature11527).
- Landau, S. M., Lal, R., O'Neil, J. P., Baker, S., and Jagust, W. J. (2009). Striatal dopamine and

References

- working memory. *Cereb Cortex* 19, 445–454. doi:[10.1093/cercor/bhn095](https://doi.org/10.1093/cercor/bhn095).
- Lange, H., Thorner, G., and Hopf, A. (1976). [Morphometric-statistical structure analysis of human striatum, pallidum and nucleus subthalamicus. III. Nucleus subthalamicus]. *J Hirnforsch* 17, 31–41.
- Langley, P., Laird, J. E., and Rogers, S. (2009). Cognitive architectures: Research issues and challenges. *Cognitive Systems Research* 10, 141–160.
- Lapicque, L. (1907). Recherches quantitatives sur l'excitation électrique des nerfs traitée comme une polarisation. *J. Physiol. Pathol. Gen.* 9, 620–635.
- Lardeux, S., Pernaud, R., Paleressompouille, D., and Baunez, C. (2009). Beyond the reward pathway: coding reward magnitude and error in the rat subthalamic nucleus. *J. Neurophysiol.* 102, 2526–37. doi:[10.1152/jn.91009.2008](https://doi.org/10.1152/jn.91009.2008).
- Lavezzi, H. N., and Zahm, D. S. (2011). The mesopontine rostromedial tegmental nucleus: an integrative modulator of the reward system. *Basal Ganglia* 1, 191–200. doi:[10.1016/j.baga.2011.08.003](https://doi.org/10.1016/j.baga.2011.08.003).
- Lawrence, A. D., Sahakian, B. J., and Robbins, T. W. (1998). Cognitive functions and corticostriatal circuits: Insights from Huntington's disease. *Trends in Cognitive Sciences* 2, 379–388.
- LeCun, Y., Bengio, Y., and Hinton, G. (2015). Deep learning. *Nature* 521, 436–444. doi:[10.1038/nature14539](https://doi.org/10.1038/nature14539).
- Lecun, Y., Bottou, L., Bengio, Y., and Haffner, P. (1998). Gradient-based learning applied to document recognition. *Proc. IEEE* 86, 2278–2324. doi:[10.1109/5.726791](https://doi.org/10.1109/5.726791).
- LeDoux, J. E. (2000). Emotion circuits in the brain. *Annu. Rev. Neurosci.* 23, 155–84. doi:[10.1146/annurev.neuro.23.1.155](https://doi.org/10.1146/annurev.neuro.23.1.155).
- Lee, B., Groman, S., London, E. D., and Jentsch, J. D. (2007). Dopamine D2/D3 receptors play a specific role in the reversal of a learned visual discrimination in monkeys. *Neuropsychopharmacology* 32, 2125–2134. doi:[10.1038/sj.npp.1301337](https://doi.org/10.1038/sj.npp.1301337).
- Lee, D., and Chun, M. M. (2001). What are the units of visual short-term memory, objects or spatial locations? *Percept Psychophys* 63, 253–257.
- Lee, H. J., Wheeler, D. S., and Holland, P. C. (2011). Interactions between amygdala central nucleus and the ventral tegmental area in the acquisition of conditioned cue-directed behavior

- in rats. *Eur. J. Neurosci.* 33, 1876–84. doi:[10.1111/j.1460-9568.2011.07680.x](https://doi.org/10.1111/j.1460-9568.2011.07680.x).
- Lehky, S. R., and Tanaka, K. (2007). Enhancement of object representations in primate perirhinal cortex during a visual working-memory task. *J Neurophysiol* 97, 1298–1310.
- Leung, L. S., and Yim, C. Y. (1993). Rhythmic delta-frequency activities in the nucleus accumbens of anesthetized and freely moving rats. *Can. J. Physiol. Pharmacol.* 71, 311–20. Available at: <http://www.ncbi.nlm.nih.gov/pubmed/8104675>.
- Levy, R., Friedman, H. R., Davachi, L., and Goldman-Rakic, P. S. (1997). [Differential activation of the caudate nucleus in primates performing spatial and nonspatial working memory tasks.](#) *J Neurosci* 17, 3870–3882.
- Levy, R., Hutchison, W. D., Lozano, A. M., and Dostrovsky, J. O. (2002). Synchronized neuronal discharge in the basal ganglia of parkinsonian patients is limited to oscillatory activity. *J Neurosci* 22, 2855–2861. doi:[20026193](https://doi.org/20026193).
- Lewis, S. J. G., Dove, A., Robbins, T. W., Barker, R. A., and Owen, A. M. (2004). Striatal contributions to working memory: A functional magnetic resonance imaging study in humans. *Eur J Neurosci* 19, 755–760.
- Linke, R., and Schwegler, H. (2000). Convergent and complementary projections of the caudal paralaminar thalamic nuclei to rat temporal and insular cortex. *Cereb Cortex* 10, 753–771.
- Liu, Z., Richmond, B. J., Murray, E. A., Saunders, R. C., Steenrod, S., Stubblefield, B. K., et al. (2004). DNA targeting of rhinal cortex D2 receptor protein reversibly blocks learning of cues that predict reward. *Proc Natl Acad Sci U S A* 101, 12336–12341.
- Ljungberg, T., Apicella, P., and Schultz, W. (1992). Responses of monkey dopamine neurons during learning of behavioral reactions. *J. Neurophysiol.* 67, 145–63. Available at: <http://www.ncbi.nlm.nih.gov/pubmed/1552316>.
- Lokwan, S. J., Overton, P. G., Berry, M. S., and Clark, D. (1999). Stimulation of the pedunculo-pontine tegmental nucleus in the rat produces burst firing in A9 dopaminergic neurons. *Neuroscience* 92, 245–54. Available at: <http://www.ncbi.nlm.nih.gov/pubmed/10392847>.
- Luciana, M., and Nelson, C. A. (1998). [The functional emergence of prefrontally-guided working memory systems in four- to eight-year-old children.](#) *Neuropsychologia* 36, 273–293.
- Luck, S. J., and Vogel, E. K. (1997). The capacity of visual working memory for features and conjunctions. *Nature* 390, 279–281.

References

- Ludvig, E. A., Conover, K., and Shizgal, P. (2007). The effects of reinforcer magnitude on timing in rats. *J. Exp. Anal. Behav.* 87, 201–18. Available at: <http://www.pubmedcentral.nih.gov/articlerender.fcgi?artid=1832167/&tool=pmcentrez/&rendertype=abstract>.
- Ludvig, E. A., Sutton, R. S., and Kehoe, E. J. (2008). Stimulus representation and the timing of reward-prediction errors in models of the dopamine system. *Neural Comput.* 20, 3034–54. doi:10.1162/neco.2008.11-07-654.
- Ludvig, E. A., Sutton, R. S., Verbeek, E., and Kehoe, E. J. (2009). A computational model of hippocampal function in trace conditioning. *Adv. Neural Inf. Process. Syst.* 21, 993–1000.
- Lustig, C., Matell, M. S., and Meck, W. H. (2005). Not “just” a coincidence: Frontal-striatal interactions in working memory and interval timing. *Memory* 3/4, 441–448. Available at: <http://www.bibsonomy.org/bibtex/2ccb5a59033ebd0fad86dc4267f1547dc/brian.mingus>.
- Luzardo, A., Ludvig, E. A., and Rivest, F. (2013). An adaptive drift-diffusion model of interval timing dynamics. *Behav. Processes* 95, 90–99. Available at: <http://www.sciencedirect.com/science/article/pii/S0376635713000247>.
- Maass, W., and Zador, A. M. (1999). [Dynamic stochastic synapses as computational units.](#) *Neural Comput* 11, 903–917.
- Mailly, P., Charpier, S., Menetrey, A., and Deniau, J.-M. (2003). [Three-dimensional organization of the recurrent axon collateral network of the substantia nigra pars reticulata neurons in the rat.](#) *J Neurosci* 23, 5247–5257.
- Mancall, E. L., and Brock, D. G. (2011). *Gray’s clinical neuroanatomy: The anatomic basis for clinical neuroscience.* Elsevier Health Sciences.
- Maren, S., and Quirk, G. J. (2004). Neuronal signalling of fear memory. *Nat. Rev. Neurosci.* 5, 844–52. doi:10.1038/nrn1535.
- Markram, H. (2006). The blue brain project. *Nat Rev Neurosci* 7, 153–60.
- Markram, H., Lubke, J., Frotscher, M., and Sakmann, B. (1997). Regulation of Synaptic Efficacy by Coincidence of Postsynaptic APs and EPSPs. *Science* (80-). 275, 213–215. doi:10.1126/science.275.5297.213.
- Markram, H., Wang, Y., and Tsodyks, M. (1998). Differential signaling via the same axon of neocortical pyramidal neurons. *Proc. Natl. Acad. Sci.* 95, 5323–5328.

doi:[10.1073/pnas.95.9.5323](https://doi.org/10.1073/pnas.95.9.5323).

- Martin-Soelch, C., Linthicum, J., and Ernst, M. (2007). Appetitive conditioning: neural bases and implications for psychopathology. *Neurosci. Biobehav. Rev.* 31, 426–40. doi:[10.1016/j.neubiorev.2006.11.002](https://doi.org/10.1016/j.neubiorev.2006.11.002).
- Matell, M. S., and Meck, W. H. (2000). Neuropsychological mechanisms of interval timing behavior. *BioEssays* 22, 94–103. Available at: <http://www.bibsonomy.org/bibtex/23ff219ef9d6fd6b6214587ad1254f7ed/brian.mingus>.
- Matell, M. S., and Meck, W. H. (2004). Cortico-striatal circuits and interval timing: coincidence detection of oscillatory processes. *Cogn. Brain Res.* 21, 139–170. Available at: <http://www.sciencedirect.com/science/article/pii/S0926641004001697>.
- Matsuda, W., Furuta, T., Nakamura, K. C., Hioki, H., Fujiyama, F., Arai, R., et al. (2009). Single nigrostriatal dopaminergic neurons form widely spread and highly dense axonal arborizations in the neostriatum. *J Neurosci* 29, 444–453. doi:[10.1523/JNEUROSCI.4029-08.2009](https://doi.org/10.1523/JNEUROSCI.4029-08.2009).
- Matsumoto, M., and Hikosaka, O. (2007). Lateral habenula as a source of negative reward signals in dopamine neurons. *Nature* 447, 1111–5. doi:[10.1038/nature05860](https://doi.org/10.1038/nature05860).
- Matsumoto, M., and Hikosaka, O. (2009). Two types of dopamine neuron distinctly convey positive and negative motivational signals. *Nature* 459, 837–41. doi:[10.1038/nature08028](https://doi.org/10.1038/nature08028).
- McClure, S. M., Berns, G. S., and Montague, P. R. (2003). Temporal prediction errors in a passive learning task activate human striatum. *Neuron* 38, 339–46. Available at: <http://www.ncbi.nlm.nih.gov/pubmed/12718866>.
- McCormick, D. A., Connors, B. W., Lighthall, J. W., and Prince, D. A. (1985). Comparative electrophysiology of pyramidal and sparsely spiny stellate neurons of the neocortex. *J Neurophysiol* 54, 782–806.
- McDannald, M., Kerfoot, E., Gallagher, M., and Holland, P. C. (2004). Amygdala central nucleus function is necessary for learning but not expression of conditioned visual orienting. *Eur. J. Neurosci.* 20, 240–8. doi:[10.1111/j.0953-816X.2004.03458.x](https://doi.org/10.1111/j.0953-816X.2004.03458.x).
- McGinty, V. B., and Grace, A. A. (2009). Activity-dependent depression of medial prefrontal cortex inputs to accumbens neurons by the basolateral amygdala. *Neuroscience* 162, 1429–36. doi:[10.1016/j.neuroscience.2009.05.028](https://doi.org/10.1016/j.neuroscience.2009.05.028).
- McNab, F., and Klingberg, T. (2008). Prefrontal cortex and basal ganglia control access to work-

References

- ing memory. *Nat Neurosci* 11, 103–107. doi:[10.1038/nn2024](https://doi.org/10.1038/nn2024).
- Meck, W. H. (2006). Neuroanatomical localization of an internal clock: a functional link between mesolimbic, nigrostriatal, and mesocortical dopaminergic systems. *Brain Res.* 1109, 93–107. doi:[10.1016/j.brainres.2006.06.031](https://doi.org/10.1016/j.brainres.2006.06.031).
- Melchitzky, D. S., and Lewis, D. A. (2001). [Dopamine transporter-immunoreactive axons in the mediodorsal thalamic nucleus of the macaque monkey](#). *Neuroscience* 103, 1033–1042.
- Mena-Segovia, J., Bolam, J. P., and Magill, P. J. (2004). Pedunculo-pontine nucleus and basal ganglia: Distant relatives or part of the same family? *Trends Neurosci* 27, 585–588. doi:[10.1016/j.tins.2004.07.009](https://doi.org/10.1016/j.tins.2004.07.009).
- Meunier, M., Bachevalier, J., Mishkin, M., and Murray, E. A. (1993). Effects on visual recognition of combined and separate ablations of the entorhinal and perirhinal cortex in rhesus monkeys. *J Neurosci* 13, 5418–5432.
- Middleton, F. A., and Strick, P. L. (1996). [The temporal lobe is a target of output from the basal ganglia](#). *Proc Natl Acad Sci U S A* 93, 8683–8687.
- Miller, E. K., and Cohen, J. D. (2001). An integrative theory of prefrontal cortex function. *Annu Rev Neurosci* 24, 167–202.
- Miller, E. K., Erickson, C., and Desimone, R. (1996). Neural mechanisms of visual working memory in prefrontal cortex of the macaque. *J Neurosci* 16, 5154–5167.
- Miller, E. K., Gochin, P. M., and Gross, C. G. (1993a). Suppression of visual responses of neurons in inferior temporal cortex of the awake macaque monkey by addition of a second stimulus. *Brain Res* 616, 25–29.
- Miller, E. K., Li, L., and Desimone, R. (1993b). Activity of neurons in anterior inferior temporal cortex during a short-term memory task. *J Neurosci* 13, 1460–1478.
- Minsky, M. (1968). *Semantic information processing*. Cambridge, MA: MIT Press.
- Mirenowicz, J., and Schultz, W. (1994). [Importance of unpredictability for reward responses in primate dopamine neurons](#). *J Neurophysiol* 72, 1024–1027.
- Mirolli, M., Santucci, V. G., and Baldassarre, G. (2013). Phasic dopamine as a prediction error of intrinsic and extrinsic reinforcements driving both action acquisition and reward maximization: A simulated robotic study. *Neural Netw* 39, 40–51. doi:[10.1016/j.neunet.2012.12.012](https://doi.org/10.1016/j.neunet.2012.12.012).

- Miyachi, S., Lu, X., Imanishi, M., Sawada, K., Nambu, A., and Takada, M. (2006). Somatotopically arranged inputs from putamen and subthalamic nucleus to primary motor cortex. *Neurosci Res* 56, 300–308. doi:[10.1016/j.neures.2006.07.012](https://doi.org/10.1016/j.neures.2006.07.012).
- Mogami, T., and Tanaka, K. (2006). Reward association affects neuronal responses to visual stimuli in macaque te and perirhinal cortices. *J Neurosci* 26, 6761–6770.
- Momiyama, T., Sim, J. A., and Brown, D. A. (1996). Dopamine D1-like receptor-mediated presynaptic inhibition of excitatory transmission onto rat magnocellular basal forebrain neurones. *J Physiol* 495 (Pt 1), 97–106.
- Mongillo, G., Amit, D. J., and Brunel, N. (2003). [Retrospective and prospective persistent activity induced by hebbian learning in a recurrent cortical network](#). *Eur J Neurosci* 18, 2011–2024.
- Montague, P. R., Dayan, P., and Sejnowski, T. J. (1996). A framework for mesencephalic dopamine systems based on predictive Hebbian learning. *J. Neurosci.* 16, 1936–47. Available at: <http://www.ncbi.nlm.nih.gov/pubmed/8774460>.
- Morita, M., and Suemitsu, A. (2002). [Computational modeling of pair-association memory in inferior temporal cortex](#). *Brain Res Cogn Brain Res* 13, 169–178.
- Morris, R. W., and Bouton, M. E. (2006). Effect of unconditioned stimulus magnitude on the emergence of conditioned responding. *J. Exp. Psychol. Anim. Behav. Process.* 32, 371–85. doi:[10.1037/0097-7403.32.4.371](https://doi.org/10.1037/0097-7403.32.4.371).
- Morrison, A., Straube, S., Plesser, H. E., and Diesmann, M. (2007). Exact subthreshold integration with continuous spike times in discrete-time neural network simulations. *Neural Comput.* 19, 47–79. doi:[10.1162/neco.2007.19.1.47](https://doi.org/10.1162/neco.2007.19.1.47).
- Muller, J. F., Mascagni, F., and McDonald, A. J. (2007). Postsynaptic targets of somatostatin-containing interneurons in the rat basolateral amygdala. *J. Comp. Neurol.* 500, 513–529. doi:[10.1002/cne.21185](https://doi.org/10.1002/cne.21185).
- Murray, E. A. (2007). The amygdala, reward and emotion. *Trends Cogn. Sci.* 11, 489–97. doi:[10.1016/j.tics.2007.08.013](https://doi.org/10.1016/j.tics.2007.08.013).
- Murray, E. A., Gaffan, D., and Mishkin, M. (1993). Neural substrates of visual stimulus-stimulus association in rhesus monkeys. *J Neurosci* 13, 4549–4561.
- Murray, E. A., and Richmond, B. J. (2001). Role of perirhinal cortex in object perception, memory, and associations. *Curr Opin Neurobiol* 11, 188–193.

References

- Murray, and Bussey (1999). [Perceptual-mnemonic functions of the perirhinal cortex](#). *Trends Cogn Sci* 3, 142–151.
- Mushiake, H., and Strick, P. L. (1995). [Pallidal neuron activity during sequential arm movements](#). *J Neurophysiol* 74, 2754–2758.
- Mutch, J., Knoblich, U., and Poggio, T. (2010). CNS: a GPU-based framework for simulating cortically-organized networks. Cambridge, MA: MIT-CSAIL-TR-2010-013 / CBCL-286, Massachusetts Institute of Technology.
- N'guyen, S., Thurat, C., and Girard, B. (2014). Saccade learning with concurrent cortical and sub-cortical basal ganglia loops. *Front Comput Neurosci* 8, 48. doi:[10.3389/fncom.2014.00048](https://doi.org/10.3389/fncom.2014.00048).
- Nakahara, H., Doya, K., and Hikosaka, O. (2001). Parallel cortico-basal ganglia mechanisms for acquisition and execution of visuomotor sequences - a computational approach. *J Cogn Neurosci* 13, 626–647.
- Nakamura, K., and Kubota, K. (1995). Mnemonic firing of neurons in the monkey temporal pole during a visual recognition memory task. *J Neurophysiol* 74, 162–178.
- Nakamura, K., Matsumoto, K., Mikami, A., and Kubota, K. (1994). [Visual response properties of single neurons in the temporal pole of behaving monkeys](#). *J Neurophysiol* 71, 1206–1221.
- Nakamura, K., and Ono, T. (1986). Lateral hypothalamus neuron involvement in integration of natural and artificial rewards and cue signals. *J. Neurophysiol.* 55, 163–81. Available at: <http://www.ncbi.nlm.nih.gov/pubmed/3512788>.
- Nambu, A. (2011). Somatotopic organization of the primate basal ganglia. *Front Neuroanat* 5, 26. doi:[10.3389/fnana.2011.00026](https://doi.org/10.3389/fnana.2011.00026).
- Nambu, A., Kaneda, K., Tokuno, H., and Takada, M. (2002). [Organization of corticostriatal motor inputs in monkey putamen](#). *J Neurophysiol* 88, 1830–1842.
- Nawrot, M., Aertsen, A., and Rotter, S. (1999). Single-trial estimation of neuronal firing rates: from single-neuron spike trains to population activity. *J. Neurosci. Methods* 94, 81–92. Available at: <http://www.ncbi.nlm.nih.gov/pubmed/10638817>.
- Naya, Y., Yoshida, M., Takeda, M., Fujimichi, R., and Miyashita, Y. (2003). Delay-period activities in two subdivisions of monkey inferotemporal cortex during pair association memory task. *Eur J Neurosci* 18, 2915–2918.

- Nicola, S. M. (2007). The nucleus accumbens as part of a basal ganglia action selection circuit. *Psychopharmacology (Berl)*. 191, 521–50. doi:[10.1007/s00213-006-0510-4](https://doi.org/10.1007/s00213-006-0510-4).
- Nicola, S. M., Surmeier, J., and Malenka, R. C. (2000). Dopaminergic modulation of neuronal excitability in the striatum and nucleus accumbens. *Annu Rev Neurosci* 23, 185–215.
- Nishijo, H., Hori, E., Tazumi, T., and Ono, T. (2008). Neural correlates to both emotion and cognitive functions in the monkey amygdala. *Behav. Brain Res.* 188, 14–23. doi:[10.1016/j.bbr.2007.10.013](https://doi.org/10.1016/j.bbr.2007.10.013).
- Nishijo, H., Ono, T., Uwano, T., Kondoh, T., and Torii, K. (2000). Hypothalamic and amygdalar neuronal responses to various tastant solutions during ingestive behavior in rats. *J. Nutr.* 130, 954S–9S. Available at: <http://www.ncbi.nlm.nih.gov/pubmed/10736360>.
- Niv, Y., Daw, N. D., Joel, D., and Dayan, P. (2007). Tonic dopamine: opportunity costs and the control of response vigor. *Psychopharmacology (Berl)*. 191, 507–20. doi:[10.1007/s00213-006-0502-4](https://doi.org/10.1007/s00213-006-0502-4).
- Nordlie, E., Gewaltig, M.-O., and Plesser, H. E. (2009). Towards reproducible descriptions of neuronal network models. *PLoS Comput. Biol.* 5, e1000456. doi:[10.1371/journal.pcbi.1000456](https://doi.org/10.1371/journal.pcbi.1000456).
- O’Doherty, J. P., Dayan, P., Friston, K., Critchley, H., and Dolan, R. J. (2003). Temporal difference models and reward-related learning in the human brain. *Neuron* 38, 329–37. Available at: <http://www.ncbi.nlm.nih.gov/pubmed/12718865>.
- O’Donnell, P., and Grace, A. A. (1995). Synaptic interactions among excitatory afferents to nucleus accumbens neurons: hippocampal gating of prefrontal cortical input. *J. Neurosci.* 15, 3622–39. Available at: <http://www.ncbi.nlm.nih.gov/pubmed/7751934>.
- O’Reilly, R. C., and Frank, M. J. (2006). Making working memory work: a computational model of learning in the prefrontal cortex and basal ganglia. *Neural Comput.* 18, 283–328. doi:[10.1162/089976606775093909](https://doi.org/10.1162/089976606775093909).
- O’Reilly, R. C., Frank, M. J., Hazy, T. E., and Watz, B. (2007). PVLV: The primary value and learned value pavlovian learning algorithm. *Behav Neurosci* 121, 31–49.
- Obeso, J. A., Rodriguez-Oroz, M. C., Javier Blesa, F., and Guridi, J. (2006). The globus pallidus pars externa and parkinson’s disease. Ready for prime time? *Exp Neurol* 202, 1–7. doi:[10.1016/j.expneurol.2006.07.004](https://doi.org/10.1016/j.expneurol.2006.07.004).
- Ohbayashi, M., Ohki, K., and Miyashita, Y. (2003). Conversion of working memory to motor

References

- sequence in the monkey premotor cortex. *Science* 301, 233–236.
- Oja, E. (1982). A simplified neuron model as a principal component analyzer. *J. Math. Biol.* 15, 267–73. Available at: <http://www.ncbi.nlm.nih.gov/pubmed/7153672>.
- Olshausen, B. A., and Field, D. J. (1997). [Sparse coding with an overcomplete basis set: A strategy employed by V1?](#) *Vision Res* 37, 3311–3325.
- Ono, T., Nishijo, H., and Uwano, T. (1995). Amygdala role in conditioned associative learning. *Prog. Neurobiol.* 46, 401–422. Available at: <http://www.sciencedirect.com/science/article/pii/030100829500008J>.
- Oprisan, S. A., and Buhusi, C. V. (2011). Modeling pharmacological clock and memory patterns of interval timing in a striatal beat-frequency model with realistic, noisy neurons. *Front. Integr. Neurosci.* 5, 52. doi:[10.3389/fnint.2011.00052](https://doi.org/10.3389/fnint.2011.00052).
- Oudeyer, P.-Y., and Kaplan, F. (2007). What is intrinsic motivation? A typology of computational approaches. *Front Neurorobot* 1, 6. doi:[10.3389/neuro.12.006.2007](https://doi.org/10.3389/neuro.12.006.2007).
- Owen, A. M., Herrod, N. J., Menon, D. K., Clark, J. C., Downey, S. P., Carpenter, T. A., et al. (1999). [Redefining the functional organization of working memory processes within human lateral prefrontal cortex.](#) *Eur J Neurosci* 11, 567–574.
- Packard, M. G., and Knowlton, B. J. (2002). Learning and memory functions of the basal ganglia. *Annu Rev Neurosci* 25, 563–593. doi:[10.1146/annurev.neuro.25.112701.142937](https://doi.org/10.1146/annurev.neuro.25.112701.142937).
- Pan, W.-X., and Hyland, B. I. (2005). Pedunculopontine tegmental nucleus controls conditioned responses of midbrain dopamine neurons in behaving rats. *J. Neurosci.* 25, 4725–32. doi:[10.1523/JNEUROSCI.0277-05.2005](https://doi.org/10.1523/JNEUROSCI.0277-05.2005).
- Pan, W.-X., Schmidt, R., Wickens, J. R., and Hyland, B. I. (2005). Dopamine cells respond to predicted events during classical conditioning: Evidence for eligibility traces in the reward-learning network. *J Neurosci* 25, 6235–6242. doi:[10.1523/JNEUROSCI.1478-05.2005](https://doi.org/10.1523/JNEUROSCI.1478-05.2005).
- Pape, H.-C., and Pare, D. (2010). Plastic synaptic networks of the amygdala for the acquisition, expression, and extinction of conditioned fear. *Physiol. Rev.* 90, 419–63. doi:[10.1152/physrev.00037.2009](https://doi.org/10.1152/physrev.00037.2009).
- Parent, A., and Hazrati, L. N. (1995a). Functional anatomy of the basal ganglia. I. The cortico-basal ganglia-thalamo-cortical loop. *Brain Res Brain Res Rev* 20, 91–127.

- Parent, A., and Hazrati, L. N. (1995b). Functional anatomy of the basal ganglia. II. The place of subthalamic nucleus and external pallidum in basal ganglia circuitry. *Brain Res Brain Res Rev* 20, 128–54.
- Parker, A., Eacott, M. J., and Gaffan, D. (1997). [The recognition memory deficit caused by mediodorsal thalamic lesion in non-human primates: A comparison with rhinal cortex lesion.](#) *Eur J Neurosci* 9, 2423–2431.
- Partiot, A., Vérin, M., Pillon, B., Teixeira-Ferreira, C., Agid, Y., and Dubois, B. (1996). [Delayed response tasks in basal ganglia lesions in man: Further evidence for a striato-frontal cooperation in behavioural adaptation.](#) *Neuropsychologia* 34, 709–721.
- Pennartz, C. M. (1995). [The ascending neuromodulatory systems in learning by reinforcement: Comparing computational conjectures with experimental findings.](#) *Brain Res Brain Res Rev* 21, 219–245.
- Petrides, M. (2000). [Dissociable roles of mid-dorsolateral prefrontal and anterior inferotemporal cortex in visual working memory.](#) *J Neurosci* 20, 7496–7503.
- Pihlajamäki, M., Tanila, H., Hänninen, T., Könönen, M., Mikkonen, M., Jalkanen, V., et al. (2003). Encoding of novel picture pairs activates the perirhinal cortex: An fMRI study. *Hippocampus* 13, 67–80.
- Plenz, D., and Aertsen, A. (1996). [Neural dynamics in cortex-striatum co-cultures–i. Anatomy and electrophysiology of neuronal cell types.](#) *Neuroscience* 70, 861–891.
- Plenz, D., and Kital, S. T. (1999). A basal ganglia pacemaker formed by the subthalamic nucleus and external globus pallidus. *Nature* 400, 677–682. doi:[10.1038/23281](https://doi.org/10.1038/23281).
- Pozo, K., and Goda, Y. (2010). Unraveling mechanisms of homeostatic synaptic plasticity. *Neuron* 66, 337–351. doi:[10.1016/j.neuron.2010.04.028](https://doi.org/10.1016/j.neuron.2010.04.028).
- Price, T. F., Peterson, C. K., and Harmon-Jones, E. (2012). The emotive neuroscience of embodiment. *Motivation and Emotion* 36, 27–37. doi:[10.1007/s11031-011-9258-1](https://doi.org/10.1007/s11031-011-9258-1).
- Ranganath, C. (2006). Working memory for visual objects: Complementary roles of inferior temporal, medial temporal, and prefrontal cortex. *Neurosci* 139, 277–289.
- Ranganath, C., Cohen, M. X., Dam, C., and D'Esposito, M. (2004). Inferior temporal, prefrontal, and hippocampal contributions to visual working memory maintenance and associative memory retrieval. *J Neurosci* 24, 3917–3925.

References

- Ranganath, C., and D'Esposito, M. (2005). Directing the mind's eye: Prefrontal, inferior and medial temporal mechanisms for visual working memory. *Curr Opin Neurobiol* 15, 175–182.
- Rao, R. P. N. (2010). Decision making under uncertainty: a neural model based on partially observable markov decision processes. *Front. Comput. Neurosci.* 4, 146. doi:[10.3389/fncom.2010.00146](https://doi.org/10.3389/fncom.2010.00146).
- Rast, A., Galluppi, F., Davies, S., Plana, L., Patterson, C., Sharp, T., et al. (2011). Concurrent heterogeneous neural model simulation on real-time neuromimetic hardware. *Neural Networks* 24, 961–978. doi:<http://dx.doi.org/10.1016/j.neunet.2011.06.014>.
- Raybuck, J. D., and Lattal, K. M. (2013). Bridging the interval: Theory and Neurobiology of Trace Conditioning. *Behav. Processes*. doi:[10.1016/j.beproc.2013.08.016](https://doi.org/10.1016/j.beproc.2013.08.016).
- Redgrave, P., and Gurney, K. (2006). The short-latency dopamine signal: A role in discovering novel actions? *Nat Rev Neurosci* 7, 967–975.
- Redgrave, P., Gurney, K., and Reynolds, J. (2008). What is reinforced by phasic dopamine signals? *Brain Res. Rev.* 58, 322–39. doi:[10.1016/j.brainresrev.2007.10.007](https://doi.org/10.1016/j.brainresrev.2007.10.007).
- Redgrave, P., Prescott, T. J., and Gurney, K. (1999). Is the short-latency dopamine response too short to signal reward error? *Trends Neurosci* 22, 146–151.
- Redgrave, P., Rodriguez, M., Smith, Y., Rodriguez-Oroz, M. C., Lehericy, S., Bergman, H., et al. (2010). Goal-directed and habitual control in the basal ganglia: Implications for parkinson's disease. *Nat Rev Neurosci* 11, 760–772. doi:[10.1038/nrn2915](https://doi.org/10.1038/nrn2915).
- Rempel-Clower, N. L., and Barbas, H. (2000). The laminar pattern of connections between prefrontal and anterior temporal cortices in the rhesus monkey is related to cortical structure and function. *Cereb Cortex* 10, 851–865.
- Repovs, G., and Baddeley, A. (2006). The multi-component model of working memory: Explorations in experimental cognitive psychology. *Neuroscience* 139, 5–21. doi:[10.1016/j.neuroscience.2005.12.061](https://doi.org/10.1016/j.neuroscience.2005.12.061).
- Reutimann, J., Yakovlev, V., Fusi, S., and Senn, W. (2004). Climbing neuronal activity as an event-based cortical representation of time. *J. Neurosci.* 24, 3295–303. doi:[10.1523/JNEUROSCI.4098-03.2004](https://doi.org/10.1523/JNEUROSCI.4098-03.2004).
- Reynolds, J. N. J., and Wickens, J. R. (2002). Dopamine-dependent plasticity of corticostriatal synapses. *Neural Networks* 15, 507–521. Available at: <http://www.sciencedirect.com/scie>

[nce/article/pii/S089360800200045X](https://doi.org/10.1038/35092560).

Reynolds, J. N., Hyland, B. I., and Wickens, J. R. (2001). A cellular mechanism of reward-related learning. *Nature* 413, 67–70. doi:[10.1038/35092560](https://doi.org/10.1038/35092560).

Reynolds, J. N., and Wickens, J. R. (2000). [Substantia nigra dopamine regulates synaptic plasticity and membrane potential fluctuations in the rat neostriatum, in vivo](#). *Neuroscience* 99, 199–203.

Riesenhuber, M., and Poggio, T. (1999). Hierarchical models of object recognition in cortex. *Nat. Neurosci.* 2, 1019–25. doi:[10.1038/14819](https://doi.org/10.1038/14819).

Rivest, F., Kalaska, J. F., and Bengio, Y. (2010). Alternative time representation in dopamine models. *J. Comput. Neurosci.* 28, 107–30. doi:[10.1007/s10827-009-0191-1](https://doi.org/10.1007/s10827-009-0191-1).

Rivest, F., Kalaska, J. F., and Bengio, Y. (2013). Conditioning and time representation in long short-term memory networks. *Biol. Cybern.* doi:[10.1007/s00422-013-0575-1](https://doi.org/10.1007/s00422-013-0575-1).

Robbins, T. W., and Everitt, B. J. (1996). Neurobehavioural mechanisms of reward and motivation. *Curr. Opin. Neurobiol.* 6, 228–36. Available at: <http://www.ncbi.nlm.nih.gov/pubmed/8725965>.

Rodriguez-Oroz, M. C., Jahanshahi, M., Krack, P., Litvan, I., Macias, R., Bezard, E., et al. (2009). Initial clinical manifestations of parkinson’s disease: Features and pathophysiological mechanisms. *Lancet Neurol* 8, 1128–1139. doi:[10.1016/S1474-4422\(09\)70293-5](https://doi.org/10.1016/S1474-4422(09)70293-5).

Rolls, E. T. (2000). Hippocampo-cortical and cortico-cortical backprojections. *Hippocampus* 10, 380–388.

Rolls, E., and Deco, G. (2001). *Computational neuroscience of vision*. Oxford Univ. Press.

Romanski, L. M. (2007). Representation and integration of auditory and visual stimuli in the primate ventral lateral prefrontal cortex. *Cereb Cortex* 17 Suppl 1, i61–i69. doi:[10.1093/cercor/bhm099](https://doi.org/10.1093/cercor/bhm099).

Rose, J., Schmidt, R., Grabemann, M., and Güntürkün, O. (2009). Theory meets pigeons: the influence of reward-magnitude on discrimination-learning. *Behav. Brain Res.* 198, 125–9. doi:[10.1016/j.bbr.2008.10.038](https://doi.org/10.1016/j.bbr.2008.10.038).

Rossum, M. C. W. van, and Turrigiano, G. G. (2001). Correlation based learning from spike timing dependent plasticity. *Neurocomputing* 38-40, 409–415.

References

- Rougier, N. P. (2009). Implicit and explicit representations. *Neural Netw* 22, 155–160. doi:[10.1016/j.neunet.2009.01.008](https://doi.org/10.1016/j.neunet.2009.01.008).
- Rougier, N. P., and Fix, J. (2012). DANA: distributed numerical and adaptive modelling framework. *Network* 23, 237–53. doi:[10.3109/0954898X.2012.721573](https://doi.org/10.3109/0954898X.2012.721573).
- Rougier, N. P., Noelle, D. C., Braver, T. S., Cohen, J. D., and O'Reilly, R. C. (2005). Prefrontal cortex and flexible cognitive control: Rules without symbols. *Proc Natl Acad Sci U S A* 102, 7338–7343. doi:[10.1073/pnas.0502455102](https://doi.org/10.1073/pnas.0502455102).
- Rougier, N. P., and Vitay, J. (2006). Emergence of attention within a neural population. *Neur Netw* 19, 573–581.
- Rowe, J. B., Toni, I., Josephs, O., Frackowiak, R. S., and Passingham, R. E. (2000). [The prefrontal cortex: Response selection or maintenance within working memory?](#) *Science* 288, 1656–1660.
- Rueda-Orozco, P. E., Mendoza, E., Hernandez, R., Aceves, J. J., Ibanez-Sandoval, O., Galarraga, E., et al. (2009). Diversity in long-term synaptic plasticity at inhibitory synapses of striatal spiny neurons. *Learn Mem* 16, 474–478. doi:[10.1101/lm.1439909](https://doi.org/10.1101/lm.1439909).
- Rumelhart, D. E., Hinton, G. E., and Williams, R. J. (1986). "Learning internal representations by error propagation," in *Parallel distributed processing: Explorations in the microstructure of cognition*, eds. D. E. Rumelhart and J. L. McClelland (Cambridge, MA: MIT Press), 318–362.
- Sah, P., Faber, E. S. L., Lopez De Armentia, M., and Power, J. (2003). The amygdaloid complex: anatomy and physiology. *Physiol. Rev.* 83, 803–34. doi:[10.1152/physrev.00002.2003](https://doi.org/10.1152/physrev.00002.2003).
- Sakai, K., and Miyashita, Y. (1991). Neural organization for the long-term memory of paired associates. *Nature* 354, 152–155. doi:[10.1038/354152a0](https://doi.org/10.1038/354152a0).
- Samejima, K., and Doya, K. (2007). Multiple representations of belief states and action values in corticobasal ganglia loops. *Ann. N. Y. Acad. Sci.* 1104, 213–28. doi:[10.1196/annals.1390.024](https://doi.org/10.1196/annals.1390.024).
- Sánchez-González, M. A., García-Cabezas, M. A., Rico, B., and Cavada, C. (2005). The primate thalamus is a key target for brain dopamine. *J Neurosci* 25, 6076–6083. doi:[10.1523/JNEUROSCI.0968-05.2005](https://doi.org/10.1523/JNEUROSCI.0968-05.2005).
- Schiller, J., Major, G., Koester, H. J., and Schiller, Y. (2000). NMDA spikes in basal dendrites of cortical pyramidal neurons. *Nature* 404, 285–289.

- Schroll, H., Beste, C., and Hamker, F. H. (2015). Combined lesions of direct and indirect basal ganglia pathways but not changes in dopamine levels explain learning deficits in patients with huntington's disease. *Eur J Neurosci* 41, 1227–1244. doi:[10.1111/ejn.12868](https://doi.org/10.1111/ejn.12868).
- Schroll, H., Vitay, J., and Hamker, F. H. (2012). Working memory and response selection: a computational account of interactions among cortico-basalganglio-thalamic loops. *Neural Netw.* 26, 59–74. doi:[10.1016/j.neunet.2011.10.008](https://doi.org/10.1016/j.neunet.2011.10.008).
- Schroll, H., Vitay, J., and Hamker, F. H. (2014). Dysfunctional and compensatory synaptic plasticity in Parkinson's disease. *Eur. J. Neurosci.* 39, 688–702. doi:[10.1111/ejn.12434](https://doi.org/10.1111/ejn.12434).
- Schultz, W. (1998). Predictive reward signal of dopamine neurons. *J Neurophysiol* 80, 1–27.
- Schultz, W., Apicella, P., and Ljungberg, T. (1993). Responses of monkey dopamine neurons to reward and conditioned stimuli during successive steps of learning a delayed response task. *J. Neurosci.* 13, 900–13. Available at: <http://www.ncbi.nlm.nih.gov/pubmed/8441015>.
- Schultz, W., Apicella, P., Scarnati, E., and Ljungberg, T. (1992). Neuronal activity in monkey ventral striatum related to the expectation of reward. *J. Neurosci.* 12, 4595–610. Available at: <http://www.ncbi.nlm.nih.gov/pubmed/1464759>.
- Schultz, W., Dayan, P., and Montague, P. R. (1997). A neural substrate of prediction and reward. *Science* 275, 1593–9. Available at: <http://www.ncbi.nlm.nih.gov/pubmed/9054347>.
- Seamans, J. K., and Yang, C. R. (2004). The principal features and mechanisms of dopamine modulation in the prefrontal cortex. *Prog. Neurobiol.* 74, 1–58. doi:[10.1016/j.pneurobio.2004.05.006](https://doi.org/10.1016/j.pneurobio.2004.05.006).
- Searle, J. R. (1980). Minds, brains, and programs. *Behavioral and Brain Sciences* 3, 417–424.
- Seger, C. A. (2008). How do the basal ganglia contribute to categorization? Their roles in generalization, response selection, and learning via feedback. *Neurosci Biobehav Rev* 32, 265–278. doi:[10.1016/j.neubiorev.2007.07.010](https://doi.org/10.1016/j.neubiorev.2007.07.010).
- Seger, C. A., and Spiering, B. J. (2011). A critical review of habit learning and the basal ganglia. *Front Syst Neurosci* 5, 66. doi:[10.3389/fnsys.2011.00066](https://doi.org/10.3389/fnsys.2011.00066).
- Selemon, L. D., and Goldman-Rakic, P. S. (1985). [Longitudinal topography and interdigitation of corticostriatal projections in the rhesus monkey.](#) *J Neurosci* 5, 776–794.
- Semba, K., and Fibiger, H. C. (1992). Afferent connections of the laterodorsal and the pedunculo-pontine tegmental nuclei in the rat: a retro- and antero-grade transport and immunohisto-

References

- chemical study. *J. Comp. Neurol.* 323, 387–410. doi:[10.1002/cne.903230307](https://doi.org/10.1002/cne.903230307).
- Sesack, S. R., and Grace, A. A. (2010). Cortico-Basal Ganglia reward network: microcircuitry. *Neuropsychopharmacology* 35, 27–47. doi:[10.1038/npp.2009.93](https://doi.org/10.1038/npp.2009.93).
- Shen, W., Flajolet, M., Greengard, P., and Surmeier, D. J. (2008). Dichotomous dopaminergic control of striatal synaptic plasticity. *Science* 321, 848–51. doi:[10.1126/science.1160575](https://doi.org/10.1126/science.1160575).
- Shimokawa, T., and Shinomoto, S. (2009). Estimating instantaneous irregularity of neuronal firing. *Neural Comput.* 21, 1931–51. doi:[10.1162/neco.2009.08-08-841](https://doi.org/10.1162/neco.2009.08-08-841).
- Simen, P., Balci, F., Souza, L. de, Cohen, J. D., and Holmes, P. (2011). A model of interval timing by neural integration. *J. Neurosci.* 31, 9238–53. doi:[10.1523/JNEUROSCI.3121-10.2011](https://doi.org/10.1523/JNEUROSCI.3121-10.2011).
- Singh, T., McDannald, M. A., Takahashi, Y. K., Haney, R. Z., Cooch, N. K., Lucantonio, F., et al. (2011). The role of the nucleus accumbens in knowing when to respond. *Learn. Mem.* 18, 85–7. doi:[10.1101/lm.2008111](https://doi.org/10.1101/lm.2008111).
- Skinner, B. F. (1938). *The behavior of organisms*. New York: Appleton-Century-Crofts.
- Smith, A., Li, M., Becker, S., and Kapur, S. (2006). Dopamine, prediction error and associative learning: A model-based account. *Network* 17, 61–84. doi:[10.1080/09548980500361624](https://doi.org/10.1080/09548980500361624).
- Smith, J. D., Redford, J. S., Gent, L. C., and Washburn, D. A. (2005). Visual search and the collapse of categorization. *J Exp Psychol Gen* 134, 443–460.
- Smith, K. S., Tindell, A. J., Aldridge, J. W., and Berridge, K. C. (2009). Ventral pallidum roles in reward and motivation. *Behav. Brain Res.* 196, 155–167. doi:[10.1016/j.bbr.2008.09.038](https://doi.org/10.1016/j.bbr.2008.09.038).
- Song, S., Miller, K. D., and Abbott, L. F. (2000). Competitive Hebbian learning through spike-timing-dependent synaptic plasticity. *Nat. Neurosci.* 3, 919–26. doi:[10.1038/78829](https://doi.org/10.1038/78829).
- Sporns, O., and Alexander, W. H. (2002). Neuromodulation and plasticity in an autonomous robot. *Neural Netw.* 15, 761–74. Available at: <http://www.ncbi.nlm.nih.gov/pubmed/12371525>.
- Spratling, M. W. (1999). Pre-synaptic lateral inhibition provides a better architecture for self-organizing neural networks. *Network* 10, 285–301.
- Srivastava, N., Hinton, G., Krizhevsky, A., Sutskever, I., and Salakhutdinov, R. (2014). Dropout: A simple way to prevent neural networks from overfitting. *J. Mach. Learn. Res.* 15, 1929–

1958.

- Stimberg, M., Goodman, D. F. M., Benichoux, V., and Brette, R. (2014). Equation-oriented specification of neural models for simulations. *Front. Neuroinform.* 8, 6. doi:[10.3389/fninf.2014.00006](https://doi.org/10.3389/fninf.2014.00006).
- Stocco, A., Lebiere, C., and Anderson, J. R. (2010). Conditional routing of information to the cortex: A model of the basal ganglia's role in cognitive coordination. *Psychol Rev* 117, 541–574. doi:[10.1037/a0019077](https://doi.org/10.1037/a0019077).
- Stopper, C. M., and Floresco, S. B. (2011). Contributions of the nucleus accumbens and its subregions to different aspects of risk-based decision making. *Cogn. Affect. Behav. Neurosci.* 11, 97–112. doi:[10.3758/s13415-010-0015-9](https://doi.org/10.3758/s13415-010-0015-9).
- Suri, R. E., and Schultz, W. (1999). A neural network model with dopamine-like reinforcement signal that learns a spatial delayed response task. *Neuroscience* 91, 871–90.
- Suri, R. E., and Schultz, W. (2001). Temporal difference model reproduces anticipatory neural activity. *Neural Comput.* 13, 841–62. Available at: <http://www.ncbi.nlm.nih.gov/pubmed/11255572>.
- Surmeier, D. J., Ding, J., Day, M., Wang, Z., and Shen, W. (2007). D1 and D2 dopamine-receptor modulation of striatal glutamatergic signaling in striatal medium spiny neurons. *Trends Neurosci* 30, 228–235. doi:[10.1016/j.tins.2007.03.008](https://doi.org/10.1016/j.tins.2007.03.008).
- Sutton, R. (1988). Learning to predict by the methods of temporal differences. *Machine Learning* 3, 9–44. doi:[10.1007/BF00115009](https://doi.org/10.1007/BF00115009).
- Sutton, R. S., and Barto, A. G. (1981). Toward a modern theory of adaptive networks: expectation and prediction. *Psychol. Rev.* 88, 135–70. Available at: <http://www.ncbi.nlm.nih.gov/pubmed/7291377>.
- Sutton, R. S., and Barto, A. G. (1998). *Reinforcement learning: An introduction*. MIT press.
- Suzuki, T., Miura, M., Nishimura, K., and Aosaki, T. (2001). Dopamine-dependent synaptic plasticity in the striatal cholinergic interneurons. *J Neurosci* 21, 6492–6501.
- Suzuki, W. A., and Amaral, D. G. (1994). Perirhinal and parahippocampal cortices of the macaque monkey: Cortical afferents. *J Comp Neurol* 350, 497–533.
- Suzuki, W. A., Miller, E. K., and Desimone, R. (1997). Object and place memory in the macaque entorhinal cortex. *J Neurophysiol* 78, 1062–1081.

References

- Tachibana, Y., and Hikosaka, O. (2012). The primate ventral pallidum encodes expected reward value and regulates motor action. *Neuron* 76, 826–37. doi:[10.1016/j.neuron.2012.09.030](https://doi.org/10.1016/j.neuron.2012.09.030).
- Takada, M., Tokuno, H., Nambu, A., and Inase, M. (1998). [Corticostriatal projections from the somatic motor areas of the frontal cortex in the macaque monkey: Segregation versus overlap of input zones from the primary motor cortex, the supplementary motor area, and the premotor cortex.](#) *Exp Brain Res* 120, 114–128.
- Takeda, M., Naya, Y., Fujimichi, R., Takeuchi, D., and Miyashita, Y. (2005). Active maintenance of associative mnemonic signal in monkey inferior temporal cortex. *Neuron* 48, 839–848. doi:[10.1016/j.neuron.2005.09.028](https://doi.org/10.1016/j.neuron.2005.09.028).
- Tan, C. O., and Bullock, D. (2008). A local circuit model of learned striatal and dopamine cell responses under probabilistic schedules of reward. *J. Neurosci.* 28, 10062–74. doi:[10.1523/JNEUROSCI.0259-08.2008](https://doi.org/10.1523/JNEUROSCI.0259-08.2008).
- Tanaka, K. (2000). Mechanisms of visual object recognition studied in monkeys. *Spat. Vis.* 13, 147–63. Available at: <http://www.ncbi.nlm.nih.gov/pubmed/11198228>.
- Tanimura, Y., King, M. A., Williams, D. K., and Lewis, M. H. (2011). Development of repetitive behavior in a mouse model: Roles of indirect and striosomal basal ganglia pathways. *Int J Dev Neurosci* 29, 461–467. doi:[10.1016/j.ijdevneu.2011.02.004](https://doi.org/10.1016/j.ijdevneu.2011.02.004).
- Taylor, J. G. (1999). Neural bubble dynamics in two dimensions: foundations. *Biol Cybern* 80, 393–409.
- Taylor, K. I., Moss, H. E., Stamatakis, E. A., and Tyler, L. K. (2006). Binding crossmodal object features in perirhinal cortex. *Proc Natl Acad Sci U S A* 103, 8239–8244.
- Tepper, J. M., Wilson, C. J., and Koós, T. (2008). Feedforward and feedback inhibition in neostriatal GABAergic spiny neurons. *Brain Res Rev* 58, 272–281. doi:[10.1016/j.brainresrev.2007.10.008](https://doi.org/10.1016/j.brainresrev.2007.10.008).
- Thibeault, C. M., Hoang, R. V., and F. C., H. (2011). A Novel Multi-GPU Neural Simulator. in *3rd int. Conf. Bioinforma. Comput. Biol. (BICoB 2011)* (New Orleans, LA: ISCA), 146–151.
- Thompson, R. F., and Steinmetz, J. E. (2009). The role of the cerebellum in classical conditioning of discrete behavioral responses. *Neuroscience* 162, 732–55. doi:[10.1016/j.neuroscience.2009.01.041](https://doi.org/10.1016/j.neuroscience.2009.01.041)
- Thorndike, E. L. (1911). *Animal intelligence: Experimental studies*. Macmillan.
- Tindell, A. J., Berridge, K. C., and Aldridge, J. W. (2004). Ventral pallidal representation

- of pavlovian cues and reward: population and rate codes. *J. Neurosci.* 24, 1058–69. doi:[10.1523/JNEUROSCI.1437-03.2004](https://doi.org/10.1523/JNEUROSCI.1437-03.2004).
- Tobler, P. N., Fiorillo, C. D., and Schultz, W. (2005). Adaptive coding of reward value by dopamine neurons. *Science* 307, 1642–5. doi:[10.1126/science.1105370](https://doi.org/10.1126/science.1105370).
- Tomita, H., Ohbayashi, M., Nakahara, K., Hasegawa, I., and Miyashita, Y. (1999). Top-down signal from prefrontal cortex in executive control of memory retrieval. *Nature* 401, 699–703.
- Turrigiano, G. G. (2008). The self-tuning neuron: synaptic scaling of excitatory synapses. *Cell* 135, 422–35. doi:[10.1016/j.cell.2008.10.008](https://doi.org/10.1016/j.cell.2008.10.008).
- Turrigiano, G. G., and Nelson, S. B. (2004). Homeostatic plasticity in the developing nervous system. *Nat Rev Neurosci* 5, 97–107.
- Tye, K. M., Cone, J. J., Schairer, W. W., and Janak, P. H. (2010). Amygdala neural encoding of the absence of reward during extinction. *J. Neurosci.* 30, 116–25. doi:[10.1523/JNEUROSCI.4240-09.2010](https://doi.org/10.1523/JNEUROSCI.4240-09.2010).
- Ungerleider, L. G., and Mishkin, M. (1982). “Two cortical visual systems,” in *Analysis of visual behavior*, eds. D. J. Ingle, M. A. Goodale, and R. J. W. Mansfield (Cambridge, MA: The MIT Press), 549–586.
- Usuda, I., Tanaka, K., and Chiba, T. (1998). Efferent projections of the nucleus accumbens in the rat with special reference to subdivision of the nucleus: biotinylated dextran amine study. *Brain Res.* 797, 73–93. Available at: <http://www.ncbi.nlm.nih.gov/pubmed/9630528>.
- Uttal, W. R. (2015). *Macroneural theories in cognitive neuroscience*. Psychology Press.
- van der Meulen, J. A. J., Joosten, R. N. J. M. A., de Bruin, J. P. C., and Feenstra, M. G. P. (2007). Dopamine and noradrenaline efflux in the medial prefrontal cortex during serial reversals and extinction of instrumental goal-directed behavior. *Cereb Cortex* 17, 1444–1453. doi:[10.1093/cercor/bhl057](https://doi.org/10.1093/cercor/bhl057).
- Velik, R. (2012). AI reloaded: Objectives, potentials, and challenges of the novel field of brain-like artificial intelligence. *BRAIN. Broad Research in Artificial Intelligence and Neuroscience* 3.
- Vijayraghavan, S., Wang, M., Birnbaum, S. G., Williams, G. V., and Arnsten, A. F. T. (2007). Inverted-u dopamine D1 receptor actions on prefrontal neurons engaged in working

References

- memory. *Nat Neurosci* 10, 376–384. doi:[10.1038/nn1846](https://doi.org/10.1038/nn1846).
- Vitay, J., Dinkelbach, H. Ü., and Hamker, F. H. (2015). ANNarchy: A code generation approach to neural simulations on parallel hardware. *Front Neuroinform* 9, 19. doi:[10.3389/fninf.2015.00019](https://doi.org/10.3389/fninf.2015.00019).
- Vitay, J., and Hamker, F. H. (2008). Sustained activities and retrieval in a computational model of the perirhinal cortex. *J. Cogn. Neurosci.* 20, 1993–2005. doi:[10.1162/jocn.2008.20147](https://doi.org/10.1162/jocn.2008.20147).
- Vitay, J., and Hamker, F. H. (2010). A computational model of Basal Ganglia and its role in memory retrieval in rewarded visual memory tasks. *Front. Comput. Neurosci.* 4. doi:[10.3389/fncom.2010.00013](https://doi.org/10.3389/fncom.2010.00013).
- Vitay, J., and Hamker, F. H. (2014). Timing and expectation of reward: A neuro-computational model of the afferents to the ventral tegmental area. *Front Neurorobot* 8, 4. doi:[10.3389/fnbot.2014.00004](https://doi.org/10.3389/fnbot.2014.00004).
- Vogels, T. P., and Abbott, L. F. (2005). Signal propagation and logic gating in networks of integrate-and-fire neurons. *J. Neurosci.* 25, 10786–95. doi:[10.1523/JNEUROSCI.3508-05.2005](https://doi.org/10.1523/JNEUROSCI.3508-05.2005).
- Voorn, P., Vanderschuren, L. J. M. J., Groenewegen, H. J., Robbins, T. W., and Pennartz, C. M. A. (2004). Putting a spin on the dorsal-ventral divide of the striatum. *Trends Neurosci* 27, 468–474. doi:[10.1016/j.tins.2004.06.006](https://doi.org/10.1016/j.tins.2004.06.006).
- Walker, A. G., and Steinmetz, J. E. (2008). Hippocampal lesions in rats differentially affect long- and short-trace eyeblink conditioning. *Physiol. Behav.* 93, 570–8. doi:[10.1016/j.physbeh.2007.10.018](https://doi.org/10.1016/j.physbeh.2007.10.018).
- Walt, S. van der, Colbert, S. C., and Varoquaux, G. (2011). The NumPy Array: A Structure for Efficient Numerical Computation. *Comput. Sci. Eng.* 13, 22–30. doi:[10.1109/MCSE.2011.37](https://doi.org/10.1109/MCSE.2011.37).
- Wan, H., Aggleton, J. P., and Brown, M. W. (1999). Different contributions of the hippocampus and perirhinal cortex to recognition memory. *J Neurosci* 19, 1142–1148.
- Wang, X.-J. (2002). Probabilistic decision making by slow reverberation in cortical circuits. *Neuron* 36, 955–68. Available at: <http://www.ncbi.nlm.nih.gov/pubmed/12467598>.
- Watanabe, Y., and Funahashi, S. (2004). Neuronal activity throughout the primate mediodorsal nucleus of the thalamus during oculomotor delayed-responses. II. Activity encoding visual versus motor signal. *J Neurophysiol* 92, 1756–1769. doi:[10.1152/jn.00995.2003](https://doi.org/10.1152/jn.00995.2003).

- Webster, M. J., Bachevalier, J., and Ungerleider, L. G. (1994). [Connections of inferior temporal areas TE0 and TE with parietal and frontal cortex in macaque monkeys](#). *Cereb Cortex* 4, 470–483.
- Wickens, J. R., and Oorshcot, D. E. (2000). "Neuronal dynamics and surround inhibition in the neostriatum: A possible connection," in *Brain dynamics and the striatal complex*, eds. R. Miller and J. R. Wickens (Australia: Harwood Academic Publishers), 141–150.
- Williams, S., Olike, L., Vuduc, R., Shalf, J., Yelick, K., and Demmel, J. (2007). Optimization of sparse matrix-vector multiplication on emerging multicore platforms. in *Proc. 2007 ACM/IEEE conf. Supercomput. - SC '07* (New York, New York, USA: ACM Press), 1. doi:[10.1145/1362622.1362674](#).
- Wiltscut, J., and Hamker, F. H. (2009). Efficient coding correlates with spatial frequency tuning in a model of V1 receptive field organization. *Vis Neurosci* 26, 21–34. doi:[10.1017/S0952523808080966](#).
- Winn, P. (2006). How best to consider the structure and function of the pedunculo-pontine tegmental nucleus: Evidence from animal studies. *J Neurol Sci* 248, 234–250. doi:[10.1016/j.jns.2006.05.036](#).
- Winstanley, C. A., Baunez, C., Theobald, D. E. H., and Robbins, T. W. (2005). Lesions to the subthalamic nucleus decrease impulsive choice but impair autoshaping in rats: the importance of the basal ganglia in Pavlovian conditioning and impulse control. *Eur. J. Neurosci.* 21, 3107–16. doi:[10.1111/j.1460-9568.2005.04143.x](#).
- Witt, K., Pulkowski, U., Herzog, J., Lorenz, D., Hamel, W., Deuschl, G., et al. (2004). Deep brain stimulation of the subthalamic nucleus improves cognitive flexibility but impairs response inhibition in parkinson disease. *Arch Neurol* 61, 697–700. doi:[10.1001/archneur.61.5.697](#).
- Wolf, J. A., Moyer, J. T., Lazarewicz, M. T., Contreras, D., Benoit-Marand, M., O'Donnell, P., et al. (2005). NMDA/AMPA ratio impacts state transitions and entrainment to oscillations in a computational model of the nucleus accumbens medium spiny projection neuron. *J. Neurosci.* 25, 9080–95. doi:[10.1523/JNEUROSCI.2220-05.2005](#).
- Wolf, M. E., Sun, X., Mangiavacchi, S., and Chao, S. Z. (2004). Psychomotor stimulants and neuronal plasticity. *Neuropharmacology* 47 Suppl 1, 61–79. doi:[10.1016/j.neuropharm.2004.07.006](#).
- Woodman, G. F., and Luck, S. J. (2007). Do the contents of visual working memory automatically influence attentional selection during visual search? *J Exp Psychol Hum Percept Perform* 33, 363–377. doi:[10.1037/0096-1523.33.2.363](#).

References

- Wu, G.-Y., Yao, J., Hu, B., Zhang, H.-M., Li, Y.-D., Li, X., et al. (2013). Reevaluating the role of the hippocampus in delay eyeblink conditioning. *PLoS One* 8, e71249. doi:[10.1371/journal.pone.0071249](https://doi.org/10.1371/journal.pone.0071249).
- Wu, W., Black, M. J., Mumford, D., Gao, Y., Bienenstock, E., and Donoghue, J. P. (2004). Modeling and decoding motor cortical activity using a switching Kalman filter. *IEEE Trans. Biomed. Eng.* 51, 933–42. doi:[10.1109/TBME.2004.826666](https://doi.org/10.1109/TBME.2004.826666).
- Yang, C. R., and Seamans, J. K. (1996). Dopamine D1 receptor actions in layers V-VI rat prefrontal cortex neurons in vitro: Modulation of dendritic-somatic signal integration. *J Neurosci* 16, 1922–1935.
- Yin, H. H., Knowlton, B. J., and Balleine, B. W. (2004). [Lesions of dorsolateral striatum preserve outcome expectancy but disrupt habit formation in instrumental learning.](#) *Eur J Neurosci* 19, 181–189.
- Yoshioka, M., Matsumoto, M., Togashi, H., and Saito, H. (1996). [Effect of conditioned fear stress on dopamine release in the rat prefrontal cortex.](#) *Neurosci Lett* 209, 201–203.
- Zahm, D. S., and Heimer, L. (1990). Two transpallidal pathways originating in the rat nucleus accumbens. *J. Comp. Neurol.* 302, 437–46. doi:[10.1002/cne.903020302](https://doi.org/10.1002/cne.903020302).
- Zahrt, J., Taylor, J. R., Mathew, R. G., and Arnsten, A. F. (1997). Supranormal stimulation of D1 dopamine receptors in the rodent prefrontal cortex impairs spatial working memory performance. *J Neurosci* 17, 8528–8535.
- Zaytsev, Y. V., and Morrison, A. (2014). CyNEST: a maintainable Cython-based interface for the NEST simulator. *Front. Neuroinform.* 8, 23. doi:[10.3389/fninf.2014.00023](https://doi.org/10.3389/fninf.2014.00023).
- Zenke, F., and Gerstner, W. (2014). Limits to high-speed simulations of spiking neural networks using general-purpose computers. *Front. Neuroinform.* 8, 76. doi:[10.3389/fninf.2014.00076](https://doi.org/10.3389/fninf.2014.00076).
- Zheng, T., and Wilson, C. J. (2002). [Cortico-striatal combinatorics: The implications of cortico-striatal axonal arborizations.](#) *J Neurophysiol* 87, 1007–1017.
- Zirnsak, M., Beuth, F., and Hamker, F. H. (2011). Split of spatial attention as predicted by a systems-level model of visual attention. *Eur. J. Neurosci.* 33, 2035–45. doi:[10.1111/j.1460-9568.2011.07718.x](https://doi.org/10.1111/j.1460-9568.2011.07718.x).
- Zola-Morgan, S., Squire, L. R., Amaral, D. G., and Suzuki, W. A. (1989). Lesions of perirhinal and parahippocampal cortex that spare the amygdala and hippocampal formation produce

severe memory impairment. *J Neurosci* 9, 4355–4370.

